



Universitat Autònoma de Barcelona

ADVERTIMENT. L'accés als continguts d'aquesta tesi doctoral i la seva utilització ha de respectar els drets de la persona autora. Pot ser utilitzada per a consulta o estudi personal, així com en activitats o materials d'investigació i docència en els termes establerts a l'art. 32 del Text Refós de la Llei de Propietat Intel·lectual (RDL 1/1996). Per altres utilitzacions es requereix l'autorització prèvia i expressa de la persona autora. En qualsevol cas, en la utilització dels seus continguts caldrà indicar de forma clara el nom i cognoms de la persona autora i el títol de la tesi doctoral. No s'autoritza la seva reproducció o altres formes d'explotació efectuades amb finalitats de lucre ni la seva comunicació pública des d'un lloc aliè al servei TDX. Tampoc s'autoritza la presentació del seu contingut en una finestra o marc aliè a TDX (framing). Aquesta reserva de drets afecta tant als continguts de la tesi com als seus resums i índexs.

ADVERTENCIA. El acceso a los contenidos de esta tesis doctoral y su utilización debe respetar los derechos de la persona autora. Puede ser utilizada para consulta o estudio personal, así como en actividades o materiales de investigación y docencia en los términos establecidos en el art. 32 del Texto Refundido de la Ley de Propiedad Intelectual (RDL 1/1996). Para otros usos se requiere la autorización previa y expresa de la persona autora. En cualquier caso, en la utilización de sus contenidos se deberá indicar de forma clara el nombre y apellidos de la persona autora y el título de la tesis doctoral. No se autoriza su reproducción u otras formas de explotación efectuadas con fines lucrativos ni su comunicación pública desde un sitio ajeno al servicio TDR. Tampoco se autoriza la presentación de su contenido en una ventana o marco ajeno a TDR (framing). Esta reserva de derechos afecta tanto al contenido de la tesis como a sus resúmenes e índices.

WARNING. The access to the contents of this doctoral thesis and its use must respect the rights of the author. It can be used for reference or private study, as well as research and learning activities or materials in the terms established by the 32nd article of the Spanish Consolidated Copyright Act (RDL 1/1996). Express and previous authorization of the author is required for any other uses. In any case, when using its content, full name of the author and title of the thesis must be clearly indicated. Reproduction or other forms of for profit use or public communication from outside TDX service is not allowed. Presentation of its content in a window or frame external to TDX (framing) is not authorized either. These rights affect both the content of the thesis and its abstracts and indexes.



**Development of electrochemical
(bio)sensors and microanalytical systems.
Application to the wine industry.**

Pablo Giménez Gómez

Tesis Doctoral

**Programa de doctorado en Electroquímica. Ciencia y
Tecnología.**

**Dirigida por Cecilia Jiménez Jorquera y Manuel Gutiérrez
Capitán**

Tutor: Iluminada Gallardo García

Departamento de Química

Facultad de Ciencias

2017



Memoria presentada para aspirar al Grado de Doctor por la
Universidad Autónoma de Barcelona.
Facultad de Ciencias.
Electroquímica. Ciencia y Tecnología.

La doctora Cecilia Jiménez Jorquera, Investigadora Científica, y el Doctor Manuel Gutiérrez Capitán, Investigador post-doctoral contratado, ambos con destino en el Instituto de Microelectrónica de Barcelona (IMB-CNM) del Consejo Superior de Investigaciones Científicas,

CERTIFICAN QUE:

Los trabajos incluidos en la presente memoria titulada: *Development of electrochemical (bio)sensors and microanalytical systems. Application to the wine industry*, han sido realizados bajo su dirección por Pablo Giménez Gómez, licenciado en Ingeniería Química, en las instalaciones del Instituto de Microelectrónica de Barcelona. Para que conste y tenga los efectos pertinentes en el departamento de Química de la Universidad Autónoma de Barcelona, firman la presente certificación el 19 de Abril de 2017.

Visto Bueno

Dra. Cecilia Jiménez Jorquera
(codirectora)

Dr. Manuel Gutiérrez Capitán
(codirector)

Dra. Ilumina Gallardo García
(tutora)

Bellaterra, Abril 2017

PUBLISHED ARTICLES INCLUDED IN THE THESIS

- I. **Multisensor portable meter for environmental applications.** P. Giménez-Gómez, R. Escudé-Pujol, C. Jiménez-Jorquera, M. Gutiérrez-Capitán. *IEEE Sensors Journal* 11 (2015), 6517-6523.
- II. **Monitoring of malolactic fermentation in wine using electrochemical bienzymatic biosensor for L-Lactate with long term stability.** P. Giménez-Gómez, M. Gutiérrez-Capitán, F. Capdevila, A. Puig-Pujol, C. Fernández-Sánchez, C. Jiménez-Jorquera. *Analytica Chimica Acta* 905 (2016), 126-133.
- III. **Portable Electronic Tongue Based on Microsensors for the Analysis of Cava Wines.** P. Giménez-Gómez, R. Escudé-Pujol, F. Capdevila, A. Puig-Pujol, C. Jiménez-Jorquera, M. Gutiérrez-Capitán. *Sensors* 16 (2016), 1796.
- IV. **Analysis of free and total sulfur dioxide in wine by using a gas-diffusion analytical system with pH detection.** P. Giménez-Gómez, M. Gutiérrez-Capitán, F. Capdevila, A. Puig-Pujol, S. Muñoz, A. Tobeña, A. Miró, C. Jiménez-Jorquera. *Food Chemistry* 228 (2017), 518-525.
- V. **Robust L-malate bienzymatic biosensor to enable the on-site monitoring of malolactic fermentation of red wines.** P. Giménez-Gómez, M. Gutiérrez-Capitán, F. Capdevila, A. Puig-Pujol, C. Fernández-Sánchez, C. Jiménez-Jorquera. *Analytica Chimica Acta* 954 (2017), 105-113.

LIST OF PROJECTS AND CONTRACTS RELATED TO THE THESIS

Ayuda predoctoral de Formación de Personal Investigador (FPI), correspondiente a la convocatoria del 2012, BES-2012-055534, en el marco del Plan Nacional de Investigación Científica, Desarrollo e Innovación 2008-2011.

Desarrollo de una tecnología híbrida Si/polímero para la fabricación de un lab on a chip (SIPLAB)

TEC2011-29045-C04-01

Instituciones: Instituto de Microelectrónica de Barcelona (IMB-CNM), CSIC; Instituto de Microelectrónica de Madrid (IMM-CNM), CSIC; Universidad de Sevilla; IRTA-INCAVI

Duración: Enero 2012-Octubre 2014

IP y Coordinador del proyecto (BIOLOC): Cecilia Jiménez Jorquera

Importe del proyecto: 120.274 €(Total: 304.118 €)

Biosensores de larga duración integrados en tecnología planar para análisis bioquímico en LOC (BIOSENSLOC)

TEC2014-54449-C3-1-R

Instituto de Microelectrónica de Barcelona (IMB-CNM), CSIC; Instituto de Microelectrónica de Madrid (IMM-CNM), CSIC; Universidad de Sevilla

Duración: Enero 2015-Diciembre 2017

IP y Coordinador del proyecto: Xavier Muñoz Berbel/ Carlos Dominguez Horna

Importe del proyecto: 147.983,00 €

ISFET based system for detection of acetic acid and SO₂ in wine barrels

Convenio Directo: Sapere corporation, California, USA

Duración: Octubre 2014- Diciembre 2016

Importe del contrato: 30.000 €

Sistema multisensor para determinación de sulfitos y grado alcohólico en enología

Convenio Directo: Biosystems, España

Duración: Enero 2012- Enero 2013

Importe del contrato: 68.000 €

INDEX

List of abbreviations.....	1
Summary.....	3
Summary in Spanish.....	7
<u>Chapter1: General Introduction.....</u>	11
1.1 Electrochemical sensors and biosensors.....	13
1.1.1 Potentiometric sensors.....	14
1.1.1.1 Ion-Sensitive Field Effect Transistors (ISFETs).....	15
1.1.1.2 ISFETs with ion selective membranes (ChemFETs).....	18
1.1.2 Amperometric enzymatic biosensors.....	19
1.1.2.1 Immobilization strategies of enzymes.....	27
1.1.2.1.1 Entrapment in electrosynthesized polypyrrole membranes...30	
1.1.2.2 L-lactate amperometric biosensors.....	34
1.1.2.3 L-malate amperometric biosensors.....	38
1.2 Multiparametric sensor systems: Electronic tongues.....	42
1.2.1 Advanced mathematical tools for signal processing.....	43
1.3 Miniaturization of the analytical systems.....	45
1.4 References.....	48
<u>Chapter 2: Objectives.....</u>	55
<u>Chapter 3: Experimental.....</u>	59
3.1 Reagents and solutions.....	61
3.2 Devices and equipment.....	62
3.3 Fabrication of the transducers.....	63
3.3.1 pH-ISFETs.....	63
3.3.2 ISFETs with membranes selective to ions (ChemFETs).....	65
3.3.3 Microelectrodes.....	66

3.4	Fabrication, optimization and characterization of the amperometric biosensors.....	69
3.4.1	Enzymes and enzymes/co-factor ratio assessments.....	69
3.4.2	Immobilization strategies to fabricate the amperometric biosensors.....	70
3.4.2.1	Physical adsorption and cross linking.....	71
3.4.2.2	Covalent immobilization.....	71
3.4.2.3	Entrapment into electrosynthesized polypyrrole membrane.....	72
3.4.2.3.1	L-lactate amperometric biosensor.....	73
3.4.2.3.2	L-malate amperometric biosensor.....	74
3.5	Fabrication of the microanalytical flow systems.....	76
3.5.1	Systems based on pH-ISFETs.....	76
3.5.1.1	Free and total SO ₂ determination.....	76
3.5.1.2	Free SO ₂ and acetic acid determination.....	78
3.5.2	Simultaneous determination of L-lactate and L-malate.....	79
3.6	Optimization of the microanalytical flow systems.....	83
3.6.1	Free and total SO ₂ determination.....	83
3.6.1.1	Optimization of the flow system and analytical assessment.....	84
3.6.2	Free SO ₂ and acetic acid determination.....	85
3.6.2.1	Free SO ₂	86
3.6.2.2	Acetic acid.....	87
3.6.3	Microanalytical flow system for L-lactate and L-malate detection.....	87
3.7	Multiparametric system for the analysis of cava wines.....	89
3.8	Analysis of real wines samples.....	91
3.8.1	Free and total SO ₂ determination.....	91
3.8.2	Free SO ₂ and acetic acid determination.....	92
3.8.3	L-lactic and L-malic acid determination.....	93
3.8.4	Analysis of Cava wines.....	94

3.9	References.....	96
Chapter 4:Results and discussions.....		97
4.1	Microanalytical flow systems based on gas-diffusion and pH-ISFET for the determination of free/total SO ₂ and acetic acid.....	99
4.1.1	Microanalytical flow system for free and total S _{O2} determination.....	104
4.1.1.1	Optimization of the system.....	104
4.1.1.2	Evaluation of the system performance.....	108
4.1.1.3	Analysis of wine samples.....	109
4.1.2	Microanalytical flow system for free SO ₂ and acetic acid determination.....	116
4.1.2.1	Optimization of the system for free SO ₂ determination.....	116
4.1.2.2	Optimization of the system for acetic acid determination.....	117
4.1.2.3	Analysis of wine samples.....	121
4.1.2.3.1	Acetic acid.....	121
4.1.2.3.2	Free SO ₂	122
4.1.2.3.3	Acetic acid and free SO ₂	123
4.2	L-lactate amperometric biosensor.....	127
4.2.1	Optimization of the LOX:HRP ratio.....	127
4.2.2	Optimization of the conditions for the immobilization of chemical reagents on the transducer surface.....	128
4.2.2.1	Adsorption and cross linking with glutaraldehyde.....	128
4.2.2.2	Covalent immobilization.....	129
4.2.2.3	Entrapment into electrosynthesized PPy membranes.....	130
4.2.3	Selection of the biosensor immobilization method.....	136
4.2.4	Monitoring of the L-lactic acid during the malolactic fermentation in wine samples.....	137
4.2.5	Comparison with other L-lactate electrochemical biosensors.....	141
4.3	L-malate amperometric biosensor.....	142
4.3.1	Optimization of the DP:MDH and (DP:MDH):NAD ⁺ ratios.....	142

4.3.2	Selection of the redox mediator.....	143
4.3.3	Selection of the biosensor architecture.....	147
4.3.4	Evaluation of the biosensor performance.....	148
4.3.5	Monitoring of the malolactic fermentation in wine samples with L-malate biosensor.....	151
4.3.6	Comparative study with other others L-malate amperometric biosensors.....	152
4.4	Microanalytical flow system for simultaneous determination of L-lactate and L-malate.....	154
4.4.1	Electrosynthesis of the electrochemical biosensors.....	154
4.4.2	Characterization of the amperometric biosensors.....	156
4.4.3	Malolactic fermentation monitoring with the dual fluidic system.....	158
4.5	Multiparametric system based on an electronic tongue for the analysis of Cava wines.....	160
4.5.1	Characterization of the sensors.....	160
4.5.2	Analysis Cava Wine samples.....	162
4.5.2.1	Classification of the samples.....	162
4.5.2.2	Quantification of Legal Parameters.....	163
4.5.2.3	Quantification of other parameters.....	165
4.6	References.....	167
	<u>Chapter 5: Conclusions</u>	169
	Conclusions in Spanish	175
	Annex	181

LIST OF ABBREVIATIONS

Symbol	Meaning
AFM	Atomic force microscope
BSA	Bovine serum albumin
CE	Counter electrode
ChemFET	ISFET with ion selective membrane
CNM	Centro Nacional de Microelectrónica
CV	Cyclic voltammetry
DIW	Deionized water
DMSO	Dimethyl sulfoxide
DP	Diaphorase
DTSP	Dithiobis (succinimidyl propionate)
ELISA	Enzyme-linked immunosorbent assay
GTQ	Grupo de Transductores Químicos
HAR	Hexaammineruthenium (III) chloride
HRP	Horseradish peroxidase
IMB	Instituto de Microelectrónica de Barcelona
IRTA-INCAVI	Institut Català de la Vinya i el Vi
ISE	Ion-selective-electrode
ISFET	Ion-sensitive Field Effect Transistor
IUPAC	International Union of Pure and Applied Chemistry
LDA	Linear discriminant analysis
LDH	L-lactate dehydrogenase
LOD	Limit of detection
LOX	Lactate oxidase
MDH	Malate dehydrogenase
MISFET	Metal-Insulator-Semiconductor Field Effect Transistor
MLF	Malolactic fermentation

NAD ⁺ /NADH	Nicotinamide adenine dinucleotide
ORP	Oxidation-reduction potential
PB	Phosphate buffer
PCB	Printed circuit board
PDMS	Polydimethylsiloxane
PLS	Partial least squares
PMMA	Polymethylmethacrylate
PPy	Polypyrrole
PSA	Pressure-sensitive-adhesive
PVC	Polyvinyl chloride
PVDF	Polyvinylidene fluoride
RE	Reference electrode
SAM	Self-assembled monolayer
THF	Tetrahydrofuran
TTF	Tetrathiafulvalene
VAD	Volumetric alcoholic degree
WE	Working electrode

Summary

Monitoring of food processes guarantee the quality of the final product. This is primarily remarkable in the wine industry, especially in the Mediterranean Region, where thousands of wine cellars and companies are producing this high benefit beverage. This growing market needs to guarantee quality standards and the consumer protection by monitoring several parameters along the winemaking processes. Application of electrochemical (bio)sensors in this field is promising due to their simplicity, fast response, low-cost and easy miniaturization for on-site detection. Besides, biosensors are a good alternative to expensive and tedious traditional methods applied in specialized laboratories.

In this Thesis, the development of electrochemical (bio)sensors fabricated with microelectronic technology and its implementation in fast-prototyped flow systems for the monitoring of chemical parameters of interest in the winemaking industry, is reported. As electrochemical (bio)sensors, Ion-Sensitive-Field-Effect-Transistors (ISFETs), microelectrodes with platinum and gold as electroactive metal and amperometric bienzymatic biosensors, have been used.

This work has been done with the collaboration of the Institut Català de la Vinya i el Vi (IRTA-INCAVI), which is the official body of the Generalitat de Catalunya for the protection of designations of origin (D.O.) of Catalan wines, as well as for their quality assurance and promotion. IRTA-INCAVI has supplied wine samples, with their respective analytics performed using standard methods.

This manuscript is the result of five papers published in international journals and contains five chapters organized as Introduction, Objectives, Experimental, Results and Discussion and Conclusions. In the introduction chapter, the theoretical principles and the state-of-the-art of the ISFETs and amperometric biosensors developed in this Thesis are described. The methods for enzyme immobilization on sensors and in particular those based on polypyrrole polymers are explained. Finally, the implementation of electrochemical sensors in multiparametric systems (electronic tongues) and in flow analytical systems is reviewed.

In the experimental chapter is described in detail the fabrication of all the (bio)sensors and microanalytical flow systems used, the methodology of characterization of them, including the procedure for wine measurements.

Regarding Results and discussion chapter, the different sections describe the specific goals achieved. Firstly, ISFETs were applied for the determination of free and total sulfur dioxide in wine samples. A simple microanalytical flow system based on the separation of the analyte from the sample with a permeable gas diffusion membrane and its indirect detection with a pH-ISFET, was proposed. The validation of the system was carried out using a total of 70 wine samples and two standard methods, the Ripper and the Paul method. This study was performed in the framework of a contract with the private company Biosystems S.A. (Spain).

The good results obtained with this system encouraged us to develop a more compact flow system for the simultaneous determination of free sulfur dioxide and acetic acid. This small-sized microanalytical flow system integrated in only one module the gas-diffusion membrane, the ISFET and the reference electrode, accomplishing the requirements of measurement in a barrel. This system was also evaluated by comparing the results obtained for wine samples with those obtained with the official methods. This study was performed in the framework of a contract with the company Sapere Co. (CA, USA).

On the other hand, the development of amperometric enzymatic biosensors for the determination of L-lactate and L-malate was carried out. They were fabricated by modifying the metal surface of the microelectrodes with polymeric membranes of polypyrrole synthesized electrochemically. These three-dimensional matrices allowed the entrapment of the biochemical reagents involved in the bienzymatic reaction. The amperometric biosensors showed an excellent working stability, retaining more than 90 % of its original sensitivity after 40 days. This allowed their application to monitor the malolactic fermentation of red wines, showing a good agreement with the standard colorimetric method.

Once both amperometric biosensors were optimized, a new silicon-chip was designed and fabricated for simultaneous determination of both parameters. This chip was

assembled in a small-size flow system for on-line analysis of L-lactate and L-malate. Finally, the microanalytical flow system was successfully evaluated with wine samples.

The application of a portable electronic tongue based on microsensors for the analysis of Cava wine was also described. The system contained an array of microsensors formed by six ISFETs sensitive to pH, Na⁺, K⁺, Ca²⁺, Cl⁻ and CO₃²⁻, one conductivity sensor, one redox potential sensor and two amperometric gold microelectrodes. This system, combined with chemometric tools, was applied to the analysis of 78 Cava wine samples, classifying them according to the ageing time (using a Linear Discriminant Analysis) and quantifying the total acidity, pH, volumetric alcoholic degree, potassium, conductivity, glycerol and methanol parameters (using Partial Least Squares regressions).

Summary in Spanish

La monitorización de los procesos alimentarios garantiza la calidad del producto final. Esto es especialmente importante en la industria del vino, y más concretamente en la región mediterránea, donde miles de bodegas y empresas productoras están relacionadas con este sector. Este mercado creciente necesita garantizar los estándares de calidad y la protección del consumidor mediante el seguimiento de varios parámetros a lo largo de los procesos de elaboración del vino. La aplicación de los (bio)sensores electroquímicos es prometedora debido a su simplicidad, respuesta rápida, miniaturización a bajo coste y su fácil implementación para la detección in situ. Además, los biosensores son una buena alternativa a los tediosos métodos tradicionales aplicados en laboratorios especializados.

En esta tesis se presenta el desarrollo de (bio)sensores electroquímicos fabricados con tecnología microelectrónica y su implementación en sistemas de flujo fabricados con técnicas de prototipado rápido, para la monitorización de parámetros químicos de interés en la industria vinícola. Como (bio)sensores electroquímicos se han utilizado Transistores de Efecto Campo Sensibles a Iones (ISFETs), microelectrodos de platino y oro como metal electroactivo y biosensores bienzimáticos amperométricos.

Este trabajo ha sido realizado con la colaboración del Instituto Catalán de la Vinya y el Vi (IRTA-INCAVI), órgano oficial de la Generalitat de Catalunya para la protección de las denominaciones de origen (DO) de los vinos catalanes, así como para el aseguramiento y promoción de su calidad. IRTA-INCAVI ha suministrado muestras de vino, con sus respectivas analíticas realizadas utilizando métodos estándar.

Esta Tesis es el resultado de cinco artículos publicados en revistas internacionales y contiene cinco capítulos organizados en Introducción, Objetivos, Experimental, Resultados y Discusión y Conclusiones. En el capítulo de Introducción se describen los principios teóricos y el estado del arte de los ISFETs y biosensores amperométricos desarrollados en esta Tesis. Se explican los métodos para la inmovilización de enzimas en sensores y en particular los basados en polímeros de polipirrol. Finalmente, se revisa la implementación de sensores electroquímicos en sistemas multiparamétricos (lenguas electrónicos) y en sistemas analíticos de flujo.

En el capítulo de Experimental se describe en detalle la fabricación de todos los (bio)sensores y sistemas de flujo microanalíticos utilizados, la metodología de caracterización de los mismos, incluyendo el procedimiento para las mediciones del vino.

En el capítulo de Resultados y Discusión, las diferentes secciones describen los objetivos específicos alcanzados. En primer lugar, se aplicaron ISFETs para la determinación de dióxido de azufre libre y total en muestras de vino. Se propuso un sistema de flujo microanalítico sencillo basado en la separación del analito de la muestra con una membrana de difusión permeable a gases y su posterior detección indirecta con un ISFET de pH. La validación del sistema se llevó a cabo utilizando un total de 70 muestras de vino y dos métodos estándar, el de Ripper y el de Paul. Este estudio se realizó en el marco de un contrato con la empresa privada Biosystems S.A. (España).

Los buenos resultados obtenidos con este sistema nos animaron a desarrollar un sistema de flujo más compacto para la determinación simultánea de dióxido de azufre libre y ácido acético. Este sistema de flujo microanalítico de pequeño tamaño permitió integrar en un solo módulo la membrana de difusión de gas, el ISFET y el electrodo de referencia, cumpliendo los requisitos de medición en barricas. Este sistema también se evaluó comparando los resultados obtenidos para las muestras de vino con los obtenidos con los métodos oficiales. Este estudio se realizó en el marco de un contrato con la empresa Sapere Co. (CA, EE.UU.).

Por otro lado, se realizó el desarrollo de biosensores enzimáticos amperométricos para la determinación de L-lactato y L-malato. Se fabricaron modificando la superficie metálica de los microelectrodos con membranas poliméricas de polypirrol sintetizadas electroquímicamente. Estas matrices tridimensionales permitieron el atrapamiento de los reactivos bioquímicos implicados en la reacción bienzimática. Los biosensores amperométricos mostraron una excelente estabilidad de trabajo, conservando más del 90% de su sensibilidad original después de 40 días. Esto permitió su aplicación para monitorizar la fermentación maloláctica de los vinos tintos, mostrando resultados análogos a los obtenidos con el método colorimétrico estándar.

Una vez que se optimizaron ambos biosensores amperométricos, se diseñó y fabricó un nuevo chip de silicio para la determinación simultánea de ambos parámetros. Este chip fue montado en un sistema de flujo de pequeño tamaño para el análisis en línea de L-lactato y L-malato. Finalmente, el sistema de flujo microanalítico fue evaluado con éxito con muestras de vino.

También se describió la aplicación de una lengua electrónica portátil basada en microsensores para el análisis de Cava. El sistema contenía una serie de microsensores formados por seis ISFETs sensibles al pH, Na⁺, K⁺, Ca²⁺, Cl⁻ y CO₃²⁻, un sensor de conductividad, un sensor de potencial redox y dos microelectrodos amperométricos de oro. Este sistema, combinado con herramientas de análisis quimiométricas, se aplicó al análisis de 78 muestras de Cava, clasificándolas según el tiempo de envejecimiento (utilizando un Análisis Discriminante Lineal) y cuantificando la acidez total, el pH, el grado alcohólico volumétrico, el potasio, la conductividad, el glicerol y el metanol (utilizando regresiones de mínimos cuadrados parciales).

Chapter 1: General Introduction

Today's wine industry is facing a dynamic global market. The monitoring of several chemical parameters involved in the different steps of the winemaking process allows guaranteeing the quality of the final product. For example, the control of the SO₂ concentration during the ageing of the wine is quite important because works as preservative, but it is toxic in excess. The acetic acid concentration has to be also strongly controlled during this process because is related to the flavor and the aroma of the wine. Other important process in the winemaking of red wines is the malolactic fermentation (MLF), in which the L-malic acid is converted to L-lactic and other volatile acids. The monitoring of both acids (L-malic and L-lactic) along the different days of the MLF process is related to the sourness, the taste and the color of the final wine. Traditional methods applied in the winemaking industry are carried out off-line in laboratories with complex equipment. Therefore, they are tedious, time-consuming and requires costly infrastructure. Off-line measurements have the inconvenience that it is not possible to apply corrective actions on time. This makes portable microanalytical flow systems for real-time monitoring of these parameters quite attractive for the winemaking industry.

This thesis is focused on the development of several electrochemical (bio)sensors and microanalytical flow systems for the analysis of several parameters of interest in the wine industry. To this aim, the combination of the advantages of the microelectronic technology for sensors fabrication and the fast-prototyping techniques for fluidic systems is proposed. Next sections offer a general view of the sensors and fluidic technologies used in this work.

1.1 Electrochemical sensors and biosensors

Chemical sensors are one of the most promising areas in analytical chemical research due to their advantages over conventional analytical methods. They provide a fast response, are easy to use and can be applied in field. They also can be implemented in more compact portable devices and are cheaper. They can be applied in fields as diverse as clinical diagnosis, food monitoring or environmental control. As it is defined by the International Union of Pure and Applied Chemistry (IUPAC), a chemical sensor is a device which transforms chemical information from an analyte between multiple analytes present in the same sample matrix into an analytical useful signal. It consists on a recognition element

which interacts with the analyte providing the selectivity to the sensor and a transducer that converts the signal to an analytical signal (Figure 1.1) [1]

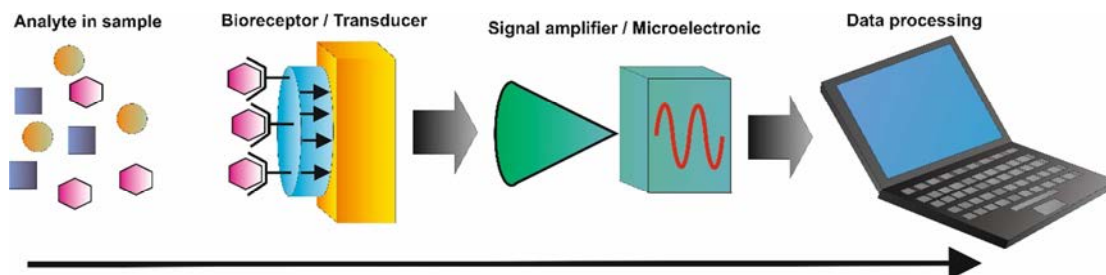


Figure 1.1 Scheme of a chemical (bio)sensor function.

Depending on the operating principle of the transducer, the chemical sensors can be classified in optical, transforming the recognition element change into an optical phenomenon; electrochemical, transforming the electrochemical interaction analyte-electrode into an electrical signal; mass sensitive, measuring a mass change due to the accumulation of the analyte/product of reaction, magnetic, based on the change of paramagnetic properties of an analyte; thermometric, measuring the heat changes of the chemical reaction involving the analyte and others based on physical properties, such as X , β or Γ radiation. Sensors are called biosensors when biological material (enzymes, antibodies, DNA, cells) is immobilized on or is in contact with the transducer.

Electrochemical sensors have among chemical sensors the possibility to miniaturize the instrumentation hence to have portable devices [2]. Electrochemical sensors can be classified depending on the type of transduction phenomena in potentiometric, voltamperometric or impedimetric sensors. This kind of biosensors will be dealt in this work.

1.1.1 Potentiometric sensors

Potentiometric sensors are based on the potential gap between a working electrode (WE) and a reference electrode (RE), at zero current [3]. This potential is related to the activity of the analyte in the solution, which is considered an effective concentration, in contact with the electrode surface. This relation is described by the Nernst equation (Equation 1.1)

$$E = E^0 + \left(\frac{RT}{z_M n F} \right) \ln(a_{M^{n+}}) \quad \text{(Equation 1.1)}$$

Where E is the potential of the electrode in the surface/solution interphase, E^0 is the standard potential of the electrode, R is the gas constant ($8.314 \text{ J K}^{-1} \text{ mol}^{-1}$), T is the absolute temperature in Kelvin (K), F is the Faraday constant ($9.6485 \times 10^4 \text{ C mol}^{-1}$), $z_M n$ is the charge of the ion, and $a_{M^{n+}}$ is the ion activity in solution.

The majority of potentiometric sensors are ion-selective-electrodes (ISEs) [4]. The selectivity to ions of these sensors is due to a membrane that contains a specie that reacts reversibly and selectively with the ion analyte, namely recognition element. The difference of voltage generated at the membrane-solution interphase is theoretically dependent on the logarithm of the ion activity, as described by the Nernst Equation.

1.1.1.1 Ion-Sensitive Field Effect Transistors (ISFETs)

Ion-Sensitive Field Effect Transistors (ISFETs) are considered a special type of potentiometric sensors since their response is following an approximation of the Nernst equation [5].

ISFETs have a similar structure of a Metal-Insulator-Semiconductor Field Effect Transistor (MISFET) [6]. This is formed by a p-Si substrate with two zones (source and drain) doped with n-type semiconductor and separated by a p-type channel (Figure 1.2). The gate of the MISFET is formed by the p-type channel, a dielectric layer and a metal electrode. When the gate insulator is formed by a thin layer of thermally growth silicon oxide is called MOSFET and when it is a double layer of silicon oxide/silicon nitride is called MNOSFET.

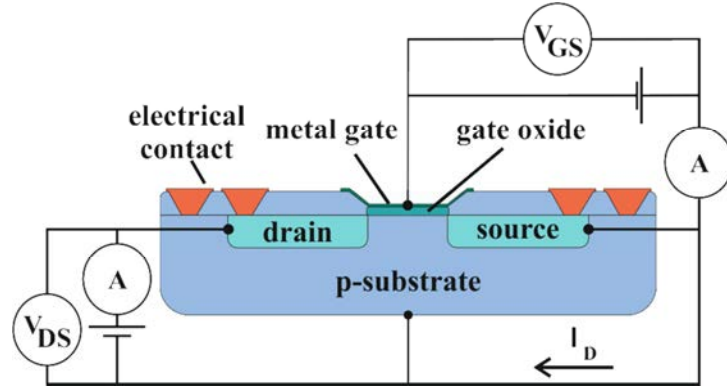


Figure 1.2 General structure and polarization scheme of a MISFET.

The MISFET behavior is based on the field effect, which is an electrical field between the drain and the source (V_{DS}) created when a perpendicular potential is applied in the metal gate (V_{GS}). This potential has associated a drain current (I_D) between the drain and the source. The general equation that relates all these parameters and the characteristics of the gate materials for a specific case of V_{DS} value is expressed in Equation 1.2:

$$I_D = \bar{\mu}_n C_{OX} \frac{W}{L} \left[(V_{GS} - V_{th}) V_{DS} - \frac{V_{DS}^2}{2} \right] \text{ for } V_{GS} - V_{th} \geq V_{DS} \quad \text{(Equation 1.2)}$$

Where V_{th} is the threshold voltage or the minimum gate voltage to achieve the electrical field between the drain and the source; $\bar{\mu}_n$ is the surface mobility of the electron; W is width of the channel; L is the length of the channel; and C_{OX} is the capacitance of gate insulator per unit area.

In the case of an ISFET, the metal gate of a MISFET is removed and it is substituted by an electrolyte and a RE. Then the dielectric layer (typically oxide layers) is in direct contact with the liquid media and the interaction between them causes an electrical double layer and consequently an electrochemical potential drop depending on the solution composition in a similar way that happens in a glass electrode [7]. This potential drop is recorded by the RE (Figure 1.3).

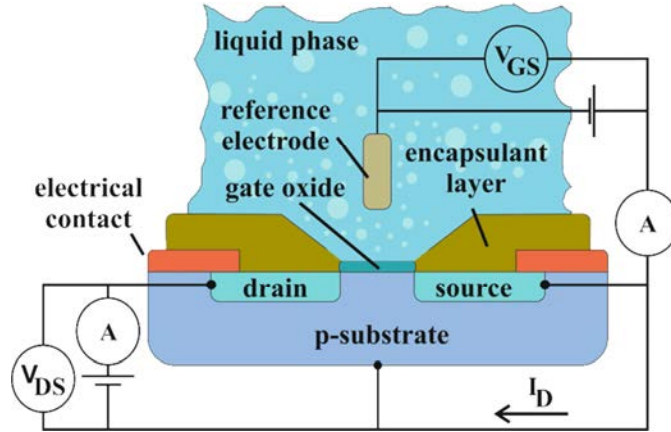


Figure 1.3 General structure and polarization scheme of an ISFET.

The difference of potential caused by electrochemical interactions between the gate dielectric and the solution depends on the material properties of the dielectric and the composition of the solution, particularly on its pH value. This dependence can be expressed by an Equation 1.3, similar to the Nernst equation.

$$\Psi_0 = 2.303 \frac{KT}{q} \frac{\beta}{\beta+1} (pH_{pzc} - pH) \quad \text{(Equation 1.3)}$$

Where Ψ_0 is the surface electrode potential; K is the Boltzmann constant ($1.38064852 \times 10^{-23} \text{ m}^2 \text{ kg s}^{-2} \text{ K}^{-1}$); T is the absolute temperature in Kelvin (K); q is the charge density; pH_{pzc} is the pH reference value at which the surface charge and the potential are equal to zero; β is a constant depending on the reactive capacity of active sites of the dielectric material.

The value of β depends of the nature of the inorganic oxides (sensitive to the H^+ ions) deposited in the gate of the ISFET (SiO_2 , SiN_4 , Al_2O_3 , Ta_2O_5). At high values of β the pH response is equal to Nernstian.

The main advantages of ISFETs over ISEs are their smaller size, their solid-state nature, the possibility of their mass-fabrication, the short response time and the low output impedance. These advantages can be exploited for applications such as environmental monitoring, clinical analysis and control of industrial processes, mainly in the food

industry. For in situ or on-line measurements, ISFETs become competitive due to their small size and robustness. Some works have been reported using pH-ISFETs for different applications, such as the measurement of ammonia in water [8], in-situ monitoring of marine environment [9], the pH of drain droplets [10], the detection of microorganisms in water [11] and the bacterial activity [12]. Besides biomedical applications [13] have been described like gynecologic control [14], intraluminal monitoring [15], monitoring of the DNA hybridization [16], health control [17] or pH monitoring of urine [18].

1.1.1.2 ISFETs with ion selective membranes (ChemFETs)

In the same way as an ISE, the gate of the ISFET can be modified with membranes selective to an ion of interest in the sample [19, 20]. The main components forming the membrane are the ionophore, the plasticizer and the polymeric matrix. The ionophore is the recognition element and has to be stable and highly soluble in the plasticizer; the plasticizer retains and dissolves the ionophore (it is also called the dissolvent); and the polymeric matrix allows the entrapment of these elements in a three-dimensional membrane. The first polymeric material used as membrane was the polyvinyl chloride (PVC), which entrapped all the materials of the selective sensor maintaining good mechanical properties (homogeneity, flexibility and stability). Nevertheless, PVC has a very poor adherence to the dielectric gate of ISFETs, therefore new strategies were proposed to solve this problem. Some alternatives, such as the chemical modification of the ISFET gate and covalent attachment of the PVC membrane [21] or the use of modified PVC [22] were proposed, the use of photocurable polymers by means of UV light attached to the silanized ISFET gate was the strategy most accepted [23, 24]. Apart from the good adherence of these membranes, these can be patterned onto the ISFET by photolithographic methods, thus being compatible with the microelectronic technology. Among several types of photocurable polymers membranes, acrylate polyurethanes family was developed by the researchers of the Grupo de Transductores Químicos (GTQ) at the Instituto de Microelectrónica de Barcelona (IMB-CNM) [25, 26], Others polymers such as polysiloxanes [27] and polymethacrylates [22] have been also proposed.

The polymeric matrix proposed by the GTQ is formed by an acrylate oligomer with high reactivity and low volatility, a cross linker agent with a reactive diluent used to

increase the UV-cure rate, maintaining the selectivity and increasing the sensitivity of the electrode and a photoinitiator that allows the radical-polymerization. The ion-selective membrane is completed by adding the ionophore, the plasticizer and, in some formulations, a lipophilic salt. This last component is used to reduce the response time, the electric resistance and the barrier at the membrane/solution interface.

The behavior of ISFETs with ion selective membrane is based on the not-polarized interface between the membrane and the solution. The Nernstian potential (E) through the interface, due to the equilibrium of the ion to determine between the solution and the surface of the membrane, is recorded, following the Equation 1.4.

$$E = E^0 + \frac{RT}{z_i F} (\ln a_i) \quad \text{(Equation 1.4)}$$

Where E is the potential of the electrode in the surface/solution membrane; E^0 is the standard potential of the electrode; R is the gas constant ($8.314 \text{ J K}^{-1} \text{ mol}^{-1}$); T is the absolute temperature in kelvin (K); F is the Faraday constant ($9.6485 \times 10^4 \text{ C mol}^{-1}$); z_i is charge of the ion; and a_i is the ion activity in solution.

Regarding the applications of modified ISFETs with membranes selective to ions, many works have been reported in the literature. Water monitoring [28], acid rain monitoring [29], soil samples measuring [30], water analysis [31-34], biomedical control [35], sensors for anionic surfactants [36] or pesticides detection [37] are some of these applications.

1.1.2 Amperometric enzymatic biosensors

The first amperometric enzymatic biosensor was described by Updike and Hicks in 1967 [38]. Their functioning is based on the current measurement resulted from the redox process of an electroactive specie in a bio-chemical reaction [39]. The current density is proportional to the electroactive specie concentration in the sample solution, as it is described by the Faraday's law. This specie is reduced or oxidized on the surface of the electrode depending on its nature and the applied potential. The reaction of the transfer rate

of the redox specie is defined considering the electrochemical reaction $Ox + ne^- \rightarrow Red$ and the first Faraday's law (Equation 1.5)

$$i = \frac{dQ}{dt}$$

$$N = \frac{Q}{nF} \quad \text{(Equation 1.5)}$$

$$v = \frac{dN}{dt} = \frac{i}{nF}$$

Where i is the current (A); Q is the charge (C); t is the time (s); n is the number of electrons consumed by the redox reaction; F is the Faraday constant ($9.6485 \times 10^4 \text{ C mol}^{-1}$); N is de number of electrolyzed moles; v is the transfer rate (mol s^{-1}).

The most common techniques of determination are amperometry and cyclic voltammetry depending on if the current is measured at a constant potential or during controlled variations of the potential, respectively. Cyclic voltammetry is one of the most used techniques for the study of redox processes. As is shown in Figure 1.4, the method is based on a linear sweep potential from E_i (initial potential) to E_λ (reversal potential), followed by a reverse linear sweep potential till E_f (final potential). The current passing through the electrode immersed in a solution without stirring is recorded along the sweep potential to obtain a cyclic voltammogram (Figure 1.5). When the difference between E_{pa} (potential in which the specie is oxidized) and E_{pc} (potential in which the specie is reduced) is lower than $35 \text{ n}^{-1} \text{ mV}$, the redox system is reversible and the plot potential versus current is very similar during the direct and the reverse sweep.

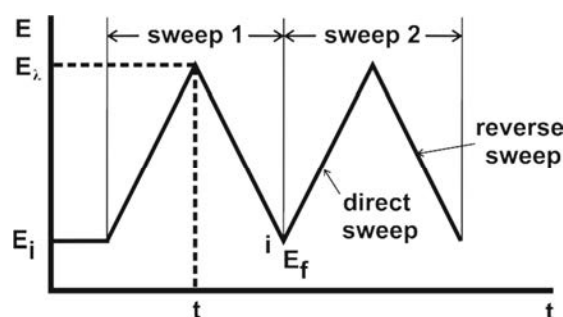


Figure 1.4 Scheme of the profile of E vs time for a cyclic voltammetry

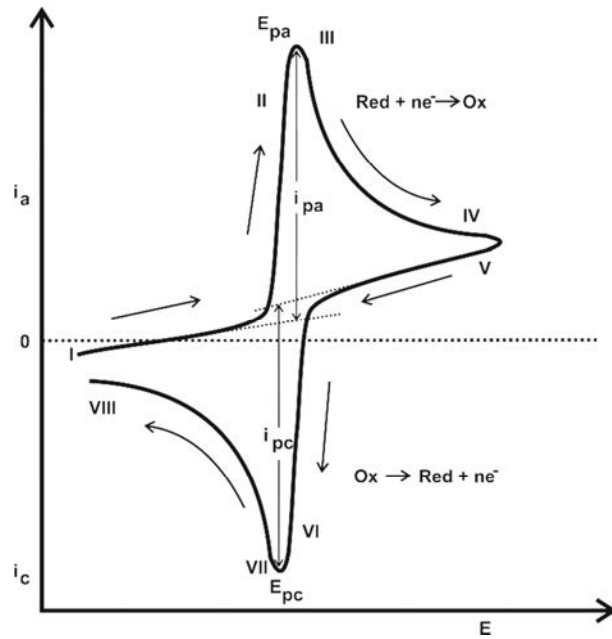


Figure 1.5. Typical cyclic voltammogram for an electrochemical specie. Narrows indicate the direction of the sweep.

The most interesting parameters obtained from the cyclic voltammetry are the peak currents (i_{pc} and i_{pa}), the ratio i_{pa}/i_{pc} and the potential difference between the peak in which the specie is oxidized and the peak in which the specie is reduced ($E_{pa}-E_{pc}$). The potential difference between peaks for a reversible system and a stable electrochemical reaction is defined by Equation 1.6.

$$\Delta E_p = E_{pa} - E_{pc} \approx \frac{59}{n} mV \quad \text{Equation 1.6}$$

Where E_{pa} and E_{pc} are the anodic and the cathodic potential peak, respectively (in mV); and n is the number of electrons consumed by the redox reaction. The average potential between the potential peaks is defined as standard potential, E° (Equation 1.7).

$$E^\circ = \frac{E_{pa} + E_{pc}}{2} \quad \text{Equation 1.7}$$

For a reversible system i_{pa} and i_{pc} values are the same, therefore $i_{pa}/i_{pc} \approx 1$ regardless the sweep potential rate and the coefficients of diffusion.

Regarding the chronoamperometric technique, it records the current generated at the electrode as a function of time when a potential step is applied to the electrode (Figure 1.6). If a reduction reaction is present, the step from the initial potential (E_i , in which there is not current related to redox process) to the final potential (E_s , in which all the oxidized specie on the surface of the electrode is reduced) causes a high current due to the reduction of the chemical specie. Resulting from this crossing current, a net flow of the oxidized specie to the electrode surface (proportional to the concentration gradient on the surface of the electrode) appears. The evolution with the time of the current value follows the Cottrell's equation (Equation 1.8).

$$i(t) = i_d(t) = \frac{nFAD_{Ox}^{1/2}C_{Ox}^*}{\pi^{1/2}t^{1/2}} \quad \text{Equation 1.8}$$

Where i is the current (A); t is the time (s); n is the number of electrons consumed by the redox reaction; F is the Faraday constant ($9.6485 \times 10^4 \text{ C mol}^{-1}$); A is the electrode area (cm^2); C_{Ox}^* is the concentration of the oxidized specie in the electrode surface (mol cm^{-3}); D_{Ox} is the coefficient of diffusion ($\text{cm}^2 \text{ s}^{-1}$).

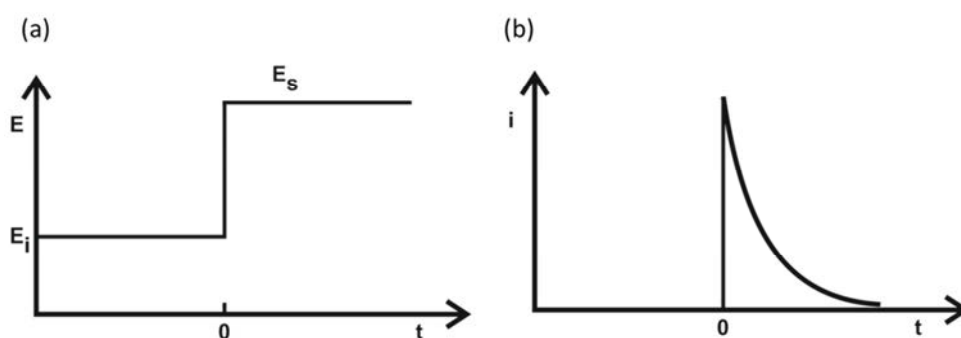
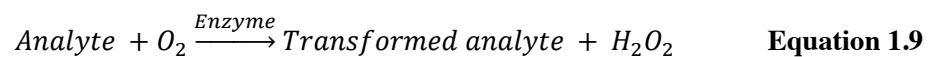


Figure 1.6 Profiles of the excitation signal evolution with time for a chronoamperometric test; (a) Potential drop; (b) Current response

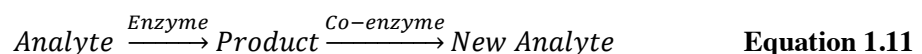
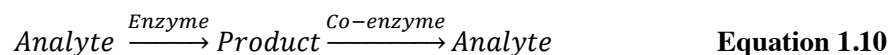
The chronoamperometric technique is the most used for electrochemical biosensors, in which the biological material is deposited on top of the electrode to be intimately connected to the transducer. The use of biosensors has important advantages over conventional methods for molecules detection, such as the use of low reagent and

biological compound volumes, low limits of detection, easy manufacturing and low cost of the control instrumentation.

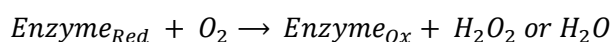
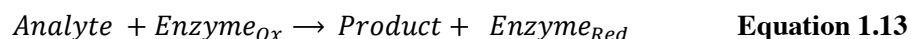
The two most common biological elements used for the fabrication of biosensors are the enzymes [37, 38] and the immuno compounds (antibodies and antigens) [40]. These bio-receptors are highly selective to specific analytes. Particularly enzymes allow the catalysis of chemical reactions implying a substrate that usually is the analyte of interest, improving the selectivity and the time of response [41]. The enzymes are classified in several groups depending on the catalyzed reaction: oxidoreductases catalyzing oxide-reduction reactions; transferases catalyzing the transfer of a chemical group from one to another substrate; hydrolases catalyzing hydrolysis reactions; lyases cleaving bonds by elimination, leaving double bonds or rings or adding group to double bonds; isomerases catalyzing geometric or structural changes within one molecule; and ligases catalyzing the joining together of two molecules coupled with the hydrolysis of a diphosphate bond in ATP or similar triphosphate. The simplest catalytic reaction is shown in Equation 1.9. In this, the enzyme catalyzes a chemical reaction in which the substrate (analyte) is transformed in the presence of other chemical reagent as co-factor (O_2 in this case).



Two or more enzymes can be used for improving the biosensor capacity/performance. By using other enzyme (co-enzyme), the sensitivity of the biosensor can be improved thanks to the regeneration of the analyte (Equation 1.10). The use of co-enzymes allows also obtaining new products more easily detectable for the transducer (Equation 1.11) or removing interferences (Equation 1.12) [42].



For the fabrication of amperometric biosensors, the most interesting enzymes are the oxidases, the peroxidases and the dehydrogenases. Regarding the oxidases enzymes, they have a strongly attached co-factor inside the enzymatic structure. The oxygen is the re-oxidant agent and the final product is hydrogen peroxide or water, depending on the donor capacity of the enzyme (Equation 1.13).



The electrochemical oxidation (or reduction) of the hydrogen peroxide or the oxygen on the transducer surface can be related to the concentration of the analyte in the solution. Nevertheless, these processes have important drawbacks because high overpotentials have to be applied for oxidizing the hydrogen peroxide, giving rise to the oxidation of other species in the solution that can interfere the response of the biosensor [43, 44]. This drawback could be solved if a direct electronic transfer between the enzyme and the electrode is used [45], because lower overpotentials had to be applied for obtaining the biosensor response. As the active centers of the enzymes are very inaccessible, the use of redox mediators allows reducing the working potential because the concentration of the analyte in the solution can be related to the electrochemical faradic current of their redox process (Figure 1.7). In addition, if for the oxidation of the reduced mediator the protons are not involved, the electrochemical response of the biosensor does not depend on the pH of the solution. In summary, the ideal mediator should be able to react rapidly with the oxidized/reduced enzyme without reversible heterogeneous kinetics, the potential for the regeneration of its oxidized/reduced form should be low and pH independent, the oxidized/reduced forms should be stable and the reduced form should not react with oxygen [46]. Several redox mediators for the fabrication of amperometric biosensors based on oxidases have been widely used, such as tetrathiafulvalene (TTF), Meldola's Blue, ferrocene or others [47-49].

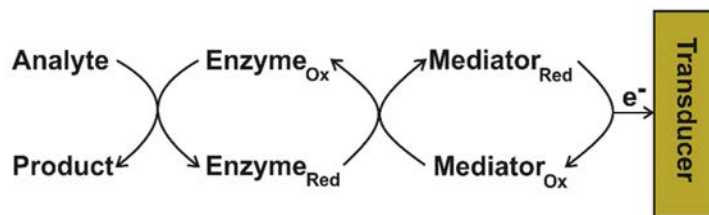
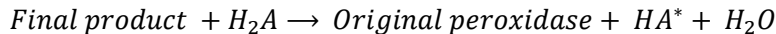
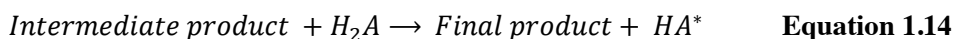
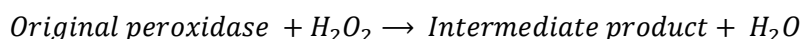


Figure 1.7 Scheme of an enzymatic reaction with a redox mediator.

Peroxidases are enzymes often used for the determination of hydrogen peroxide and small organic peroxides. The reaction with the hydrogen peroxide is shown in the Equation 1.14. The original peroxidase is oxidized to intermediate product in presence of the hydrogen peroxide. Then, the intermediate product is oxidized to the final product, which is reduced in a final step, recovering the original peroxidase. Phenolics compounds, hexacyanoferrates, ascorbate or others are used as electron donor species [50].



Horseshoe peroxidase (HRP) is the most studied peroxidase as biological catalyst in the development of enzyme-based amperometric biosensors. It is a redox hemoglycoprotein with the active site in the sixth coordination position of Fe(III) in the Fe(III) protoporphyrin IX prosthetic group [51]. In this case, the HRP [Fe(III)] is oxidized by hydrogen peroxide to form water and an oxidized form of HRP, denoted HRP I. The reduction of HRP I back into the HRP [Fe(III)] occurs in two separate one-electron steps. The complete process is depicted in the Figure 1.8 [51]. For an ideal biosensor, the enzyme regeneration must take place at the electrode surface with a fast electron transfer between electrodes and metalloproteins. In order to achieve it, many electrochemical studies of small-molecule electrode-active mediators have been carried out [52]. The analytical system follows the reaction scheme described previously in Figure 1.7. In its last step, the redox mediator is re-reduced on the transducer surface and the faradaic current associated to this process is stoichiometrically related to the amount of hydrogen peroxidase in the medium. The hydrogen peroxidase determination is important in fields as diverse as the

cosmetic, environmental or food industry, therefore a large number of amperometric biosensors based on HRP have been described [53-55]. The use of HRP combined with other oxidase enzyme (bienzymatic biosensors) is quite extended (Figure 1.8) and allows the determination of interesting analytes at lower potentials that the required for the direct detection of hydrogen peroxidase [56-58].

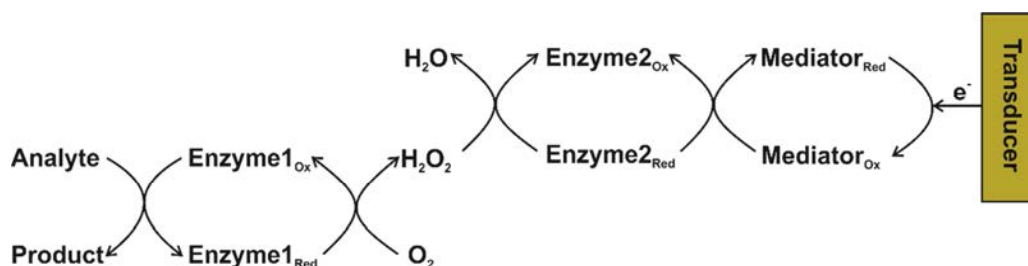


Figure 1.8 Schematic representation of an amperometric biosensor involving the use of two enzymes and a redox mediator (bienzymatic biosensor).

The group of dehydrogenase enzymes catalyzes the chemical reactions which are not-dependent of the molecular oxygen (Figure 1.9). In this case, the reduced co-factor can recover the enzyme in presence of other acceptor of electrons/protons different from oxygen.

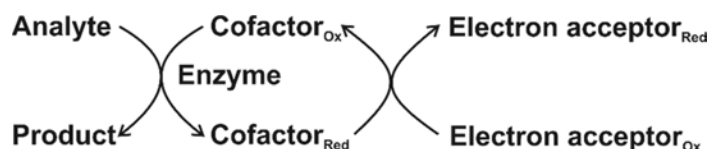


Figure 1.9 Sequence of an oxidation reaction of an amperometric biosensor catalyzed by a dehydrogenase enzyme.

The dehydrogenase enzymes nicotinamide adenine dinucleotide (NAD^+) or nicotinamide adenine dinucleotide phosphate (NADP^+) are the main group of redox enzymes. The electrochemistry of the redox couple NAD^+/NADH has been studied extensively by Gorton [59] (Figure 1.10). The oxidizing capacity of the enzyme is very low, therefore the presence of their equivalent dehydrogenase is necessary (NADH or NADPH). If a second reaction step is coupled (using the NADH or NADPH produced or the reaction product) for stimulating the product formation, the resulting current of the oxidized NADH or NADPH can be stoichiometrically related to the analyte concentration.

Nevertheless, the electrochemical reaction is high irreversible and produce collateral reaction affecting the surface of the transducer [60]. Using a two-electron acceptor as redox mediator or a second enzymatic step in presence of the diaphorase (DP) enzyme allow solving this problem [61].

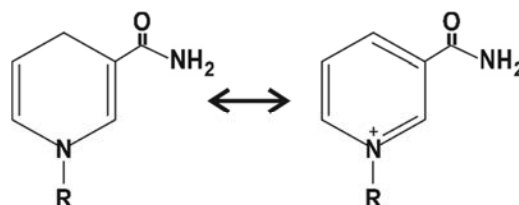


Figure 1.10 Scheme of the redox couple NAD^+/NADH molecule

1.1.2.1 Immobilization strategies of enzymes

One of the most important steps of the fabrication of enzymatic amperometric biosensors is the immobilization of the enzyme on the transducer surface. The immobilization process should be reproducible and offer high stability to achieve efficient biosensors with good analytical performance -working stability, sensitivity, limit of detection, selectivity and fast response-. The biological elements immobilized on the transducer surface should maintain their initial structure and activity for long-times after the immobilization, and they have to be strongly attached to the surface for avoiding their leak from the transducer.

In general, the immobilization of enzymes can be obtained by physical (adsorption, entrapment) or chemical (covalent attachment, cross linking) strategies. The strategies used in this thesis are the physical adsorption (and cross linking), the covalent attachment and the entrapment into electrosynthesized polypyrrole (PPy) membranes (Figure 1.11). Each of these methods has some advantages and drawbacks, therefore its selection depends on the specific application of the biosensor.

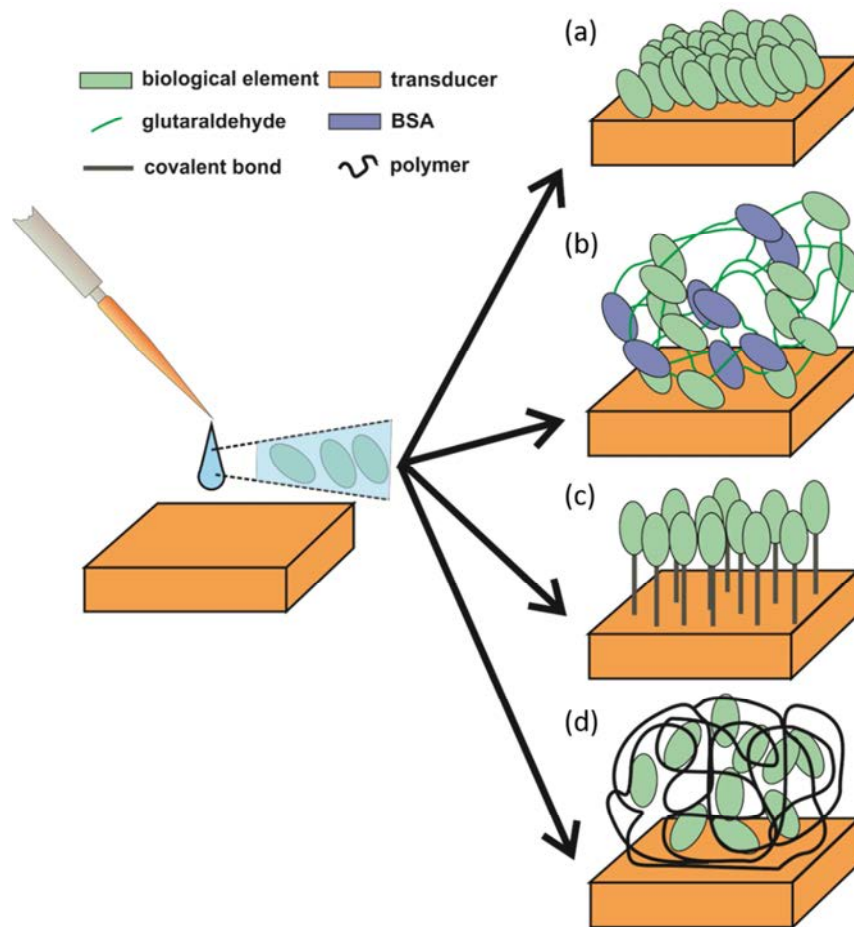


Figure 1.11. Scheme of different strategies for the enzymes immobilization on the transducer surface: (a) physical adsorption; (b) physical adsorption with cross linking; (c) covalent attachment; and (d) entrapment into electro-synthesized polypyrrole membrane.

Physical adsorption is based on the deposition of an enzyme on the surface of the transducer and its attachment through weak bonds (Figure 1.11a). This is a simple, fast and low cost method. The adsorption is based on weak bonds such as electrostatic or hydrophobic interactions, hydrogen bonds or Van Der Waals's bonds. One of the worst drawbacks of this method is the possible attachment of the enzymes on the transducer surface in unfavorable orientation, causing a decrease of its activity. Other drawback is the quick desorption of the enzymes when there are changes in temperature, pH or ionic strength. Therefore, the working-stability of the biosensors based on this immobilization strategy is not quite good. Despite these disadvantages, many amperometric biosensors using this immobilization technique have been described in literature. These biosensors

show a good sensitivity, reproducibility and stability for a few weeks for the determination of analytes as diverse as hydrogen peroxide [62], glucose [63] or lactate [64]. The working stability of the physical adsorbed enzymes can be improved by combining the physical adsorption with the chemical method of cross-linking. For this methodology, the biological elements are cross-linked each to other with some bifunctional agents as glutaraldehyde [65] in presence of functionally inert proteins as bovine serum albumin (BSA) (Figure 1.11b). This method improves the strength of the physical bonds. Nevertheless, the use of cross-linker can cause significant changes in the activity of the enzymes. Many biosensors based on this methodology of immobilization are described in the literature for the determination of glucose [66], ethanol [67] or urea [68], between many other analytes.

Other chemical method of immobilization widely used for biological elements is the covalent attachment. Here, some functional groups of the enzymes, not essential for their activity, are bonded covalently to the surface of the transducer (Figure 1.11c). Previously to the attachment, the surface of the transducer is activated with some multifunctional reagent, including functional groups such as $-SH$, $-CN$, $-COOH$ or $-NH_2$. Then, the functional group of the enzyme (amino, carboxylic, phenolic) is covalently attached to the modified surface of the transducer (Figure 1.12).

The amino group is the most functional target used for the immobilization of enzymes because they are usually on their outer surface and are more accessible for conjugation without denaturing their structure. These groups can be attached to the transducer surface by modifying it with NHS esters, which are reactive groups formed by carboimide-activation of carboxylate molecules (Figure 1.12). Several analytes (lactate, glutamate, etc.) have been detected using this methodology in the last years [69-71]

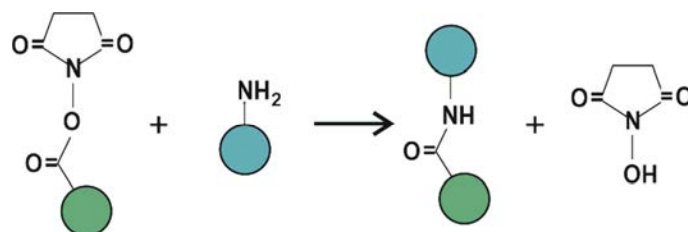


Figure 1.12 Scheme of the chemical conjugation between the NHS ester group and the amine group of a biological element.

The main advantages of the covalent coupling are the strength of the binding (minimizing the leakage of the biological element) and its simplicity. Nevertheless, the chemical modification of the biological element causes its denaturation meaning in a smaller number of enzymes immobilized.

Another strategy for the immobilization of enzymes on the transducer surface is the entrapment. For this method, the biological elements are entrapped inside a three-dimensional polymeric matrix (Figure 1.11d). This method minimizes the loss of the enzymes activity because they are not chemical modifications during the process, improving the working stability of the biosensor. Meanwhile, the enzyme can suffer from leakage into the solution or some mass transfer resistance to the chemical reagents involve in the determination reaction can be observed in some cases.

Although the matrices used for the entrapment of biological elements can be of materials as diverse as polydimethylsiloxane (PDMS) [72], photopolymers [73], silica gel [74], carbon paste [75] or polysaccharides [76], the conducting polymers are one of the most promising materials.

1.1.2.1.1 Entrapment in electrosynthesized polypyrrole membranes

The biosensors fabricated by electrochemical polymerization processes for entrapping the biomolecules in a polymeric matrix allow a controlled immobilization on the transducer surface. The method is based on the application of a potential or current to a solution containing the monomer and the biological elements to be entrapped. The potential or current applied induces the electrochemical oxidation of the monomer. Conducting polymers contain a π -conjugated system alternating single and double bonds in the polymer chain which confer upon them the charge transfer property, making it compatible for integration with redox enzymes and allowing electron transfer to the electrode surface [77]. Besides, the simple anodic oxidation of the monomer at an applied potential allows direct deposition of the polymer on the electrode with the simultaneous entrapment of the enzyme into the matrix with a controlled spatial distribution [78]. However, this immobilization method needs high concentration of the monomer (0.05 - 0.5 M) and the enzymes (0.2 – 3.5 mg L⁻¹) in the electrosynthesis solution. Moreover, the estimation of entrapped enzyme

cannot be calculated directly as the difference between the concentration of enzymes before and after the electropolymerization [79].

Although many conducting polymers, such as polyaniline, polyphenol, polythiophene, polyvinylalcohol, polyvinylsulfonate or polyacrylamide, have been applied to the development of amperometric biosensors [80-84], the PPy has some advantages over them. PPy has a high stable electrical conductivity, is acceptably stable in ambient conditions [85] and can be easily prepared electrochemically from a variety of electrolytes, including aqueous solutions [86]. PPy has a good adherence to the transducer surface, increasing the transducer area due to its ramified polymer membrane. Moreover, the properties of the electrosynthesized PPy membrane can be controlled by changing the conditions applied during the electrochemical polymerization [87]. The simple one-step electrochemical procedure used for the enzyme immobilization also allows preserving the enzyme activity [88]. In addition, the three-dimensional matrix of PPy prevents the leaching out of the entrapped enzymes [89].

Several mechanisms have been proposed for the polymerization of the pyrrole monomer [90], but the most acceptable is that based on the radical cation formation, radical coupling and deprotonation (Figure 1.13). PPy is formed by anodic oxidation of the monomer at specified potentials. When enzyme is present in the monomer solution, the polymerization produces the entrapment of the enzyme within the matrix. This is favored because at the operational pH, which is greater than their isoelectric point, PPy has a positive charge and the enzyme a negative charge, and then an electrostatic interaction is produced between both compounds. The first step produced is the oxidation of the monomer at an electrode potential leading to the generation of extremely reactive π -radical cations (Figure 1.13a). These radical cations can react in a second step with another monomeric radical cation, an oligomeric radical cation or a neutral monomer, to form a dimeric radical cation (Figure 1.13b). The dimeric radical cation may lose a proton to form dimers or oligomers which are predominantly α,α' -coupled (Figure 1.13c). As the dimers and oligomers formed have lower oxidation potentials than the monomer itself, it indicates that formation of PPy involves a nucleation step and polymer formation that leads to chain propagation and finally precipitation of the polycationic polymer on the anode surface

(Figure 1.13d) [77]. This deposition of the conducting polymer on the electrode surface occurs only when the length has surpassed a polymer specific solubility limit [91, 92].

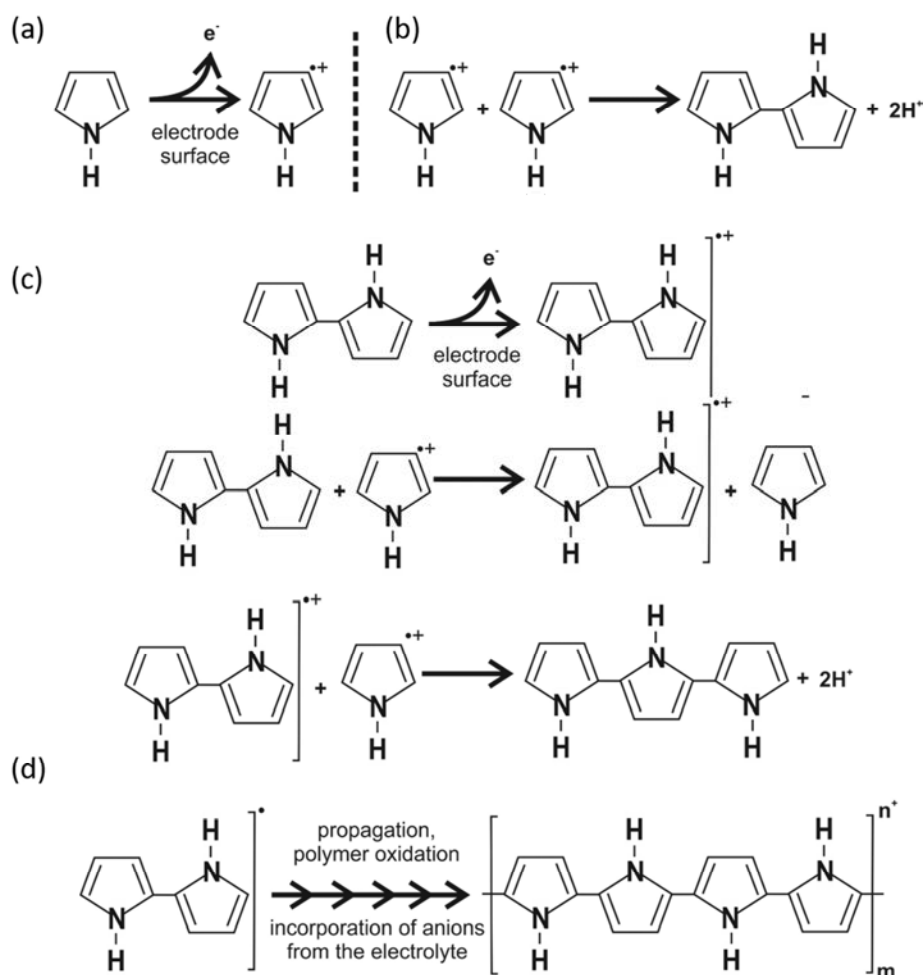


Figure 1.13. Sequence of the polypyrrole electrochemical polymerization: (a) oxidation of the monomer and formation of reactive π -radical cations; (b) formation of the dimeric radical cation; (c) formation of oligomers α, α' -coupled; (d) nucleation, propagation and precipitation of the polypyrrole

There are many factors influencing the electrochemical synthesis of PPy [93] such as the electrolyte, the temperature, the electrode material or the selected electrochemical technique [94]. The major limitations of electrochemical synthesis of electroconducting polymers on numerous metals are the relatively high potentials required for monomer oxidation. At these potentials, most metals are dissolved (i.e. iron, steel, copper) or form nonconductive passive layers (i.e. aluminum and its alloys). For that reason, the

electrochemical synthesis should be performed on inert metal electrodes, such as platinum, gold, graphite, glassy carbon or indium tin oxide (ITO) glass [95-97].

Some properties of electrosynthesized PPy are dependent on the applied electrochemical technique [98]. Generally, electrochemical techniques used for synthesis of PPy are galvanometry, potentiometry or cyclic voltammetry. Galvanostatic technique allows the generation of polypyrrole at a constant rate (current density). The PPy film, obtained at the end of the polymerization is in its doped and conductive form [99]. Besides, this technique allows controlling the thickness of PPy film by adjusting the duration of the polymerization process or the accumulated charge during the process. Potentiostatic polymerization technique is referred to the application of a constant positive (for oxidative polymerization) potential. It is necessary to choose the potential high enough for getting polymerization, but low enough to avoid undesired secondary reactions and over oxidation of the polymer [100]. In this case, the obtained polymer is also in doped state. During the application of cyclic voltammetry technique for the electrochemical polymerization, the transducer is subjected to cyclic regular change of the potential during which electroconducting polymer changes between its conducting and not conducting form [99]. Electrochemical synthesis of PPy is performed in a three-electrode cell, although galvanostatic synthesis can be performed in a two electrode system [98]. In a three-electrode electrochemical cell, the WE operates as anode and on its surface, the deposition of the PPy is carried out. Reduction of solvent, dissolved oxygen or other compounds of the electrolyte occurs at the CE, while RE controls the potential.

The composition of the solution used for the electrochemical synthesis of polymer involves the monomer, the solvent and the acid which serves as source of dopant ions or counter ions [101]. The solvent should be able to dissolve the monomer and should be stable at the potential applied during the electrosynthesis. Most of the electrochemical syntheses of conducting polymers are carried out in aqueous solutions because they are cheap, easy handling and friendly-environment. However, various organic solvents are also used (acetonitrile, dichloromethane, propylene carbonate) [98]. Dopant or counter ions are incorporated into the polymer structure during its electrosynthesis for compensating positive charge on anode. Their presence and properties affect the morphology,

conductivity, electrochemical activity and the polymerization process [98], therefore they have to be chemically and electrochemically stable. Temperature has also impact on electrochemical synthesis of electroconducting polymers because the free radicals obtained in the anodic process react with oxygen in a reaction high-sensitive to temperature; therefore the increase in temperature decrease the polymerization efficiency [98].

Many amperometric biosensors using this immobilization strategy have been reported for glucose [102], hydrogen peroxide [103], nitrate [104], levetiracetam [105], glutamate [106], tyramine [107], cholesterol [108] or urea [109].

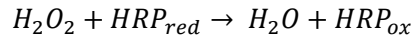
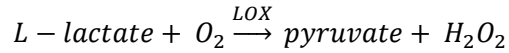
1.1.2.2 L-lactate amperometric biosensors

The determination of lactate is very important for the clinical diagnostics for assessing patient health conditions and studying of diseases [110]. The monitoring of lactate is also important in sports medicine [111], because the lactate concentration in blood changes depending on the human activity. This concentration is around 1 mM under rest conditions [112], 12 mM during normal training and 25 mM during intense activity [113]. For clinical care, the control of lactate levels in blood plasma is very useful in order to make a comparison between the produced and the consumed lactate. Unusual amounts of lactate can notify the presence of some medical anomaly, such as hemorrhagic shock or pulmonary embolism [114].

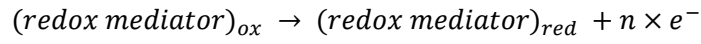
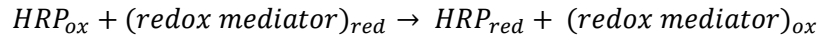
The lactate concentration has also a big relevance in the food industry [115-117]. In this field, the lactate is related to many fermentation processes, in different industries such as milk, vegetables, fruits, orange juices or wines. The amount of lactate is intensely connected to the freshness or quality of the final product [118]. In the winemaking industry, the L-lactic acid concentration is related to the quality of the final product [119]. It is produced mainly in the malolactic fermentation (MLF), in which the transformation of the L-malic acid into L-lactic acid and CO₂ takes place.

Analytical methods, such as high performance liquid chromatography (HPLC) [120], fluorometry [121], magnetic resonance spectroscopy [122] or colorimetry [123], are the most applied for lactate determination. Although these methods are precise and reliable,

they are time consuming and use costly equipment. However, amperometric biosensors are a good alternative to these conventional methods. They are easy to use, can be applied in field, and provide rapid response with high specificity, low-cost and user-friendly [124]. Among them, amperometric biosensors based on redox reactions catalyzed by oxidoreductase enzymes have been of widespread use [125]. These enzymes show additional advantages like their natural origin and no toxicity, high specificity and stability under moderate working conditions of pH and temperature. One of the most common strategies for the L-lactate determination makes use of L-lactate dehydrogenase (LDH) in presence of NAD^+/NADH as co-enzyme [126]. However, the derived biosensor devices show several drawbacks related to the necessity of incorporating the NAD^+ cofactor, which in turn requires the implementation of a potential step once the sensor response is recorded in order to regenerate it. This step is carried out at relatively high potentials (above 300 mV), and this can cause interferences of other electroactive species present in the samples. Another alternative is the use of lactate oxidase (LOX) as recognition element. This enzyme catalyzes the L-lactate oxidation to produce pyruvate and hydrogen peroxide in the presence of dissolved oxygen. The hydrogen peroxide can then be reduced and the resulting cathodic current is stoichiometrically related to the L-lactate concentration in the sample. Here, the main drawback is that a high overpotential for the direct detection of H_2O_2 is needed and this again can cause interferences of other oxidable species present in the samples. In order to circumvent this difficulty, a LOX based biosensor comprising an electrochemical dissolved oxygen sensor has been reported [127]. Other more widespread strategies are based on the incorporation of a second enzyme, namely horseradish peroxidase (HRP) that catalyzes the reduction of H_2O_2 to H_2O in the presence of a suitable redox mediator that is concomitantly oxidized [128-130]. The determination of L-lactate is based on the oxidation of the L-lactate to pyruvate and H_2O_2 in presence of LOX. Then, the hydrogen peroxide is reduced in presence of HRP and the HRP is regenerated thanks to a reduced redox mediator, which is oxidized. This is again reduced back by applying an adequate potential and the recorded faradaic current is stoichiometrically related to the L-lactate concentration in the sample (Equation 1.15).



Equation 1.15



Detection of these oxidized species takes place at low enough potentials to avoid any possible interference from the sample. Moreover, the resulting biosensor shows enhanced sensitivity thanks to the application of the LOX /HRP cascade enzyme reaction [46].

The chosen immobilization procedure should be studied in detail and optimized in order to maximize the working stability over time. As has been explained above, the enzyme entrapment in three-dimensional matrices [131] allows the simple one-step fabrication without modification of the enzyme structure, meaning an improvement of the lifetime of the biosensor [103]. Conducting polymers, in particular PPy, have a stable electrical conductivity and can be electrogenerated under biocompatible conditions, in agreement with the enzyme requirements. Only a few works have been reported based on a two-enzyme co-immobilization process onto the transducer surface using polymers. They make use of the polymer as a surface for the further enzyme physical adsorption [64] or covalent immobilization [132], but no paper has been reported describing the simultaneous one-step immobilization of LOX and HRP enzymes in an electrosynthesized PPy matrix.

Table 1.1 summarizes the electrochemical biosensors described in literature for the analysis of L-lactate in the food industry. Best analytical response of sensitivity, linear range and limit of detection has been achieved when the bienzymatic reaction based on LOX and HRP have been used. It should also be highlighted that even though some of those biosensor devices have been applied to the L-lactic acid determination in real samples, such as beers, wines or milk, the working stability of the described biosensors do not enable the real-time monitoring of long-term processes.

Table 1.1. L-lactate electrochemical biosensors described in the literature.

Enzymes	Electrode	Mediator	Immobilization	Sensitivity	Linear range (M)	LOD (M)	Stability	Samples	Reference
LOX/HRP	Carbon	Ferrocene	MWCNT/PS membrane	116880 $\mu\text{A M}^{-1} \text{cm}^{-2}$	1.1×10^{-6} - 5.6×10^{-5}	5.6×10^{-7}	40 % after 2 weeks	Wine Beer	[130]
LOX/HRP	Carbon		Screen printed	0.84 $\mu\text{A M}^{-1} \text{L}$ (flow system)	1×10^{-5} - 2×10^{-4}	1×10^{-6}	90 % after 50 injections	Yoghurt Milk	[129]
LOX/HRP	Gold disk	TTF	MPA-SAM	2711 $\mu\text{A M}^{-1}$	4.2×10^{-7} - 2×10^{-5}	4.2×10^{-7}	91 % after 5 days	Synthetic wines	[128]
LDH	Glassy carbon		MWCNT-CHIT	8300 $\mu\text{A M}^{-1} \text{cm}^{-2}$	5×10^{-6} - 1.2×10^{-4}	7.6×10^{-7}	65 % after 7 days		[133]
LOX/LDH	ITO		PANI physical absorption	0.038 $\mu\text{A M}^{-1}$	1×10^{-4} - 1×10^{-3}	5×10^{-5}	3 weeks		[134]
LOX	Gold	PVI-Os	CNT-CHIT	0.0197 $\mu\text{A M}^{-1} \text{cm}^{-2}$	Up to 8×10^{-4}	5×10^{-6}			[135]

* ITO: indium tin oxide; TTF: tetrathiafulvalene; PVI-Os: polyvinylimidazole-Os; MWCNT: Multiwalled carbon nanotubes; PS: polystyrene; MPA: 3-mercaptopropionic acid; SAM: self-assembled monolayer; CNT: carbon nanotubes; CHIT: chitosan.

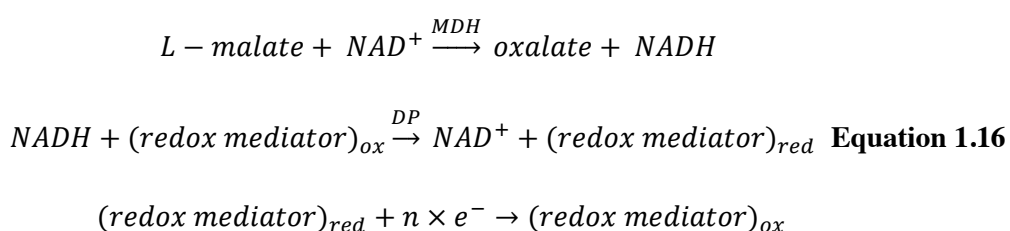
1.1.2.3 L-malate amperometric biosensors

L-malate is a component of the citric acid cycle and it is found in all living organisms. Its determination is especially important in the manufacture of wine, beer, bread, fruit and vegetable products [136-139], as well as in cosmetics and pharmaceuticals. It is one of the most important fruit acids and has the highest concentration of all acids in wine. L-Malic acid finds many applications as a food preservative (E296) and flavor enhancing compound, such as in the manufacture of low calorie drinks [140].

In the wine industry, the level of L-malic acid is monitored, along with L-lactic acid, during malolactic fermentation. L-malic acid is one of the principal organic acids in grapes [141]. It is mainly synthesized via glycolysis and its concentration depends on the climatic conditions and temperature during harvesting and crushing of the grapes [142]. However, the presence of L-malic acid affects the final quality of the wine by deteriorating its biochemical and microbial stability, and hence its sensorial quality and freshness. This is why an adjustment of the acidity is performed in red wines by malolactic fermentation, wherein the L-malic acid is converted to L-lactic acid and CO₂ by lactic acid bacteria action [143]. During alcoholic fermentation, yeast strain converts grape sugars, glucose and fructose, into ethanol. Once these sugars are consumed, the yeast concentration decreases and the lactic acid bacteria (LAB) perform the malolactic fermentation using the malolactic enzymes [144]. Natural or induced malolactic fermentation is carried out in the production of all red wines.

The conventional analytical methods for the determination of L-malic acid are chromatography [145] and electrophoresis [146]. These methods require the use of bulky expensive equipment and are time consuming. Alternative enzymatic approaches based on the detection of nicotinamide adenine dinucleotide (NADH) by absorbance were also reported [147]. In them, L-malic acid is oxidized to oxaloacetate in presence of NAD⁺ and catalyzed by L-malate dehydrogenase (L-MDH) enzyme. Then, the produced NADH is detected by absorbance at 340 nm and stoichiometrically related to the L-malic acid in the sample. However, this procedure has to be carried out in an external laboratory and is reagent consuming. The application of amperometric biosensors for in-field determination of malic acid appears to be an excellent option for the strict and continuous control of the fermentation processes in the food industry. These are based on different enzymatic approaches [148-152], but the most applied one

makes use of a cascade bienzymatic reaction involving the catalytic reactions of L-MDH enzyme in the presence of NAD^+ as co-factor, and consecutively of Diaphorase (DP) enzyme coupled to an appropriate redox mediator. The enzymatic process started with the oxidation of the analyte of interest to oxalate in presence of the enzyme MDH and the co-factor NAD^+ , which is reduced to NADH. The reduced co-factor is then re-oxidized in presence of the enzyme DP and the redox mediator, which is reduced. Finally, the redox mediator is re-oxidized on the transducer surface, and the faradaic current associated to this process is stoichiometrically related to the L-malate concentration in the sample (Equation 1.16).



The readout of this reaction can be carried out by spectrophotometry [153] or amperometry [128, 154]. Amperometric biosensors are characterized by its small size, low manufacturing costs, potential portability for in-situ analysis, low volume reagent consumption, wide linear response range and high selectivity and reproducibility [155]. Different redox mediators can be selected to record the biosensor amperometric signal. The careful selection of a mediator is fundamental for the successful performance of the developed device [46]. In the case of those NAD-dependent enzyme reactions, the mediator participates in the electrocatalytic regeneration of the NAD^+ cofactor. In this context, the most commonly used mediators are organics dyes [156] and inorganic redox ions [157]. Although the mediator is commonly added in solution during the biosensor performance, a lot of work has also been done on the incorporation of the mediator on the transducer surface together with the rest of biochemicals (enzymes and cofactors) in order to construct reagentless biosensors that are easier to use and show enhanced sensitivities [158]. Several electrochemical biosensors for the L-malate using MDH as enzyme are shown in Table 1.2. Regarding the application of coupled enzyme reactions, there is one biosensor using just MDH and most of them also incorporate DP for improving the sensitivity. Regarding the linear range, the obtained in the work based on physical absorption was narrow compared to the biosensors adding the mediator in solution and to the biosensor using covalent coupling as immobilization method. A

biosensor applied to the monitoring of the malolactic fermentation in red wines must show a long-term working stability under continuous use because the fermentation process takes around 30 days. Some of the biosensors in Table 1.2 show storage stability values, showing excellent results after months or years. However, the working biosensor stability is significantly worse, this being restricted to few days and thus limiting the biosensor performance for long-term applications. Finally, some biosensors have been applied to the determination of L-malate in wines samples and one of them has been tested in synthetic wines samples simulating the malolactic fermentation process. But any of them has been assessed using real samples collected during the malolactic fermentation of red wines.

Table 1.2. L-malate amperometric biosensors based on MDH described in the literature.

Enzymes	Electrode	Mediator	Immobilization	Sensitivity ($\mu\text{A M}^{-1}$)	Linear range (M)	LOD (M)	Stability	Samples	Reference
MDH/DP	Carbon-Paste	Ferricyanide in solution	entrapment in the carbon paste	-	1.5×10^{-5} - 1.5×10^{-3}	1.5×10^{-5}	90 % after 1 month of storage	-	[159]
MDH/DP	Carbon	Ferricyanide in solution	dialysis membrane	-	1×10^{-5} - 1.3×10^{-3}	1×10^{-5}	100 % after 5 month of storage or 5 assays	Wines	[160]
MDH	SWCNT		physical absorption	4.55×10^{-1}	2×10^{-4} - 8×10^{-4}	3.3×10^{-7}	75 % after 5 measures 63 % after 7 days or 30 assays or 90 % after 1 year of storage	-	[161]
MDH/DP	Gold planar electrode	Ferricyanide in solution	chitosan layers	5.50×10^{-4}	1.5×10^{-6} - 5.2×10^{-4}	5.4×10^{-6}		Wines	[154]
MDH/DP	Gold disk	TTF	MPA-SAM and dialysis membrane	1.58×10^3	5.2×10^{-7} - 2×10^{-5}	5.2×10^{-7}	90 % after 7 days	Synthetic MLF	[128]

*TTF: tetrathiafulvalene; MPA: 3-mercaptopropionic acid; SAM: self-assembled monolayer; SWCNT: single-wall carbon nanotubes;

1.2 Multiparametric sensor systems: Electronic tongues

Historically, multiparametric sensor systems applied to organoleptic analysis of food were called electronic tongues and noses since the aim of these systems was to imitate the human senses of taste and smell [162]. In 1982 the concept of “taste sensor” was described for the first time by Toko et al. [163] but it was not until the second half of the 80s when it had its greatest expansion [164, 165]. The IUPAC defined the electronic tongue as “a multisensor system, which consists of a number of low-selective sensors and uses advanced mathematical procedures for signal processing based on the pattern recognition and/or multivariate analysis (artificial neural networks (ANNs), principal component analysis (PCA), etc.)” [166]. The sensors array produces a signal pattern that can be correlated to certain features or qualities of the sample. These systems are able to imitate the taste sense but also to perform classification and discrimination, qualitative analysis and quantitative analysis of multiple components simultaneously.

Sensors of different nature can be used for the fabrication of electronic tongue systems: optical [167], mass [168] or biosensors [169]. However, the electrochemical ones are the most used. Among them, microelectrodes fabricated with semiconductor technology present some advantages that make them particularly suitable for integration into arrays for on-site measurements, such as the miniaturization, robustness, high reproducibility, low output impedance, mass fabrication, and ease of integration with the electronic circuitry [170]. In addition, one special technique is the data fusion of various measurement techniques (potentiometry, amperometry, conductance, spectrophotometry, gas sensing). These systems are called hybrid electronic tongues because they merge variables of different nature. This approach was already reported in the end of nineties as a powerful way to improve the performance of sensor technologies to the analysis of wines [171]. Since then, just four hybrid electronic tongues for wine have appeared in the bibliography, including those that also merge optical variables [172-175].

Electronic tongues have demonstrated their reliability and versatility in a broad range of fields, such as clinical diagnostic [176], environmental monitoring [177], agro food analysis [178], industrial processes control [179] and pharmaceutical analysis [180]. It is in the food quality and safety control where the applicability of these multisensor

systems has been most extended [181]. However, most electronic tongue systems reported until now for food quality are laboratory versions [181], partly due to the use of large-sized sensors and data collection equipment. On one hand, the miniaturization of the electronic tongue has been approached by using individual wire electrodes [182] or developing integrated arrays of sensors. Usually, these arrays have a planar configuration and include layers of conductive inks or pastes sequentially deposited onto insulating and chemically-inert substrates. Depending on the thickness of these layers, integrated arrays of sensors have been fabricated by using screen-printed methods (thick-film technology) and applied as portable devices for monitoring drinking waters [182] and beer discrimination [183]. Additionally, thin-film technologies have been also used to fabricate integrated multisensor systems combined with flow injection analysis [170] and portable taste sensors [184], both by using standard photolithographic techniques.

1.2.1 Advanced mathematical tools for signal processing

The quality of the output data from sensors is a key factor in the multivariate analysis. The memory effect or hysteresis and the signal drift, defined as the slow non-random change of the sensor signal along time when it is immersed in a solution with a constant concentration and temperature [185] are two typical phenomena especially of the potentiometric sensors. These problems can be solved considering the analytical signal as the difference between the absolute signal measured by the electrode and the signal of a background solution with constant composition. Besides, the importance between the different variables (potential, current, etc.) have to be balanced using different strategies, such as the centering (the signals from each sensor is referred to the arithmetic mean signal of them), the standardization (the signals are treated for having the same standard deviation), the auto-scale (resulting from the combination between the centering and the standardization methods) or the normalization (the signal have to be treated for being included in a defined interval). The method used in this thesis is the auto-scale and the centering.

As the sensors present cross-response to different analytes in the sample, a great amount of complex data are generated that must be processed by chemometric tools. According to the definition of the International Chemometrics Society, chemometrics is the

chemical discipline that uses mathematical and statistical methods to design or select optimal procedures and experiments, and to provide maximum chemical information by analyzing chemical data. There are different data processing tools used with the electronic tongue systems [186] aimed to classify samples and to carried out qualitative analysis, such as the Principal Component Analysis (PCA) or the Linear Discriminant Analysis (LDA). Other methods, as the Partial Least Squares (PLS) or Artificial Neural Networks (ANNs) are applied for quantification purposes. The most challenging aspect of these tools is that with the minimum number of sensors, we can obtain a high amount of quality patterns [187] and rich chemical information about sample [188]. The methods used in this thesis are the PLS and the LDA.

The PLS regression is a standard method in chemometrics for multivariate calibration. It is based on the reduction of the number of variables without losing the quality of the original multidimensional information. The new variables generated, which are called principal components or factors, are in fact linear combinations of the original ones. Then, the least squares regression is performed using these new variables. Therefore, the set of samples is divided in two subsets: the calibration one, which is used to construct the response model, and the prediction one, which is afterwards interpolated in the generated to model in order to evaluate it. As the first components contain much information for predicting samples, during the calibration step, the PLS algorithm not only uses the information given by the signals of the sensors, but also the information given by the concentrations of the analytes. The PLS regression is applied to analytical systems with a large number of variables and a small number of samples [189].

Regarding the LDA method, it is also based on a reduction of variables. LDA is a supervised method, therefore assumes a previous knowledge of the group membership of each sample in the training set. In this case, the new variables are called discriminant functions (DFs) and they are linear combinations of the original variables that produce the best discrimination between the different groups of samples, allowing to show the similarities and differences more simply and direct. It provides a classification model characterized by a linear dependence of the classification scores with respect to the descriptors (groups defined previously), which maximize the ratio between-class variance

and minimize the ratio of within-class variance. The classification power of the model generated can be evaluated using a prediction set of samples or using a “leaving one-out” cross-validation procedure. In the latter procedure, the whole sample data minus one observation are used for the estimation of the discriminant functions, and then the omitted sample is interpolated and classified by the model.

1.3 Miniaturization of the analytical systems

The interest of monitoring chemical parameters for in-situ or on-line applications like the food industry or environmental water monitoring has been increasing in the last years. This interest lies on the rapid detection of unexpected changes to offer a solution in time. Traditionally, these analyses have been carried out in external laboratories using costly equipment and time-consuming procedures. Therefore, miniaturized and portable analytical systems would be highly valuable to have information in real time. In addition, the miniaturization of the system would give rise to several improved operational features, such as short analysis time, reduced reagent consumption, lower power consumption and low fabrication and maintenance costs.

Microanalytical flow systems allow on-line analysis of the sample directly from the process stream, therefore the determination of the analyte can be carried out on time. For extracting and processing the sample, the automated sampling system can work in intermittent or continuous method [190]. Intermittent methods require injection of a portion of the sample stream into the flow system, meanwhile continuous methods allow the sample flowing continuously through the flow system. Therefore, continuous on-line process is the best technique to offer real-time monitoring of analytes. These methods can be classified into those injecting (Flow-injection analysis (FIA) or Sequential-injection analysis (SIA)) [191] or aspirating [192] the sample into the system. FIA is the most valuable technique for on-line process monitoring, as has been reported for food industry or environmental monitoring applications [193-202]. Regarding the detection techniques used in these flow systems, most of them are electrochemical sensors. FIA methods for monitoring sulfur species during electrochemical production of polysulfides [203] or for the determination of metal-binding carbohydrates in plant extracts by amperometry [204] have been reported.

Gas-diffusion membranes are also widely used in on-line monitoring for separating the analyte of interest from the sample. Since Van der Linden used them for the determination of ammonia, carbon dioxide, cyanide and sulfur dioxide [205] at the beginning of the 1980s, the use of gas-diffusion membranes have been extensively described in fields like water analysis [206-208] or food industry [209, 210].

Materials for the fabrication of the microanalytical flow-systems should be robust, low-cost and easy manufacturing. The materials proposed in the first years of microfluidic research were glass, ceramics, quartz or silicon [211]. Although these were a good choice for prototyping due to their reproducible fabrication, they presented some problems of integration of all the elements of the system like sensors and passive fluidic elements in the same substrate. Nowadays, polymers are a good alternative due to their simplicity of fabrication and low cost [212], among them polydimethylsiloxane (PDMS) has been proposed due to its biocompatibility, its optical transparence and its low cost [213]. Although there are several methods for PDMS prototyping, the soft lithography or replica molding is the most extended in laboratories [214] for the fabrication of fluidic devices [215]. However, the PDMS has some disadvantages like its soft mechanical properties, short lifetime and the difficulties of fabrication process escalation for mass production. The use of polymethylmethacrylate (PMMA) [216] could be an alternative to PDMS.

The PMMA is a robust thermoplastic material with interesting mechanical properties, such as stiffness and hardness. It can be used under environmental conditions [217, 218] and can be manufactured by rapid-prototyping techniques [219]. The most common fast prototyping techniques are the milling and the laser ablation [220, 221]. The mechanical milling uses a cutter for removing the material from the workpiece without its chemical modification [222]. The laser ablation method is based on a high-intensity laser beam focused onto the material and its movement in x and y directions for generating the desired pattern [223]. In contrast to mechanical milling, the laser ablation mechanism is a complex combination of photochemical and photothermal processes [224]. During the process, some chemical bonds are broken by the photon absorption process and others are broken thermally. Among the laser ablation methods, CO₂-laser, emitting at 10.6 μm wavelength, ablates all the material photothermally [224]. Besides, CO₂-laser emits

radiation continuously; therefore the temperature of the irradiated spot rises so fast that the material will first melt and then decomposed, leaving a void in the workpiece. In the case of PMMA, the material vaporizes in the form of monomers when it reaches its boiling temperature. The power setting, the moving speed of the laser beam and the repetition rate of the beam over the same channel are controlled by the user [225]. The use of these techniques for the PMMA mechanizing in fluidic systems has been extensively reported [225-230]. An example of a microanalytical flow system integrating sensors in a PMMA module for on-line measurements of copper (II) ions in water has been described [231].

1.4 References

1. Hulanicki, A., S. Glab, and F. Ingman, *Pure and Applied Chemistry*, 1991. **63**(9): p. 1247-1250.
2. Thevenot, D.R., et al., *Biosensors & Bioelectronics*, 2001. **16**(1-2): p. 121-131.
3. Cattrall, R.W., *Chemical Sensors*. 1997, New York: Oxford University Press.
4. Moody, G.J. and J.D.R. Thomas., *Talanta*, 1972. **19**(5): p. 623-&.
5. Jimenez, C., Bratov, A., Abramova, N., Baldi, A., *ISFET Based Sensors: Fundamentals and Applications*, A.S. Publishers, Editor. 2006. p. 151-196.
6. Sze, S.M., *Physics of Semiconductor Devices*. 1981, New York: John Wiley and Sons.
7. Bockris, J.O., Reddy, A. K. N., *Modern Electrochemistry*. 2000, New York: Kluwer Academic and Plenum Press.
8. Alegret, S., et al., *Analytica Chimica Acta*, 1990. **231**(1): p. 53-58.
9. Le Bris, N. and D. Birot., *Analytica Chimica Acta*, 1997. **356**(2-3): p. 205-215.
10. Poghosian, A., et al., *Sensors and Actuators B-Chemical*, 2001. **76**(1-3): p. 634-638.
11. Cambiaso, A., et al., *Sensors and Actuators B-Chemical*, 1996. **34**(1-3): p. 245-251.
12. Bettaieb, F., et al., *Bioelectrochemistry*, 2007. **71**(2): p. 118-125.
13. Cheung, P.W., *Ieee Transactions on Biomedical Engineering*, 1984. **31**(8): p. 581-581.
14. Oelssner, W., H. Kaden, and H. Bellee, *Biomedizinische Technik*, 1993. **38**(3): p. 38-41.
15. Duroux, P., et al., *Gut*, 1991. **32**(3): p. 240-245.
16. Sakurai, T. and Y. Husimi, *Analytical Chemistry*, 1992. **64**(17): p. 1996-1997.
17. Han, J.H., et al., *Sensors and Actuators B-Chemical*, 2000. **66**(1-3): p. 203-204.
18. Grases, F., et al., *Springerplus*, 2014. **3**: p. 5.
19. Kaminski, R.K., *Instrumentation Technology*, 1969. **16**(9): p. 41-&.
20. Pungor, E. and K. Toth, *Analyst*, 1970. **95**(1132): p. 625-&.
21. Clechet, P. and N. Jaffrezicrenault, *Advanced Materials*, 1990. **2**(6-7): p. 293-298.
22. Moody, G.J., J.M. Slater, and J.D.R. Thomas, *Analyst*, 1988. **113**(5): p. 699-703.
23. Beltran, A., et al., *Electroanalysis*, 2002. **14**(3): p. 213-220.
24. Munoz, J., et al., *Biosensors & Bioelectronics*, 1997. **12**(7): p. 577-585.
25. Artigas, J., et al., *Computers and Electronics in Agriculture*, 2001. **31**(3): p. 281-293.
26. Bratov, A., et al., *Analytical Chemistry*, 1995. **67**(19): p. 3589-3595.
27. Vanderwal, P.D., A. Vandenberg, and N.F. Derooij, *Sensors and Actuators B-Chemical*, 1994. **18**(1-3): p. 200-207.
28. Jimenez, C., I. Marques, and J. Bartroli, *Analytical Chemistry*, 1996. **68**(21): p. 3801-3807.
29. Wakida, S.I., et al., *Water Air and Soil Pollution*, 2001. **130**(1-4): p. 625-630.
30. Dieffenbach, A. and E. Matzner, *Plant and Soil*, 2000. **222**(1-2): p. 149-161.
31. Campanella, L., et al., *Sensors and Actuators B-Chemical*, 1995. **27**(1-3): p. 329-335.
32. Humenyuk, I., et al., *Microelectronics Journal*, 2006. **37**(6): p. 475-479.
33. Orozco, J., et al., *Measurement Science and Technology*, 2007. **18**(3): p. 935-940.
34. Temple-Boyer, P., et al., *Microelectronics Reliability*, 2004. **44**(3): p. 443-447.
35. Barbaro, A., et al., *Advanced Materials*, 1992. **4**(6): p. 402-408.
36. Sanchez, J., et al., *Analytica Chimica Acta*, 1999. **382**(1-2): p. 157-164.
37. Flores, F., et al., *Analytical and Bioanalytical Chemistry*, 2003. **376**(4): p. 476-480.
38. Updike, S.J. and G.P. Hicks, *Nature*, 1967. **214**(5092): p. 986-&.
39. Eggins, B., *Chemical sensors and biosensors. Analytical Techniques in the Sciences*. 2002, West Sussex: John Wiley & Sons.
40. Sadik, O.A. and G.G. Wallace, *Analytica Chimica Acta*, 1993. **279**(2): p. 209-212.
41. Dzyadevych, S.V., et al., *Irbm*, 2008. **29**(2-3): p. 171-180.
42. Julio Reviejo, A., Pingarrón, J. M., *Biosensores electroquímicos. Una herramienta para el análisis medioambiental, alimentario y clínico*. 2000, Anales de la Real Sociedad Española de Química. p. 5-15.

43. Misra, H.P. and I. Fridovich, *Analytical Biochemistry*, 1976. **70**(2): p. 632-634.
44. Rorth, M. and P.K. Jensen, *Biochimica Et Biophysica Acta*, 1967. **139**(1): p. 171-&.
45. Heller, A., *Journal of Physical Chemistry*, 1992. **96**(9): p. 3579-3587.
46. Chaubey, A. and B.D. Malhotra, *Biosensors & Bioelectronics*, 2002. **17**(6-7): p. 441-456.
47. Pei, J.H. and X.Y. Li, *Electroanalysis*, 1999. **11**(17): p. 1266-1272.
48. Rodriguez, M.C. and G.A. Rivas, *Electroanalysis*, 1999. **11**(8): p. 558-564.
49. Zhang, X.J., et al., *Electroanalysis*, 1999. **11**(13): p. 945-949.
50. Gorton, L., *Electroanalysis*, 1995. **7**(1): p. 23-45.
51. Dunford, H.B., *Peroxidases in Chemistry and Biology*, ed. K.E. J. Everse, M. Grisham Vol. II. 1991, New York: CRC Press. 1-24.
52. Dasgupta, S. and M.D. Ryan, *Bioelectrochemistry and Bioenergetics*, 1980. **7**(3): p. 587-594.
53. Lin, M.S., S.Y. Tham, and G.A. Rechnitz, *Electroanalysis*, 1990. **2**(7): p. 511-516.
54. Reviejo, A.J., et al., *Journal of Electroanalytical Chemistry*, 1994. **374**(1-2): p. 133-139.
55. Wang, J., A. Ciszewski, and N. Naser, *Electroanalysis*, 1992. **4**(8): p. 777-782.
56. Yang, L., et al., *Analytical Chemistry*, 1995. **67**(8): p. 1326-1331.
57. Cayuela, G., et al., *Analyst*, 1998. **123**(2): p. 371-377.
58. Wang, J. and M. Ozsoz, *Electroanalysis*, 1990. **2**(8): p. 647-650.
59. Gorton, L., *Electrochemistry of NAD(P)⁺/NAD(P)H*, in *Encyclopedia of Electrochemistry*, A.J. Bard and M. Stratmann, Editors. 2002, Wiley-VCH: Weinheim. p. 67-143.
60. Schuhmann, W. and H.L. Schmidt, *Advances in Biosensors*, A.P.F. Turner, Editor. 1992, JAI Press: London. p. 79-130.
61. Hart, J.P., et al., *Electroanalysis*, 1999. **11**(6): p. 406-411.
62. Wang, J., et al., *Talanta*, 2009. **77**(4): p. 1454-1459.
63. Ekanayake, E.M.I.M., D.M.G. Preethichandra, and K. Kaneto, *Biosensors & Bioelectronics*, 2007. **23**(1): p. 107-113.
64. Chaubey, A., et al., *Analytica Chimica Acta*, 2000. **407**(1-2): p. 97-103.
65. Sheldon, R.A., *Biochemical Society Transactions*, 2007. **35**: p. 1583-1587.
66. Yonemori, Y., et al., *Analytica Chimica Acta*, 2009. **633**(1): p. 90-96.
67. Luo, P., et al., *Forensic Science International*, 2008. **179**(2-3): p. 192-198.
68. Mikkelsen, S.R. and G.A. Rechnitz, *Analytical Chemistry*, 1989. **61**(15): p. 1737-1742.
69. Delvaux, M. and S. Demoustier-Champagne, *Biosensors & Bioelectronics*, 2003. **18**(7): p. 943-951.
70. Rahman, M.A., et al., *Analytical Chemistry*, 2005. **77**(15): p. 4854-4860.
71. Wu, H.M., et al., *Electrochimica Acta*, 1994. **39**(3): p. 327-331.
72. Hanko, M., et al., *Analytical and Bioanalytical Chemistry*, 2006. **386**(5): p. 1273-1283.
73. Leca, B. and J.L. Marty, *Biosensors & Bioelectronics*, 1997. **12**(11): p. 1083-1088.
74. Salinas-Castillo, A., et al., *Biosensors & Bioelectronics*, 2008. **24**(4): p. 1053-1056.
75. Svancara, I., et al., *Electroanalysis*, 2009. **21**(1): p. 7-28.
76. Azmi, N.E., et al., *Analytical Biochemistry*, 2009. **388**(1): p. 28-32.
77. Singh, M., P.K. Kathuroju, and N. Jampana, *Sensors and Actuators B-Chemical*, 2009. **143**(1): p. 430-443.
78. Gerard, M., A. Chaubey, and B.D. Malhotra, *Biosensors & Bioelectronics*, 2002. **17**(5): p. 345-359.
79. Cosnier, S., *Applied Biochemistry and Biotechnology*, 2000. **89**(2-3): p. 127-138.
80. Eftekhari, A., *Synthetic Metals*, 2004. **145**(2-3): p. 211-216.
81. Shan, D., et al., *Materials Science & Engineering C-Biomimetic and Supramolecular Systems*, 2008. **28**(2): p. 213-217.
82. Lupu, S., et al., *Sensors*, 2013. **13**(5): p. 6759-6774.
83. Nien, P.C., T.S. Tung, and K.C. Ho, *Electroanalysis*, 2006. **18**(13-14): p. 1408-1415.
84. Vedrine, C., S. Fabiano, and C. Tran-Minh, *Talanta*, 2003. **59**(3): p. 535-544.

85. Cochequerente, L., et al., *Electroanalysis*, 1993. **5**(8): p. 647-652.
86. Wang, J. and M. Musameh, *Analytica Chimica Acta*, 2005. **539**(1-2): p. 209-213.
87. Schuhmann, W., et al., *Biosensors & Bioelectronics*, 1991. **6**(8): p. 689-697.
88. Cosnier, S., *Biosensors & Bioelectronics*, 1999. **14**(5): p. 443-456.
89. Ramanavicius, A., A. Kausaite, and A. Ramanaviciene, *Analyst*, 2008. **133**(8): p. 1083-1089.
90. Sadki, S., et al., *Chemical Society Reviews*, 2000. **29**(5): p. 283-293.
91. Asavapiriyant, S., et al., *Journal of Electroanalytical Chemistry*, 1984. **177**(1-2): p. 229-244.
92. Schuhmann, W., et al., *Biosensors & Bioelectronics*, 1997. **12**(12): p. 1157-1167.
93. Matyjaszewski, K. and T. Davys, *Handbook of radical polymerization*. 2002, Hoboken: John Wiley & Sons.
94. Pringle, J.M., et al., *Polymer*, 2004. **45**(5): p. 1447-1453.
95. Jugovic, B., et al., *Materials Chemistry and Physics*, 2009. **114**(2-3): p. 939-942.
96. Grgur, B.N., et al., *Journal of Power Sources*, 2012. **217**: p. 193-198.
97. Inzelt, G., et al., *Electrochimica Acta*, 2000. **45**(15-16): p. 2403-2421.
98. Wallace, G.G., et al., *Conductive Electroactive Polymers*. 2009, Boca Raton: Telyor & Francis Group.
99. Heinze, J., B.A. Frontana-Uribe, and S. Ludwigs, *Chemical Reviews*, 2010. **110**(8): p. 4724-4771.
100. Kankare, K., *Conducting polymers: Basic Methods of Synthesis and Characterization*, in *Electrical and Optical Polymer Systems: Fundamentals, Methods and Applications*, D. Wise, et al., Editors. 1998, CRC Press: New York. p. 167-199.
101. *Conducting Polymers-Theory, S., Properties and and T.A.S. Characterization*, J. Reynolds, Eds., CRC, *Conducting Polymers-Theory, Sinthesis, Properties and Characterization*. 2007, New York: CRCPress, Teyor & Francis Group.
102. Uang, Y.M. and T.C. Chou, *Biosensors & Bioelectronics*, 2003. **19**(3): p. 141-147.
103. Razola, S.S., et al., *Biosensors & Bioelectronics*, 2002. **17**(11-12): p. 921-928.
104. Sohail, M. and S.B. Adeloju, *Sensors and Actuators B-Chemical*, 2008. **133**(1): p. 333-339.
105. Alonso-Lomillo, M.A., et al., *Bioelectrochemistry*, 2009. **74**(2): p. 306-309.
106. Simsek, S., E. Aynaci, and F. Arslan, *Artificial Cells Nanomedicine and Biotechnology*, 2016. **44**(1): p. 356-361.
107. Apetrei, I.M. and C. Apetrei, *Sensors and Actuators B-Chemical*, 2013. **178**: p. 40-46.
108. Singh, S., A. Chaubey, and B.D. Malhotra, *Analytica Chimica Acta*, 2004. **502**(2): p. 229-234.
109. Adeloju, S.B., S.J. Shaw, and G.G. Wallace, *Analytica Chimica Acta*, 1996. **323**(1-3): p. 107-113.
110. Bakker, J., et al., *American Journal of Surgery*, 1996. **171**(2): p. 221-226.
111. Parra, A., et al., *Analytica Chimica Acta*, 2006. **555**(2): p. 308-315.
112. Kost, G.J., *Critical Reviews in Clinical Laboratory Sciences*, 1993. **30**(2): p. 153-202.
113. Beneke, R. and S.P. vonDuvillard, *Medicine and Science in Sports and Exercise*, 1996. **28**(2): p. 241-246.
114. Fowler, R.A., et al., *Journal of Critical Care*, 2003. **18**(3): p. 181-191.
115. Mazzei, F., et al., *Food Chemistry*, 1996. **55**(4): p. 413-418.
116. Ghanbari, M., et al., *Food Science and Technology*, 2013. **54**(2): p. 315-324.
117. Stiles, M.E., *International Journal of General and Molecular Microbiology*, 1996. **70**(2-4): p. 331-345.
118. Shapiro, F. and N. Silanikove, *Food Chemistry*, 2010. **119**(2): p. 829-833.
119. Lonvaud-Funel, A., *International Journal of General and Molecular Microbiology*, 1999. **76**(1-4): p. 317-331.
120. Milagres, M.P., et al., *Food Chemistry*, 2012. **135**(3): p. 1078-1082.

121. Galban, J., S. Demarcos, and J.R. Castillo, *Analytical Chemistry*, 1993. **65**(21): p. 3076-3080.
122. Soares, D.P. and M. Law, *Clinical Radiology*, 2009. **64**(1): p. 12-21.
123. Barker, S.B. and W.H. Summerson, *Journal of Biological Chemistry*, 1941. **138**(2): p. 535-554.
124. Kimmel, D.W., et al., *Analytical Chemistry*, 2012. **84**(2): p. 685-707.
125. May, S.W., *Current Opinion in Biotechnology*, 1999. **10**(4): p. 370-375.
126. Silber, A., C. Brauchle, and N. Hampp, *Sensors and Actuators B-Chemical*, 1994. **18**(1-3): p. 235-239.
127. Makovos, E.B. and C.C. Liu, *Biotechnology and Bioengineering*, 1985. **27**(2): p. 167-170.
128. Gamella, M., et al., *Talanta*, 2010. **81**(3): p. 925-933.
129. Ghamouss, F., et al., *Analytica Chimica Acta*, 2006. **570**(2): p. 158-164.
130. Perez, S. and E. Fabregas, *Analyst*, 2012. **137**(16): p. 3854-3861.
131. Herrero, A.M., et al., *European Food Research and Technology*, 2004. **219**(5): p. 556-559.
132. Casimiri, V. and C. Burstein, *Biosensors & Bioelectronics*, 1996. **11**(8): p. 783-789.
133. Marquette, C.A., A. Degiuli, and L.J. Blum, *Biosensors & Bioelectronics*, 2003. **19**(5): p. 433-439.
134. Tsai, Y.C., S.Y. Chen, and H.W. Liaw, *Sensors and Actuators B-Chemical*, 2007. **125**(2): p. 474-481.
135. Cui, X.Q., et al., *Biosensors & Bioelectronics*, 2007. **22**(12): p. 3288-3292.
136. Cowles, H.W., *Journal of the American Chemical Society*, 1908. **30**(8): p. 1285-1288.
137. O'Connell, M. and W. Silvers, *Journal of Allergy and Clinical Immunology*, 2000. **105**(1): p. S137-S137.
138. Sansville, T.J., *Food Manufacture*, 1969. **44**(10): p. 50-+.
139. Weiss, J.M., C.R. Downs, and H.P. Corson, *Industrial and Engineering Chemistry*, 1923. **15**: p. 628-630.
140. Sha, R.Y. and C.G. Cai, *Research Journal of Biotechnology*, 2016. **11**(10): p. 22-26.
141. *The Biochemistry of Organic Acids in the Grape*, in *The Biochemistry of the Grape Berry*, H. Gerós, M. Chaves, and S. Delrot, Editors. 2012, Bentham Books. p. 67-88.
142. Boulton, R.B., et al., *Principles and Practices of Winemaking*. 1999, New York: Springer Science.
143. Ribereau-Gayon, P., et al., *The Microbiology of Wine and Vinifications*, in *Handbook of Enology. 2 ed.* 2006, John Wiley & Sons.
144. Bony, M., et al., *Febs Letters*, 1997. **410**(2-3): p. 452-456.
145. Vonach, R., B. Lendl, and R. Kellner, *Journal of Chromatography A*, 1998. **824**(2): p. 159-167.
146. Mato, I., S. Suarez-Luque, and J.F. Huidobro, *Food Chemistry*, 2007. **102**(1): p. 104-112.
147. *L-malic acid: enzymatic method (OIV Compendium ed. 1990, revised by 377/2009)*, *OIV-MA-AS313-11* 2009, International Organisation of Vine and Wine (OIV).
148. Bucur, B., et al., *Biosensors & Bioelectronics*, 2006. **21**(12): p. 2290-2297.
149. Esti, M., et al., *Analytica Chimica Acta*, 2004. **513**(1): p. 357-364.
150. Gurban, A.M., et al., *Analytical Letters*, 2006. **39**(8): p. 1543-1558.
151. Mazzei, F., F. Botre, and G. Favero, *Microchemical Journal*, 2007. **87**(1): p. 81-86.
152. Gallarta, F., F. Javier Sainz, and C. Saenz, *Analytical and Bioanalytical Chemistry*, 2007. **387**(6): p. 2297-2305.
153. de Santana, J.F.S., M.F. Belian, and A.F. Lavorante, *Analytical Sciences*, 2014. **30**(6): p. 657-661.
154. Monosik, R., et al., *Central European Journal of Chemistry*, 2012. **10**(1): p. 157-164.
155. Grieshaber, D., et al., *Sensors*, 2008. **8**(3): p. 1400-1458.
156. Schlereth, D.D., E. Katz, and H.L. Schmidt, *Electroanalysis*, 1995. **7**(1): p. 46-54.

157. Somasundrum, M., J. Hall, and J.V. Bannister, *Analytica Chimica Acta*, 1994. **295**(1-2): p. 47-57.
158. Barendrecht, E., *Journal of Applied Electrochemistry*, 1990. **20**(2): p. 175-185.
159. Miertus, S., et al., *Biosensors & Bioelectronics*, 1998. **13**(7-8): p. 911-923.
160. Katrlík, J., et al., *Analytica Chimica Acta*, 1999. **379**(1-2): p. 193-200.
161. Arvinte, A., L. Rotariu, and C. Bala, *Sensors*, 2008. **8**(3): p. 1497-1507.
162. Nagle, H.T., R. Gutierrez-Osuna, and S.S. Schiffman, *Ieee Spectrum*, 1998. **35**(9): p. 22-34.
163. Toko, K., *Sensors and Actuators B-Chemical*, 2000. **64**(1-3): p. 205-215.
164. Moore, S.W., et al., *Sensors and Actuators B-Chemical*, 1993. **16**(1-3): p. 344-348.
165. Pearce, T.C., et al., *Analyst*, 1993. **118**(4): p. 371-377.
166. Vlasov, Y., et al., *Pure and Applied Chemistry*, 2005. **77**(11): p. 1965-1983.
167. Kirby, R., et al., *Analytical Chemistry*, 2004. **76**(14): p. 4066-4075.
168. Abraham, J.K., et al., *Identification of soft drinks using MEMS-IDT microsensors*, in *Smart Structures and Materials 2005: Smart Electronics, Memes, Biomemes, and Nanotechnology*, V.K. Varadan, Editor. 2005. p. 414-424.
169. Alonso, G.A., R. Munoz, and J.-L. Marty, *Analytical Letters*, 2013. **46**(11): p. 1743-1757.
170. Moreno i Codinachs, L., et al., *Ieee Sensors Journal*, 2008. **8**(5-6): p. 608-615.
171. Toko, K., *Measurement Science and Technology*, 1998. **9**(12): p. 1919-1936.
172. Buratti, S., et al., *Food Chemistry*, 2007. **100**(1): p. 211-218.
173. Di Natale, C., et al., *Sensors and Actuators B-Chemical*, 2000. **69**(3): p. 342-347.
174. Rodriguez-Mendez, M.L., et al., *Ieee Sensors Journal*, 2004. **4**(3): p. 348-354.
175. Gutierrez, M., et al., *Analyst*, 2010. **135**(7): p. 1718-1725.
176. Gutierrez, M., S. Alegret, and M. del Valle, *Biosensors & Bioelectronics*, 2008. **23**(6): p. 795-802.
177. Rudnitskaya, A., et al., *Talanta*, 2001. **55**(2): p. 425-431.
178. Gutierrez, M., et al., *Journal of Agricultural and Food Chemistry*, 2008. **56**(6): p. 1810-1817.
179. Winquist, F., et al., *Sensors and Actuators B-Chemical*, 2005. **111**: p. 299-304.
180. Gutes, A., et al., *Microchimica Acta*, 2007. **157**(1-2): p. 1-6.
181. Baldwin, E.A., et al., *Sensors*, 2011. **11**(5): p. 4744-4766.
182. Ouyang, Q., J. Zhao, and Q. Chen, *Food Research International*, 2013. **51**(2): p. 633-640.
183. Blanco, C.A., et al., *Journal of Food Engineering*, 2015. **157**: p. 57-62.
184. Tahara, Y., et al., *Sensors*, 2013. **13**(1): p. 1076-1084.
185. Buck, R.P. and E. Lindner, *Pure and Applied Chemistry*, 1994. **66**(12): p. 2527-2536.
186. Richards, E., C. Bessant, and S. Saini, *Electroanalysis*, 2002. **14**(22): p. 1533-1542.
187. Baret, M., et al., *Talanta*, 1999. **50**(3): p. 541-558.
188. Winquist, F., et al., *Analytica Chimica Acta*, 2000. **406**(2): p. 147-157.
189. Lomillo, M.A.A., O.D. Renedo, and M.J.A. Martinez, *Analytica Chimica Acta*, 2001. **449**(1-2): p. 167-177.
190. Callis, J.B., D.L. Illman, and B.R. Kowalski, *Analytical Chemistry*, 1987. **59**(9): p. A624-&.
191. Valcarcel, M. and M.D.L. Decastro, *Journal of Chromatography*, 1987. **393**(1): p. 3-23.
192. Goto, M., *Trac-Trends in Analytical Chemistry*, 1983. **2**(4): p. 92-94.
193. Forman, L.W., B.D. Thomas, and F.S. Jacobson, *Analytica Chimica Acta*, 1991. **249**(1): p. 101-111.
194. Ogawa, K., et al., *Analytical and Bioanalytical Chemistry*, 2002. **373**(4-5): p. 211-214.
195. Sariahmetoglu, M., et al., *Analytical Letters*, 2003. **36**(4): p. 749-765.
196. Valero, F., et al., *Biotechnology and Bioengineering*, 1990. **36**(6): p. 647-651.
197. Kanda, Y. and M. Taira, *Analytical Sciences*, 2003. **19**(5): p. 695-699.
198. Navratil, M., et al., *Process Biochemistry*, 2001. **36**(11): p. 1045-1052.

199. Rhee, J.I., M. Yamashita, and T. Scheper, *Analytica Chimica Acta*, 2002. **456**(2): p. 293-301.
200. Wiryawan, A., *Laboratory Robotics and Automation*, 2000. **12**(3): p. 142-148.
201. Fitsev, I.M. and G.K. Budnikov, *Industrial Laboratory*, 1999. **65**(12): p. 761-772.
202. Li, Y.S., *Bunseki Kagaku*, 1996. **45**(1): p. 107-108.
203. Chai, X.S. and L.G. Danielsson, *Process Control and Quality*, 1996. **8**(4): p. 159-166.
204. Weber, G. and J. Messerschmidt, *Fresenius Journal of Analytical Chemistry*, 2000. **367**(4): p. 356-358.
205. Vanderlinden, W.E., *Analytica Chimica Acta*, 1983. **151**(2): p. 359-369.
206. Alegret, S., et al., *Analyst*, 1989. **114**(11): p. 1443-1447.
207. Monser, L., N. Adhoum, and S. Sadok, *Talanta*, 2004. **62**(2): p. 389-394.
208. Oshima, M., et al., *Analytical Sciences*, 2001. **17**(11): p. 1285-1290.
209. Azevedo, C.M.N., et al., *Analytica Chimica Acta*, 1999. **387**(2): p. 175-180.
210. Dhaouadi, A., et al., *Food Chemistry*, 2007. **103**(3): p. 1049-1053.
211. Gardeniers, J.G.E., R.E. Oosterbroek, and A. van den Berg, *Lab-on-a-Chip*, 2003, p. 37-64.
212. Guber, A.E., et al., *Chemical Engineering Journal*, 2004. **101**(1-3): p. 447-453.
213. Bhagat, A.A.S., P. Jothimuthu, and I. Papautsky, *Lab on a Chip*, 2007. **7**(9): p. 1192-1197.
214. Yu, H.B., et al., *Sensors and Actuators B-Chemical*, 2009. **137**(2): p. 754-761.
215. Friend, J. and L. Yeo, *Biomicrofluidics*, 2010. **4**(2).
216. Vandenberg, J. and T. Junkers, *Polyacrylates*, in *Handbook of thermoplastics*, O. Olabisi and K. Adewale, Editors. 2016, CRS Press: London. p. 169-192.
217. Beaton, A.D., et al., *Sensors and Actuators B-Chemical*, 2011. **156**(2): p. 1009-1014.
218. Kwakye, S. and A. Baeumner, *Analytical and Bioanalytical Chemistry*, 2003. **376**(7): p. 1062-1068.
219. Chua, C.K., K.F. Leong, and C.S. Lim, *Rapid prototyping: Principles and Applications*. 2010: World Scientific Publishing Company.
220. Rahman, M., et al., *International Journal of Machine Tools & Manufacture*, 2010. **50**(4): p. 344-356.
221. Bartnik, A., et al., *Applied Physics B-Lasers and Optics*, 2009. **96**(4): p. 727-730.
222. Mousinho, A.P., R.D. Mansano, and A.C.S. de Arruda, *Microelectronics Journal*, 2003. **34**(5-8): p. 651-653.
223. Yeh, J.T.C., *Journal of Vacuum Science & Technology a-Vacuum Surfaces and Films*, 1986. **4**(3): p. 653-658.
224. Mohammed, M.I., et al., *Journal of Micromechanics and Microengineering*, 2017. **27**(1).
225. Klank, H., J.P. Kutter, and O. Geschke, *Lab on a Chip*, 2002. **2**(4): p. 242-246.
226. Hong, T.-F., et al., *Microfluidics and Nanofluidics*, 2010. **9**(6): p. 1125-1133.
227. Chen, P.-C., et al., *International Journal of Advanced Manufacturing Technology*, 2014. **71**(9-12): p. 1623-1630.
228. Friedrich, C., et al., *Proceedings of the Tenth Annual Meeting - the American Society for Precision Engineering*. 1995. 284-287.
229. Sanahuja, D., et al., *Lab on a Chip*, 2015. **15**(7): p. 1717-1726.
230. Pujol-Vila, F., et al., *Sensors and Actuators B-Chemical*, 2016. **222**: p. 55-62.
231. Gibson, C.; Byrne, P.; Gray, D.; MacCraith, B.; Paul, B.; Tyrrell, E., Design of a micro-fluidic sensor for high sensitivity copper (II) sensing applications. In *Opto-Ireland 2002: Optics and Photonics Technologies and Applications, Pts 1 and 2*, Blau, W. J.; Donegan, J. F.; Duke, A. F.; MacCraith, J. A.; McMillan, N. D.; Oconnor, G. M.; Omongain, E.; Toal, V.; McLaughlin, J. A., Eds. Spie-Int Soc Optical Engineering: Bellingham, 2003; Vol. 4876, pp 615-622.

Chapter 2: Objectives

Today's wine industry is facing a dynamic global market. The monitoring of several chemical parameters involved in the different steps of the winemaking process allows guaranteeing the quality of the final product. Traditional methods used in the wine cellars are carried out off-line in laboratories with conventional analytical equipment or tedious and time-consuming methods. These off-line measurements have the inconvenience that it is not possible to apply corrective actions on time. Use of microanalytical flow systems will provide real-time monitoring of these parameters and will result an attractive solution for monitoring winemaking processes.

This thesis is focused on the development of several electrochemical (bio)sensors and microanalytical flow systems for the analysis of several parameters of interest in the wine industry. To this aim, the combination of the advantages of the microelectronic technology for sensors fabrication and the fast-prototyping techniques for fluidic systems is proposed. In order to gain this aim, the following general objectives have been set:

1. Fabrication of several sensors with microelectronic technology. These sensors will be pH-ISFETs and ISFETs with ion selective membranes and microelectrodes of platinum and gold as electroactive metal for amperometric measurements. The last will be modified with enzymatic membranes to obtain biosensors.
2. Characterization of these (bio)sensors with electrochemical techniques to assess their response characteristics.
3. Fabrication of flow systems with low-cost and fast-prototyping polymers, such as PSA or PMMA, manufactured by micromilling and CO₂-laser ablation. These flow systems will provide a better functionality of the sensors and automatization of the analytical system.

More specific objectives, addressed to measure specific parameters for wine monitoring will be:

4. Design, fabrication and evaluation of a microanalytical flow system for monitoring the free and total SO₂ concentration in wines samples. The system will combine the use of pH-ISFETs and a gas-diffusion membrane to avoid potential interferences.

5. Design, fabrication and evaluation of a microanalytical flow system based on the above methodology for monitoring the free SO₂ and acetic acid concentration in wines samples. The possibility of simultaneously determining both parameters using the same pH-ISFET and gas-diffusion membrane will be evaluated.
6. Development of a microanalytical flow system for monitoring the malolactic fermentation (MLF) process in red wine samples. This objective will be carried out in several steps:
 - 6.1. Fabrication and optimization of an amperometric bienzymatic L-lactate biosensor based on the modification of the microelectrodes with biological elements. Different strategies of immobilization will be studied and the best one will be applied to the monitoring of the L-lactic acid in samples recollected during the MLF process.
 - 6.2. Fabrication and optimization of an amperometric bienzymatic L-malate biosensor based on the modification of the microelectrodes with biological elements. This will be applied to the monitoring of the L-malic acid in samples recollected during the MLF process.
 - 6.3. Design, fabrication and optimization of a microanalytical flow system based on the two biosensors described above for the simultaneous determination of L-lactate and L-malate. The system will be also validated in samples recollected during the MLF process.
7. Design, development and evaluation of a multiparametric analytical system based on the use of the sensors described in the point 1. The analysis of cava wine samples will be assessed with the combination of the sensor and chemometric tools.

Chapter 3: Experimental

3.1 Reagents and solutions

All reagents used were of high purity, analytical grade or equivalent and were purchased from Sigma-Aldrich (Spain), unless stated otherwise. All solutions were prepared using deionized water (DIW).

For the analysis of free and total sulfur dioxide by using a gas-diffusion microanalytical flow system with pH-ISFET detection, a solution containing 0.1 M sodium hydroxide (NaOH), 5 % (v/v) glycerol and 0.1 M sodium sulfite (Na_2SO_3) was used as stock for preparing the calibration solutions and was renewed every 10 days.

For the determination of acetic acid, stock solutions of 1 M acetic acid and 0.1 M potassium acetate (CH_3COOK) were prepared and renewed every 10 days for the calibration and the carrier solutions preparation, respectively.

During the development of the electrochemical bienzymatic biosensor for the L-lactate determination, 5- μL 0.8 U μL^{-1} Lactate oxidase (LOX, from *Pediococcus* sp., lyophilized powder, ≥ 20 U mg^{-1} solid) aliquots were prepared and stored in a freezer at -20 °C. Horseradish peroxidase (HRP, type VI-A, essentially salt-free, lyophilized powder, 250-330 U mg^{-1} solid) was stored in a refrigerator at 4 °C and used as received. A 0.05 M phosphate buffer (PB) solution prepared with potassium phosphate monobasic (KH_2PO_4) was used at pH 6.8 for all the optimization and electrochemical characterization experiments.

For the fabrication, optimization and characterization of the L-malate bienzymatic biosensor, Diaphorase (DP, from *Clostridium kluveri*, lyophilized powder, 3-20 U mg^{-1} solid) and β -Nicotinamide adenine dinucleotide hydrate (NAD^+ , $\geq 96.5\%$ enzymatic, from yeast) were stored in a freezer at -20 °C and used as received. 15- μL 2.4 U μL^{-1} Malate dehydrogenase (MDH, from porcine heart, freeze-dried material, ≥ 119 U mg^{-1} solid, Sorachim, S.A.) aliquots were prepared and stored in a freezer at -20 °C. A 0.05 M PB solution prepared with KH_2PO_4 and adjusted at pH 7 with NaOH 0.1 M was used for all the optimization and electrochemical characterization experiments.

For the full integrated electrochemical microanalytical flow system for the simultaneously determination of L-malate and L-lactate by amperometric bienzymatic

biosensors, a PB solution with 0.05 KH_2PO_4 at pH 7 and 0.5 M KCl was used for the optimization of the characterization conditions and the electrochemical experiments. 1-mL 0.1 M NAD^+ solution was prepared daily. 15- μL 5 $\text{U } \mu\text{L}^{-1}$ MDH and 10- μL 1 $\text{U } \mu\text{L}^{-1}$ LOX aliquots were prepared and stored in a freezer at $-20\text{ }^\circ\text{C}$.

In case of the multiparametric system based on a portable electronic tongue for the analysis of cava wines, for ISFET calibration, stock solutions with ionic salts with concentrations of 10^{-4} , 10^{-2} and 1.0 M were prepared. In the case of those sensitive to cations (Na^+ , K^+ and Ca^{2+}), the corresponding chloride salts were considered. For the Cl^- and CO_3^{2-} ions, solutions of NaCl and NaHCO_3 , respectively, were prepared. For the pH ISFET calibration, a buffer solution containing 0.04 M boric acid, 0.04 M acetic acid, 0.04 M phosphoric acid and 0.1 M KNO_3 as background was prepared. Five water solutions containing different concentrations of KCl were prepared in order to obtain conductivities in the range between 0.80 and 13.07 mS cm^{-1} . A standard solution of 1416 $\mu\text{S cm}^{-1}$ at $25\text{ }^\circ\text{C}$ (Crison Instruments, Barcelona, Spain) was used for the repeatability study during conductivity tests. ORP standard solutions with nominal potentials of 220 mV and 468 mV at $25\text{ }^\circ\text{C}$ (Panreac, Barcelona, Spain) were used as received. For amperometric measurements, a 0.1 M potassium ferricyanide ($\text{K}_3[\text{Fe}(\text{CN})_6]$, Panreac) solution, a 0.1 M KNO_3 solution and a 0.1 M potassium phosphate buffer at pH 5.5 were prepared. Ethanol 96% (Panreac) and 6 M H_2SO_4 solution were used for the electrodes cleaning.

3.2 Devices and equipment

As RE, a Ag/AgCl (3.0 M KCl) double junction (Orion 92-02-00, Thermo Fisher Scientific Inc., Waltham, MA USA) was used. For measurements with one ISFET, a RE and the ISFET were connected to a home-made electronic interface for recording and amplifying the signal. This was connected to a data-acquisition card (NI USB 6259, National Instruments, Austin, TX) to do the analogical/digital conversion. The signal was treated and displayed with a computer and a software program LabView 2013 (National Instruments).

For the analysis of cava wines, the conductivity sensor, the ORP sensor and the two amperometric gold microelectrodes were connected to a multi-sensor meter developed in the IMB-CNM premises. For the measurements with the six ISFETs, a multi-ISFET meter

also designed and performed in the IMB-CNM premises was used. The devices were connected to a laptop PC and controlled using the LabView software.

The electrochemical measurements carried out with the amperometric biosensors were performed with an Autolab electrochemical workstation (PGSTAT-100 potentiostat – galvanostat, Ecochemie, Uthecht, The Netherlands) controlled with GPES (General Purpose Electrochemical System) software. During the individual biosensor's characterization, the three-electrode cell was completed with an Ag/AgCl RE and the integrated on-chip auxiliary electrode as CE.

For the morphological characterization of the polypyrrole films, an atomic force microscope (AFM, Nanoscope IV from Veeco, USA) operated in tapping mode, a scanning electron microscope (SEM, Auriga from Carl Zeiss, Spain) operated at 5–10 kV and a focused ion beam equipment (FIB, Crossbeam 1560 XB from Carl Zeiss) were used.

3.3 Fabrication of the transducers

3.3.1 pH-ISFETs

The ISFETs were fabricated at the IMB-CNM according to the Negative-channel Metal-oxide Semiconductor (NMOS) technology developed by the GTQ [1]. The ISFETs sensitive to pH has a nitride gate (Si_3N_4). The main steps of the fabrication process for a pH-ISFET are summarized in Figure 3.1. The wafers used are <100> p-type silicon wafers with $1.5 \times 10^{16} \text{ cm}^{-3}$ boron doping for ensuring low field leakage currents. As the first step, a thick field oxide layer (8000 Å) is grown on the silicon wafer. Then, the layer is patterned with the first mask, defining the drain and the source zone which is implanted with phosphorous and a thin layer of oxide is grown and patterned with the second mask (Figure 3.1a). After, a thin oxide is grown (780 Å) and a nitride layer is deposited (1000 Å) using Low Pressure Chemical Vapor Deposition (LPCVD) to define the gate dielectric (Figure 3.1b). A third mask is used to pattern the nitride layer and let only on the gate area. Using the fourth mask, the thin oxide layer is patterned and the electrical contacts are opened (Figure 3.1c). Then, a 0.5 μm aluminum layer is deposited (Figure 3.1d). The metal connections are patterned with the fifth mask and two layers are deposited

(3000 Å of oxide and 4000 Å of nitride) using Plasma Enhanced CVD (Figure 3.1e). Finally, these layers are patterned using last mask (Figure 3.1f). Each chip has a size of $3 \times 3 \text{ mm}^2$ and has a gate area of $10 \mu\text{m} \times 500 \mu\text{m}$ (Figure 3.1g). Apart from the ISFET, the chip contains a MOSFET with the same geometrical characteristics to check the technology.

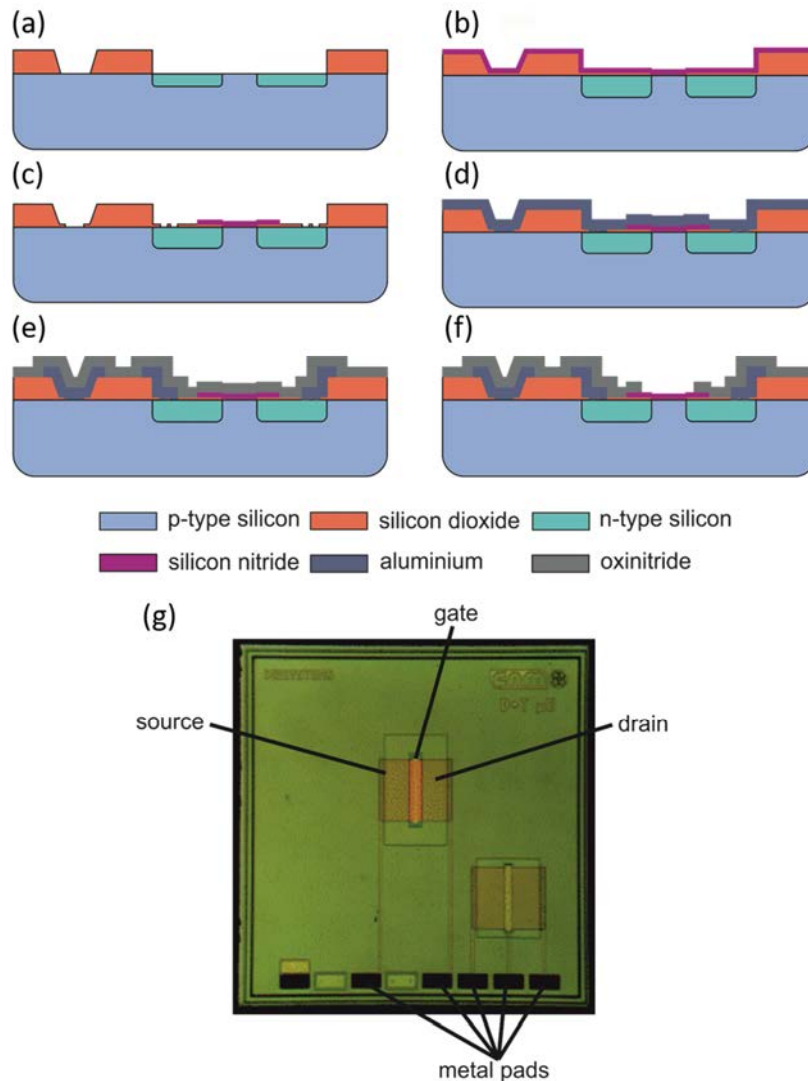


Figure 3.1. Main steps of the fabrication process of pH-ISFET (a-f) and photography of the final chip.

The last step in the process of ISFET fabrication is the dicing of the wafer in individual chips. Then, they are fixed using an epoxy resin (EPO-TEK® H77, Epoxy Technology, USA) on a printed circuit board (PCB) and the electrical connections between

the metal pads of the chip and the copper tracks of the PCB are bonded with gold wires (Figure 3.2). Finally, a 500 μm resin layer formed by a photocurable polymer is deposited to encapsulate and protect the electronics parts of the chip leaving free the ISFET gate [2]. This step avoids the short-circuit by contact between the electrical connections of the chip and the sample solution. This polymer is constituted by EBECRYL® 600 (1,6-Hexanediol diacrylate, Allnex, Germany) and IRGACURE ®651 (Ciba Geigy, Sweden) and it is deposited by semi-automatic process using a photolithographic aligner.

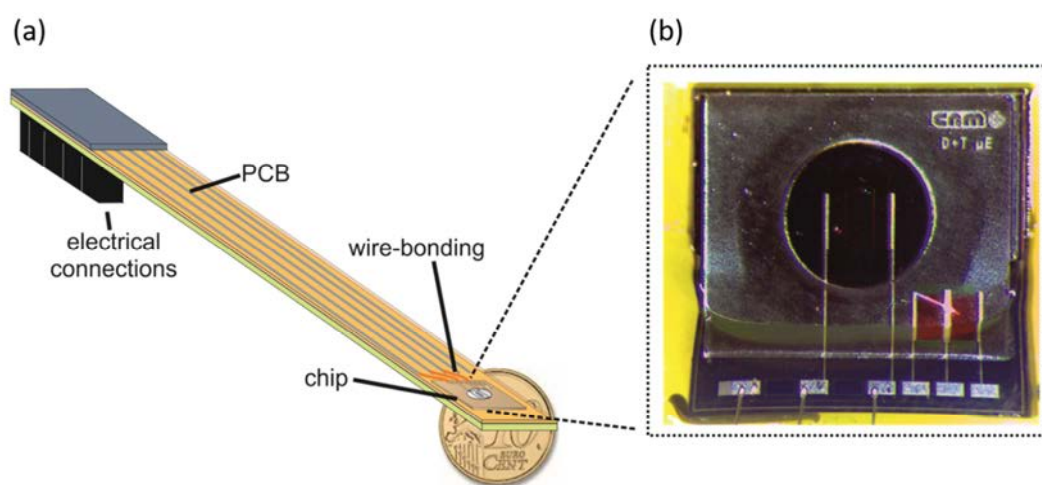


Figure 3.2. (a) Drawing of the encapsulated pH-ISFET on a PCB and (b) photography detailing the ISFET chip.

3.3.2 ISFETs with membranes selective to ions (ChemFETs)

For the fabrication of the ISFETs with membrane selective to ions, a standard protocol developed by the GTQ has been followed [3, 4]. ISFETs with silicon oxide gates (SiO_2) were used in order to improve the adherence of the membranes. Previously to the membrane deposition, the gate of the ISFET is thoroughly cleaned with ethanol (96 %) and DIW, and dried with nitrogen. Then, the gate surface is silanized (using a 3-(trimethoxysilyl) propyl methacrylate solution in ethanol) during 1 h at 80 °C to obtain a good attachment between the acrylate groups of the membrane and the gate chip. After cleaning and drying the chip again, the membrane is deposited.

Membranes are formed by the ionophore, the plasticizer, the lipophilic salt and the polymeric matrix. This polymer is prepared by mixing 82 % of urethane acrylate oligomer

(EBECRYL® 270, Allnex, Germany), 17 % of the reactive diluent and cross linker agent 1,6-hexanediol diacrylate (HDDA, Allnex) and 0.5 % of photoinitiator IRGACURE ® 651 (Ciba Geigy, Sweden). The composition in percentage of each compound of the membrane depends on the ion to determine (Table 3.1). The membrane solution is prepared by mixing all the compounds together and adding 0.5 mL of tetrahydrofuran (THF) to dissolve the mixture. Then, the container with the solution is introduced in an ultrasonic device to homogenize. Finally, the container is leaving open overnight for evaporating the THF solvent.

Table 3.1. Membranes composition (% in weight) for the ISFETs selective to ions.

Ion	Ionophore / %	Lipophilic salt / %	Plasticizer BEHS ⁶ / %	Polymeric matrix / %	Irradiation time / s	Reference
K ⁺	Valinomycin / 2	KtCIPhB ⁵ / 0.5	38.5	59	15	[4]
Na ⁺	TBCATA ¹ / 1.8	KtCIPhB ⁵ / 0.4	38.5	59	15	[5]
Ca ²⁺	TCHOPA ² / 1	KtCIPhB ⁵ / 0.6	38.5	59	15	[6]
Cl ⁻	TDDMACl ³ / 50	–	–	50	60	[5]
CO ₃ ²⁻	Hex-TFA ⁴ / 5.6	TDDMACl ³ / 2.8	34.4	57.2	60	[7]

¹4-tert-Butylcalix[4]arenetetraacetic acid tetraethyl ester; ²N, N', N'-Tetracyclohexyl-3-oxopentanamide; ³Tridodecylmethylammonium chloride; ⁴4-hexyltrifluoroacetophenone; Potassium tetrakis (4-chlorophenyl); ⁶ Bis (2-ethylhexyl) sebacate

In order to obtain membranes with a thickness between 150 and 200 μm , 5 μL of the membrane solution are deposited onto the silanized surface of the ISFET gate. A polyester protector film (MYLAR ®, Isovolta, Spain) is applied over the deposited membrane and it is photocured by irradiating with UV light (365 nm, 22 mW cm^{-2}). Then, the modified gate of the ISFET is slightly cleaned with ethanol and DIW and dried with nitrogen. Finally, the ISFET is immersed overnight in a solution 10^{-3} M of its ion of interest in order to condition the selective membrane.

3.3.3 Microelectrodes

The microelectrodes were fabricated at the IMB-CNM according to standard photolithographic techniques and using a lift-off process [7]. As a first step, the silicon

wafer is oxidized forming a silicon dioxide layer (1000 nm) for isolating the metal electrodes from the silicon wafer. Then, the wafer was spin-coated with a photoresist and exposed to UV light through a patterned mask to define the geometry of the metal electrodes (Figure 3.3a). After, a double metal layer (25 nm titanium and 150 nm platinum, or 20 nm chrome and 100 nm gold) is deposited by electron-beam evaporation (Figure 3.3b). The photoresist is removed with acetone (this is the lift-off process) and the metal electrodes and contacts are exposed. Afterwards, a passivation layer of silicon oxide (600-700 nm) is deposited by plasma enhanced chemical vapor deposition (PECVD) (Figure 3.3c.). Another photoresist layer is then deposited (Figure 3.3d) and developed to define the chip patters (Figure 3.3e). Finally, the area of the metal microelectrodes and the electrical pads are opened by wet etching using hydrofluoric acid (HF) and the photoresist is removed with acetone (Figure 3.3f).

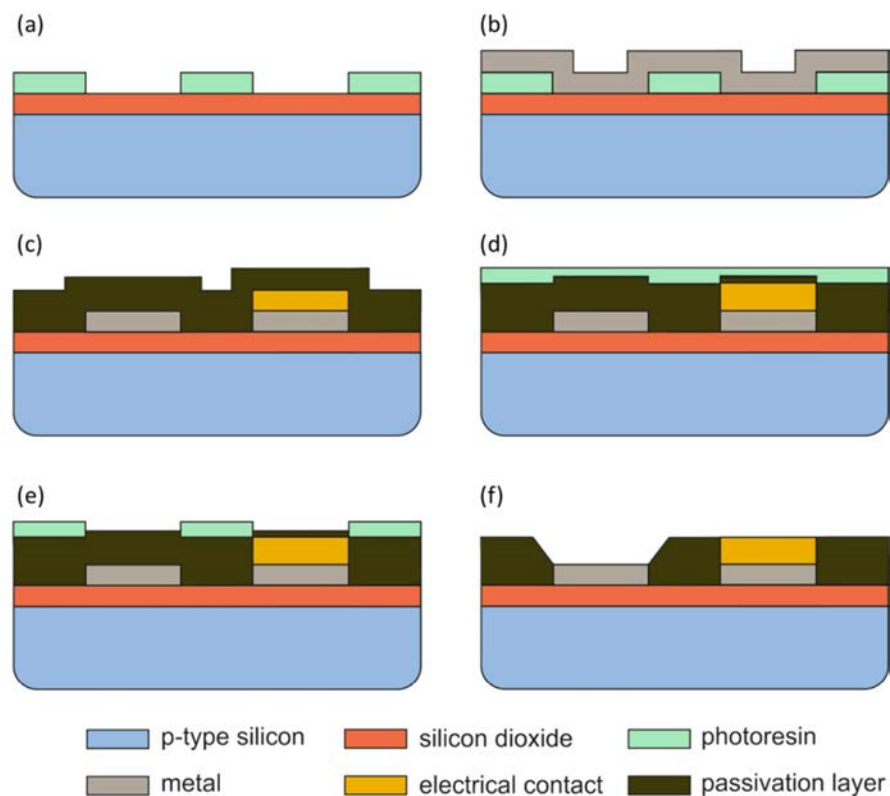


Figure 3.3. Main steps of the fabrication process of the microelectrodes.

During the development of this thesis, four designs of microelectrodes have been used (Figure 3.4). Two of them used gold as metal and the other two used platinum. Regarding the gold microelectrodes, two amperometric chips designs with the size

3 × 3.5 mm were used: one contained only a WE with a surface of 4.510 mm² (Figure 3.4a) and other with an WE inner electrode (1.62 mm²) and a CE surrounding the WE (2.77 mm²) (Figure 3.4b). These were used for individual amperometric measures. A platinum 4-bar microelectrode (3 × 3.5 mm) formed by two rectangular external electrodes (2 × 0.7 mm) and two internal ones (2 × 0.24 mm) separated each of other 0.24 mm (Figure 3.4c) was used for conductimetric tests. Finally, an amperometric platinum microelectrode (11 × 9 mm) formed by four lined up electrodes separated 0.6 mm between them was used for carrying out simultaneous amperometric test with two WEs. From the left to the right, the first electrode (2 × 2.5 mm) was used as CE, the two internal ones (1 × 2.5 mm) were used as WEs and the last one (1 × 2.5 mm) was used as pseudo-RE (Figure 3.4d).

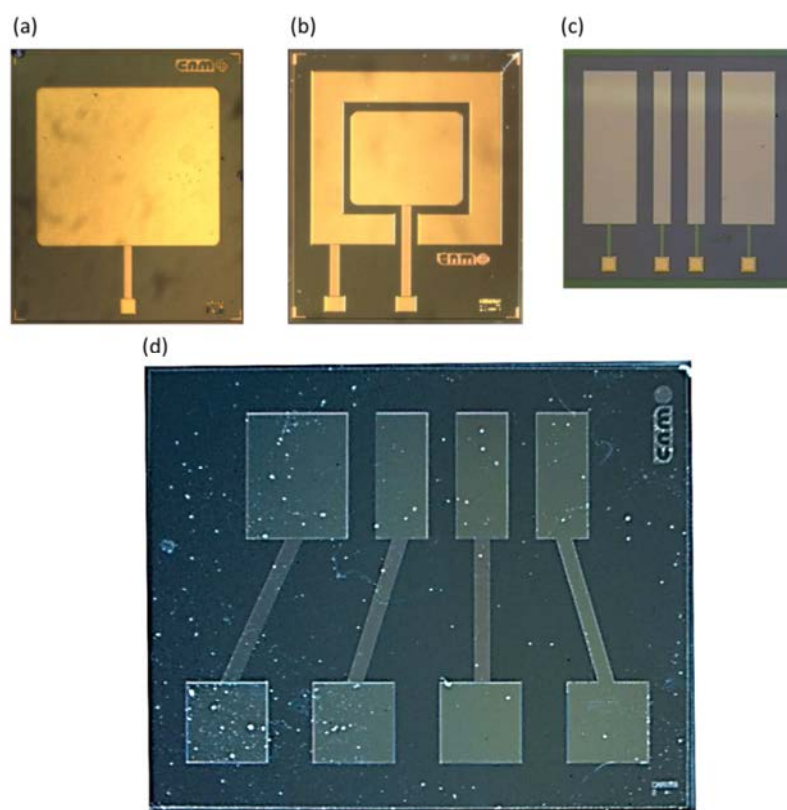


Figure 3.4. Pictures of the microelectrodes: (a) amperometric gold microelectrode formed by one WE.; (b) amperometric gold microelectrode formed by an inner WE and an external CE; (c) platinum 4-bar microelectrode for conductivity tests; and (d) amperometric platinum microelectrode formed –from left to right- by a CE, two WEs and a RE.

Once the microelectrodes were fabricated, they were fixed on PCBs and their pads were wire bonded with the pads of the PCB to establish the electrical connections. Finally,

they were encapsulated as was explained for the ISFETs, but using a heat cured epoxy resin (EPO-TEK® H77).

3.4 Fabrication, optimization and characterization of the amperometric biosensors

3.4.1 Enzymes and enzymes/co-factor ratio assessments

The optimization of the ratio between the enzymes and the co-factor used for the L-lactate and L-malate determinations was carried out off-chip in solution using 96-well low-binding polystyrene enzyme-linked immunosorbent assay (ELISA) plates (Corning Inc., USA) and a Thermo Electron Multiskan EX plate reader (Thermo Fisher Scientific). The absorbance value of the redox mediator potassium ferricyanide ($K_3[Fe(CN)_6]$ $\geq 99\%$) was recorded at 405 nm [8].

In the case of the L-lactate determination, the LOX:HRP ratio was checked using 100- μ L PB solutions containing 0.1 M KCl, 2 mM of potassium ferrocyanide, 2 mM of L-lactate (L-(+)-Lactic acid, $\geq 98\%$) and different amounts of the two enzymes. The LOX activity was set to 0.2 U and six activities of HRP (0 U, 2 U, 4 U, 6 U, 8 U and 10 U) were tested. Therefore, the LOX:HRP ratios studied were 1:0, 1:10, 1:20, 1:30, 1:40.

For the L-malate determination, the enzymes and co-factor ratios were also optimized. Firstly, DP:MDH ratio was studied using 100- μ L PB solutions containing 0.1 M KCl, 2 mM potassium ferricyanide, 2 mM L-malate (L-(-)-Malic acid, $\geq 99\%$) and different amounts of the two enzymes. A fixed DP activity of 0.5 U was set and six activities of MDH (0 U, 1 U, 2 U, 3 U, 4 U and 5 U) were tested, these resulting in DP:MDH ratios of 1:0, 1:2, 1:4, 1:6, 1:8 and 1:10, respectively. Secondly, (DP:MDH): NAD^+ ratio was optimized using in this case 100- μ L PB solutions containing 0.1 M KCl, 2 mM of potassium ferricyanide, 2 mM of L-malate, 0.5 U of DP, 3 U of MDH and different amounts of NAD^+ (0 mM, 0.05 mM, 0.1 mM, 0.2 mM, 0.5 mM, 1 mM and 2 mM) whose corresponding (DP:MDH): NAD^+ ratios were 1:0, 1:2, 1:4, 1:6, 1:8 and 1:10, respectively.

In each case, the solution was analyzed in triplicate after being stirred for 45 s and then leaving it 10 min for taking place the enzymatic reaction.

3.4.2 Immobilization strategies to fabricate the amperometric biosensors

Before the modification of the microelectrode surface, this was cleaned and activated according to previous works by our group [9]. Firstly, they were carefully cleaned using 96 % ethanol, H₂SO₄ 6 M and DIW. Then, an electrochemical activation was performed in a 0.1 M KNO₃ solution by applying 20 cyclic voltammetric scans in a potential range from +0.8 V to -2.2 V at 100 mV s⁻¹. The effectiveness of this activation process was verified in a 0.1 M KNO₃ solution containing 1 mM potassium ferricyanide [10].

Three common immobilization strategies [11] were evaluated for the L-lactate biosensor: physical adsorption with cross-linking, covalent immobilization and polymer entrapment. They were compared in terms of sensitivity, linear range, limit of detection to L-lactate and working stability over 5 days. As the process associated with the L-lactate determination was based on the reduction of the oxidized redox mediator (potassium ferrocyanide), chronoamperometric measurements were carried out at +0.075 V (vs Ag/AgCl) in PB containing 0.1 M KCl, 2 mM potassium ferrocyanide and 80 U HRP (when was necessary) and increasing concentrations of L-lactate, in a range from 1×10⁻⁷ to 1×10⁻³ M. Each L-lactate concentration was measured in triplicate. Then, for the biosensor fabricated with the selected immobilization strategy, selectivity studies were carried out in PB solutions containing 0.1 M KCl, 2 mM ferrocyanide and 1×10⁻⁵ M concentrations of glucose, glycerol, gluconic acid, L-malate, tartaric acid, fructose, acetic acid, ethanol or ascorbic acid interferences. Besides, the working stability of the developed biosensor fabricated with the selected immobilization strategy was tested in an extended time by carrying out periodic calibrations (every 2 or 4 days) in a L-lactate concentration range from 1×10⁻⁶ M to 1×10⁻⁴ M during 52 days. All the biosensors were thoroughly rinsed with DIW and stored in PB at 4°C when not in use.

For the physical absorption and the covalent immobilization, a gold one-microelectrode electrochemical cell was used. In case of the polymer entrapment strategy, gold two-microelectrode electrochemical cells and platinum four-microelectrode electrochemical cells were used as transducers.

3.4.2.1 Physical adsorption and cross linking

In order to check the adsorption of the enzymes onto the gold microelectrodes, the study was carried out in several steps. Firstly, the bienzymatic reaction associated to the L-lactate determination was evaluated immobilizing only the LOX on the gold surface. 10 μL of the PB solution containing 4 U of LOX was dropped on the amperometric microelectrode (Figure 3.5a). Secondly, both enzymes (LOX and HRP) were immobilized by dropping 10 μL of the PB solution containing 4 U of LOX and 80 U of HRP on the transducer surface (Figure 3.5b). Finally, 10 μL of the PB solution containing 4 U of LOX and 80 U of HRP, 1% (v/v) glutaraldehyde as cross linker and 20 mg mL^{-1} of bovine serum albumin (BSA) as inert protein was dropped on the gold surface (Figure 3.5c).

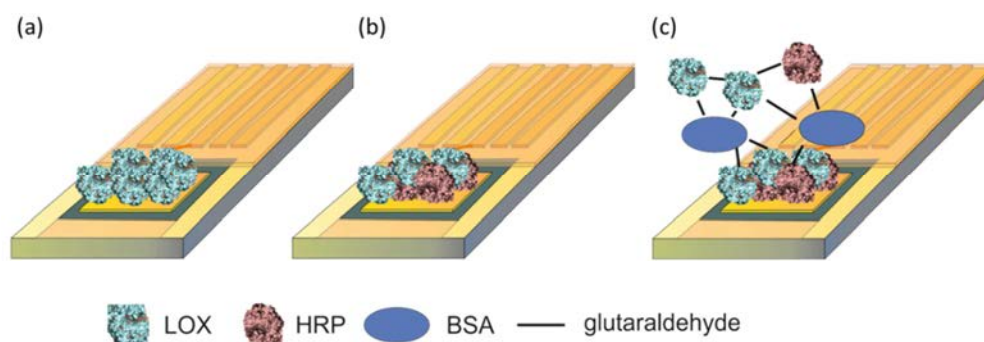


Figure 3.5. Scheme of the steps for the physical adsorption with cross linking strategy.

3.4.2.2 Covalent immobilization

A self-assembled monolayer (SAM) [12] was formed on the surface of the gold transducer immersing the microelectrode 1 h at room temperature into a 10 mL of dimethyl sulfoxide (DMSO) solution with 4 mM dithiobis(succinimidyl propionate) (DTSP) (Figure 3.6a). After, the microelectrode was thoroughly rinsed with DMSO and distilled water in order to remove the thiol molecules weakly adsorbed. 10 μL of a PB solution containing 4 U of LOX and 80 U of HRP was then deposited on the surface of the SAM-modified microelectrode and kept at 4 $^{\circ}\text{C}$ overnight (Figure 3.6b). In this way, both enzymes were covalently attached to the carboxylic groups of the DTSP. Finally, the modified microelectrode was immersed in a 10 mL of PB solution with 0.05 % (v/v) of Tween® 20 during 1 h under stirring for removing the adsorbed enzymes molecules from the surface of the microelectrode (Figure 3.6c).

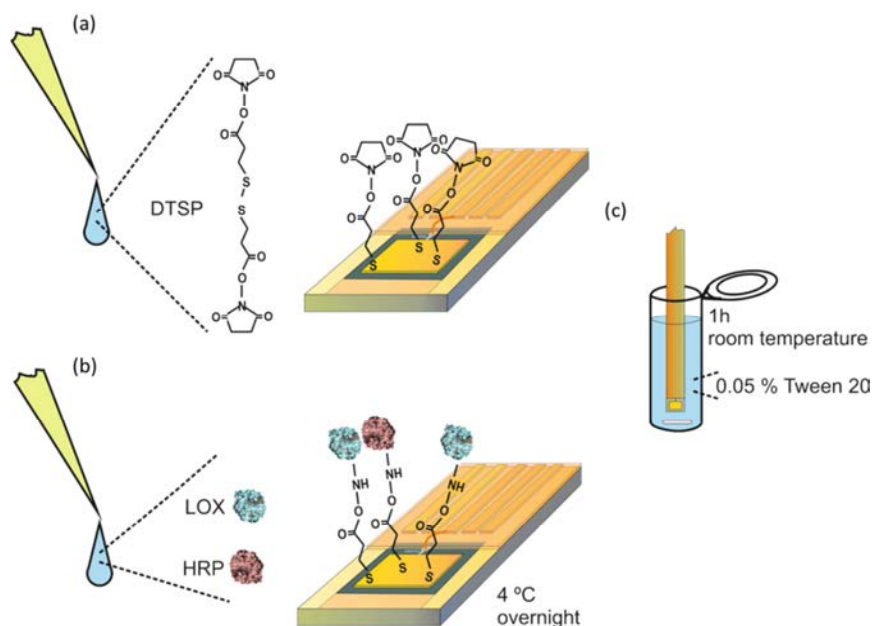


Figure 3.6. Scheme of the steps of the covalent immobilization strategy.

3.4.2.3 Entrapment into electrosynthesized polypyrrole membrane

For the polymer entrapment immobilization method, pyrrole (reagent grade, 98%) was distilled every week and stored in a freezer at $-20\text{ }^{\circ}\text{C}$. Electrosynthesis of all the PPy films were carried out under potentiostatic conditions at a set potential optimized by cyclic voltammetry. In order to ensure a low consumption of reagents during the polymer film fabrication, a $20\text{ }\mu\text{L}$ cell formed by two $3\text{ mm} \times 30\text{ mm} \times 20\text{ mm}$ PMMA layers was designed and fabricated using a CO_2 -laser system (Epilog Mini 24, Epilog Laser, USA) (Figure 3.7). This laser writer is controlled by a PC as a conventional printer. The bottom layer was milled to host the transducer. The top layer was also machined to define the well of the electrochemical cell. Both parts were fixed with screws and an O-ring was used to avoid the fluid leakage. A 2-mm diameter stainless steel wire and a 0.5 mm diameter silver wire were used as CE and pseudo-RE, respectively.

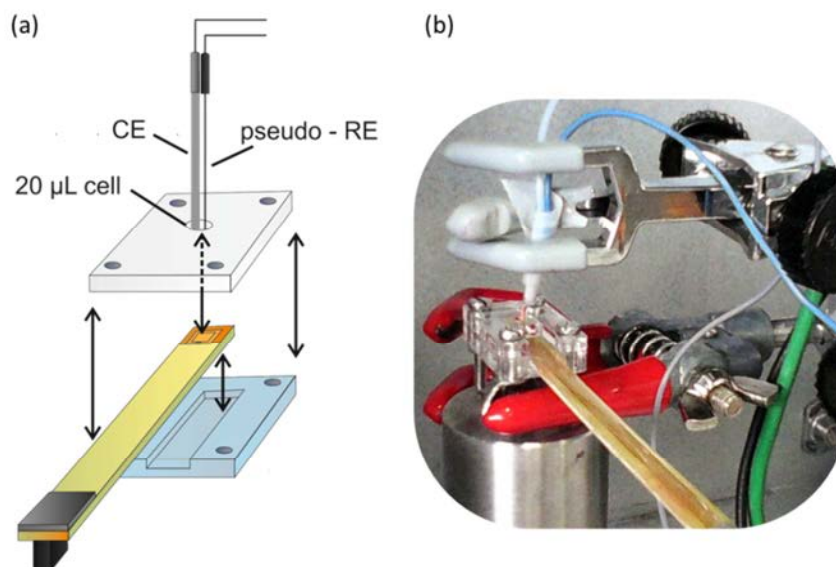


Figure 3.7. (a) Drawing of the cell and (b) photography of the set up used for the PPy membrane fabrication.

3.4.2.3.1 *L*-lactate amperometric biosensor

The *L*-lactate biosensor was the first one fabricated and optimized following the polymer entrapment strategy (Figure 3.8). Therefore, the chemical parameters of the polymerization conditions were optimized. The nature of the required counter-ion (or dopant agent), the pyrrole concentration and the number of enzymes in the electrogeneration solution were studied. As counter-ion, three electrolytes (lithium perchlorate (LiClO_4), potassium nitrate (KNO_3) and potassium chloride (KCl)) were tested in 20 μL PB (pH 7) containing 0.5 M pyrrole, 4 U of LOX and 80 U of HRP. The counter-ion concentration was fixed to 0.1 M [13]. Then, the effect of the monomer concentration and the concentration of both enzymes were sequentially studied in PB solutions. Four pyrrole concentrations (0.2 M, 0.4 M, 0.5 M and 0.8 M) and three LOX:HRP activity ratios (2:40, 4:80 and 6:120, in U) were selected. The accumulation charge was fixed to 500 mC cm^{-2} , according to the bibliography [14], in order to guarantee an efficient enzyme entrapment and the reproducibility of the PPy film thickness.

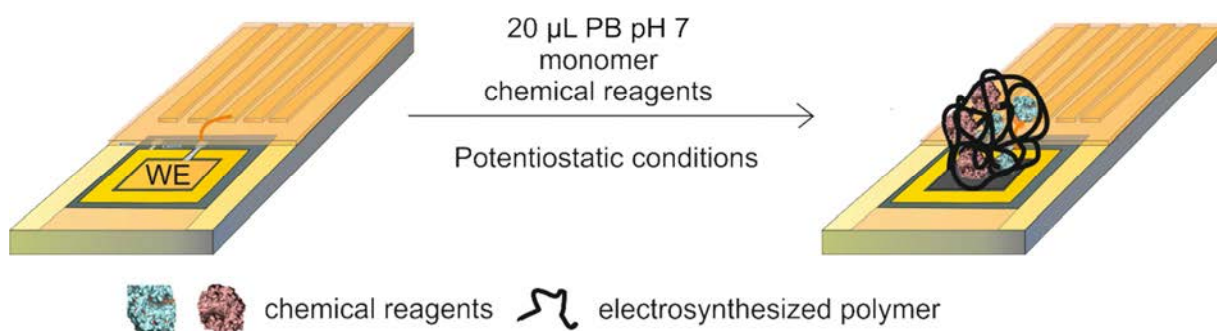


Figure 3.8. Scheme of the polymer entrapment immobilization strategy.

3.4.2.3.2 *L*-malate amperometric biosensor

The *L*-malate biosensor was fabricated with the same electrogeneration conditions previously optimized for the *L*-lactate biosensor. In contrast to the *L*-lactate biosensor, the redox mediator was also incorporated to the PPy membrane. Thus, the electrogeneration was carried out in two consecutive potentiostatic steps. In the first step, the redox mediator was entrapped in the polymeric membrane for ensuring the good electron transfer with the transducer surface and avoiding competition with the other species (enzymes and co-factor) during the membrane growth. The concentration of the redox mediator was fixed to 10 mM to ensure its excess against the other chemical reagents involved in the bienzymatic process. The accumulation charge during this electrogeneration was fixed to 250 mC cm⁻².

In order to decide the most convenient redox mediator for this biosensor, previous studies on the electrocatalytic oxidation of NADH [15, 16] were followed and eight organic compounds (2,6-Dichlorophenolindophenol sodium salt hydrate $\geq 90\%$, Gallocyanine 90%, Toluidine Blue O 80%, Nile Blue A $\geq 75\%$, 1,1'-Dimethylferrocene 95%, Methyl Red sodium salt, Ferrocene 98% and Tetrathiafulvalene 97%) and two inorganic salts (Hexaammineruthenium (III) chloride (Ru(NH₃)₆Cl₃ 98%, HAR) and Potassium ferricyanide) were tested as redox mediators. Cyclic voltammetric experiments were performed using the gold microelectrode, in 10 mL PB solutions (pH 7) containing 0.1 M KCl and 2 mM of each redox mediator. In case of 1,1'-dimethylferrocene and tetrathiafulvalene, a 10% ethanol was added to the aqueous solution in order to improve their solubility. The redox processes ascribed to each mediator were compared in terms of reversibility, current and redox potential values as well as solubility. Then, they were

incorporated to the PPy membrane during its electrogeneration. The stability inside the membrane was tested by comparing the cyclic voltammogram response in PB solutions right after the electrosynthesis and 24 h later.

Once chosen the redox mediator, the enzymes (MDH and DP) and the co-factor (NAD⁺) were entrapped in a new PPy membrane, fixing the accumulation charge to 500 mC cm⁻². Using these electrosynthesis conditions, three different biosensor architectures that differ in the immobilization of the different components, were assessed: Biosensor 1, the redox mediator was not immobilized; Biosensor 2, the NAD⁺ co-factor was not immobilized and Biosensor 3, both the redox mediator and the co-factor were immobilized on the microelectrode surface.

Chronoamperometric measurements were carried out by applying a set overpotential that depended on the selected redox mediator. This potential allowed re-oxidizing the reduced mediator generated during the bienzymatic process and the faradaic current recorded was stoichiometrically related to the L-malate concentration in the sample. The biosensors were calibrated in 10 mL PB solutions (pH 7) containing L-malate in a concentration range between 1×10⁻⁷ M and 1×10⁻⁵ M. All the measurements were done by triplicate.

Firstly, a study of the working stability of the different biosensor architectures was performed. The study consisted of periodic calibrations for over 40 days. The biosensors were stored in PB at 4 °C when not in use.

Once the more stable architecture was selected, the biosensor performance was assessed in terms of repeatability, reproducibility, sensitivity, linear range and limit of detection to L-malate using three biosensors fabricated under the same experimental conditions.

In order to evaluate the selectivity of the optimized biosensor, chronoamperometric measurements were performed in PB solutions containing 5×10⁻⁷ M concentrations of glycerol, glucose, gluconic acid, fructose, acetic acid, citric acid, ethanol, L-lactate, tartaric acid, or ascorbic acid as interferences.

3.5 Fabrication of the microanalytical flow systems

3.5.1 Systems based on pH-ISFETs

The developed microanalytical flow systems were based on the separation of the analyte of interest (SO_2 or acetic acid) from the sample by using the acid/base characteristics of the analyte and a gas-diffusion membrane. The cells including the gas-diffusion membrane and the pH-ISFET were designed and fabricated for each application. For total SO_2 determination, a pretreatment chamber for the sample was also designed and machined.

3.5.1.1 Free and total SO_2 determination

For the total sulfur dioxide determination, a cell for an alkaline pretreatment of the sample was designed and fabricated with a micromilling machine (Roland MDX-40, Roland Digital Group Iberia, Spain) (Figure 3.9). This was formed by two pieces of PMMA, one defining the chemical reactor of 3 ml volume with a height of 10 mm and an inner diameter of 8 mm, and the other (height of 3 mm and diameter of 15 mm) for covering the reactor and allowing the fluidic connections. Finally, two screws were used for fixing both pieces.

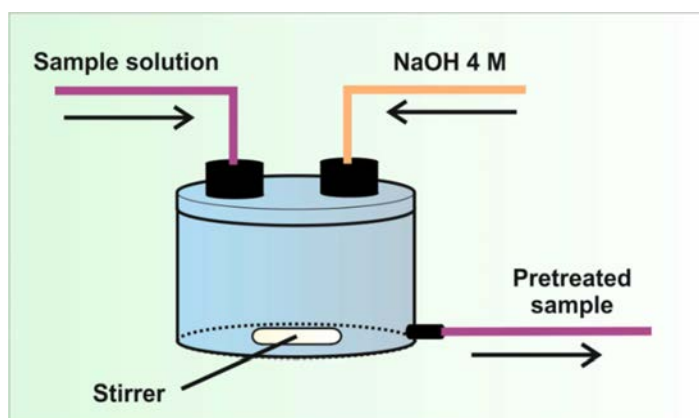


Figure 3.9. Scheme of the alkaline pretreatment cell used for the total SO_2 determination.

A homemade PMMA gas-diffusion cell containing a polyvinylidene fluoride (PVDF, VHP09050 Durapore®, Hydrophobic Plain White, 0.22 μm pore size, from Merck Millipore, Darmstadt, Germany) gas-permeable membrane was used to separate the analyte from the sample. This type of hydrophobic membrane has already demonstrated a good

performance for the proposed application [16]. The gas-diffusion cell was formed by four individual PMMA layers (60 mm width×60 mm length) fabricated with a micromilling machine (Figure 3.10). The two external layers (5 mm of thickness) allowed the coupling of the flow tubes to the two internal layers (3 mm of thickness). Using a total of eight screws, the PVDF gas-permeable membrane was fixed between the two internal layers. A concentric spiral was defined on each internal layer in order to obtain the highest area of contact between both sides of the membrane.

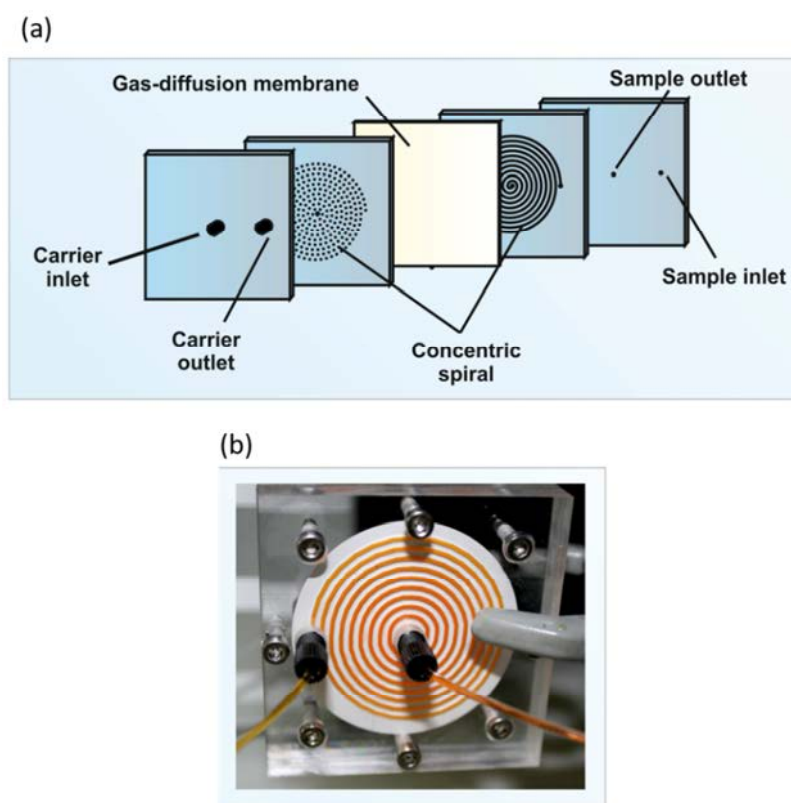


Figure 3.10. (a) Layer-by-layer scheme and (b) picture of the gas-diffusion cell.

The flow cell hosting a pH-ISFET and an Ag/AgCl (3.0 M KCl) RE for the flow measurement was also designed and fabricated. This cell was made of PMMA and aluminum (Figure 3.11). This cell was fabricated by the external company Blumeprot (Vilassar de Mar, Spain) on request. Figure 11c details the design inside the cell, where the pH-ISFET and the RE are placed, and the fluidic contacts between them are depicted. The carrier solution enters on top, arrives to the sensor and flows till the RE before leaving the

cell. The use of O-rings in the RE hole avoids the leakage of liquid and the O-ring on the pH-ISFET allows its adjustment in the cell.

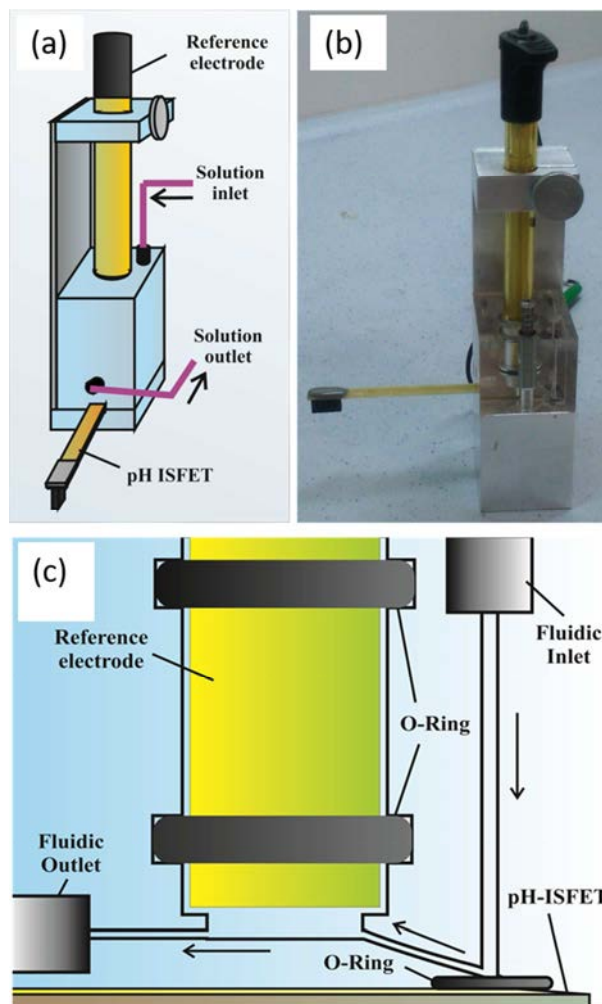


Figure 3.11. (a) Detailed scheme of the flow cell containing the RE and the pH-ISFET. (b) Picture of the measurement cell. (c) Detailed scheme of the cross-section cell. The arrows indicate the flow direction.

3.5.1.2 Free SO_2 and acetic acid determination

The flow assembly containing the sensors and the gas-diffusion chamber were designed and fabricated using PMMA and pressure-sensitive-adhesive (PSA) mechanized with a CO_2 -laser system. This flow assembly has total dimensions of 3 cm width, 7 cm length and 2 cm height and was fabricated with different layers of PMMA and PSA (Figure 3.12). This defines a 150 μ L chamber for the gas diffusion process (5 mm width \times 10 mm length \times 3 mm height). A space was also defined for positioning the pH-ISFET with the

fluidic channels of the assembly. Finally, a 340 μL chamber for a standard RE was also mechanized. The flow channels had a diameter of 1 mm. There were two fluidic inlets and two fluidic outlets to full control the performance of the assembly. The PMMA layers were fixed using 2-layer-PSA as adhesive. The two fluidic PMMA/PSA structures were fixed with 8 screws (1 mm diameter) to allow easy assembly and disassembly of the system. Two O-ring junctions were used for the ISFET and the RE in order to avoid the fluidic leakage. The PVDF gas-diffusion membrane was the same that was used for the free/total SO_2 determination system described previously. As RE, a double junction Ag/AgCl was used. The pH-ISFET and the RE were connected to a data-acquisition card controlled by a PC.

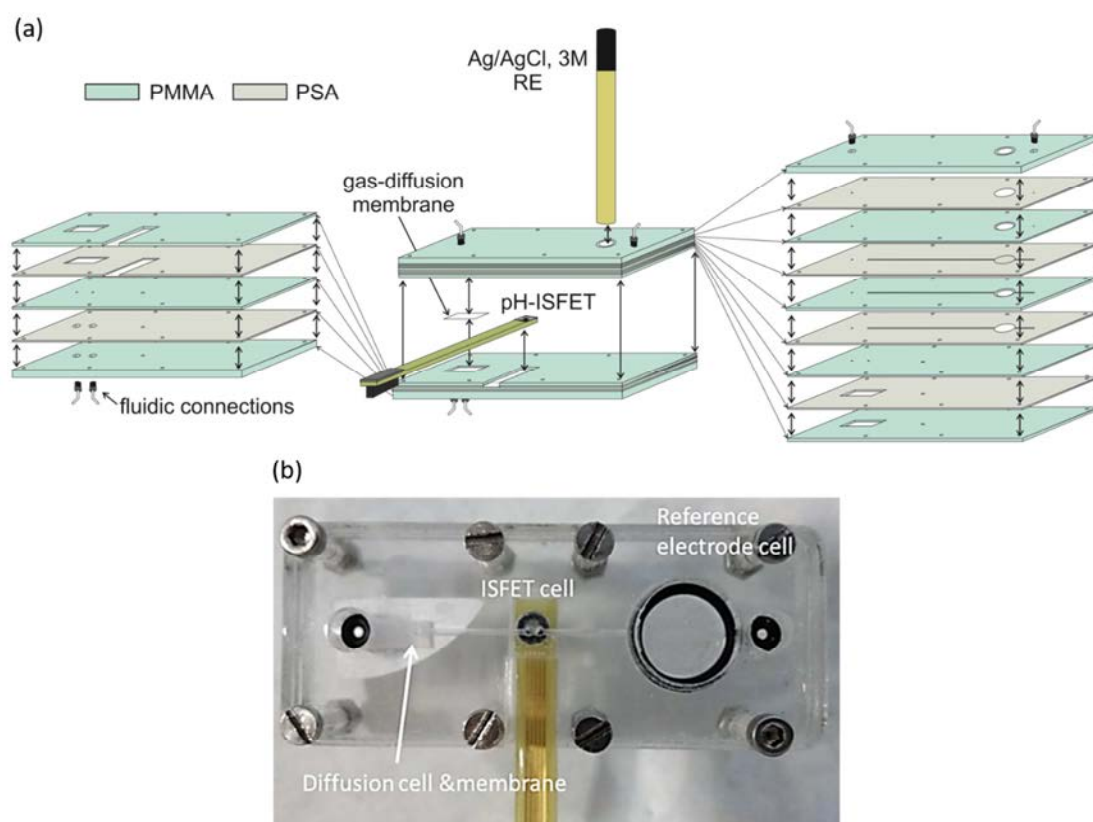


Figure 3.12. (a) Drawing and (b) photography from the top of the PMMA/PSA assembly used for SO_2 and acetic acid determination.

3.5.2 Simultaneous determination of L-lactate and L-malate

For measuring simultaneously L-lactate and L-malate, the sensor chip was integrated in a low-cost, robust and portable PMMA/PSA module formed by two structures with several individual layers (17 mm width \times 30 mm length) of different thickness. The

novelty of this chamber regarding the previous described is that the sensor chip has not been encapsulated in a PCB, being easier its integration in the fluidic chamber. The first structure is used to place the silicon chip. A PMMA layer (3 mm thick) is fixed to other PMMA layer (0.5 mm thick) using 2-layer-PSA as adhesive. In this way, the defined hold (9 mm width×11 mm length×0.5 mm height) allowed the positioning and alignment of the silicon chip with the fluidic part contained in the second PMMA/PSA structure (Figure 3.13a). The second structure had a different design depending if it was used for the fabrication or for the characterization of the biosensors. For the fabrication of the biosensors, the second structure is formed by a PMMA layer (3 mm thick) which sealed a 50 μ L reservoir (facing with the platinum microelectrodes of the silicon chip) and a space (2.5 mm width×10.5 mm) to fix the electrical connections (Figure 3.13b). For these connections, four spherical conn spring loaders (0.5 mm width×2.54 mm length, RS Components, Switzerland) were used. The electrochemical cell is completed with a 2-mm diameter stainless steel wire and a 1.5 mm diameter Ag /AgCl (3M KCl) flexible Dri-Ref (World Precision Instruments, Sarasota, USA) used as CE and RE, respectively.

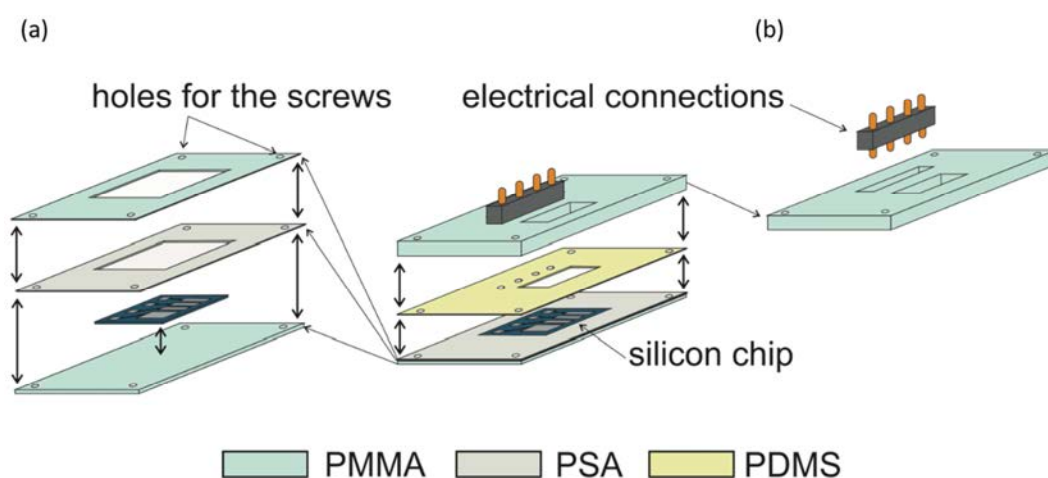


Figure 3.13. Drawing of the cell used for the biosensors fabrication formed by (a) the structure placing the chip and (b) the structure containing the electrochemical cell.

The surface of the platinum microelectrodes was electro-modified applying the conditions optimized for the individual biosensors (see section 3.4.2.3). For deposition of the PPy film, a cell potential of +0.7 V (vs the Dri-Ref) was applied in PB solutions (generation solution) containing 0.4 M pyrrole, 0.1 M KCl and the entrapped enzymes. For

making the L-lactate biosensor, the generation solution incorporated 10 U of LOX and 200 U of HRP, and these were entrapped in a 500 mC cm⁻² electrosynthesized PPy membrane. In case of the L-malate biosensor, the reagents were entrapped in two membranes. The first membrane (250 mC cm⁻²) entrapping the redox mediator. Secondly, a 500 mC cm⁻² PPy membrane was electrosynthesized using the generation solution and also containing 7.5 U of DP and 45 U of MDH for entrapping the enzymes.

In all cases, after the electro-deposition, the microelectrodes were cleaned with a PB solution for removing the reagents physically adsorbed on the PPy surface and were stored at 4°C in PB solution when they were not in use.

For the characterization of the biosensors in the flow cell, the second PMMA/PSA structure was formed by eight layers (17 mm width/30 mm length). This structure (Figure 3.14) contained the characterization reservoir, the fluidic channels and the electrical connections with the chip. The small-size reservoir (10 μL) faced with the four microelectrodes of the chip. The fluidic channels (1 mm width, 7 mm length) were connected with two holes (1mm diameter) to enable fluidic connection between layers. The top PMMA layer (5 mm) contained 5 mm fitting threads (facing with the holes of the other layers) for connecting with fittings and allowing the fluidic inlet and outlet of the samples. The layers were bonded using 70 μm thick double-sided PSA as adhesive. The samples were pumped through Teflon pump tubes (1.0 mm inner diameter) using a peristaltic pump. The PMMA fluidic structures were fixed with 1 mm diameter screws (allowing easy assembly and disassembly of the system) and using a 180 μm thick PDMS layer to avoid the fluid leakage.

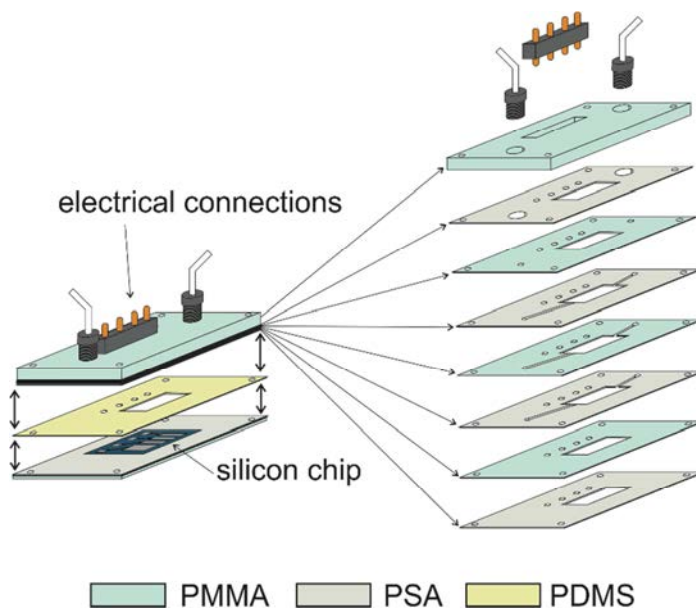


Figure 3.14. Drawing of the cell used for the biosensors characterization

3.6 Optimization of the microanalytical flow systems

3.6.1 Free and total SO₂ determination

The microanalytical flow system for SO₂ measurement illustrated in Figure 3.15 was fabricated. Two peristaltic pumps (403U/VM3, Watson Marlow, UK) were used to pump carrier and sample solutions. Teflon pump tubes had an internal diameter of 1.0 mm (Teknokroma, Barcelona, Spain) and Polyether ether ketone (PEEK) tubes connecting different devices had 0.75 mm of inner diameter (Teknokroma). The system is formed by the gas-diffusion module described in the Figure 3.10 for separating the SO₂ from the sample and the measurement cell hosting the pH-ISFET and the RE described in the Figure 3.11. The electrochemical cell was connected to a data-acquisition card controlled by a PC. For the determination of total SO₂, the sample was treated in the cell described in the Figure 3.9 with an alkaline solution in order to release all the bound sulfur dioxide of the sample [17]. This 3-mL cell was placed in the sample channel as depicted in figure 3.15.

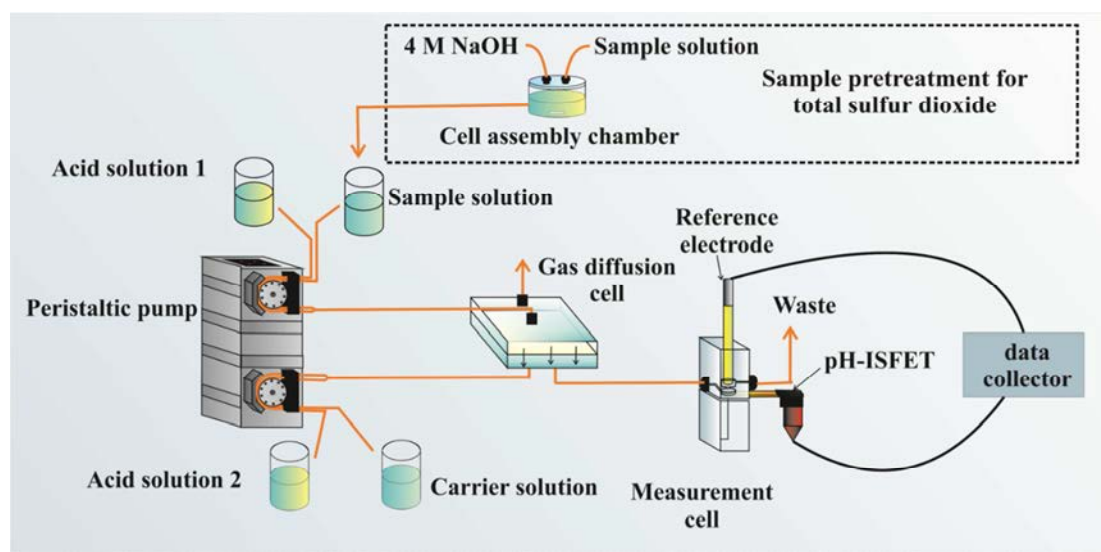


Figure 3.15. Drawing of the flow system used for the determination of free and total sulfur dioxide.

For the free SO₂ measurement, the sample or calibration solution was pumped and mixed 1:1 in volume with a HCl solution (Acid solution 1) to convert all the hydrogen sulfite present to SO₂. In parallel, the pH of the carrier solution was also adjusted by mixing 1:1 in volume with the Acid solution 2. When the sample stream arrives to the gas-diffusion cell, the SO₂ diffuses through the membrane and it is collected by the acceptor

solution. Then, the pH change generated in the carrier is measured with the ISFET (in mV) under stop-flow conditions during 2 min for each sample and the analytical signal collected corresponds to the mean potential value of the last 30 s. The calibration of the system was performed in triplicate using five solutions in the range 1 mg L^{-1} - 60 mg L^{-1} of SO_2 in DIW with 12 % (v/v) ethanol. In order to obtain the calibration curve, this signal (in mV) was plotted versus the logarithm of the SO_2 concentration (in mg L^{-1}).

For the determination of total SO_2 , for the sample pretreatment, 1.5 mL of sample was mixed with 1.5 mL of 4 M NaOH and let to react. After the treatment of the sample was completed, the sample (pH around 11) was mixed with a high concentration of HCl (Acid solution 1) to reduce in situ the pH value below 1. The flow system for the carrier channel was the same as described above for the determination of free SO_2 . Five solutions of sulfur dioxide in the range of 30 mg L^{-1} - 300 mg L^{-1} were used to obtain the calibration curve.

3.6.1.1 Optimization of the flow system and analytical assessment

Several hydrodynamic and chemical parameters of the flow system were optimized for improving the analytical characteristics of the SO_2 detection.

For that, a set of calibration solutions in the range from 30 mg L^{-1} to 300 mg L^{-1} of total sulfur dioxide were used to perform the calibration in triplicate. Firstly, the length of the tubes for mixing the sample with the HCl 4 M was a critical parameter to achieve the pH adjustment. The optimization of tubes' length was carried out for the determination of total sulfur dioxide since a more drastic change in pH is required (from pH 11 to 1). Two lengths of tubes (10 and 20 cm) were checked using a flow rate of 1.00 mL min^{-1} . The alkaline pretreatment of the sample was performed by mixing 1:1 the sample with NaOH 4 M during 3 min under stop flow conditions. The influence of four different flow rates (0.25 , 0.50 , 0.75 and 1.00 mL min^{-1}) was also checked. In relation to the performance of the gas-diffusion cell, it was tested if the diffusion of SO_2 could be improved stopping the flow –after the 5 min under continuous flow- for 2 min before the analysis. Moreover, the flow mode - parallel current and countercurrent flow- in both sides of the membrane was also checked.

Regarding the alkaline pretreatment of the sample for the determination of total sulfur dioxide, the time of digestion in stop flow (1, 2 or 3 min) and the stirring conditions were optimized by using a set of 16 wine samples and comparing the results obtained with a commercial equipment based on the iodimetric method.

In order to avoid the hysteresis and the clogging of the diffusion membrane, a method for cleaning the system was proposed and tested. The aim was to recover the baseline of the carrier solution after each measurement with wine samples. For that, a HCl solution with a concentration in the range from 0.1 M to 1 M was flowed at 1 mL min^{-1} through the wine sample channel between 1 and 5 min.

After the hydrodynamic parameters were fixed, the chemical parameters were optimized. The HCl concentration of the Acid solution 1 channel was tested in order to assure the total conversion of hydrogen sulfite to sulfur dioxide in the sample. The experiments consisted on mixing (1:1 in volume) a set of 3 wine samples with a set of HCl solutions (Acid solution 1). These solutions were from 0.1 M to 1 M and from 1 M to 4 M HCl for the free and total sulfur dioxide, respectively. The final pH of the mixed solution was checked using a pH-meter for ensuring a pH value below 1. In the same way, the HCl concentration in the Acid solution 2 channel was varied (from 10^{-7} M to 10^{-3} M) to study five different pH values of the carrier solution, specifically pH 3.50, 4.00, 4.75, 6.00 and 6.50.

Finally, the matrix effect was tested in the presence of some substances contained in wine that could affect the response of the system. For that, calibration curves in a range from 1 mg L^{-1} to 60 mg L^{-1} of free SO_2 were carried out adding an average concentration of several compounds in the calibration solutions [18]. First 12 % ethanol, then the most common ions ($7.75 \text{ mg L}^{-1} \text{NO}_3^-$, $500 \text{ mg L}^{-1} \text{H}_2\text{PO}_4^-$, $700 \text{ mg L}^{-1} \text{SO}_4^{2-}$, $210 \text{ mg L}^{-1} \text{K}^+$, $107.2 \text{ mg L}^{-1} \text{Mg}^{2+}$, $90.6 \text{ mg L}^{-1} \text{Ca}^{2+}$ and $100 \text{ mg L}^{-1} \text{Cl}^-$) and finally adding 5 g L^{-1} of acid malic and 2.5 g L^{-1} of tartaric acid.

3.6.2 Free SO_2 and acetic acid determination

A scheme of the fluidic performance of the assembly for free SO_2 and acetic acid determination is schematized in Figure 3.16. The difference between the two

microanalytical flow systems is that for the acetic acid detection, the channel with HCl for conditioning the carrier solution is removed and only the carrier channel is used. This assembly integrates the diffusion cell and the sensing chamber in the same module. Two peristaltic pumps (403U/VM3) were used for pumping the solutions. The peristaltic pumps and the PMMA assembly were connected with Teflon pump tubes with an internal diameter of 1.0 mm (Teknokroma).

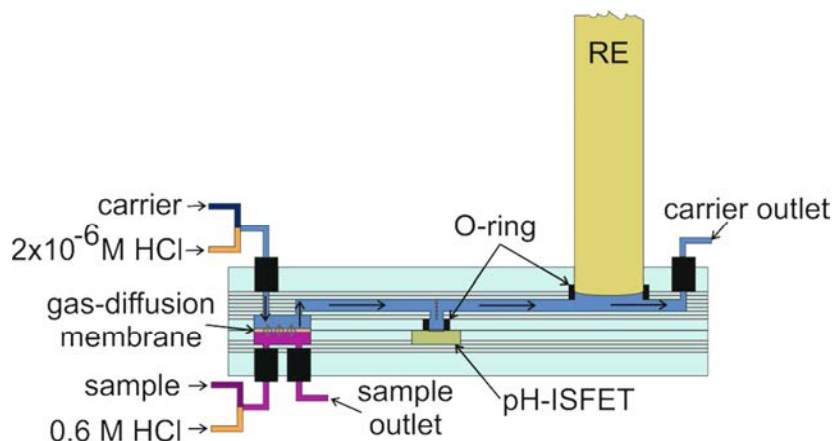


Figure 3.16. Scheme of the assembly for the free SO₂ and acetic acid determination.

3.6.2.1 Free SO₂

The optimized chemical parameters for the free SO₂ microanalytical flow system of the previous section were used in this case. At the lower side the gas-diffusion chamber, the sample (or calibration solution) was pumped at 0.25 mL min⁻¹ and mixed 1:1 in volume with a 0.6 M HCl solution. The calibration solutions (5- 60 mg L⁻¹ of SO₂) were prepared every day from a stock solution of 400 ppm of SO₂, diluted in a buffer solution (without SO₂). The last two solutions were provided by the company Biosystems. At the upper side, the carrier solution was mixed 1:1 with 2×10⁻⁶ M HCl to get pH 6. The carrier was prepared every day from a stock solution as was explained for the free and total SO₂ microanalytical flow system. When the adjusted sample arrived to the gas-diffusion cell, the SO₂ diffused through the membrane and it was collected by the carrier solution. The pH change generated in the carrier was measured with the pH-ISFET.

3.6.2.2 Acetic acid

For the acetic acid determination, the sample (or calibration solution) was also pumped at 0.25 mL min^{-1} and mixed 1:1 in volume with a 0.6 M HCl solution to deliver all the acetic acid. The calibration solutions (200-1400 mg L^{-1} of acetic acid) were prepared every day from a stock solution of 1 M of acetic acid, diluted in a background solution containing the main species present in wines (12 % in volume of ethanol, 0.12 mM KNO_3 , 5.26 mM KH_2PO_4 , 4.41 mM MgSO_4 , 2.26 mM CaCl_2 , 19.0 mM malic acid, 33.0 mM potassium bitartrate and 13.9 mM NaOH). At the upper side of the gas-diffusion membrane, the carrier solution (DIW solution with potassium acetate and 0.01 M KCl), prepared every day from a stock solution of 0.1 M of potassium acetate, was flowed at 0.5 mL min^{-1} . When the adjusted sample and the carrier arrived to the gas-diffusion chamber, the acetic acid from the sample passed through the membrane and was collected by the carrier solution. Then, all the acetic acid was converted to acetate, causing a pH change of the carrier solution which is recorded by the pH-ISFET.

The hydrodynamic conditions of the system and their effect on the diffusion of the acetic acid were evaluated. Firstly, the procedure was carried out in continuous flow conditions, flowing the carrier solution and the adjusted sample at a total flow of 0.5 mL min^{-1} during 7 min for each calibration solution/sample. The signal taken for each sample was those recorded by the pH-ISFET during the last 20 s of each step. Secondly, stop flow conditions were also evaluated. The time of contact between the carrier and the sample in the gas-diffusion chamber for obtaining a good diffusion was evaluated using an acid/base colorimetric reagent and an image recorder.

Finally, the chemical conditions for the carrier solution were evaluated. On one hand, three concentrations of the potassium acetate (10^{-2}M , 10^{-3}M and 10^{-4}M) in the carrier solution were checked under the hydrodynamics conditions optimized previously. On the other hand, the pH of the carrier solution in a range from 3 to 7 was also evaluated.

3.6.3 Microanalytical flow system for L-lactate and L-malate detection

Using the PMMA/PSA assembly described in the Figure 3.14, the system was characterized. Cyclic voltammetric experiments were performed in PB solutions (pH 7)

containing 0.5 M KCl (characterization solution). Chronoamperometric measurements were carried out by applying an overpotential of -0.35V and -0.40 V (vs. platinum pseudo-RE), for the L-lactate and the L-malate determination, respectively. Characterization PB solutions adding 2 mM ferrocyanide potassium and L-lactate in a concentration range between 1×10^{-7} M and 1×10^{-5} M were used for the L-lactate biosensor characterization. In the case of the L-malate biosensor, characterization PB solutions including 5 mM NAD^+ and L-malate in a concentration range between 1×10^{-7} M and 1×10^{-5} M were used.

A scheme of the fluidic performance of the assembled PMMA/PSA system is illustrated in Figure 3.17. The PB solution used for characterizing each biosensor described above flowed under continuous mode through the module during 30 s at 0.25 mL min^{-1} , in order to fully clean the chip between consecutive measurements. The pseudo-RE was positioned at the beginning of the fluidic reservoir avoiding the potential changes caused by the enzymatic reaction on the surface of the WEs. All the measurements were done in stop flow conditions.

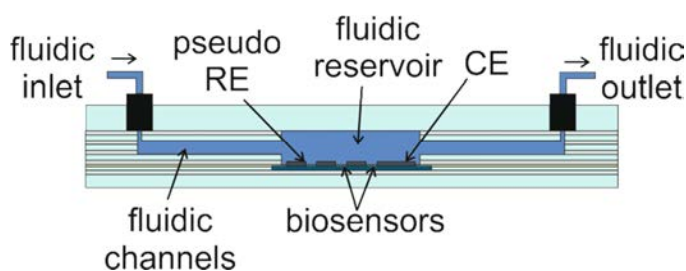


Figure 3.17. Drawing of the cross-section of the integrated assembly used for L-malate and L-lactate determination.

3.7 Multiparametric system for the analysis of cava wines

One ISFET was used for measuring pH and other five with ion-selective membranes were used for determining Na^+ , K^+ , Ca^{2+} , Cl^- and CO_3^{2-} ions. A double junction Ag/AgCl RE was employed for the potentiometric tests. Sensors based on a platinum 4-bar microelectrodes configuration were employed as conductivity sensor and ORP sensor. Finally, two gold microelectrodes were employed for chronoamperometric assays, completing the electrochemical cell with a platinum microelectrode as CE (Radiometer, Lyon, France) and a Ag/AgCl/10% (w/v) KNO_3 (Metrohm 0726 100, Herisau, Switzerland) as RE.

The signal of the conductivity and the ORP sensors was recorded with a very low consumption and portable multi-sensor meter constructed in the IMB-CNM premises. The multi-sensor meter allows the simultaneous measure of ORP, conductivity, temperature and amperometric response from analytes. A detailed explanation of the electronic design, software for data collection and global performance of this equipment is presented in [19]. For the measurements with the six ISFETs, another portable and low power consumption multi-ISFET meter was also designed and fabricated using the same equipment's. A scheme of the setup for measurement with all the microsensors is showed in Figure 3.18. Both meters were connected to a PC with a mini-USB connector for the acquisition and control of data.

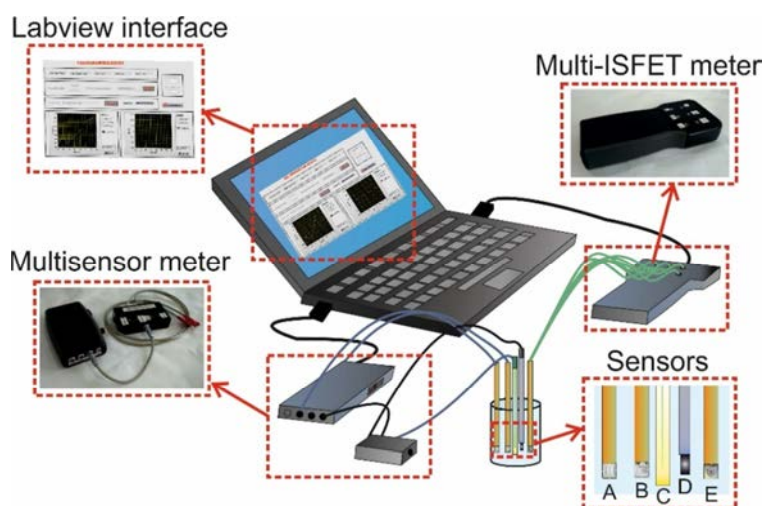


Figure 3.18. System used for the cava wines classification: (A) conductivity and ORP microsensor, (B) amperometric microsensor, (C) RE, (D) CE and (E) pH-ISFET.

For evaluating the multi-ISFET meter, the response of all sensors was evaluated by calibration against to the principal ion in the range from 10^{-8} M to 0.1 M by adding accumulated microvolumes of stock ion solutions (10^{-4} , 10^{-2} and 1.0 M) to 25 mL of DIW. In case of the pH ISFET, microvolumes of 1 M NaOH solution were added to a 50 mL of universal buffer solution to change pH from 2 to 12. All of these experiments were performed by triplicate at room temperature by using three different ISFETs of each type, prepared under the same experimental conditions.

In the case of the multi-meter, conductivity, ORP and amperometric responses were performed and compared with the results provided by Autolab commercial equipment. For conductivity tests, five KCl solutions of 0.80 mS cm^{-1} , 1.52 mS cm^{-1} , 2.82 mS cm^{-1} , 6.87 mS cm^{-1} and 13.07 mS cm^{-1} were prepared in order to evaluate the system in a wide range. The four-microelectrode sensor was immersed in each solution and the signal was recorded every 10 s during 2 min using the proposed electronic system. A study of measurement repeatability was carried out using a standard solution with nominal conductivity of $1416 \mu\text{S/cm}$, which was measured six times consecutively. ORP tests were done using the same microelectrode employed for the conductivity test. A four-electrode microsensor and a commercial RE were immersed in the standard solutions of 220 mV and 468 mV. The potential given by the system was recorded every 1 s during 3 min. This measurement was repeated three times for each ORP solution. As before, the ORP testing was completed with a study of measurement repeatability. In this case, the 220 mV standard solution was measured six times consecutively with the same sensor.

In the case of the amperometric studies, the three-electrode microsensor as WE, a commercial counter electrode and a commercial reference electrode were used. In order to evaluate the circuit performance, the ferricyanide/ferrocyanide ($\text{Fe}(\text{CN})_6^{3-}/\text{Fe}(\text{CN})_6^{4-}$) redox process was considered. A potential of + 75 mV that allowed the reduction of ferricyanide to ferrocyanide was applied. Then, calibration curves were performed in triplicate by addition of increasing concentrations of potassium ferricyanide in a 0.1 M KNO_3 background electrolyte solution in a range from 0 mM to 5 mM. Continuous stirring was used during all the measurements, to ensure the homogeneity of the solution. For each addition of ferricyanide, the current intensity was recorded every 1 s during 2 min.

3.8 Analysis of real wines samples

3.8.1 Free and total SO₂ determination

For the validation of the microanalytical system four sets of wine samples were analyzed. First, a calibration was carried out to check that the system was working correctly and to interpolate the signal obtained from each sample in the calibration curve for both free and the total SO₂ to obtain the sulfur dioxide value. In order to check the repeatability of the system and the drift of the ISFET, control solutions of 15 mg L⁻¹ and 80 mg L⁻¹ (for free and total SO₂ detection, respectively) were measured every five samples. The signal obtained was used as the baseline for correcting the calibration curve.

A set of 27 samples were used to validate the microanalytical flow system against an analytical equipment based on iodimetric determination, SO₂-Matic 23 (Crison Instruments, Barcelona, Spain). This equipment is based on the Ripper method [20] and works in a range from 0 mg L⁻¹ to 640 mg L⁻¹ of SO₂ with a resolution of 1 mg L⁻¹. 14 wine samples were used for the analysis of free sulfur dioxide: 4 white wines (CW1 to CW4) and 10 red wines (CR1 to CR10). 13 wine samples were used for the determination of total sulfur dioxide: 7 white wines (CW5 to CW10) and 6 red wines (CR2 to CR4 and CR10 to CR12).

A second set of 43 wine samples was provided by the Institut Català de la Vinya i el Vi (IRTA-INCAVI) which is an accredited laboratory (ISO 17025). These wines were analyzed by the Paul method (aeration-oxidation method) [21]. In the Paul, the free sulfur dioxide is carried over by a stream of air or nitrogen and it is fixed and oxidized by bubbling through a dilute and neutral H₂O₂ solution. Then, the sulfuric acid formed is determined by titration with a standard NaOH solution. Free sulfur dioxide is purged from the wine by entrainment at low temperature (10 °C), while total sulfur dioxide is purged from the wine by entrainment at high temperature (approximately 100 °C). Samples (analyzed with this method and the microanalytical flow system) were: 10 white wines (W1 to W10) and 15 red wines (R1 to R15) for free sulfur dioxide and 8 white wines (W11 to W18) and 10 red wines (R16 to R25) for the determination of total sulfur dioxide.

3.8.2 Free SO₂ and acetic acid determination

Several sets of wines samples were analyzed in order to test the feasibility of the developed microanalytical flow system. A set of commercial wines was analyzed by spiking the wine sample with the analyzed analyte. For that, solutions containing the same volume of wine and different concentration of acetic acid (0, 150, 500 and 1000 mg L⁻¹) or SO₂ (0, 5, 10, 15 and 40 mg L⁻¹) were used.

After that, a set of wine samples were analyzed to validate the proposed system against the official Paul (free SO₂) and potentiometric titration method (acetic acid) applied by the accredited IRTA-INCAVI laboratory. The standard method used for the acetic acid determination is based on the removing of the carbon dioxide from the sample and at once, the volatile acids are evaporated by steam distillation and titrated with sodium hydroxide. A first set of samples was analyzed for the SO₂ determination at the IRTA-INCAVI laboratories and transported to our institute. Then, each sample was analyzed with our system by triplicated. The volatile acidity was also evaluated by the IRTA-INCAVI for each sample in order of study the interference of the acetic acid concentration during the SO₂ determination. One sample (9619) was spiked in the IRTA-INCAVI laboratory with extra acetic acid and samples 9730, 9735 and 9788 were spiked after analysis at IMB-CNM with 700 mg L⁻¹ acetic acid.

Finally, the system was simultaneously validated for acetic acid and SO₂ determination at the IRTA-INCAVI laboratories. The system was first calibrated for free SO₂ (from 5 to 60 mg L⁻¹) and acetic acid (from 200 to 1400 mg L⁻¹). Then, the wine samples were tested for acetic acid and SO₂ consecutively, interpolating the signal obtained in the corresponding calibration plot. As the concentration of the analyte was obtained by the differential method (difference between the sample signal and the baseline signal), there was no necessary to use control solutions along all the analysis. 12 wine samples were analyzed for free sulfur dioxide and acetic acid: 5 red wines 3 rosé wines and 4 white wines.

3.8.3 L-lactic and L-malic acid determination

Three red wines provided by the IRTA-INCAVI were tested for the individual developed biosensors. These wines were from the 2013 vintage and their vineyards were harvested in the region of Tarragona (Spain). When the alcoholic fermentation was completed, selected bacteria of strain of *Oenococcus Oeni* were inoculated to induce the malolactic fermentation. For each wine, samples collected along this fermentation process, with a concentration of L-lactic acid and L-malic acid in a range of $0 - 2 \times 10^{-2}$ M ($0 - 1.7$ g L⁻¹ and $0-2.5$ g L⁻¹ for L-lactic and L-malic, respectively) were analyzed. Ten samples from the Wine 1 along 32 days, 5 samples from the Wine 2 along 15 days and 11 samples from the Wine 3 along 34 days were analyzed with the developed biosensor.

For measuring with the individual biosensors, a 1:100 sample dilution in PB was done in order to adjust the L-lactic acid concentration to the linear range of the L-lactate biosensor, previously calibrated. In the case of the L-malate biosensor, the samples were diluted 1:20000 (Wine 1), 1:25000 (Wine 2) and 1:10000 (Wine 3) for adjusting the L-malic concentration to the linear range of L-malate.

Three new red wines were provided by the IRTA-INCAVI to test the simultaneous determination of both analytes in the microfluidic system. 28 samples from the Wine 4 along 28 days, 5 samples from Wine 5 along 33 days and 12 samples from Wine 6 along 45 days were checked with the proposed system. The concentration range was $0-8 \times 10^{-3}$ M ($0-1.2$ g L⁻¹) and $0-6 \times 10^{-3}$ M ($0-0.5$ g L⁻¹) for malic and lactic acid, respectively. The three wines were diluted 1:10000 in PB to adjust the L-malic acid concentration to the L-malate linear range of the biosensor. For the L-lactic determination, Wine 4 and Wine 5 were diluted 1:50 and Wine 6 was diluted 1:20, in PB solutions, adjusting the concentration with the linear range of the proposed L-lactate biosensors.

Results were compared with the standard enzymatic methods used by the IRTA-INCAVI. This method is based on the enzymatically catalyzed reaction between the L-lactate or L-malate and the NAD⁺ to produce NADH, whose concentration is stoichiometrically related to the analyte concentration in the samples. The change of NADH concentration is measured spectrophotometrically at 340 nm [22].

3.8.4 Analysis of Cava wines

A total set of 78 commercial Cava wine samples from Catalonia provided by the IRTA-INCAVI were analyzed. The samples were selected according to its type, taking into account their vintage time as categorized by the Regulatory Board of Cava [23]: 20 "Young" samples (9 to 15 months), 25 "Reserva" samples (15 to 30 months) and 16 "Gran Reserva" samples (more than 30 months). A set of 17 "Rosé" Cava samples were also studied. These samples were mainly from Penedès region (Spain). White Cava wines were obtained mainly from Macabeu, Xarel·lo and Parellada grape varieties, although Chardonnay and/or Subirat parent may also be used, that is, the five different white grape varieties authorized by Regulatory Board of Cava [24]. For Rosé cava wines, Trepat, Monastrell, Grenache Noir and/or Pinot Noir might be used.

Volumetric alcoholic degree (VAD), total acidity, pH, potassium ion, conductivity, glycerol and methanol were also analyzed with reference/standard methods [24, 25] by the IRTA-INCAVI.

The analysis of wine was directly carried out in the degassed Cava sample. The ISFETs were immersed in the samples and the potentials (in mV vs. Ag/AgCl) were recorded every 10 s during 30 s using the multi-ISFET meter. The platinum 4-microelectrode sensors and the gold microelectrodes were also immersed in the wine samples and the signals were recorded every 1 s during 30 s using the multi-sensor meter. In the case of the amperometric measurements, an overpotential of +1.01 V (vs. Ag/AgCl) corresponding to the oxidation potential of polyphenols and gold from the electrode [26], respectively, was applied. The total analysis of a Cava wine sample spent less than two min.

Once all the samples were analyzed, a data matrix was constructed with the different variables to be used as the input of the chemometric tools. In this study, the input data were composed by 10 variables (pH, Na⁺, K⁺, Cl⁻, Ca²⁺, CO₃²⁻, conductivity, ORP and current recorded by the amperometric sensors at +1.01 and +1.31 V). These data were treated using different multivariate methods. The Linear Discriminant Analysis (LDA) was utilized to achieve a good classification model for the Cava wine samples. The Partial Least Squares

(PLS) regression was employed to perform the quantification of different parameters of the samples.

The original values were previously auto-scaled -all the variables were centered and set to a standard deviation equal to 1- to avoid variables from having a different influence on the model. Besides, all the obtained models were centered. On one hand, the Mahalanobis method, for measuring the distance of an observation to the centers of the groups, together with the leave-one-out cross validation method were used for the LDA model. On the other hand, the classical non-linear iterative (NIPALS) algorithm, together with the test-set validation technique was used for the PLS regressions. In this case, a fixed calibration set composed by 60 Cava wine samples was chosen. Meanwhile, the prediction set was formed by 18 samples. To control all these parameters and to perform the analyses, the Unscrambler v.9.1 informatics package (CAMO ASA, Oslo, Norway) was used.

3.9 References

1. Jimenez, C., Bratov, A., Abramova, N., Baldi, A., *ISFET Based Sensors: Fundamentals and Applications*, A.S. Publishers, Editor. 2006. p. 151-196.
2. Munoz, J., et al., *Biosensors & Bioelectronics*, 1997. **12**(7): p. 577-585.
3. Abramova, N., et al., *Talanta*, 2000. **52**(3): p. 533-538.
4. Bratov, A., et al., *Analytical Chemistry*, 1995. **67**(19): p. 3589-3595.
5. Bratov, A., N. Abramova, and C. Dominguez, *Analytica Chimica Acta*, 2004. **514**(1): p. 99-106.
6. Artigas, J., et al., *Analytica Chimica Acta*, 2001. **426**(1): p. 3-10.
7. Makarychev-Mikhailov, S., et al., *Electroanalysis*, 2003. **15**(15-16): p. 1291-1296.
8. Chakrabarti, M.H. and E.P.L. Roberts, *Journal of the Chemical Society of Pakistan*, 2008. **30**(6): p. 817-823.
9. Orozco, J., et al., *Electrochimica Acta*, 2007. **53**(2): p. 729-736.
10. Wang, J., *Study of the electrode reactions*, in *Analytical Electrochemistry*,. 2000, Wiley-VCH: New York.
11. Sassolas, A., L.J. Blum, and B.D. Leca-Bouvier, *Biotechnology Advances*, 2012. **30**(3): p. 489-511.
12. Chaki, N.K. and K. Vijayamohanan, *Biosensors & Bioelectronics*, 2002. **17**(1-2): p. 1-12.
13. Razola, S.S., et al., *Biosensors & Bioelectronics*, 2002. **17**(11-12): p. 921-928.
14. Wang, X., et al., *Synthetic Metals*, 2010. **160**(13-14): p. 1373-1381.
15. Grundig, B., et al., *Journal of Electroanalytical Chemistry*, 1995. **395**(1-2): p. 143-157.
16. Schuhmann, W., et al., *Biosensors & Bioelectronics*, 1991. **6**(8): p. 689-697.
17. Sarudi, I. and J. Kelemen, *Talanta*, 1998. **45**(6): p. 1281-1284.
18. Hans-Ferdinand, L. and J.F. Jackson, *Wine Analysis*. 1998: Springer.
19. Gimenez-Gomez, P., et al., *Ieee Sensors Journal*, 2015. **15**(11): p. 6517-6523.
20. Gamella, M., et al., *Talanta*, 2010. **81**(3): p. 925-933.
21. Grieshaber, D., et al., *Sensors*, 2008. **8**(3): p. 1400-1458.
22. Katrlík, J., et al., *Analytica Chimica Acta*, 1999. **379**(1-2): p. 193-200.
23. Ministerio de Agricultura, P.y.A., *In BOE-A-1991-28079, Secretaría General Técnica: Madrid, 1991; p 37587*. 1991, ORDEN de 14 de noviembre de 1991 por la que se aprueba el Reglamento de la Denominación "Cava" y de su Consejo Regulador. .
24. Commision, E., *Community methods for the analysis of wines. Tech. Rep. 2676/90 EEC*. 1990: Brussels.
25. International Organization of Vine and Wine(OIV), *Compendium of International Methods of Wine and Must Analysis*. 2005, ORDEN de 14 de noviembre de 1991 por la que se aprueba el Reglamento de la Denominación "Cava" y de su Consejo Regulador. : Paris. p. Vol. 1-2.
26. Gutierrez, M., et al., *Sensors*, 2011. **11**(5): p. 4840-4857.

Chapter 4: Results and discussions

4.1 Microanalytical flow systems based on gas-diffusion and pH-ISFET for the determination of free/total SO₂ and acetic acid

Sulfur dioxide is added to wine during winemaking to prevent the microbial spoilage, oxidation and color changes due to undesirable enzymatic and non-enzymatic reactions [1]. Monitoring of total and free SO₂ content in wine is critical during wine storage and processing to ensure protection from chemical and microbiological agents and to adhere to prevailing legislation. The presence of even low concentrations of SO₂ can induce severe diseases in people with allergic illness or food intolerance symptoms [2]. Furthermore, high concentrations of sulfur dioxide affect the final quality of the wine, mainly the smell and the taste and can inhibit the malolactic fermentation. The maximum level of total and free sulfur dioxide is fixed in the European Community by the International Organization of Vine and Wine (OIV) and it depends on the type of wine (up to 150 mg L⁻¹ for red wines and up to 400 mg L⁻¹ for sweet white wines). If the total sulfur dioxide content exceeds 10 mg L⁻¹, it must be expressed on the label of the wine bottle [3]. The analysis of SO₂ is also important during winemaking in order to control the sulfur dioxide decrease and the right amount of sulfur dioxide to add.

There are three standard methods for the determination of sulfur dioxide in wine proposed by the OIV. The Paul method, also known as the aeration-oxidation method, is the official method. In that method, the free sulfur dioxide is volatilized and carried through a separate container by a stream of air or nitrogen where it is fixed and oxidized with a dilute and neutral H₂O₂ solution. Then, the sulfuric acid formed is determined by titration with a standard NaOH solution. Free sulfur dioxide is purged from the wine by entrainment at low temperature (10 °C), while total sulfur dioxide is purged from the wine by entrainment at high temperature (approximately 100 °C) [4]. However, this method is tedious since it requires flushing of the sample, use large sample volumes and the precision depends on the experience of the technician. The Ripper method is based on an iodimetric titration [5]. This is the most widely used in cellars due to its simplicity and short analysis time. Nevertheless, it suffers from many interferences and the end point observation in red wines is difficult due to the use of colorimetric indicators. The third recommended method is based on theoretical models [6] and allows calculating the molecular sulfur dioxide content as percentage of free SO₂ according to pH, temperature and alcoholic strength [7].

Alternative methods based on direct detection of sulfur dioxide in wine are electrochemical biosensors. They have a high selectivity due to the use of enzymatic recognition [8-10]. However, these biosensors suffer from low stability due to the inactivation of the bio-elements.

Other alternatives to standard methods that permit the automation of the analysis are those based on flow analysis mainly using flow injection analysis (FIA) [11, 12] and Sequential Injection analysis (SIA) [13]. The most interesting aspect of these methods is that they allow the separation of the analyte from the sample using a diffusion cell and a hydrophobic membrane. The methodology is based on the acid/base characteristics of sulfur dioxide. The sample is acidified to pH lower than 1 to convert all sulfur dioxide to the SO₂ form. This gas is diffused through the gas permeable membrane and collected by an acceptor stream. The most usual detection technique is colorimetric having a reagent on the acceptor channel such as pararosaniline [14, 15], p-aminoazobenzene [16], malachite green [17] or luminol [18]. Some of these techniques were commercialized in the past (i.e. FIAstar analytical system from FOSS), however, they have been substituted by other detection techniques due to the toxicity of the colorimetric reagents and the use of expensive complex measuring devices.

Amperometric detection using non-modified glassy carbon electrodes [19] or modified electrodes (Thanh, Decnopweever, & Kok, 1994) implemented in FIA systems have also been described in the literature. The main problem of this detection method was the loss of sensitivity of electrodes. An alternative detection method using a pH-ISFET (Ion-Sensitive Field-Effect Transistor) combined with a FIA system was proposed in [20]. These authors evaluated the system with water solutions but no wine samples were analyzed. However the paper pointed out the interest of using ISFETs as pH sensors. ISFETs are sensors fabricated with microelectronic technology. Their functioning is based on a MOS (Metal-Oxide Semiconductor) transistor with a Si₃N₄ dielectric membrane instead of a metal. This membrane behaves in a similar way as a glass electrode, therefore ISFETs have potentiometric response and follow Nerstian law. Nevertheless, due to their semiconductor device characteristics, they have several advantages, such as small size, they have the dimensions of a chip, in this case 3×3 mm², they are solid state by nature as they

are fabricated on silicon, they are mass fabricated, and show a short response time and long term stability [21].

Today's winemakers are moving away from manual titrations, color indicators, time consuming aeration-oxidation (AO) tests and dilution calculations to more accurate, more automatic and faster methods. It is crucial that instruments deliver information quickly, inexpensively and with high accuracy. For example, commercial methods like WineScan™ from FOSS use a gas separation method to extract the SO₂ from the sample and a FTIR (Fourier Transform Infrared Spectroscopy) interferometer that scans the full infrared spectrum. This system is rapid, automatic and can measure other parameters than SO₂. However, this equipment requires laboratory infrastructure.

Volatile acidity is other important parameter for being monitored during the winemaking process because is linked to the quality of the wine sample [22]. An excess of volatile acidity is mainly related to high concentration of acetic acid, which is produced in small concentration at the beginning of alcoholic fermentation. During this process, its level increases to a maximum and then starts decreasing. On the other hand, during the MLF there is a slight increase of volatile acidity due to the breakdown of citric acid.

Wine naturally has a volatile acidity of 0.36 – 0.48 g L⁻¹, expressed in acetic acid. This value tends to increase slightly during aging. Higher values indicate bacterial activity. Volatile acidity is not easily detectable for humans in normal wine if the concentration is below 0.72 g L⁻¹ (acetic acid), meaning a no effect on its flavor. Above this value, the smell becomes acid and the flavor deteriorates, becoming harsh and bitter on the finish. In view of the impact of total acidity on the wine quality, the maximum level of acetic acid is also controlled by the OIV in Europe, depending on the wine class (up to 1.2 g L⁻¹ for most of wines, although some old wines can exceed this limit because they are subjected to a particular legislation) [23].

Regarding the methods applied for the acetic acid determination, the standard method proposed by the OIV determines the volatile acidity [24]. In this official method, the CO₂ is first removed from the wine. Then, volatile acids are separated from the wine by steam distillation and titrated using a standard sodium hydroxide solution. The acidity of free and combined sulfur dioxide distilled under these conditions should be subtracted from

the acidity of the distillate. Other methods for acetic acid determination based on HPLC, gas chromatography or potentiometry have been also proposed without good results due to the effect of some interferents [25, 26]. Greatest results have been described using gas-diffusion systems for avoiding the interferents of the sample matrix [27], although its large size does not allow its implementation for on-line measures.

The aim of this work is the development and validation of simple, selective, automatic and rapid methods for the determination of free/total sulfur dioxide and acetic acid in wine samples. The detection method in both cases is based on the use of a gas diffusion membrane to separate the analyte from the sample (Figure 4.1). This methodology exploits also the acid/basic characteristics of the analytes and their gas or volatile state in the acidic form. On one side of the gas-diffusion membrane, the sample is adjusted to a pH value that converts all sulfur dioxide or acetic acid to the gas form. This gas is diffused through the gas-permeable membrane and it is collected with a carrier (or acceptor) solution on the other side of the gas-diffusion membrane. Depending on the concentration of the analyte in the sample, the pH of the carrier changes, and this pH-change is recorded by the pH-ISFET. The obtained signal is correlated to the concentration of analyte in the sample. The main advantage of this method is the removing of matrix interferences, resulting in a rapid detection method with low-reagent consumption.

The diffusion ratio depends on the gas concentration but also on the concentration gradient of the analyte and the time of contact between both sides of the membrane, as well as on the pH of the carrier solution.

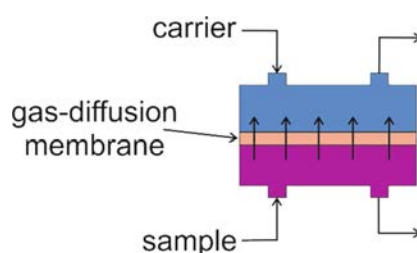


Figure 4.1. Scheme of the gas-diffusion principle cell.

Two fluidic systems including a gas-diffusion chamber and a pH-ISFET have been fabricated. Firstly, a microanalytical flow system for the determination of free and total SO_2 and secondly, a more compact microanalytical flow system for the determination of free SO_2 and acetic acid. Both methods have been optimized and validated with wine samples.

Sulfur dioxide can be present in different forms depending on the pH: molecular sulfur dioxide (SO_2), hydrogen sulfite (HSO_3^-) or sulfite (SO_3^{2-}) (Figure 4.2a). In wine it is present in two forms, as free sulfur – this is basically under the form of HSO_3^- , which is the antioxidant portion, and a small amount of dissolved SO_2 – and sulfur bound with acetaldehyde, some polyphenols, ketones, sugars or acids. The sum of both fractions corresponds to the total sulfur dioxide [28] (Figure 4.2b).

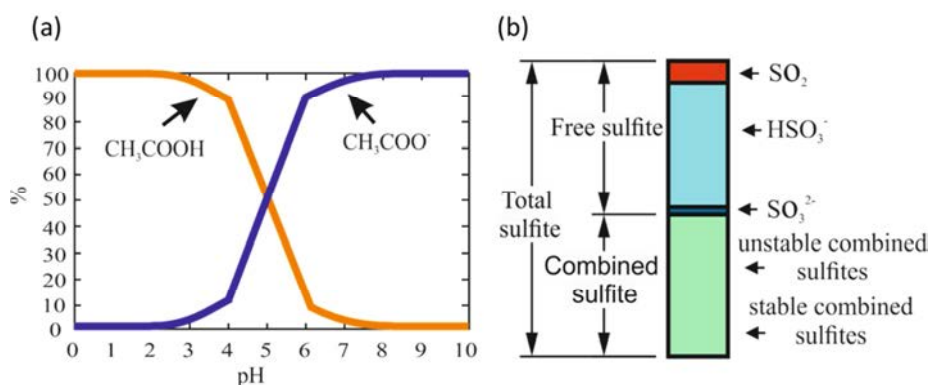


Figure 4.2. (a) Percentage of the chemical forms of sulfites as function of the pH value; and (b) scheme of the chemical forms of sulfites in wine.

The detection of SO_2 proposed is based on the conversion of all the bisulfite present in the sample to its gas form (SO_2) with the acidification of the sample to pH below 1. Then, SO_2 diffuses through the gas-diffusion membrane and it is recollected by the carrier solution adjusted to a pH value where HSO_3^- is the predominant specie, converting all the SO_2 diffused to HSO_3^- . For the detection of total SO_2 , a previous treatment of the sample for releasing all the bounded SO_2 is carried out.

The acetic acid/acetate equilibrium as function of pH is shown in Figure 4.3. In this case, the sample is acidified before arriving to the gas-diffusion chamber to have all the specie in form of acetic acid gas (pH < 3). Then, the acetic acid crosses through the membrane and is recollected by the carrier solution at pH 6 (acetate as predominant specie), converting all the diffused acetic acid to acetate.

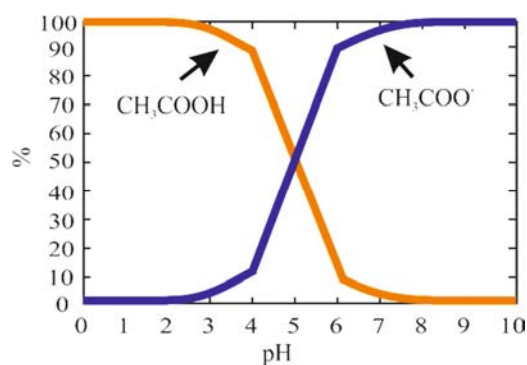


Figure 4.3 Percentage of the chemical forms of acetic acid/acetate as function of pH .

4.1.1 Microanalytical flow system for free and total SO₂ determination

The setup used for the proposed microanalytical flow system is summarized in Figure 3.15 (section 3.6.1).

4.1.1.1 Optimization of the system

The optimization of the system was performed by doing calibrations of SO₂ in a range of concentrations of 1 mg L⁻¹ - 60 mg L⁻¹ and 30 mg L⁻¹ - 300 mg L⁻¹ for free and total SO₂ determination, respectively. The parameters to be tested were the length of the tubes, the flow rate, the mode of the flow (parallel or countercurrent, stop flow or continuous flow), the conditions of the sample pretreatment for the total SO₂ determination, the cleaning method between consecutive measurements and the concentration of the solutions flowed through the fluidic system.

First, the length of the tubes for mixing the sample with the acid solution 1 was evaluated using the total sulfur dioxide system and a calibration range of 30 mg L⁻¹ - 300 mg L⁻¹. The slope of the regression curve was -34.7 ± 0.4 mV dec⁻¹ and -38.7 ± 0.5 mV dec⁻¹ for a 10 cm and 20 cm coil, respectively. When the longer coil was used, the pH fell close to 0 at the end of the coil, meanwhile the pH was stabilized at 1 when the shorter coil was used. If the pH is close to 0, the predominant specie in the sample is SO₂ gas. Therefore, the 20 cm coil was chosen for the next measurements.

Regarding the optimization of the flow rate, the sensitivity of the calibration curves (in absolute value) increased until a rate of 0.75 mL min⁻¹ (Figure 4.4). However, a rate of 0.50 mL min⁻¹ was chosen considering that the difference of sensitivity between both rates

($-38.0 \pm 0.6 \text{ mV dec}^{-1}$ and $-39.0 \pm 0.7 \text{ mV dec}^{-1}$ for 0.50 mL min^{-1} and 0.75 mL min^{-1} , respectively) does not justify the higher consumption of reagents at 0.75 mL min^{-1} .

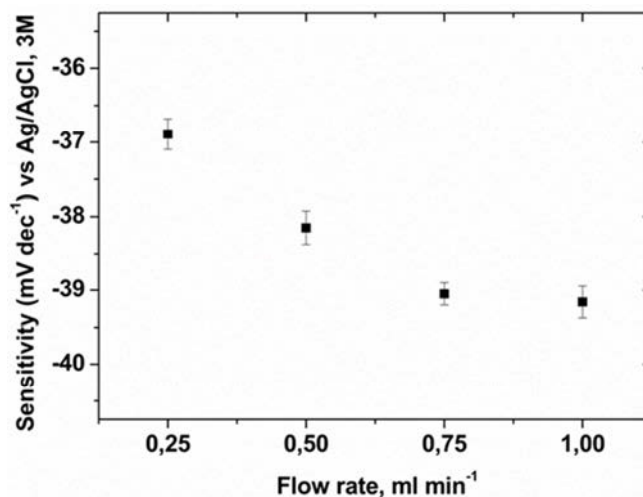


Figure 4.4. Sensitivity obtained with the total sulfur dioxide system in the range of 30 mg L^{-1} – 300 mg L^{-1} versus the pump flow rate used. Standard deviations of three calibrations carried out consecutively with the same pH-ISFET are drawn as error bars.

The use of parallel current and countercurrent flow in both sides of the diffusion cell was evaluated. The results showed a 40% higher sensitivity for the countercurrent flow (slopes of $-40.0 \pm 0.3 \text{ mV dec}^{-1}$ and $-25.5 \pm 0.7 \text{ mV dec}^{-1}$ for counter and parallel current, respectively). Also, a test increasing the time of contact by stopping the flow for 2 min after the 5 minutes of continuous flow in both sides of the membrane was carried out. However, no significant improvement was obtained (slope of $-39.3 \pm 0.6 \text{ mV dec}^{-1}$ for 5 min in continuous flow plus 2 min in stop flow vs. $-40.0 \pm 0.3 \text{ mV dec}^{-1}$ for just 5 min in continuous flow) and therefore the process was performed without stopping the flow.

For total SO_2 detection, bounded SO_2 was released under basic conditions. The process was optimized by using the pretreatment chamber described in the Experimental chapter and several wine samples (SO_2 from 30 mg L^{-1} to 105 mg L^{-1}). The best results in terms of accuracy were obtained using an initial stirring step of 3 s and then allowing reacting without stirring for 3 min before driving the sample to the microanalytical flow system. The relative errors between the values obtained with the iodimetric method and the experimental proposed system were below 10 % after this pretreatment optimization.

The proposed method for cleaning the system using HCl was checked for the determination of total sulfur dioxide in five wine samples (SO_2 from 15 mg L^{-1} to 63 mg L^{-1}). Best cleaning conditions (0.3 M HCl , 3 min) allowed the recovery of the baseline after each sample analysis (Figure 4.5). For these five measurements, the ISFET signal obtained for the baseline after each cleaning process had a relative standard deviation (RSD) of 5.1% .

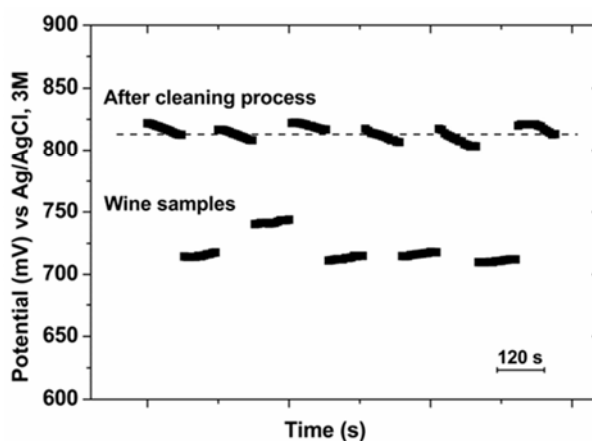


Figure 4.5. Signal recorded with the pH-ISFET in the total sulfur dioxide system for five different wine samples and recovery of the baseline after the cleaning process with 0.3 M HCl .

The carrier solution was fixed considering that SO_2 is a weak acid specie and forms HSO_3^- and SO_3^{2-} as conjugate bases. In order to obtain a stable, reproducible and linear pH change with the concentration of SO_2 , one alternative is to achieve the equilibrium with one of these conjugates. For that reason, the carrier solution used was $2 \times 10^{-5} \text{ M Na}_2\text{SO}_3$ which allows a rapid chemical equilibrium. Previous tests demonstrated that if no any conjugated species are used (i.e. water with a salt), the baseline signal is not stable due to pH variations. Besides, the pH change due to the presence of SO_2 is not reproducible and linear. The low concentration of sulfite chosen is related to its low buffering capacity, which allows a higher jump of pH against the presence of SO_2 and therefore better sensitivity. This carrier solution was adjusted initially at pH 4 (with an Acid solution 2 channel of $2 \times 10^{-4} \text{ M HCl}$) because this pH is close to the equilibrium $\text{SO}_2/\text{bisulfite}$. This carrier solution contained also 0.02 M NaCl in order to adjust the ionic strength so that the response of the pH-ISFET sensor is not affected [20].

The HCl concentration used for the Acid solution 1 channel was fixed to 0.6 M and 4 M for free and total sulfur dioxide, respectively. These concentrations allowed that the sulfite in the sample was in form of SO₂ gas (pH close to 1) before arriving to the gas-diffusion chamber. For Acid solution 2 channel, five HCl solutions in a range from 10⁻⁷ M to 10⁻³ M were tested to adjust the pH of the carrier solution in a range from 3.5 to 6.5 (HSO₃⁻ as predominant specie). The solutions (Acid solution 2 and carrier solution) were prepared separately and mixed under dynamic conditions to assure the stability of the HSO₃⁻, which is unstable at low pH. The results of this study showed that the best sensitivity (-49.1 ± 0.5 mV dec⁻¹) and linear range was obtained when a 2×10⁻⁶ M HCl was used in this channel, being the final pH value of the carrier solution 6 (Figure 4.6). At pH 6 all the SO₂ gas diffused from the sample is converted to bisulfite upon contact with the carrier solution. In conclusion, this pH 6 is optimal because it is basic enough to favor a good diffusion of the SO₂ through the membrane, but in turn acid enough to achieve a rapid pH change.

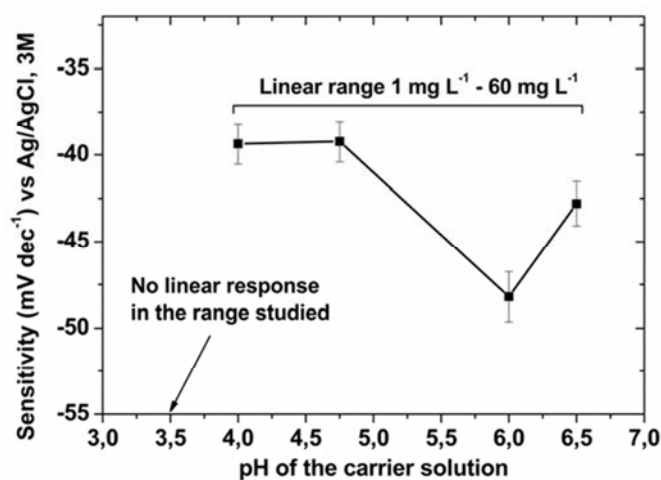


Figure 4.6. Sensitivity obtained for the determination of free sulfur dioxide in the range of 1 – 60 mg L⁻¹ versus the pH value.

To summarize, the optimum conditions for SO₂ determination were using a carrier solution containing 2×10⁻⁵ M Na₂SO₃ and 0.02 M NaCl, with a pH adjusted to mixing (1:1 in volume) with a 2×10⁻⁶ M HCl solution (Acid solution 2). Sample solutions were mixed with the Acid solution 1 (HCl 0.6 M and HCl 4 M for the determination of free and total SO₂, respectively) to get a value of pH close to 0. For total SO₂ analysis, a pretreatment

process was carried out mixing (1:1 in volume) the sample and NaOH 4M in the pre-treatment chamber during 3 seconds under stirring conditions and kept in stop flow during 3 min to achieve complete release of bound SO₂.

4.1.1.2 Evaluation of the system performance

Using the optimized experimental conditions described above, triplicate calibrations in a range from 1 mg L⁻¹ to 60 mg L⁻¹ and from 30 mg L⁻¹ to 300 mg L⁻¹ for the free and the total SO₂ determination, respectively, were done. The pH-ISFET signals and the calibration plot for the free SO₂ determination are shown in Figure 4.7a and Figure 4.7b, respectively. In Figure 4.8a and 8b are depicted the pH-ISFET signals and the calibration plots, respectively, for the total SO₂. A linear drop of the potential recorded by the pH-ISFET with the increasing concentration of SO₂ was observed in both cases. The sensitivity (slope) was $-49.6 \pm 0.7 \text{ mV dec}^{-1}$ ($r = 0.998$) and $-49.4 \pm 0.7 \text{ mV dec}^{-1}$ ($r = 0.998$) for the free and total sulfur dioxide determination, respectively. The limit of detection (LOD) was 0.5 mg L⁻¹ (calculated according to the IUPAC criterion for potentiometric sensors [29]).

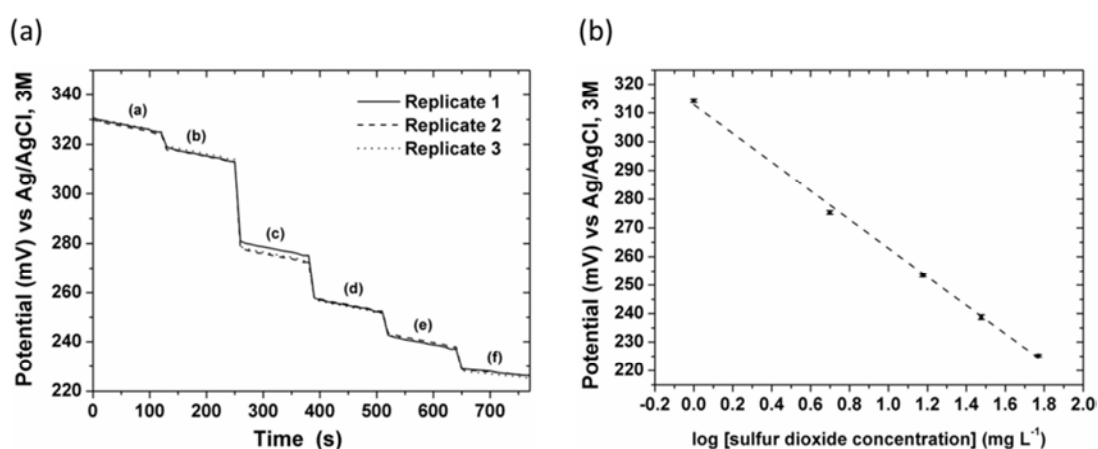


Figure 4.7. (a) pH-ISFET signals recorded by triplicate and (b) calibration curve obtained for the free sulfur dioxide system in presence of (a) 0 mg L⁻¹, (b) 1 mg L⁻¹, (c) 5 mg L⁻¹, (d) 15 mg L⁻¹, (e) 30 mg L⁻¹ and (f) 60 mg L⁻¹ of sulfur dioxide. Standard deviation of triplicated calibrations is drawn as error bars.

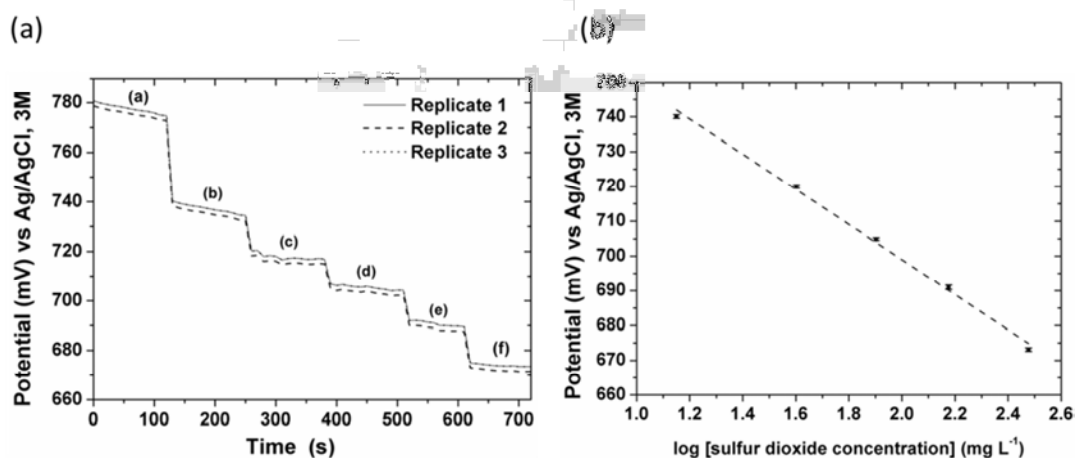


Figure 4.8. (a) pH-ISFET signals recorded by triplicate and (b) calibration curve obtained for the total SO₂ system in presence of (a) 0 mg L⁻¹, (b) 30 mg L⁻¹, (c) 40 mg L⁻¹, (d) 80 mg L⁻¹, (e) 150 mg L⁻¹ and (f) 30 mg L⁻¹ of SO₂. Standard deviation of triplicated calibrations is drawn as error bars.

To study the matrix effect, a calibration of the free SO₂ in a range from 1 mg L⁻¹ to 60 mg L⁻¹ SO₂ was performed in a solution containing 12 % ethanol. The regression curve obtained under these conditions was $E \text{ (mV)} = -46.3 \log[\text{SO}_2] + 297.4$ ($r = 0.996$). Then, common ions were added in this solution giving a curve $E \text{ (mV)} = -44.1 \log[\text{SO}_2] + 292.6$ ($r = 0.998$). Finally, malic and tartaric acid were added, resulting in a similar calibration curve, $E \text{ (mV)} = -45.5 \log[\text{SO}_2] + 294.2$ ($r = 0.996$). These results demonstrate that the presence of ethanol in the calibration solution is decreasing the sensitivity, maybe due to a reduction of the diffusion coefficient of SO₂ through the membrane. Therefore, this compound was used for next experiments in the calibration solution.

During the optimization of the proposed microanalytical flow system, a unique gas-diffusion membrane was used for a total number of 204 tests, without any decrease of the SO₂ diffusion rate.

4.1.1.3 Analysis of wine samples

The optimized microanalytical flow system was evaluated with wine samples. A previous calibration was carried out for each set of wines and control solutions of 15 mg L⁻¹ and 80 mg L⁻¹ for free and total SO₂, respectively, were measured every five samples to check the stability of the system. These control solutions showed coefficients of variation of 7 and 1% respectively that demonstrates the repeatability of the system. Two gas-diffusion membranes were used along all these tests (total of 236). The membrane was

changed when a decrease higher than 10% in the interpolated concentration of SO₂ was obtained in the control solutions. Unlike the aqueous solutions used during the optimization of the system, the complexity of the wine matrix affected the gas-diffusion membrane, blocking it after 148 consecutive tests.

Firstly, two sets of 14 and 13 wines were analyzed with the microanalytical flow system for the free and the total sulfur dioxide determination, respectively, and the results were compared with the values obtained with commercial equipment using the iodimetric method. Results of this analysis are shown in Table 4.1 and Table 4.2 for free and total SO₂, respectively. For the free sulfur dioxide determination, the relative errors are above -25 %, being lower for red wines. The negative values of these errors indicate an underestimation of values for the flow method. These lower values could be associated to a lower rate of SO₂ diffusion through the membrane in the microanalytical flow system, mainly for the white wine. On the other hand, the interferences (mainly ascorbic acid and polyphenols) present for the iodimetric method could cause an extra consumption of iodine during the titration. For total sulfur dioxide, the relative errors are below 16 % for both types of wine samples. Among these samples, 10 and 13 average values for free and total sulfur dioxide, respectively, were within the confidence interval of the iodimetric method.

Table 4.1. Values of free sulfur dioxide concentration obtained with the microanalytical flow system and with the standard iodimetric method for 14 commercial wine samples. The confidence intervals are calculated with a level of 95% (n = 3 replicates).

Wine	Free sulfur dioxide concentration (mg L ⁻¹)		Relative error (%)
	Microanalytical flow system	Iodimetric method	
CW1	26 ± 2	31 ± 6	-16
CW2	20 ± 0.8	26 ± 5	-23
CW3	26 ± 1	33 ± 6	-21
CW4	19 ± 1	25 ± 5	-24
CR1	20 ± 1	22 ± 4	-9
CR2	21 ± 0.8	23 ± 5	-9
CR3	9.0 ± 0.6	9.0 ± 2	0
CR4	22 ± 1	26 ± 5	-15
CR5	12 ± 0.5	16 ± 3	-25
CR6	21 ± 0.9	23 ± 5	-9
CR7	35 ± 1	37 ± 7	-5
CR8	24 ± 1	25 ± 5	-4
CR9	15 ± 0.6	15 ± 3	0
CR10	35 ± 1	36 ± 7	-3

* CW: white wine; CR: red wine.

Table 4.2. Values of total sulfur dioxide concentration obtained with the microanalytical flow system and with the standard iodimetric method for 13 commercial wine samples. The confidence intervals are calculated with a level of 95% (n = 3 replicates).

Wine ¹	Total sulfur dioxide concentration (mg L ⁻¹)		Relative error (%)
	Microanalytical flow system	Iodimetric method	
CW5	98 ± 5	106 ± 18	-8
CW6	105 ± 5	121 ± 21	-13
CW7	127 ± 7	121 ± 21	5
CW8	101 ± 5	103 ± 18	-2
CW9	117 ± 5	113 ± 19	3
CW10	131 ± 6	122 ± 21	7
CW11	110 ± 6	117 ± 20	-6
CR2	115 ± 7	106 ± 18	8
CR3	83 ± 4	87 ± 15	-5
CR4	66 ± 3	68 ± 12	-3
CR10	48 ± 2	43 ± 8	12
CR11	87 ± 5	104 ± 18	-16
CR12	92 ± 5	83 ± 15	11

¹ CW: white wine; CR: red wine.

The differences between both methods separating white and red wines were analyzed by the least squares method plotting the data of the microanalytical flow system vs. the iodimetric method. The results are shown in Figure 4.9 and Table 4.5. For free sulfur dioxide the slope and the correlation coefficient are close to 1 indicating a good agreement between both methods. However, a negative value of the intercept, higher for white wines, indicates an underestimation of the values obtained with the microanalytical flow system as was discussed previously. The results of the least square analysis for total sulfur dioxide are poorest due to the variance introduced by the treatment of the sample for releasing the bounded sulfur dioxide. Slopes are close to 1 but regression coefficients are not fitting ideal behavior, especially for white wines samples. The intercept value is higher than for free sulfur dioxide determination, although the uncertainty intervals include zero. This high value is more accentuated for white wines maybe due to the narrow range of concentrations analyzed.

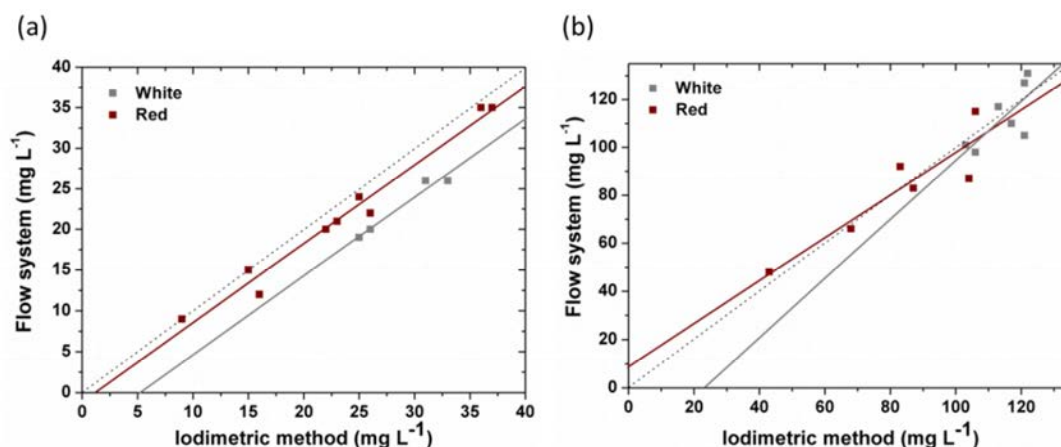


Figure 4.9. Comparative results from least squares analysis between the iodimetric method and the microanalytical flow system for (a) free SO₂ and (b) total SO₂ determination. The dotted line corresponds to the ideal correlation between methods.

A second set of 43 samples was analyzed by the accredited IRTA-INCAVI laboratory using the Paul method and the microanalytical flow system (Table 4.3 and Table 4.4). As shown, for values of free sulfur dioxide lower than 16 mg L⁻¹, the relative errors were high. We can distinguish those values near to 20 mg L⁻¹ for the Paul method (W2, W5, W6, W7, W9) that are showing errors around -40% and those values below 3 mg L⁻¹ with errors above 100 % (W10, R4, R13, R14). This last case seems to be related with the limit of quantification of our method. For values above 20 mg L⁻¹ the error is below 10%. However, most of the mean values obtained (corresponding to 16 wine samples) were within the confidence interval of the Paul method. For total sulfur dioxide, the relative errors were in general below 15 % that is quite acceptable. In addition, the mean values of 16 wine samples obtained were within the confidence interval of the Paul method.

Table 4.3. Values of free sulfur dioxide concentration obtained with the microanalytical flow system and with the standard accredited Paul method for 25 wine samples. The confidence intervals are calculated with a level of 95%.

Wine ¹	Free sulfur dioxide concentration (mg L ⁻¹)		Relative error (%)
	Microanalytical flow system (n = 3)	Accredited Paul method ²	
W 1	28 ± 2	32 ± 10	-12
W 2	11.1 ± 0.6	19 ± 6	-42
W 3	20 ± 1	21 ± 7	-5
W 4	16.4 ± 0.8	18 ± 6	-11
W 5	9.0 ± 0.4	17 ± 6	-47
W 6	12.2 ± 0.8	20 ± 6	-40
W 7	16.2 ± 0.9	24 ± 8	-33
W 8	12.0 ± 0.8	12 ± 4	0
W 9	14 ± 1	22 ± 7	-36
W 10	7.1 ± 0.5	3 ± 2	133
R 1	14.3 ± 0.7	10 ± 4	40
R 2	21.4 ± 0.9	21 ± 7	0
R 3	17 ± 1	21 ± 7	-19
R 4	8.0 ± 0.6	3 ± 2	167
R 5	18 ± 1	20 ± 6	-10
R 6	30 ± 1	28 ± 9	7
R 7	32 ± 2	27 ± 8	18
R 8	47 ± 2	41 ± 12	15
R 9	43 ± 2	32 ± 10	34
R 10	45 ± 3	39 ± 12	15
R 11	12.1 ± 0.8	9 ± 3	33
R 12	25 ± 1	22 ± 7	14
R 13	6.0 ± 0.3	2 ± 1	200
R 14	11.0 ± 0.7	2 ± 1	450
R 15	33 ± 1	31 ± 10	6

¹W: white wine; R: red wine.

² Confidence interval calculated by IRTA-INCAVI from the results of inter-comparison analysis.

Table 4.4. Values of total sulfur dioxide concentration obtained with the microanalytical flow system and with the standard accredited Paul method for 18 wine samples. The confidence intervals are calculated with a level of 95%.

Wine ¹	Free sulfur dioxide concentration (mg L ⁻¹)		Relative error (%)
	Microanalytical flow system (n = 3)	Accredited Paul method ²	
W 11	104 ± 5	105 ± 13	-1
W 12	121 ± 6	128 ± 15	-5
W 13	76 ± 4	77 ± 10	-1
W 14	73 ± 4	79 ± 10	-8
W 15	65 ± 3	69 ± 9.0	-6
W 16	72 ± 4	82 ± 10	-12
W 17	70 ± 4	74 ± 10	-5
W 18	96 ± 5	103 ± 13	-7
R16	61 ± 3	64 ± 8	-5
R17	73 ± 4	68 ± 9	7
R 18	62 ± 3	67 ± 9	-7
R 19	54 ± 6	61 ± 8	-11
R 20	85 ± 4	105 ± 13	-19
R 21	45 ± 2	43 ± 6	5
R 22	64 ± 3	74 ± 9	-13
R 23	17.4 ± 0.9	17 ± 3	0
R 24	130 ± 6	132 ± 16	-1
R 25	42 ± 2	37 ± 5	13

¹ W: white wine; R: red wine.

² Confidence interval calculated by IRTA-INCAVI from the results of inter-comparison analysis.

The results comparing both methods with the least squares regression are shown in Table 4.5 and Figure 4.10. For free sulfur dioxide, the slope in both cases, red and white wines, is close to 1, but again the values of a negative intercept for white wine indicates that the microanalytical flow system underestimates the SO₂ content due to a low diffusion rate of the SO₂ through the membrane. However, this value is lower than for the Ripper method, which is in accordance with the different sign of errors seen in Table 4.5. For red wines, the positive value of the intercept indicates the opposite effect, an overestimation of the microanalytical flow method in accordance with positive values of errors shown in Table 4.5. On the other hand, for total sulfur dioxide determination, the values of slope and regression coefficient are close to 1 indicating a good correlation between both methods. Again the values of intercept indicate certain systematic deviation with the same tendency as for free SO₂. This difference between white and red wines for almost all sets of analysis is indicating a kind of interference or matrix effect.

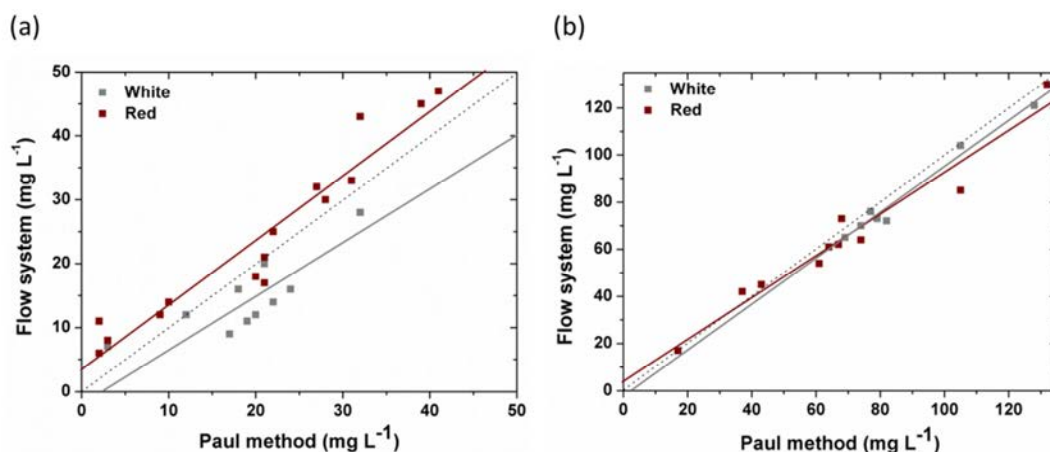


Figure 4.10. Comparative results from least squares analysis between the Paul method and the microanalytical flow system for (a) free SO₂ and (b) total SO₂ determination. The dotted line corresponds to the ideal correlation between methods.

Table 4.5. Least squares parameters obtained comparing the microanalytical flow system and the iodimetric method (Ripper method) and the Paul method. The uncertainty intervals are calculated at the 95% confidence level.

Wine	Free sulfur dioxide			Total sulfur dioxide		
	Slope	Intercept	r	Slope	Intercept	r
Ripper method						
White wine	1.0 ± 0.1	-4.7 ± 4.2	0.966	1.2 ± 0.5	-25.7 ± 58.8	0.657
Red wine	1.0 ± 0.1	-1.1 ± 1.4	0.985	0.9 ± 0.2	9.8 ± 17.1	0.885
Paul Method						
White wine	0.9 ± 0.2	-2.2 ± 4.9	0.782	1.0 ± 0.1	-3.1 ± 6.1	0.986
Red wine	1.0 ± 0.1	3.4 ± 2.0	0.956	0.9 ± 0.1	4.1 ± 5.2	0.972

As conclusion, the results obtained with the developed microanalytical flow system demonstrate the feasibility of the proposed system in a range of SO₂ from 1 mg L⁻¹ to 60 mg L⁻¹ and from 30 mg L⁻¹ to 300 mg L⁻¹ for the determination of free and total SO₂, respectively, and a LOD of 0.5 mg L⁻¹. The evaluation of the system with 70 wine samples and the comparison with two reference methods has demonstrated that there is a good correlation between both methods but an underestimation of values obtained with the microanalytical flow system for free sulfur dioxide determination in white wines is present. Even though, it is shown that this system could be feasible for a rapid and automatic analysis of wine in the cellar. It is worthwhile to notice that best comparative results are obtained with Paul method, which is an accredited laboratory method.

4.1.2 Microanalytical flow system for free SO₂ and acetic acid determination

The objective of this work was to develop a microanalytical flow system for the simultaneous detection of free SO₂ and the acetic acid by using the same methodology (pH-ISFET and gas-diffusion membrane) of detection tested previously for free and total SO₂ detection. This system was planned to be placed in a wine barrel and therefore needed some special requirements of miniaturization and reduction of reagents and sample consumption. For that reason the gas-diffusion chamber and the pH detection cell were joined in the same assembly as it is shown in Figure 3.16 (section 3.6.2). The total size of this assembly was 3 cm×7 cm×2 cm.

4.1.2.1 Optimization of the system for free SO₂ determination

Most of the chemical and hydrodynamics parameters were already optimized in the previous chapter for the free/total sulfur dioxide system.

The determination of free SO₂ was carried out under continuous flow conditions due to stop-flow did not improve the gas-diffusion rate with this chamber configuration. The flow rate was selected at 0.25 L min⁻¹. The measurement time for the sample was fixed taking into account the stabilization of the signal recorded by the pH-ISFET, thus indicating that the diffusion of the SO₂ has been completed. The optimized experimental conditions were obtained from the pH-ISFET signal recorded from triplicate calibrations in a range from 5 mg L⁻¹ to 60 mg L⁻¹ of free SO₂ (Figure 4.11a). From this figure, a time of 8 min and 6 min for the background solution (0 mg L⁻¹) and the sample/calibration solution (5, 30 or 60 mg L⁻¹), respectively, was fixed as optimal conditions in continuous flow because the signal recorded by the pH-ISFET is quite stable at this time. The analytical signal used for obtaining the calibration plot was the mean value of the last 15 s for each background or sample/calibration solution (Figure 4.11b). A linear variation of potential with the increasing concentration of SO₂ was observed, with a sensitivity of -56.1 ± 0.5 mV dec⁻¹ ($r = 0.997$) and a LOD of 4.2 mg L⁻¹ (calculated according to the IUPAC criterion for potentiometric sensors).

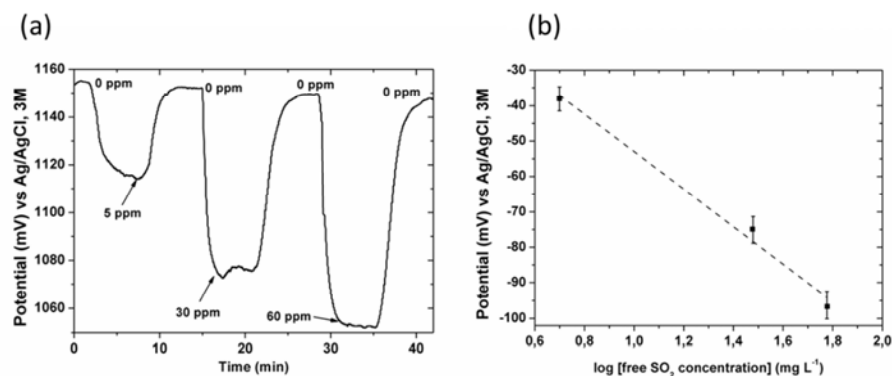


Figure 4.11. (a) pH-ISFET signals recorded and (b) calibration curve obtained for the free SO₂ determination in presence of 0 mg L⁻¹, 5 mg L⁻¹, 30 mg L⁻¹ and 60 mg L⁻¹ of SO₂. Standard deviation of triplicated calibrations is drawn as error bars.

4.1.2.2 Optimization of the system for acetic acid determination

The setup used for the acetic acid determination is depicted in in Figure 3.16 (section 3.6.2). The flow mode (continuous or stop flow), the concentration of the potassium acetate in the carrier solution and the pH of the carrier were optimized in a range of acetic acid concentration from 100 mg L⁻¹ to 1400 mg L⁻¹.

First tests for the acetic acid determination were carried out under continuous flow conditions in order to minimize measurement times. For that, the carrier (1×10⁻⁴ potassium acetate and 0.01 M KCl) and the adjusted sample with HCl 0.6 M were pumped at a total flow of 0.5 mL min⁻¹ during 7 min. The signal recorded by the pH-ISFET in triplicate in a range from 100 mg L⁻¹ to 1400 mg L⁻¹ of acetic acid is shown in Figure 4.12a. The calibration plot using the mean value of the last 15 s for each sample is shown in Figure 4.12b. As can be seen, there was not a linear fitting of the recorded signal with increasing concentration of acetic acid. This demonstrates that under continuous flow conditions there is not a good acetic acid diffusion from the sample to the carrier solution.

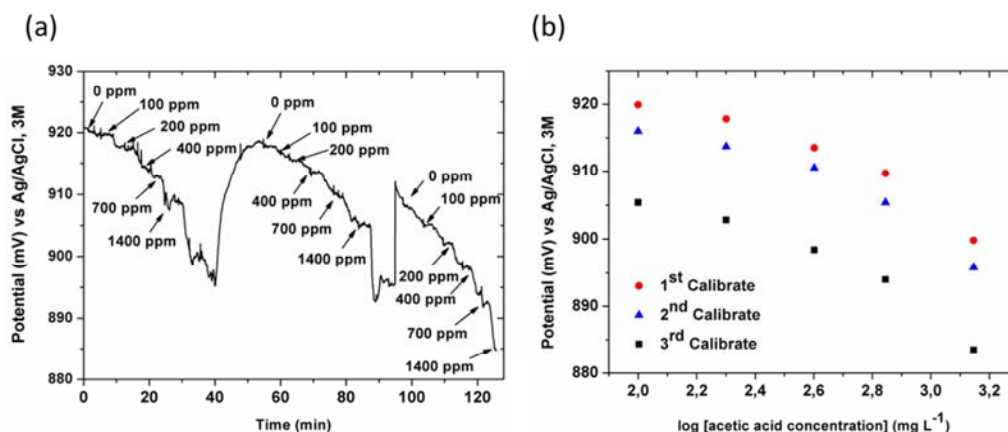


Figure 4.12. (a) pH-signal (mV) recorded by the ISFET and (b) Calibration curve obtained for the acetic acid determination in presence of 100 mg L⁻¹, 200 mg L⁻¹, 400 mg L⁻¹, 700 mg L⁻¹ and 1400 mg L⁻¹ of acetic acid.

Based on these results, stop flow conditions were checked to improve the linear fitting. For that, an experiment using colorimetric detection to visualize the diffusion of acetic acid through the membrane was performed. A 10⁻⁴ M potassium acetate carrier solution with the colorimetric indicator bromothymol blue was flowed to the gas-diffusion membrane. In the other side of the gas-diffusion chamber, a sample solution with a high concentration of acetic acid was also flowed. Both solutions were kept in contact in both sides of the membrane during 10 min, and the carrier solution chamber was recorded on video. As can be seen in the Figure 4.13, the initial color of the solution (at t = 0 min) is blue (pH above 8), indicating that the diffusion of the acetic acid from the sample to the carrier solution has not initiated. After 5 min of contact between the sample and the carrier solution, the color of the carrier solution is green, indicating that a fraction of the acetic acid from the sample has been collected by the carrier solution and its pH has decreased (around 6.5–7). Finally, after 10 min, the carrier solution is totally yellow (pH below 6), meaning that all the acetic acid from the sample has passed through the gas-diffusion membrane and has been collected by the carrier solution. Therefore, the optimized time of stop flow conditions necessary for the total acetic acid diffusion from the sample to the carrier solution was fixed at 10 min for next experiments.

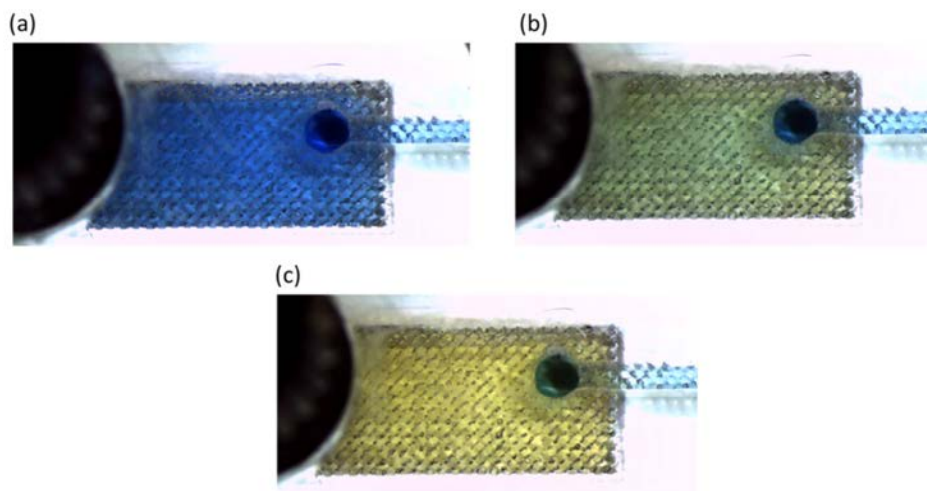


Figure 4.13. Picture of the carrier solution side chamber recorded on video in presence of the bromothymol blue: (a) at the beginning of the test; (b) after 5 min and (c) after 10 min of contact between the sample and the carrier solution in the gas-diffusion chamber.

Three different concentrations of the potassium acetate (10^{-2} M, 10^{-3} M and 10^{-4} M) in the carrier solution were checked. The carrier solution and the adjusted sample were flowed at a total flow rate of 0.5 mL min^{-1} during 5 min, and then, the flow was stopped and both solutions were in contact with the gas-diffusion membrane during 10 min. Finally, the carrier solution was flowed during 10 s at 0.5 mL min^{-1} for arriving to the pH-ISFET and the signal was recorded during 2 min in stop flow conditions. The mean value of the last 15 s was used for the calibration plot for each concentration of carrier checked. A linear response was obtained for the potassium acetate concentration of 10^{-3} and 10^{-4} M. However, sensitivity obtained for 10^{-3} M potassium acetate was twice higher than that obtained for 10^{-4} M. The stability in consecutive measurements was also higher for 10^{-3} M. Therefore, the optimal concentration of potassium acetate in the carrier solution was fixed to 10^{-3} M.

The pH of the carrier solution was also evaluated. As shown in Figure 4.3 acetic acid and acetate coexist in the pH range from 3 to 7. At pH below 4.8, the predominant specie is the acetic acid, meanwhile the acetate is the predominant one for pH above 4.8. The carrier solution, after being prepared and stabilized, had a pH around 6 (acetate as predominant specie). Two pH were tested, pH 5.5 and 7. These results showed that the sensitivity decreased when the pH of the carrier solution was adjusted, therefore the carrier without modification of its pH favor the diffusion of the acetic acid through the membrane.

The fluidic system for acetic acid determination was evaluated using the optimized conditions. The carrier solution (1×10^{-3} M CH_3COOK and 0.01 M KCl, pH 6) and the sample solution (pH close to 1, acidified with 0.6 M HCl) were pumped during 5 min at 0.5 mL min^{-1} . Then, they were in contact in both sides of the gas-diffusion membrane during 10 min in stop flow conditions, and after it, the carrier solution was flowed during 10 s at 0.5 mL min^{-1} to arrive to the pH-ISFET chamber. Finally, the signal was recorded during two minutes for each concentration of the acetic acid (range from 150 mg L^{-1} to 1400 mg L^{-1}) (Figure 4.14). Each sample was measured by triplicate.

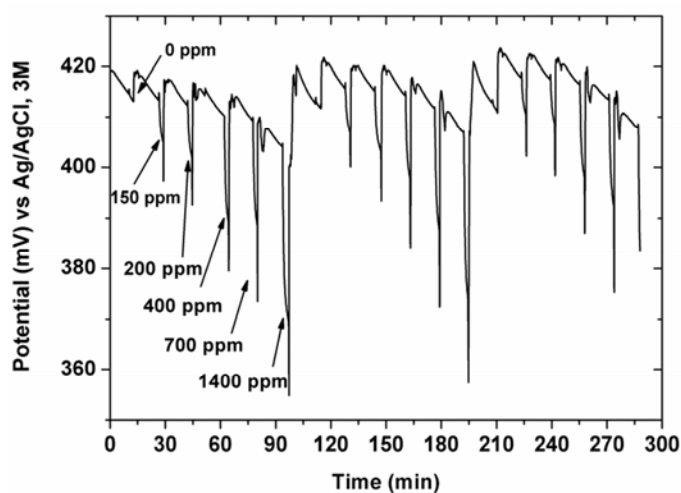


Figure 4.14. pH-signal (mV) recorded by the ISFET in presence of 150 mg L^{-1} , 200 mg L^{-1} , 400 g L^{-1} , 700 mg L^{-1} and 1400 mg L^{-1} of acetic acid.

The calibration plot was obtained using the mean value of the recorded signal of the last 15 s was for each acetic acid concentration. Although the sensitivity was very similar for the three replicates ($-34.6 \pm 2.0 \text{ mV dec}^{-1}$), the coefficient of regression was lower for the second and the third replicates (0.999 the first one and 0.980 the last one). In order to avoid the periodic use of control solutions for adjusting the calibration plot, a new strategy was proposed for plotting the calibration curves. In this case, the analytical signal taken for each sample was the difference between the sample signal at the end of the 2 min under stop flow (the same that in the previous procedure) and the signal at the end of the 10 minutes of the gas-diffusion. Using this procedure, the sensitivity changed slightly for consecutive replicates ($-32.4 \pm 1.8 \text{ mV dec}^{-1}$) and the coefficient of regression is 0.999 in all the cases.

4.1.2.3 Analysis of wine samples

The evaluation of this system with wine samples was carried out separately, first for acetic acid and after for free SO₂, and finally for both parameters

4.1.2.3.1 Acetic acid

The acetic acid system was evaluated with two commercial wines and four wines provided by the IRTA-INCAVI. Previously, the fluidic system was calibrated in a range from 100 mg L⁻¹ to 1000 mg L⁻¹. Then, each wine sample was evaluated by triplicate and the recorded signal was interpolated in the calibration plot.

The content of acetic acid in commercial wines was unknown, therefore solutions containing the same volume of wine spiked with different concentrations of acetic acid (0, 150, 500 and 1000 mg L⁻¹) were measured. The results obtained for the two commercial wines (a table wine, Don Simón, and a wine with DO Penedés, Spain, Sumarroca) are shown in Table 4.6 and Table 4.7. According to the results for Don Simon (Table 4.6), the wine had an acetic acid concentration of around 560 mg L⁻¹. This value had an important deviation (18% RSD) due to the drift of the baseline. However, wine samples with spiked acetic acid provided better results, with a RSD below 4%. The recovery values (100 × obtained value/(control+added value)) are above 98% for 500 and 1000 mg L⁻¹ samples and 94 % for 150 mg L⁻¹ spiked samples. As shown in Table 4.7, Sumarroca wine had an acetic acid concentration of 408 mg L⁻¹. This value had a low relative deviation (RSD 8%). For the spiked samples the RSD was below 6%. The recovery values for these wine samples were showing a different behavior than for Don Simon wine, since this recovery is worst for high acetic acid values.

Table 4.6. Values of acetic acid concentration obtained with the microanalytical flow system for the Don Simón wine. The standard deviation for the experimental method is represented in brackets.

Wine	Acetic acid concentration (mg L ⁻¹)		% Recovery
	Experimental (n=3)	Theoretical	
Wine	561 (104)	561	-
Wine + 150 mg L ⁻¹	671 (27)	711	94
Wine + 500 mg L ⁻¹	1038 (24)	1061	98
Wine + 1000 mg L ⁻¹	1563 (37)	1561	100

Table 4.7. Values of acetic acid concentration obtained with the microanalytical flow system for the Sumarroca wine. The standard deviation for the experimental method is represented in brackets.

Wine	Acetic acid concentration (mg L ⁻¹)		% Recovery
	Experimental (n=3)	Theoretical	
Wine	408 (35)	408	-
Wine + 150 mg L ⁻¹	544 (13)	558	94
Wine + 500 mg L ⁻¹	826 (53)	908	98
Wine + 1000 mg L ⁻¹	1184 (49)	1408	100

4.1.2.3.2 Free SO₂

Secondly, the free SO₂ system was also evaluated with one commercial wine and nine wines provided by the IRTA-INCAVI laboratory. At first, the microanalytical flow system was calibrated in a range from 5 mg L⁻¹ to 40 mg L⁻¹. Then, each wine sample was evaluated by triplicate and the recorded signal was interpolated in the calibration plot.

The same methodology that used for acetic acid was applied here: wine samples were spiked with 5, 10, 15 and 40 mg L⁻¹ of SO₂. The results are shown in Table 4.8. Theoretical SO₂ concentration corresponds to the sum of the concentration of wine (control) plus the 70 % of added SO₂, given that the other 30 % is bounded to aldehydes, ketones, sugars or acids present in wines [22]. According to the results for Don Simon, the wine has SO₂ concentration of around 23 mg L⁻¹. The recovery values obtained for spiked samples were quite satisfactory.

Table 4.8. Values of free SO₂ concentration obtained with the microanalytical flow system for the Don Simón wine sample.

Wine	Free SO ₂ concentration (mg L ⁻¹)		% Recovery
	Experimental	Theoretical	
Wine	23.2	23.2	-
Wine + 5 mg L ⁻¹	27.3	26.7	102
Wine + 10 mg L ⁻¹	27.3	30.2	90
Wine + 15 mg L ⁻¹	30.5	33.7	91
Wine + 40 mg L ⁻¹	47.1	51.2	92

Another test was carried out with a set of red, white and rosé wine samples provided by IRTA-INCAVI laboratory. Results from the microanalytical flow system were compared with them obtained with the accredited Paul method (Table 4.9). As can be seen in the Table 4.9, the repeatability of the method is quite good, given that the RSD is below 10% for almost all samples. Only the sample 9735/W* had a higher RSD value of 32%. Comparing results with those from IRTA-INCAVI we observe high relative errors for

white wines and lower errors for rose and red wines. However, the number of red and rose samples was not as much representative as white samples. There is a high dispersion of relative errors (negative and positive), which means that the difference between both methods is not due to a systematic error. In general, values obtained with our method are higher than that obtained with the IRTA-INCAVI method. It is important to notice that all values of our method are within the confidence interval of the standard method. The values of SO₂ for samples with higher concentrations of acetic acid (samples 9619, 9730, 9791) do not present the highest relative errors. Besides, the samples spiked with acetic acid in the IMB after SO₂ analysis, provide lower values than IRTA-INCAVI. This is indicative that acetic acid does not interfere in the SO₂ detection system.

Table 4.9. Values of free SO₂ concentration obtained with the microanalytical flow system and the standard method applied by the IRTA-INCAVI for several wine samples. The standard deviation for the microanalytical flow system is represented in brackets.

Wine ¹	Free SO ₂ concentration (mg L ⁻¹)			Volatile acidity (mg L ⁻¹)
	Microanalytical flow system (n=3)	Standard method ²	Relative error %	
9616/W	13.7 (0.4)	12 ± 4	14	1220
9731/W	11.3 (0.3)	9 ± 3	26	180
9733/W	18.9 (0.2)	12 ± 4	58	210
9734/W	14.0 (1.2)	21 ± 7	-33	130
9735/W	24.4 (1.8)	27 ± 9	-10	120
9735/W*	20.8 (6.7)	-	-	-
9787/RO	17.9 (0.5)	23 ± 7	-22	210
9788/RO	14.0 (0.4)	13 ± 5	8	180
9788/RO*	19.1 (0.8)	-	-	-
9730/R	34.2 (1.3)	33 ± 10	4	370
9730/R*	19.9 (2.1)	-	-	-
9791/R	16.2 (0.7)	16 ± 5	1	520

¹W: white wine; R: red wine; RO: ROSE wine

²Confidence interval calculated by IRTA-INCAVI from the results of inter-comparison analysis.

*Spiked with 700 ppm acetic acid.

4.1.2.3.3 Acetic acid and free SO₂

After the individual analysis of the free SO₂ and the acetic acid concentration in wine samples, a new set of wine samples were analyzed to validate the system for the simultaneous detection of both analytes against the official methods. All these analyses were carried out at the IRTA-INCAVI laboratories in order to compare the results between methods in real time. Once the system was calibrated for both species, the 12 wine samples were tested for acetic acid and SO₂ consecutively.

Results of the comparative analysis are shown in Table 4.10 and Table 4.11 for free SO₂ and acetic acid, respectively. It is important to notice that values for volatile acidity are referred to the volatile acids present in wine, of which the major content comes from acetic acid, therefore this value was taken as an estimation. Values for red wines showed a quite good correlation between both methods either for acetic acid and SO₂ parameters. Even for samples that had been spiked with extra sulfite the errors were very low. For rosé wines, negative error's values for SO₂ indicate an underestimation of the concentration for the proposed method, although the values of the microanalytical flow system are within the confidence interval of IRTA-INCAVI data. This underestimation is maybe related to the low diffusion rate though the membrane for low SO₂ concentrations. For acetic acid the values for samples RO2 and RO3 had a high error but of different sign, meaning that there was not a systematic error associated. For free SO₂, the relative errors are also high for these Rosé wines. The results for white wines were more dispersed. For acetic acid, the samples with high content of sugar (W2) and cava type (W3) interfered in the analysis, providing higher values. For the SO₂ analysis, the error was acceptable for the three samples except for the sparkling sample (W4), where it is supposed that the carbonic acid is interfering.

Table 4.10. Values of free SO₂ concentration obtained with the microanalytical flow system and with the standard accredited Paul method for 12 wine samples.

Wine ¹	Free SO ₂ concentration (mg L ⁻¹)		Relative error %
	Microanalytical flow system	Standard method ²	
W1	18	19 ± 6	-6
W2 ^a	25	22 ± 7	12
W3 ^b	57	46 ± 14	23
W4 ^c	21	5 ± 2	328
RO1	16	19 ± 6	-14
RO2	4	5 ± 2	-14
RO3	3	6 ± 2	-50
R1	15	15 ± 5	0
R2	13	11 ± 4	17
R3	4	4 ± 2	0
R4	14	15 ± 5	-5
R5	25	25 ± 8	0

¹ W: white wine; R: red wine.

² Confidence interval calculated by IRTA-INCAVI from the results of inter-comparison analysis.

^a High sugar content; ^b cava wine, ^c sparkling

Table 4.11. Values of acetic acid concentration obtained with the microanalytical flow system and with the standard accredited potentiometric method for 12 wine samples.

Wine ¹	Acetic acid concentration (mg L ⁻¹)		
	Microanalytical flow system	Standard method ²	Relative error %
W1	311	290 ± 47	7
W2 ^a	524	180 ± 33	191
W3 ^b	1538	230 ± 40	568
W4 ^c	172	170 ± 32	1
RO1	221	240 ± 41	-8
RO2	366	290 ± 47	26
RO3	235	350 ± 55	-33
R1	292	260 ± 43	12
R2	436	470 ± 70	-7
R3	642	700 ± 98	-8
R4	727	700 ± 98	4
R5	678	700 ± 98	-3

¹W: white wine; R: red wine.

²Confidence interval calculated by IRTA-INCAVI from the results of inter-comparison analysis.

^aHigh sugar content; ^bcava wine, ^csparkling

The data obtained for the microanalytical flow system was plotted versus those obtained by the standard methods (Figure 4.15). For free SO₂, the data from W4 sample was removed and for acetic acid the data from W2 and W3 samples were removed. The differences between both methods for free SO₂ analysis separating the wines as function of their type were analyzed by the least squares method (Table 4.12). For free SO₂, the slopes are close to 1, indicating a good agreement between both methods. The negative and positive values of the intercept for the three types of wine are in agreement with the previous comments (overestimation of concentration for white wines and our system). The value of the regression coefficient for white wines is lower than 0.9, meaning that there was not an ideal behavior.

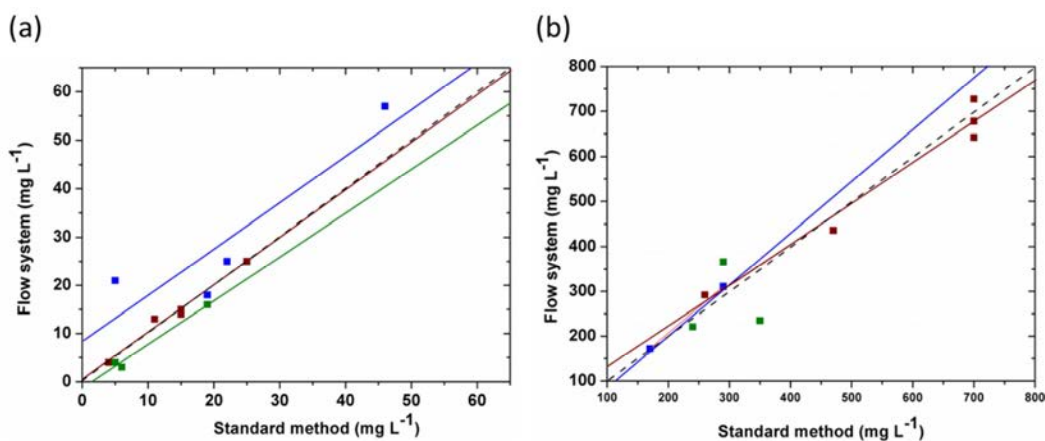


Figure 4.15. Comparative results from least squares analysis between the standard method and the microanalytical flow system for (a) free SO₂ and (b) acetic acid determination. The dotted line corresponds to the ideal correlation between methods. Red, green and blue filled squares correspond to red, rosé and white wine samples, respectively.

Table 4.12. Least squares parameters obtained comparing the microanalytical flow system and the standard method for the free SO₂ determination. The uncertainty intervals are calculated at the 95% confidence level.

Wine*	Free SO ₂		
	Slope	Intercept	r
Red wine	1.0 ± 0.1	0.6 ± 1.0	0.994
Rosé wine	1.0 ± 0.1	-1.5 ± 1.5	0.982
White wine	1.0 ± 0.1	8.2 ± 8.7	0.855

*W4 not included in the analysis of free SO₂

4.2 L-lactate amperometric biosensor

During malolactic fermentation process of wine, L-lactic acid is monitored and its evolution is strongly related with the quality of the final product. Nowadays the analysis of L-lactic acid is carried out off-line in a laboratory. Therefore, there is a clear demand for analytical tools that enabled real-time monitoring of this process in field and biosensors have positioned as a feasible alternative in this regard.

In this work, the development and characterization of a biosensor for L-lactate determination based on the co-immobilization of LOX and HRP has been described. The enzymatic reactions associated with the developed L-lactate biosensor is described in Equation 1.15 (section 1.1.2.2).

4.2.1 Optimization of the LOX:HRP ratio

In order to assess the optimal enzyme ratio whose coupled activity provided with the best analytical signal, solutions containing different LOX:HRP proportions were analyzed with a colorimetric method, as described in the experimental section 3.4.1. As it is shown in Figure 4.16, the absorbance value increased with the HRP activity and levels off at concentration values above 4 U. This HRP activity corresponded to the LOX:HRP ratio of 1:20, which was chosen for the further biosensor fabrication.

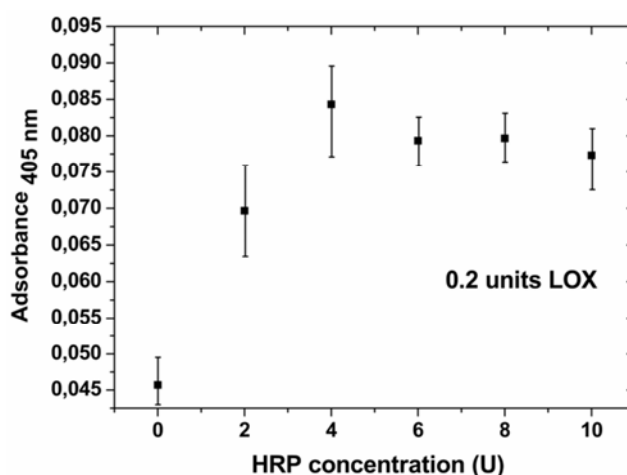


Figure 4.16. Absorbance recording of potassium ferricyanide using different LOX:HRP ratios. Measurements were carried out in PB solution containing 2 mM potassium ferrocyanide, 2 mM L-lactate, 0.2 U LOX and 0, 2, 4, 6, 8 or 10 U of HRP. Each point is the mean value of three replicates and the error bars represents the standard deviation.

4.2.2 Optimization of the conditions for the immobilization of chemical reagents on the transducer surface

Three common immobilization strategies to develop enzymatic biosensors [30] were evaluated for the L-lactate biosensor: physical adsorption with cross-linking, covalent immobilization and entrapment into an electrosynthesized polypyrrole membrane.

4.2.2.1 Adsorption and cross linking with glutaraldehyde

Firstly, 4 U LOX were physically adsorbed over the gold transducer as explained in the Section 3.4.2.1. Chronoamperometric measurements were carried out at +0.075 V (vs Ag/AgCl) in PB containing 0.1 M KCl, 2 mM potassium ferrocyanide, 80 U HRP and increasing concentrations of L-lactate, in a range from 1×10^{-7} M to 1×10^{-3} M. The faradic current associated to the reduction of the oxidized redox mediator was recorded for 120 s and the mean current value of the last 30 s was used as the analytical signal for the calibration curve shown in Figure 4.17 (blue color). There was a linear response in a concentration range from 1×10^{-5} M to 1×10^{-4} M L-lactate with a sensitivity of $(-31.4 \pm 2) \times 10^2 \mu\text{A M}^{-1} \text{cm}^{-2}$ ($r = 0.9602$). For L-lactate concentration above 1×10^{-4} M, the enzymatic biosensor was saturated, according to the normal behavior of a Michaelis-Menten enzyme kinetics [31]. Therefore, we can conclude that bi-enzymatic reaction took place because the LOX was well adsorbed on the gold surface. Three different biosensors were fabricated on the same day, obtaining a relative standard deviation (R.S.D.) of the sensitivity lower than 6 %.

In a second approach, the physical adsorption of both enzymes (4 U of LOX and 80 U of HRP) was checked following the same characterization conditions as before. Figure 4.17 (red color) shows the linear response in a concentration range from 7.5×10^{-6} M to 1×10^{-4} M with a sensitivity of $(-18.7 \pm 6) \times 10^2 \mu\text{A M}^{-1} \text{cm}^{-2}$ ($r = 0.996$) and a LOD of 6×10^{-6} M (3σ IUPAC). Three different biosensors were fabricated on the same day, obtaining a relative standard deviation (R.S.D.) lower than 5 %.

Finally, the chemical binding between the biomolecules was strengthened using glutaraldehyde as cross-linker and BSA. The new immobilization procedure was evaluated as previously. The linear response of the new biosensor was compared to the response of the previous biosensor (without cross linking) in Figure 4.17 (black color). The biosensor

sensitivity improved more than 40 % $(-74.2 \pm 3) \times 10^2 \mu\text{A M}^{-1} \text{cm}^{-2}$, $r= 0.995$), whereas linear response (L-lactate concentration from 1×10^{-6} M to 1×10^{-4} M) and the LOD (7.5×10^{-7} M, 3σ IUPAC) also improved.

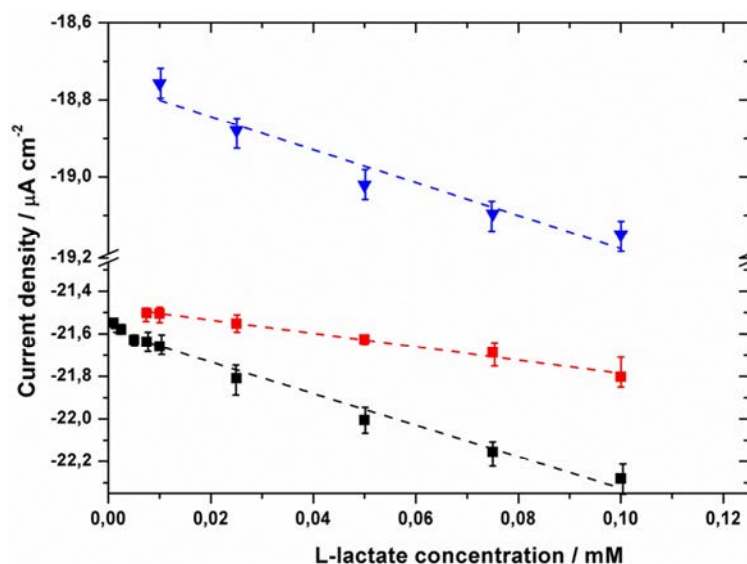


Figure 4.17. Calibration curves obtained for the three types of L-lactate biosensors: LOX adsorbed and HRP in solution (blue color); LOX and HRP physically adsorbed (red color); and LOX, HRP physically adsorbed with glutaraldehyde and BSA (black color). The error bars correspond to the standard deviation.

4.2.2.2 Covalent immobilization

4 U LOX and 80 U HRP were covalently attached on the modified gold surface of the transducer according to the procedure described in the Section 3.4.2.2. The biosensor was evaluated by chronoamperometry at +0.75 V (vs Ag/AgCl), achieving a sensitivity of $(-51.2 \pm 4) \times 10^2 \mu\text{A M}^{-1}$ ($r= 0.992$), a linear range from 1×10^{-6} M to 1×10^{-4} M and a LOD of 7.3×10^{-7} M (3σ IUPAC). The linear response is shown in Figure 4.18. Three different biosensors were fabricated on the same day, obtaining a relative standard deviation (RSD) lower than 5 %.

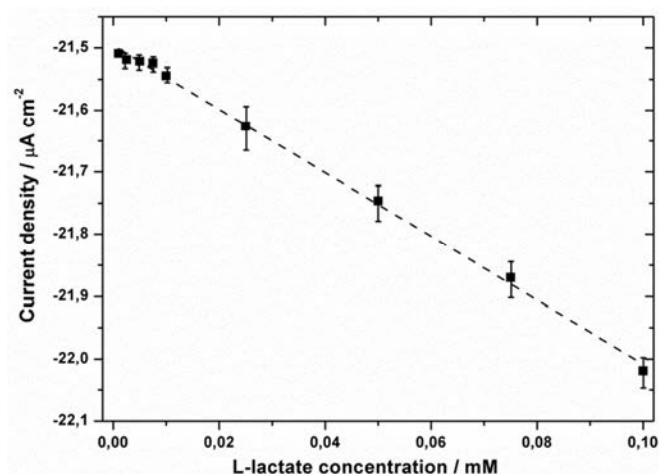


Figure 4.18. Calibration curve for the L-lactate biosensor with the LOX and the HRP covalently attached on the gold surface. The error bars correspond to the standard deviation.

4.2.2.3 Entrapment into electrosynthesized PPy membranes

As explained previously in the Section 3.4.2.3, the entrapment of enzymes into polymeric matrices allows obtaining a fast, easy and controlled method for the immobilization of biological elements on the transducer surface. For carrying out it, potentiostatic conditions were proposed. A preliminary study by cyclic voltammetry was done in order to set the potential. First and second cyclic voltammograms during PPy electrogeneration are showed and compared to the background cyclic voltammogram in Figure 4.19. The fast increase of current at potentials above +0.60 V (vs Ag pseudo-ref. electrode) in the electrogeneration solution was related to the pyrrole oxidation-polymerization. A quasi-reversible signal at a half wave potential of +0.23 V was also recorded, which could be related to the polymer film oxidation and reduction processes. From these results, the selected potential was set at +0.85 V (vs. Ag pseudo-ref. electrode).

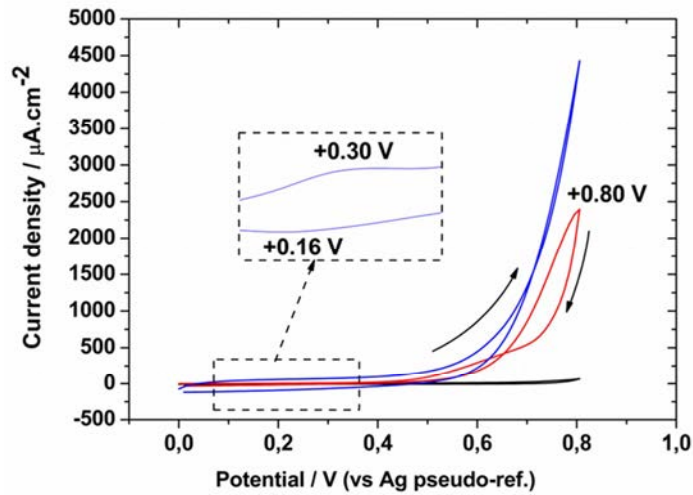


Figure 4.19. Cyclic voltammograms at 100 mV s^{-1} in the PB background solution (black color) and in the electrogeneration solution showing the oxidation/reduction peaks of the process involved in the pyrrole electrogeneration during first (red color) and second scan (blue color).

In order to ensure the reproducibility of the PPy film thickness, the charge accumulated during the PPy formation was fixed to 500 mC cm^{-2} . An example of the chronoamperometric response obtained under these conditions is shown in Figure 4.20.

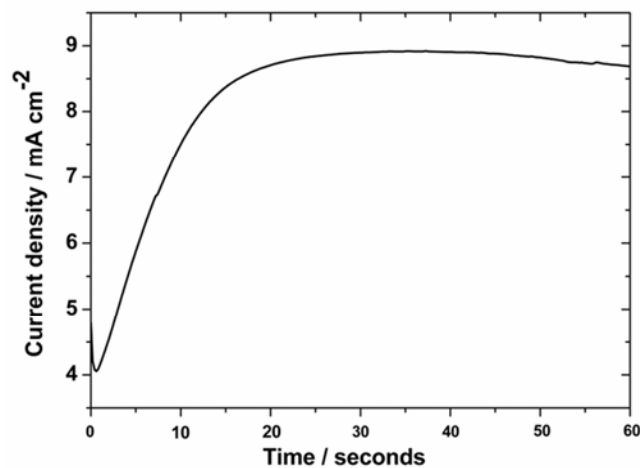


Figure 4.20. Current profile recorded during the amperometric electrogeneration of the PPy film.

The influence of three different counter ions (Cl^- , NO_3^- or ClO_4^-) on the PPy electropolymerization was assessed in terms of the sensitivity values achieved with the corresponding biosensors. Calibration curves were recorded in PB solutions containing 0.1 M KCl and L-lactate in a concentration range from $1 \times 10^{-7} \text{ M}$ to $1 \times 10^{-3} \text{ M}$. The highest

sensitivity was obtained when the PPy was generated in the presence of Cl^- ions ($-95 \times 10^2 \mu\text{A M}^{-1} \text{cm}^{-2}$), while values of $-81 \times 10^2 \mu\text{A M}^{-1} \text{cm}^{-2}$ and $-69 \times 10^2 \mu\text{A M}^{-1} \text{cm}^{-2}$ were obtained with NO_3^- and ClO_4^- , respectively. This lower sensitivity obtained with LiClO_4 and KNO_3 may be related to their oxidative power that could affect the enzyme activity. Indeed, preliminary studies carried out with HRP entrapped in PPy films showed the significant decrease of the enzyme activity when ClO_4^- ions were used.

Then, the effect of the monomer concentration on the biosensor response was studied in PB solutions containing 4 U LOX, 80 U HRP and 0.1 M KCl. Figure 4.21 depicts the biosensor sensitivity related to the monomer concentration. It is shown that the highest sensitivity was achieved for a 0.4 M pyrrole concentration. At higher concentrations of monomer, the sensitivity and the linear range of the biosensor decreased. This could be related to the generation of a thicker polymer layer with low density of enzyme that affects the diffusion of the redox mediator to reach the electrode solution interface through the membrane [32]. Also, at concentrations of pyrrole below 0.4 M no response of the biosensor was recorded and this could be related to the formation of a very thin polymer layer, which contained a low amount of enzymes entrapped in its structure.

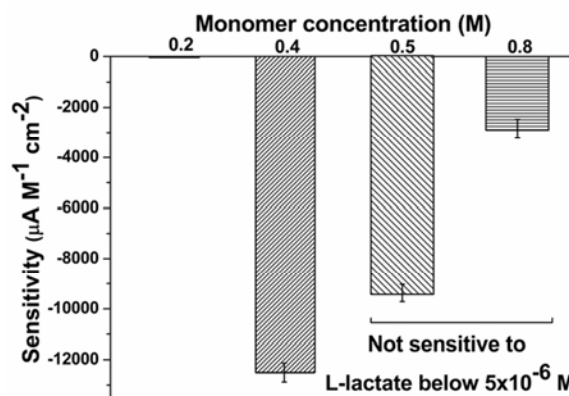


Figure 4.21. Bar plots showing the variation of biosensor sensitivity with pyrrole concentration. The error bars correspond to the standard deviation.

Finally, the effect of the LOX and HRP concentrations was evaluated in PB containing 0.4 M pyrrole and 0.1 M KCl. Three LOX:HRP concentrations (2:40, 4:80 and 6:120, in U) were tested, keeping the LOX:HRP ratio to 1:20. As can be seen in Figure

4.22, the highest sensitivity and widest linear range were achieved for the 4:80 U. Low enzyme concentrations resulted in a low amount of entrapped enzymes and a poor sensitivity. On the other hand, for high enzyme concentrations, the rate of the polypyrrole film formation decreased drastically (more than 30 minutes were required to reach the set charge of 500 mC cm^{-2}). This could be due to the transducer surface being blocked by the adsorption of the enzymes, which results in the recording of no-faradaic current and thus of no biosensor response, or to the high concentration of enzymes that could affect the polymerization rate.

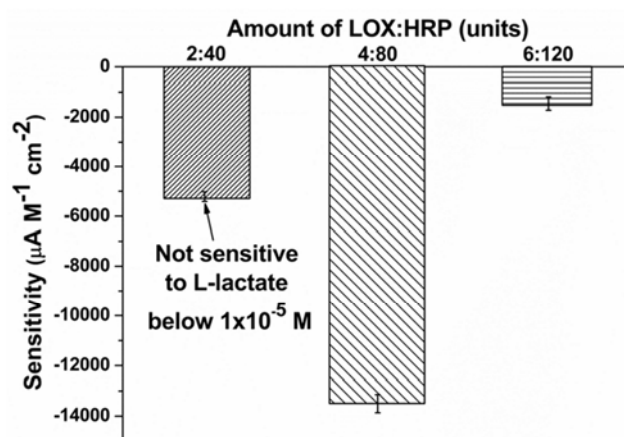


Figure 4.22. Bar plots showing the variation of biosensor sensitivity with the amount of LOX and HRP enzymes. The error bars correspond to the standard deviation.

As a summary, the optimum conditions for the electrosynthesis of the enzyme containing PPy film on the surface of the gold transducers were the following: potentiostatic conditions at $+0.85 \text{ V}$ (vs. Ag pseudo-ref. electrode) for 60 s and 500 mC cm^{-2} charge, in a PB solution containing 0.4 M pyrrole, 0.1 M KCl, 4 U of LOX and 80 U of HRP.

Once the fabrication of the biosensor was optimized, chronoamperometric measurements were carried out at $+0.075 \text{ V}$ (vs Ag/AgCl) in PB containing 0.1 M KCl, 2 mM potassium ferrocyanide and increasing concentrations of L-lactate, in a range from $1 \times 10^{-7} \text{ M}$ to $1 \times 10^{-3} \text{ M}$. The biosensor responses are shown in Figure 4.23a. As expected a more negative current density for increasing L-lactate concentrations, was obtained. The

current recorded in all cases increased and started to levels off at 100 s time after the potential application.

This current was recorded for 200 s and the mean current value of the last 60 s (140-200 s) was used as the analytical signal. From this, the sensor response was 100 s and the overall assay time is set to 200 s. The calibration curve is shown in Figure 4.23b. A linear response was observed in a concentration range from 1×10^{-6} M to 1×10^{-4} M of L-lactate with a sensitivity of $(-135 \pm 6) \times 10^2 \mu\text{A M}^{-1} \text{cm}^{-2}$ ($r = 0.998$). A limit of detection (LOD) of $5 \pm 0.2 \times 10^{-7}$ M, calculated using the 3σ IUPAC criterion was obtained. Regarding the reproducibility of the fabrication process, three different biosensors were calibrated on the same day, obtaining a relative standard deviation (R.S.D.) of the sensitivity lower than 4 %.

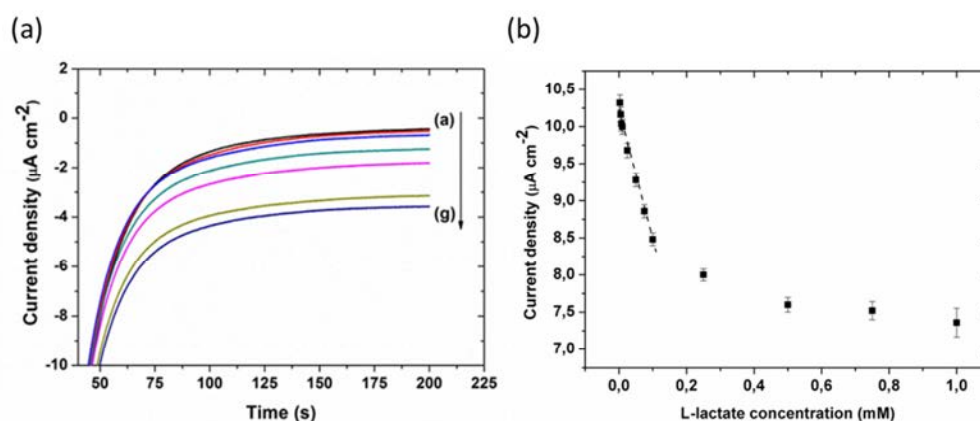


Figure 4.23. (a) Chronoamperometric response and (b) calibration curve of the PPy/LOX:HRP biosensor for L-lactate concentrations from 5×10^{-7} M (a) to 1×10^{-3} M. Each point represents the mean current value of three replicates recorded consecutively with the same biosensor, with the error bars being the corresponding standard deviation.

A morphological characterization of the PPy film was carried out. The thickness and the structure of the polymer matrix are related to the charge accumulated during the electrogeneration process and the nature and concentration of the substances involved in it (monomer, enzymes and counter-ion) [33]. A SEM image in Figure 4.24a shows the typical surface morphology of these films [34]. The roughness, opening, porosity and globular morphology of the polypyrrole films allow for the adequate enzyme loading and improve the electronic conductivity of the film. Figure 4.24b depicts a SEM image of the silicon chip, with the PPy film selectively deposited on the working electrode.

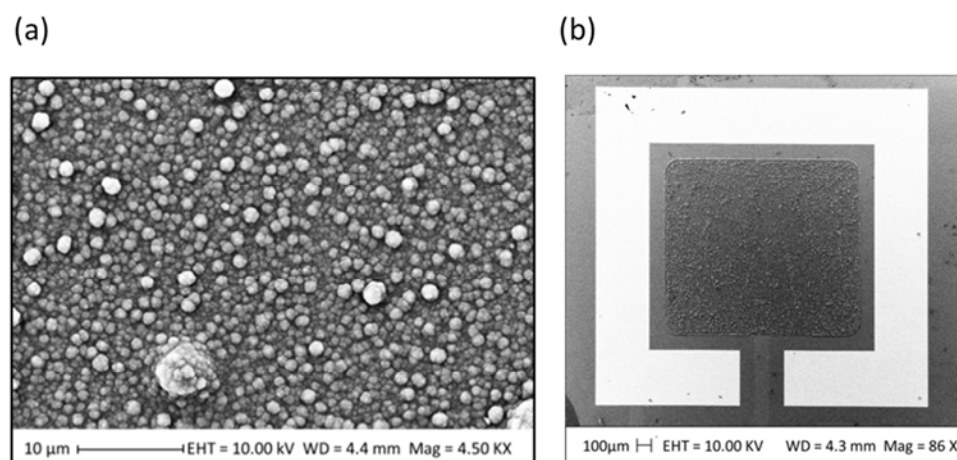


Figure 4.24. SEM images of (a) the PPy/LOX:HRP film showing the typical PPy morphology and (b) the silicon chip showing the polymer film selectively deposited on the working electrode surface.

An AFM detailed image of the PPy surface shown in Figure 4.25a, gives more information about the surface topology and roughness. A Root Mean Square (RMS) roughness of $0.24 \mu\text{m}$ was obtained. The thickness of the polypyrrole film, measured by FIB, was between $1.30\text{-}1.40 \mu\text{m}$ (Figure 4.25b).

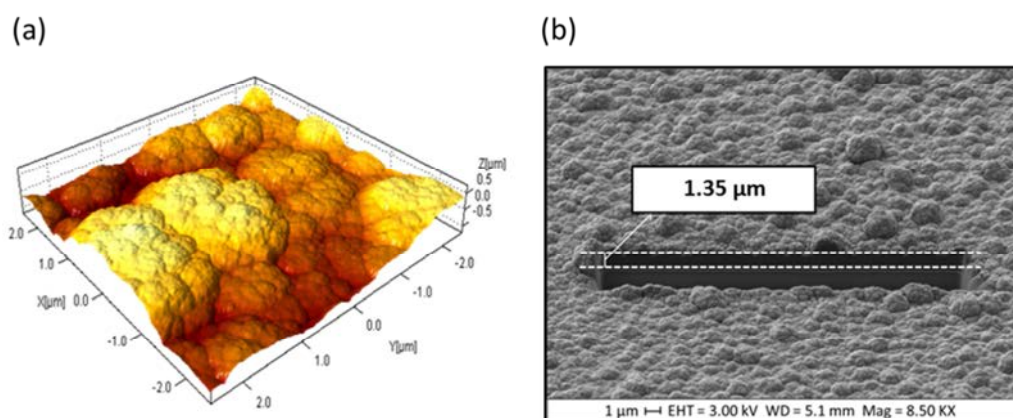


Figure 4.25. (a) AFM image of the PPy/LOX:HRP film. Scanned area: $5 \mu\text{m}^2$. (b) FIB image of the transversal membrane cut used for the estimation of the membrane thickness

4.2.3 Selection of the biosensor immobilization method

The three different biosensor immobilization strategies described in section 4.2.2 were compared in terms of sensitivity, linear range and LOD Results are summarized in Table 4.13. The sensitivity is much higher for the polymer entrapment method (60 % and 80 % compared with the physical adsorption and covalent immobilization, respectively) as was expected since for this method the biological compounds are slightly altered by the process, therefore the activity loss is much lower. The linear range of L-lactate concentration was the same for all the methods according to Michaelis-Menten enzymatic behavior, meanwhile the LOD was slightly better for the polymer entrapment. Besides, the immobilization method based on the polymer entrapment simplified the fabrication of the device with shorter production time.

Table 4.13. Analytical characteristics of the L-lactate biosensors based on three different immobilization strategies.

Protocol	Sensitivity / ($\mu\text{A M}^{-1} \text{cm}^{-2}$) $\times 10^{-2}$ (n = 3)	Linear range / M	L.O.D / M	r
Physical adsorption and cross linking	-74.2 ± 3	1×10^{-6} to 1×10^{-4}	7.5×10^{-7}	0.995
Covalent attachment	-51.2 ± 4	1×10^{-6} to 1×10^{-4}	7.3×10^{-7}	0.992
Polymer entrapment	-135 ± 6	1×10^{-6} to 1×10^{-4}	5×10^{-7}	0.998

Finally, the working stability of the biosensors prepared with these methods was evaluated and compared over 5 days. The lifetime estimated from the percentage of the initial sensitivity kept over time, is shown in Figure 4.26. For the case of the physical adsorption and cross linking, there was a pronounced loss of the signal after 3 days related to total desorption of the enzymes. This decrease was less pronounced for the biosensor with the covalent entrapment, although the sensitivity lost after 4 days is higher than 80 %. The biosensor with polymer entrapment lost less than 10% of its original sensitivity after 5 days, therefore this method appeared to be the most suitable for stable L-lactate biosensors.

According to these results, biosensors with enzymes entrapped in the polypyrrole were fully characterized and applied to the monitoring of the malolactic fermentation in wines samples.

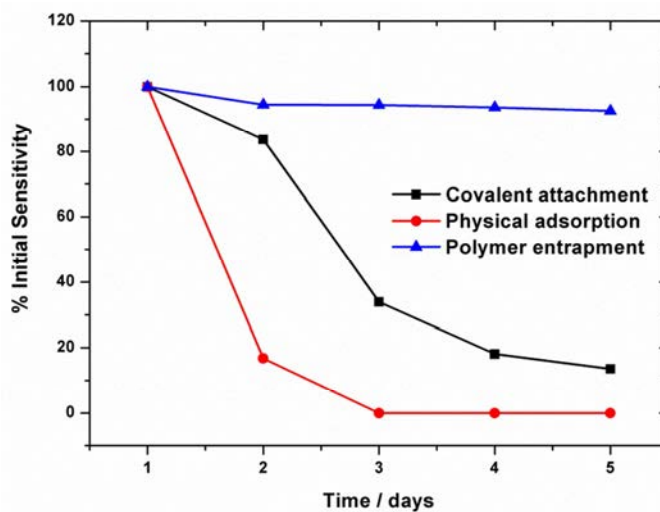


Figure 4.26. Comparative study of the working stability along 5 days for the three proposed biosensor immobilization strategies: polymer entrapment (blue color), covalent attachment (black color) and physical adsorption with cross linking (red color).

4.2.4 Monitoring of the L-lactic acid during the malolactic fermentation in wine samples.

Before the measurements with wine samples, the biosensor response to possible interferences in wine samples was assessed. For that, glycerol, glucose, gluconic acid, fructose, acetic acid, citric acid, ethanol, L-malate, tartaric acid and ascorbic acid were considered. The corresponding chronoamperometric responses are shown in Figure 4.27. Only a significant signal was obtained in the presence of ascorbic acid, due to its electrochemical oxidation at the measurement potential of +0.075 V [35]. However, red wines do not contain ascorbic acid [22] and it is not produced during the malolactic fermentation. These results demonstrate the high selectivity of the developed biosensor for the L-lactate determination.

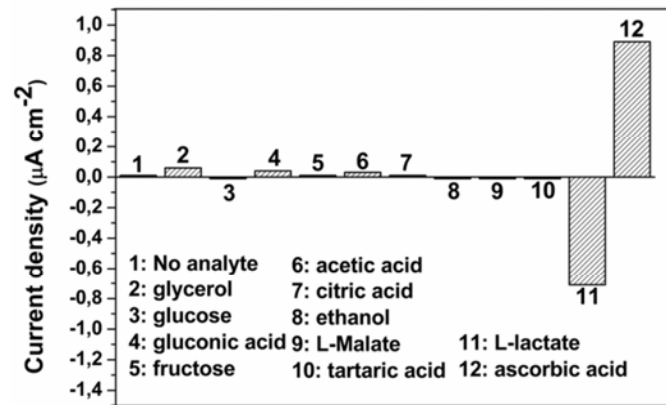


Figure 4.27. Current density response of the biosensor in solutions containing possible interferences. All of them are in a concentration of 1×10^{-5} M and were compared to the signal recorded in the background electrolyte (no analyte).

The biosensor working stability with time was studied over a longer time (52 days). When not in use, the biosensor was stored in the PB at 4 °C. As can be seen in Figure 4.28, a decrease of the sensitivity around 5 % took place during the first five days, probably related to the loss of the enzyme attached by physical absorption on the PPy film or the weaker entrapment in the PPy film (enzyme molecules closer to the outer surface of the polymer). After this time, the biosensor response remained stable and kept over 90 % of the initial sensitivity value for 42 days. From the day 45, there was a sudden decrease of the response, which could be attributed to the denaturation of the immobilized enzymes. However, this decrease represented only around 20 % of the initial sensitivity after 52 days of study.

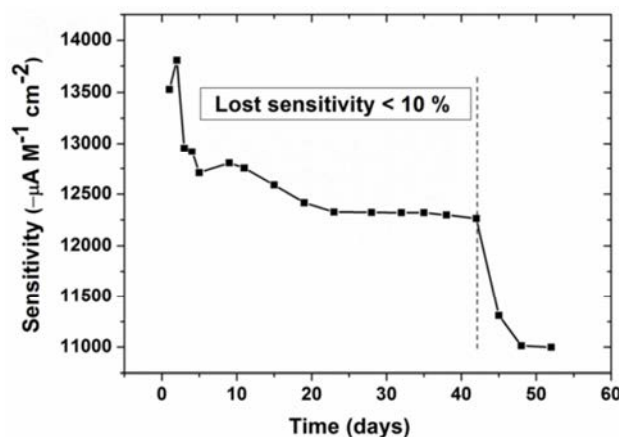


Figure 4.28. Variation of the biosensor sensitivity along 52 days.

Finally, the optimized L-lactate biosensor was applied to the monitoring of the malolactic fermentation in three different red wines. Samples collected different days during the fermentation process were provided by the IRTA-INCAVI. The 1:100 diluted wine samples were analyzed in triplicate with the biosensor. In parallel, the same samples were analyzed by the IRTA-INCAVI with the colorimetric standard method. The results from both methods were compared by plotting the L-lactic acid concentration (in g L^{-1}) versus the day of the malolactic fermentation process. As shown in Figure 4.29, there is an excellent agreement between the two values, with absolute errors below 0.09 g L^{-1} in all the cases. The evolution of the lactic acid during the fermentation processes was as expected. There was an initial slow formation, followed by an exponential increase and a final stabilization of the L-lactic acid concentration, which indicates the end of the malolactic fermentation. This behavior was particularly clear in the monitoring with "Wine 3". However, for the "Wine 1" and "Wine 2", the concentration of L-lactic acid was still increasing, which means that the process of transformation of malic acid to L-lactic acid was still in progress.

During its application, the biosensor was calibrated four times in the L-lactate concentration ranging from $1 \times 10^{-6} \text{ M}$ to $5 \times 10^{-4} \text{ M}$. These calibrations were carried out at the beginning, between the first and the second set of wines (30 analyses), between the second and the third set of wines (15 analyses) and at the end of the experiment (24 analyses). The results showed a stable sensor response, which retained over 90 % of the initial value after completing all the analyses (see Table 4.14).

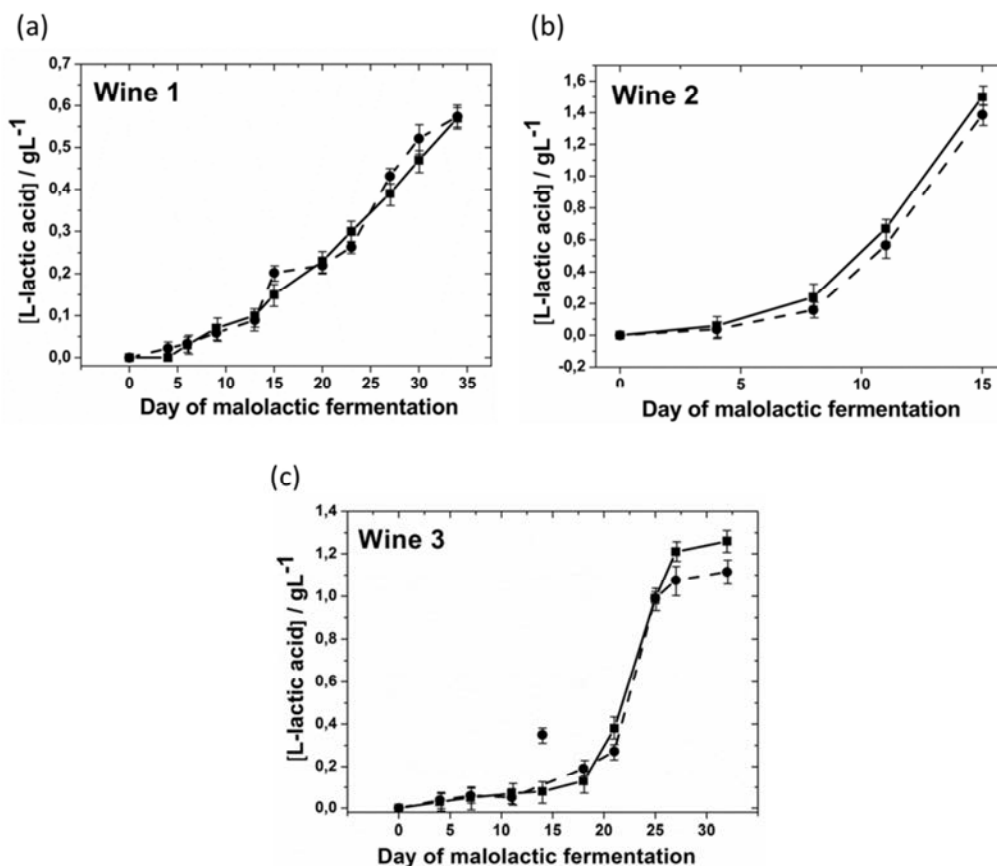


Figure 4.29. Analysis of wine samples collected during the malolactic fermentation process for three red wines. Dashed lines and filled circles show the values of L-lactic acid obtained with the colorimetric standard method and filled lines and squares ones, those measured with the proposed PPy/LOX:HRP biosensor. In the case of the biosensor, the standard deviation values of three replicates are represented as error bars in the plot. In the case of the colorimetric method, the error bars represent the uncertainty at 95 %.

Table 4.14. Data of calibration curves carried out during the analysis of the malolactic fermentation process of the three wines.

Calibration	Sensitivity / ($\mu\text{A M}^{-1} \text{cm}^{-2}$) $\times 10^{-2}$	r^2
First	-134.7	0.995
Second	-127.8	0.993
Third	-130.0	0.994
Fourth	-140.6	0.993

4.2.5 Comparison with other L-lactate electrochemical biosensors

The developed biosensor was compared with other electrochemical biosensors for L-lactate determination reported in the literature. The main characteristics of these devices are summarized in Table 1.1 in Section 1.1.2.2. Regarding the immobilization method, the proposed biosensor is the only one constructed by simultaneously entrapping both enzymes LOX and HRP in a PPy film, which simplifies the fabrication of the device. Also, biosensor production time is very short and reagent consumption has been very low.

The approach presented in this work clearly outperforms other devices in terms of operational stability and in terms of biosensor performance. It is worth mentioning that even though some of them show the required sensitivity and linear range for the measurement of L-lactic acid during the malolactic fermentation, all of them lack the long-term stability required to monitor this process, which usually takes place for up to 40 days in most wines. The proposed PPy/LOX:HRP biosensor, with a lifetime of 42 days is the only one that could be applied to this monitoring process.

It should also be highlighted that even though some of those biosensor devices have been applied to the L-lactic acid determination in real samples, such as beers, wines or milk, the long-term stability of the proposed biosensor enable the real-time of the malolactic fermentation using the same biosensor during all the process.

As conclusion, taking into account the simplicity of the biosensor fabrication, its compatibility with the microelectronic technology, the long working stability and the characteristics of the response, the developed PPy/LOX:HRP biosensor for the L-lactate acid determination represents a competitive and feasible approach for the online monitoring of malolactic fermentation in wineries.

4.3 L-malate amperometric biosensor

As explained in the introduction, this compound is one of the principal organic acids in grapes and it is converted to L-lactic acid and CO₂ by lactic acid bacteria action. The presence of L-malic acid affects the final quality of the wine by deteriorating its biochemical and microbial stability, and hence its sensorial quality and freshness. Therefore, monitoring the malolactic fermentation process is strictly required to guarantee the sensorial quality and freshness of red wines. In this chapter, the potential of a miniaturized amperometric bienzymatic biosensor as an analytical tool to be applied in such scenario is described. For that, the same methodology of enzyme immobilization that for the previous chapter is followed. A PPy membrane is generated on the surface of a gold microelectrode with the aim of entrapping the enzymes required for biosensor fabrication. Different redox mediators have been tested for selecting the most suitable in terms of signal reversibility, low oxidation potential and compatibility with the PPy membrane. A comparative study has been then conducted with three different biosensor architectures based on the partial or full immobilization of the required chemical reagents in the PPy membrane. The selected biosensor architecture has been eventually applied to the L-malic acid monitoring during the MLF of three red wines.

This L-malate biosensor is based on an enzymatic process described in Equation 1.16 (section 1.1.2.3).

4.3.1 Optimization of the DP:MDH and (DP:MDH):NAD⁺ ratios

The enzymes and co-factor relative concentrations were optimized and results are shown in Figure 4.30. The absorbance value decreased with the increase of MDH activity up to 3 U, remaining constant for higher values. Thus, the optimum DP:MDH ratio was 1:6. Then, the DP and MDH activities were fixed to 0.5 U and 3 U, respectively, and the NAD⁺ concentration was increased from 0 to 2 mM. The recorded absorbance values levelled off for NAD⁺ concentrations above 0.5 mM. Thus, the (DP:MDH):NAD⁺ ratio was set to 2:1. These ratios were selected for the further biosensor fabrication.

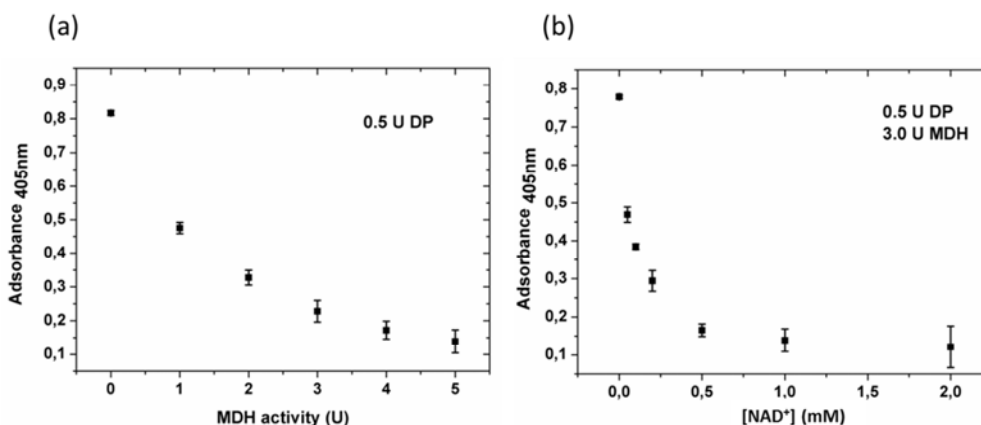


Figure 4.30. Absorbance recording of ferricyanide for different biological components ratios a) DP:MDH and b) (DP:MDH):NAD⁺. Measurements were carried out in PB solution containing 2 mM potassium ferricyanide, 2 mM L-malate and different concentration of DP, MDH and NAD⁺. Each point corresponds to the mean value of three replicates and the error bars represents the standard deviation.

4.3.2 Selection of the redox mediator

All the selected redox mediators of this study have previously been applied in amperometric biosensing [36, 37]. The corresponding cyclic voltammograms recorded with the gold microelectrodes are shown in Figure 4.31 and Figure 4.32. Table 4.15 includes the electrochemical parameters extracted from these voltammograms. Ideally, a mediator should show a fully reversible redox process taking place at low potentials, in order to avoid interferences from other species that may be present in the wine samples, and also a high current density. Also, these species should have good water solubility to allow for the strict control of the polypyrrole membrane electrosynthesis. Using the oxidation potential (E_{ox}) as the initial parameter to select these species, the lowest values were obtained for Gallocyanine, Toluidine Blue O and HAR (-250 mV, -275 mV and -180 mV, respectively). Among these three redox mediators, Gallocyanine and Toluidine Blue O showed a similar peak potential separation (ΔE_p), while this is about two times larger for HAR. Then, the ratio of oxidation to reduction peak currents was compared. Values around 1 indicate the absence of coupled chemical reactions. This is the case for Gallocyanine and HAR, while is around 2.1 for Toluidine Blue O. These three redox mediators showed oxidation peak current densities higher than $250 \mu A cm^{-2}$. Besides, all three are fully water soluble, therefore the electrosynthesis conditions of the PPy would not be modified by presence of any organic solvent.

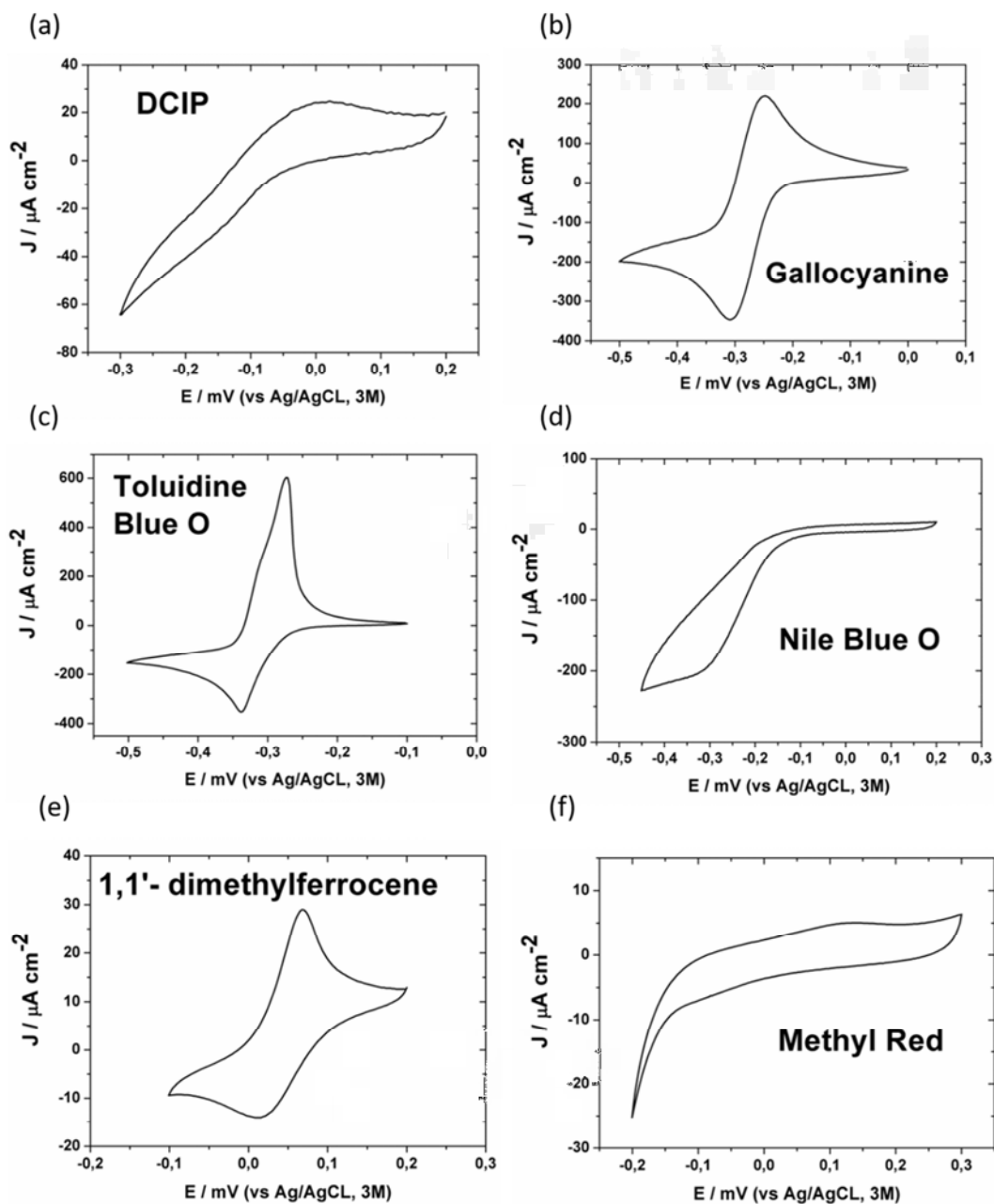


Figure 4.31. Cyclic voltammograms recorded in PBS buffer containing 2 mM of the mediator: a) 2,6-dichlorophenolindophenol sodium salt hydrate; b) Gallocyanine; c) Toluidine Blue O; d) Nile Blue A; e) 1,1-dimethylferrocene; f) Methyl Red. Scan rate = 25 mV s^{-1}

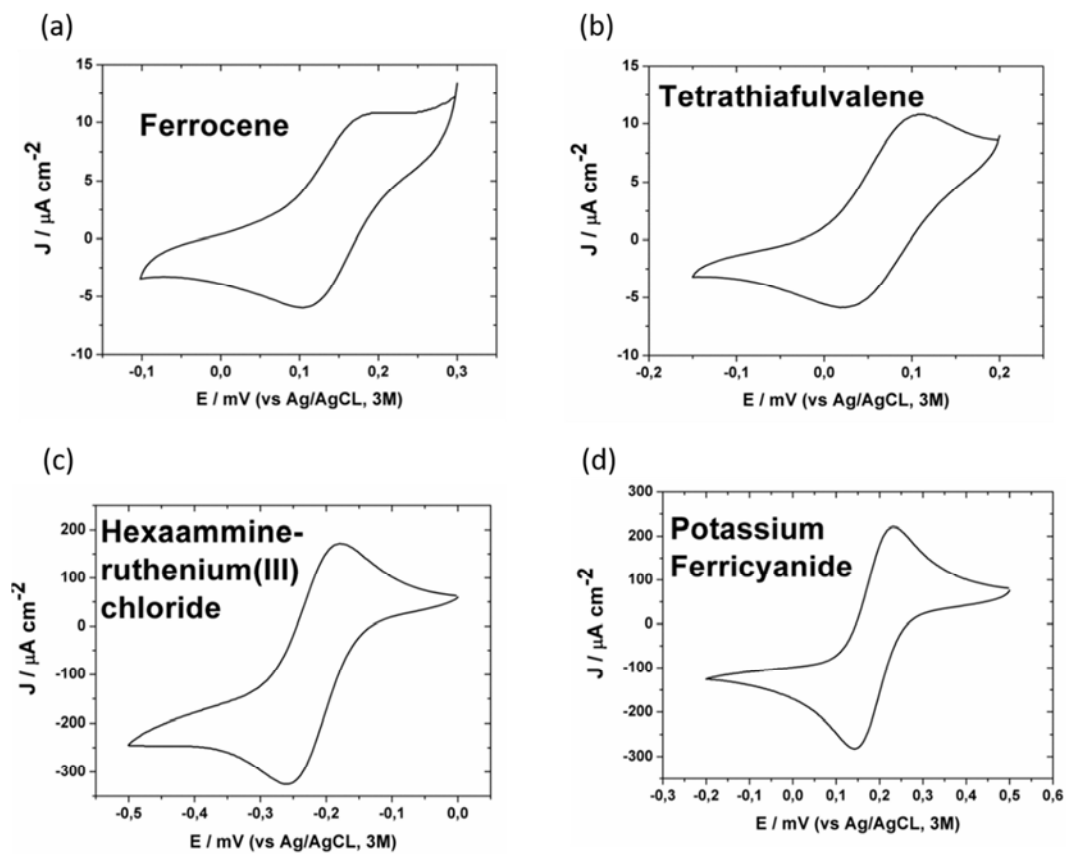
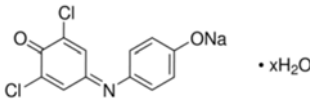
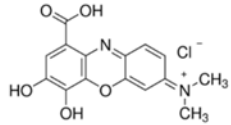
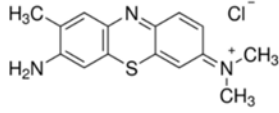
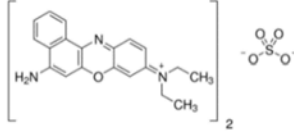
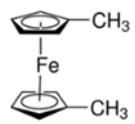
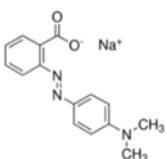
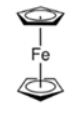
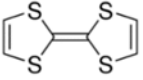
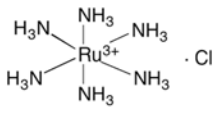
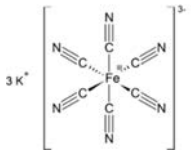


Figure 4.32. Cyclic voltammograms recorded in PBS buffer containing 2 mM of the mediator: a) Ferrocene; b) Tetrathiafulvalene; c) Hexaammineruthenium (III) chloride and d) Potassium ferricyanide . Scan rate = 25 mV s^{-1} .

Table 4.15. Chemical structures of the studied redox mediators and their main redox values obtained in solution: oxidation potential (E_{ox}), peak potential separation (ΔE_p) and the ratio between the oxidation and the reduction peak currents (I_{ox}/I_{red}).

Redox mediator	Chemical structure	E_{ox} / mV	ΔE_p / mV	$ I_{ox}/I_{red} $
2,6-Dichlorophenolindophenol sodium salt hydrate		10	55	0.4
Gallocyanine		-250	59	0.9
Toluidine Blue O		-274	66	2.1
Nile Blue A *		-	-	-
1,1'-Dimethylferrocene		68	57	1.7
Methyl Red		126	205	0.9
Ferrocene		190	85	1.3
Tetrathiafulvalene		110	94	1.8
Hexaammineruthenium (III) chloride		-180	80	0.9
Potassium ferricyanide(III)		220	120	0.8

*There is no signal of the oxidation peak current

Then, the electrogeneration of the PPy/mediator membrane on the surface of the gold transducers was carried out in solutions containing 10 mM of each of these three redox mediators. Toluidine Blue O formed a blue precipitate during the polymerization process. This is likely to be related to the polymerization of this redox mediator by the one-electron oxidation of the NH₂ group and the formation of a radical cation at the potential applied during the PPy electrosynthesis membrane [38]. By contrast, both Galloxyanine and HAR could be entrapped in the PPy membrane and the time to achieve an accumulation charge of 250 mC cm⁻² was 70 and 30 s, respectively. The resulting membranes were rinsed with PB and tested by cyclic voltammetry and then stored immersed in PB solution at 4 °C. After 24 h, the PPy/Galloxyanine- modified transducer nearly lost all its voltammetric response and the PB solution turned blue-colored, meaning that the mediator leached from the polypyrrole membrane. This may be due to charge repulsion between the positively charged pyrrole and the Galloxyanine molecules during the PPy membrane electrosynthesis that would make these species not to be efficiently entrapped and thus to be easily leached. The same experiment was repeated with PPy/HAR-modified transducer, this keeping its voltammetric response after the 24-h period. Therefore, this redox mediator was selected for the fabrication of the biosensor architecture.

4.3.3 Selection of the biosensor architecture

The working stability of the three different biosensor architectures, described in the experimental section 3.4.2.3.2, was analyzed for 38 days. The lifetime estimated from the percentage of the initial sensitivity kept over time, is shown in Figure 4.33. In the three cases, an initial decrease of the sensitivity is observed during the first eight days, probably related to partial leaching of the chemical species not tightly immobilized within the PPy membrane. This decrease was more pronounced for biosensor 3 (all reagents in the PPy membrane), which lost 30% sensitivity after 5 days and 45 % after 8 days, and biosensor 1 (redox mediator in solution), which lost 10 % sensitivity after 3 days, 20% after 7 days and 40% after 18 days. However, biosensor 2 architecture (NAD⁺ in solution) just lost 10 % after 37 days. The decrease in sensitivity of biosensor 1 and 3 is likely to be due to the fast decomposition of the entrapped NAD⁺ [39]. Biosensor 2 appeared to be the most suitable for the monitoring of L-malic acid during the red wine fermentation process, taking into account that it maintained around 90% of the initial sensitivity after 36 days. Then it suddenly decreased to 30 % of the

initial value after 37 days, probably due to the denaturation of the immobilized enzymes. This architecture was then selected and fully characterized, as described in the following sections.

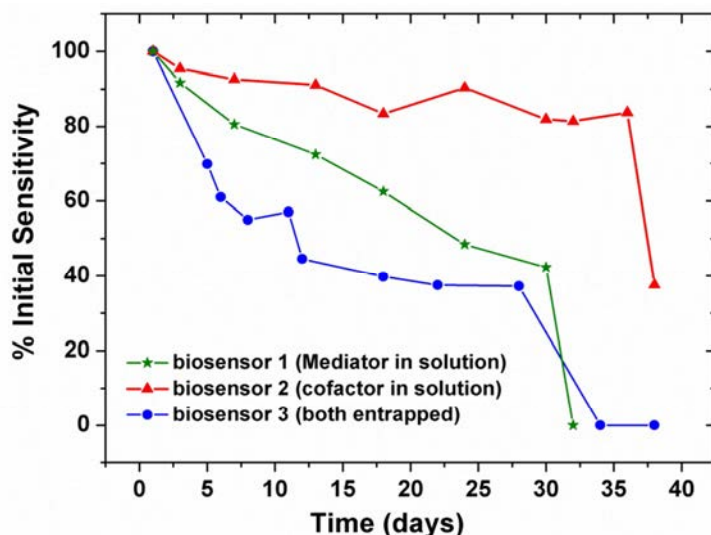


Figure 4.33. Comparative study of the working stability along 38 days for the three proposed biosensor architectures: biosensor 1 (green colored stars), biosensor 2 (red colored triangles) and biosensor 3 (blue colored circles).

4.3.4 Evaluation of the biosensor performance

The optimized biosensor was calibrated by chronoamperometry in PB solutions containing 0.1 M KCl, 5 mM NAD^+ and a L-malate concentration ranging from 1×10^{-7} M to 1×10^{-5} M. A -0.15 V potential (vs. Ag/AgCl) was chosen considering the voltammetric response of the selected redox mediator used (Figure 4.32c), at which the HAR reduced species generated by the enzymatic reaction are oxidized back to the HAR. Results are shown in Figure 4.34a. The sensor response followed an exponential trend, and the current started to level off at 70 s after initiating the measurement. The signal was recorded during 120 s and the mean current density value of the last 20 s was used as analytical signal. As expected, the recorded current density increased with the L-malate concentration. Then, it can be said that the biosensor response was 70 s and the overall assay time is set to 120 s.

The calibration curve is shown in Figure 4.34b. A linear range was observed in a concentration range from 1×10^{-7} M – 1×10^{-6} M (1.3×10^{-5} – 1.3×10^{-4} g L⁻¹) of L-malate with a sensitivity of 1365 ± 110 mA M⁻¹ cm⁻² ($r = 0.998$, $n = 5$). A limit of detection of 6.3×10^{-8} M, calculated using the 3σ IUPAC criterion, was obtained. For L-malate concentration above 1×10^{-6} M, the biosensor response is saturated, this following the

usual behavior of a Michaelis-Menten kinetic process. Regarding the biosensor reproducibility, three different devices were calibrated on the same day, obtaining a relative standard deviation (RSD) of the sensitivity lower than 10 %.

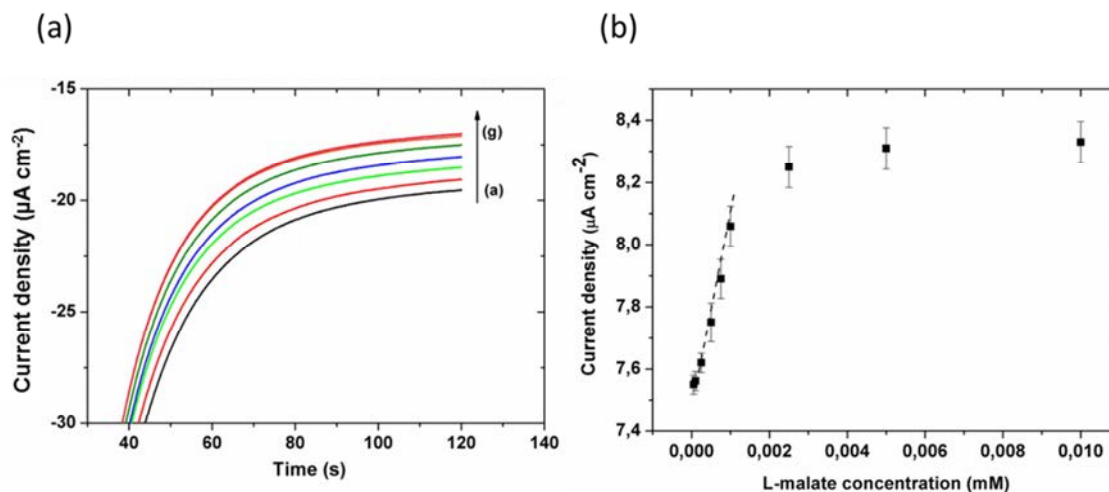


Figure 4.34. (a) Chronoamperometric response and (b) calibration curve representing the mean current value of three replicates recorded consecutively with the same biosensor of the developed biosensor for L-malate concentrations in a range of 1×10^{-7} M (a) to 5×10^{-6} M (g). Each point corresponds to the mean value of three replicates and the error bars represents the standard deviation.

The biosensor selectivity to L-malate was assessed considering the possible interferences found in wine. Results are shown in Figure 4.35. Among all of them, just ascorbic acid produced a non-negligible biosensor response that is related to the electrochemical oxidation that starts to undergo at the applied potential of -0.15 V [40]. Although ascorbic acid exists in small quantities in grapes (around 10 mg L^{-1} or 7.5×10^{-5} M), it rapidly disappears during the fermentation and initial aeration processes [22]. Therefore, it is anticipated that the red wine samples coming from the malolactic fermentation process would not contain ascorbic acid. Therefore, it can be stated that the L-malate determination is not affected by the presence of interferences.

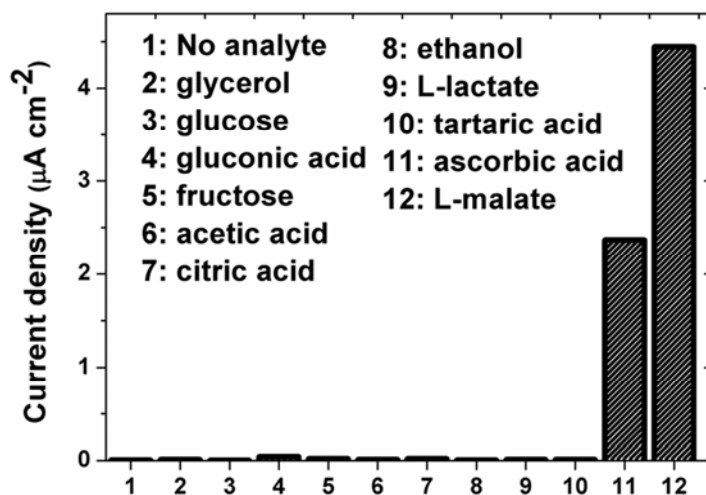


Figure 4.35. Current density response of the biosensor in solutions containing different interferents at a concentration of 5×10^{-7} M.

The PPy membrane thicknesses, measured by FIB (Figure 4.36) was $1.3 \mu\text{m}$ and $2.5 \mu\text{m}$ for the PPy/HAR and the PPy/(DP:MDH) membranes, respectively. This difference is in accordance with the electrical charge associated to the electrosynthesis of both membranes, being twice for the PPy/(DP:MDH) membrane than that of the PPy/HAR one. An additional SEM image (Figure 4.37) showed the homogeneity and roughness of the PPy membranes.

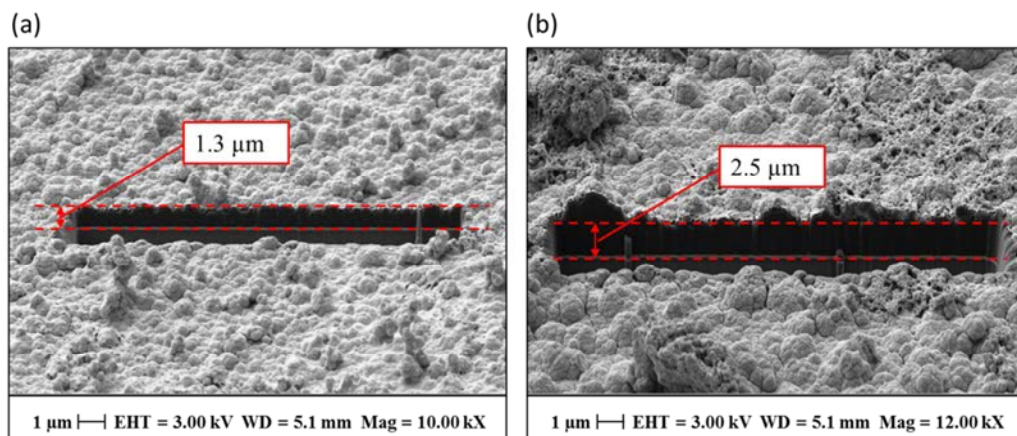


Figure 4.36. SEM images of the transversal cut done by FIB for the estimation of the thickness of (a) PPy/mediator and (c) PPy/enzymes membranes.

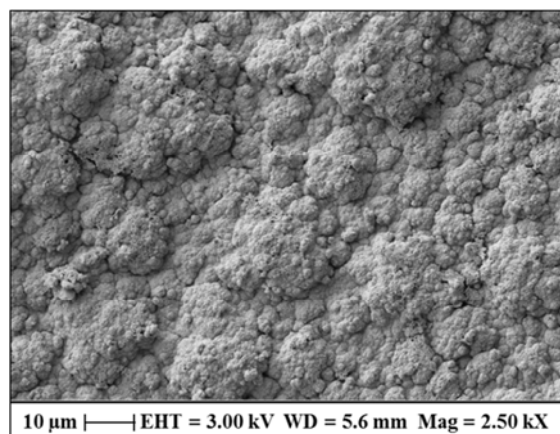


Figure 4.37. SEM image showing the morphology of the PPy membrane surface of the L-malate biosensor.

4.3.5 Monitoring of the malolactic fermentation in wine samples with L-malate biosensor

The biosensor performance for the L-malate determination in wine samples collected during the malolactic fermentation was assessed. Figure 4.38 shows the results of the analysis of samples collected from the fermentation process of three red wines and the values obtained with the standard colorimetric method. An excellent agreement was achieved with absolute errors below 0.2 g L^{-1} ($1.5 \times 10^{-3} \text{ M}$) in all the samples. As can be seen, almost all values obtained with the biosensor are within the uncertainty range at 95% of the standard method. The evolution of the malic acid during the fermentation processes was as expected. When the concentration of L-malic is below 0.3 g L^{-1} ($2.2 \times 10^{-3} \text{ M}$) for 3 consecutive determinations, the transformation to L-lactic acid is considered to end. In this case, the three wines analyzed have completed this process. During the winemaking, the detection of this end point is very important in order to microbiologically stabilize the wine by adding sulfite on time. If not, the lactic acid bacteria begin to degrade the sugars, producing an increase of acetic acid concentration in wine. This affects negatively the taste and odor of the final product. It is worth mentioning that all measurements performed in this study were carried out with the same biosensor, which retained the 90% of its initial sensitivity after analyzing more than 80 measurements, including all the wine samples as well as the calibrations carried out before and after the analysis of each wine.

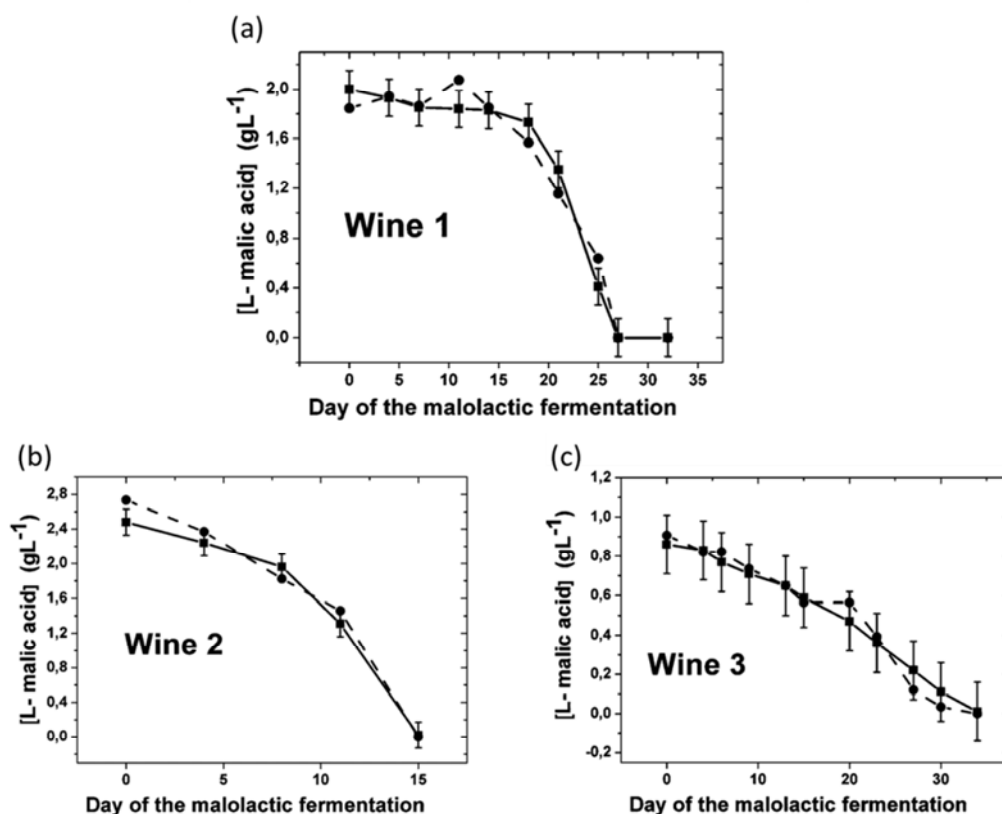


Figure 4.38. Analysis of wine samples collected during the malolactic fermentation process for three red wines. Dashed lines and filled circles show the values of L-malic acid obtained with the proposed biosensor and filled lines and squares ones are those obtained with the colorimetric standard method. In the case of the colorimetric method, the error bars represent the uncertainty at 95 %.

4.3.6 Comparative study with other others L-malate amperometric biosensors

Table 1.2 in Section 1.1.2.3 shows the analytical characteristics of other amperometric biosensors based on the use of MDH, previously reported. Regarding the application of coupled enzyme reactions, there is one biosensor using just MDH and most of them also incorporate DP for improving the sensitivity. Regarding the linear range, the obtained in this work was narrow compared to the biosensors adding the mediator in solution and to the biosensor using covalent coupling as immobilization method. However, the use of an entrapped mediator is necessary to avoid the addition in solution of more chemical reagents during the characterization. On the other hand, the polymer entrapment causes a diffusion barrier compared to the covalent coupling, but only a lineal range of one decade of magnitude is necessary for the proposal application. The biosensor described in this work clearly outperforms the other approaches in terms of sensitivity and detection limit. This may be partially related with the immobilization of the chemical species in a conductive polypyrrole membrane synthesized under

biocompatible conditions that may preserve the enzyme activity almost intact. Besides, using an electropolymerization approach enables the strict controlled deposition of the required chemical species making it compatible with the application of miniaturized transducers.

A biosensor applied to the monitoring of the malolactic fermentation must show a long-term working stability under continuous use because the fermentation process takes around 40 days. Some of the biosensors in Table 1.2 (Section 1.1.2.3) show storage stability values, showing excellent results after months or years. However, the working biosensor stability is significantly worse, this being restricted to few days and thus limiting the biosensor performance for the proposed application. The biosensor developed in this work maintains 90 % of its initial sensitivity after 37 days in solution and continuous use, being the only amperometric biosensor based on MDH reported so far that could be applied to the real-time monitoring of malolactic fermentation processes. Finally, some biosensors have been applied to the determination of L-malate in wines samples and one of them has been tested in synthetic wines samples simulating the malolactic fermentation process. However, the biosensor presented in this work is the only one that has been assessed using real samples collected during the malolactic fermentation of red wines.

As conclusions, the results obtained for the developed L-malate biosensor demonstrated that presented a very high sensitivity with a low limit of detection. Besides, the biosensor retained more than 90 % of its original sensitivity over 37 days of performance, allowing its successful application to the L-malic acid monitoring during the MLF of three red wines.

4.4 Microanalytical flow system for simultaneous determination of L-lactate and L-malate

As has been explained previously, during the malolactic fermentation of red wines, L-malic acid is mainly converted to L-lactic acid. Both acids concentration have a significant influence along the process on the quality of the final wine, therefore real-time monitoring of the malolactic fermentation would be interesting for winemaking industry. The traditional methods used at present require laboratory equipment, therefore the results are not known in real-time. The use of biosensors and analytical systems would be advantageous to meet the requirement of on-line analysis.

In the two previous chapters, the development of two amperometric biosensors has been described, with a final evaluation in wine samples. The work described in this chapter corresponds to the integration of both amperometric biosensors in a miniaturized and portable device for facilitating in-situ measurements. For that application, a new chip has been fabricated to integrate the two sensors in the same chip (Figure 3.4d, in section 3.3.3). The chip is implemented in a robust PMMA and PSA structure formed by several individual layers (17 mm × 30 mm) allowing the positioning of the chip and its alignment with the fluidic reservoir and channels. Both working electrodes are electro-modified with a three-dimensional polypyrrole membrane entrapping the enzymes and reagents involved in the bienzymatic reaction of the L-lactate and the L-malate determination.

4.4.1 Electrosynthesis of the electrochemical biosensors

The polypyrrole membranes containing the enzymes were electrosynthesized using the previously optimized conditions for the individual L-lactate and L-malate biosensors. This was performed in the microanalytical flow system described in Figure 3.13 (Section 3.5.2). A potential of +0.7 V (vs Ag/AgCl Dri-Ref) with an accumulation charge of 500 mC cm⁻² was applied for the L-lactate biosensor fabrication. For the L-malate biosensor, the electrosynthesis was carried out in two steps: one for the electrosynthesis of the PPy membrane entrapping the redox mediator (250 mC cm⁻²) and other for entrapping the enzymes (500 mC cm⁻²). The recorded responses under these conditions are shown in Figure 4.39. The time required for each electrosynthesis depended on the current density of the potentiostatic response, and this value is related to the material in which the electrodeposition was carried out and the chemicals analytes

contained in the generation solution. The recorded signals were as expected. Comparing the electroynthesis signal of the L-lactate biosensor (Figure 4.39a) with the signal for the second layer deposition of the L-malate biosensor (Figure 4.39b, red color), both of 500 mC cm^{-2} , the time spent for the L-malate (28 s) is shorter than the time spent for the L-lactate biosensor (55 s). This is because the PPy layer grows on the surface of the first PPy membrane for the L-malate biosensor, which has more active area than the platinum surface of the chip sensor.

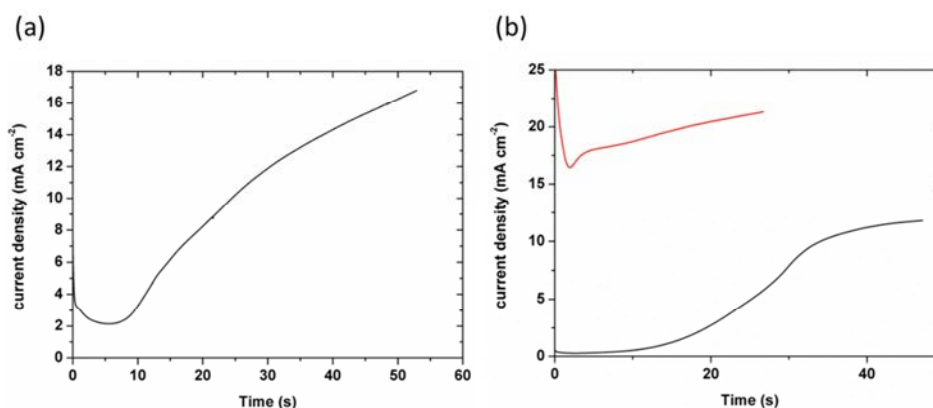


Figure 4.39. Current profile recorded during the potentiostatic electrogeneration of the PPy film for the (a) L-lactate biosensor and (b) L-malate biosensor. In (b), black and red color line corresponds to the electrogeneration of the first and the second PPy film, respectively.

Then, the electrosynthesized PPy membranes were overoxidized for both biosensors for obtaining a stable base line signal from the PPy during all the next measurements. This process was performed by cyclic voltammetry at 100 mV s^{-1} (from 0 V to +1 V) during 60 cycles in PB solutions [41]. The recorded cyclic voltammograms (number of the CV five, thirty, forty-five and sixty) during the overoxidation of the L-lactate and the L-malate biosensors are shown in Figure 4.40a and 4.40b, respectively. As was expected, the area of the cyclic voltammograms decreased with the process to achieve a stable signal.

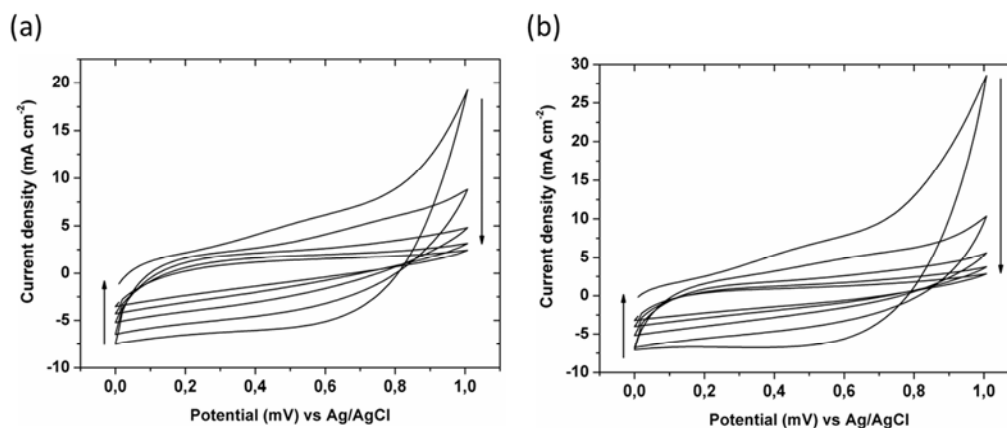


Figure 4.40. Cyclic voltammograms at 100 mV s^{-1} in PB solution recorded during the overoxidation of the (a) PPy:LOX:HRP film and the (b) PPy:redox mediator + PPy:MDH:DP films. Arrows indicate the direction in which the cycles advanced.

4.4.2 Characterization of the amperometric biosensors

The microanalytical flow system used is shown in Figure 3.14 (Section 3.5.2). The device contained the detection chamber ($10 \mu\text{L}$), the fluidic channels and the electrical connections with the chip. The solution flowed in continuous mode in the device during 30s at 0.25 mL min^{-1} and the electrochemical measurements were done in stop flow conditions.

The PB solutions used for the characterization of biosensors in the microanalytical flow system had a concentration of KCl five times higher (0.5 M) than those used for the characterization of the individual sensors under batch conditions. This increase of conductivity allowed reducing the effect of the potential drop which was observed when biosensors were measured under flow conditions. Avoiding the potential drop, the hysteresis effects of electrochemical processes in the WEs were prevented and the analytes determination over time was carried out correctly [42].

A preliminary study by cyclic voltammetry was done in order to set the potential for the chronoamperometric measurements. Two cyclic voltammograms at 20 mV s^{-1} in PB solutions were carried out for each biosensor (Figure 4.41). For the L-lactate biosensor, a high increase of the negative current associated to the reduction of the oxidized potassium ferrocyanide was observed at -0.35 V (vs Pt pseudo-RE) when 1 mM of L-lactate was added to the solution (Figure 4.41a, red line). On the other hand, for the L-malate biosensor, a high increase of the positive current associated to the re-oxidation process of the reduced HAR in presence of 1 mM of L-malate is observed in Figure

4.41b (red line). From these results, a set potential of -0.35 V and -0.4 V (vs Pt pseudo-RE) was chosen for the L-lactate and the L-malate determination, respectively.

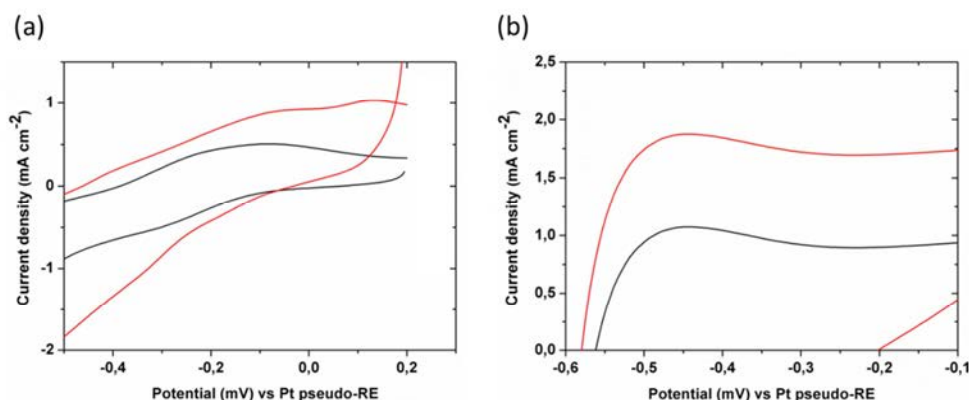


Figure 4.41. Cyclic voltammograms at 20 mV s^{-1} in a PB solution obtained in presence of 0 mM (black line) or 1 mM (red line) of the analyte (a) L-lactate and the (b) L-malate biosensor.

Then, the microanalytical flow system was calibrated by chronoamperometry. Firstly, the L-lactate biosensor was calibrated. For that the sensor chamber was filled with 0.5 M KCl PB solutions in presence of 2 mM ferrocyanide potassium and L-lactate in a concentration range between 1×10^{-7} M and 1×10^{-3} M. Then, an overpotential of -0.35 V (vs. Pt pseudo-RE) was applied and the signal was recorded during 120 s. The mean value of the current density of the last 30 s was used as analytical signal for the calibration plot (Figure 4.42a). Regarding the L-malate biosensor calibration, a set overpotential of -0.40 V (vs. Pt pseudo-RE) was applied in 0.5 M KCl PB solutions containing 5 mM NAD^+ and a L-malate concentration from 1×10^{-7} M to 1×10^{-5} M. The calibration plot was obtained by plotting the mean current density of the last 30 s of the signal recorded during 120 s versus the L-malate concentration in the solution (Figure 4.42b).

The L-lactate biosensor had a sensitivity of $(-173 \pm 8) \times 10^2 \mu\text{A M}^{-1} \text{ cm}^{-2}$ ($r = 0.997$, $n = 7$) in a linear range from 5×10^{-6} M to 1×10^{-4} M and a LOD (3σ IUPAC criterion) of $3.2 \pm 0.3 \times 10^{-6}$ M. Regarding the L-malate biosensor, a sensitivity of $(5.53 \pm 0.6) \times 10^2 \text{ mA M}^{-1} \text{ cm}^{-2}$ ($r = 0.997$, $n = 5$) in a linear range from 1×10^{-7} M to 1×10^{-6} M and a LOD $6.7 \pm 0.2 \times 10^{-8}$ M have been obtained. The RSD was calculated for both biosensors using three biosensors fabricated under the same conditions the same day, obtaining a value lower than 8 % and 6 % for the L-lactate and the L-malate biosensor, respectively.

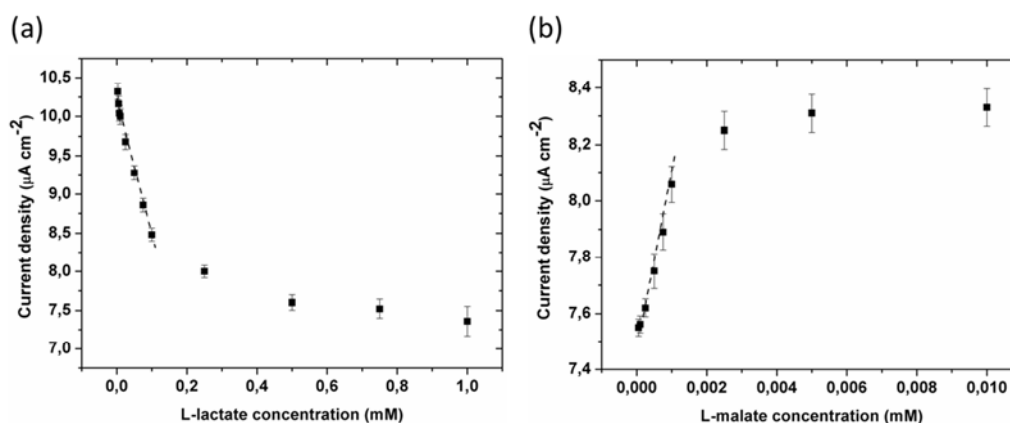


Figure 4.42. Calibration curve for the (a) L-lactate and (b) L-malate biosensor using the mean current value of three replicates recorded consecutively with the same biosensor. The error bars correspond to the standard deviation.

4.4.3 Malolactic fermentation monitoring with the dual fluidic system

Once demonstrated that the biosensors worked correctly in the fluidic system this was applied to the monitoring of the malolactic fermentation of samples recollected during this process for three red wines. Firstly, the device was calibrated for L-lactate and L-malate determination, and then, both analytes were analyzed consecutively in the samples. The results of the comparative analysis with the standard method are shown in Figure 4.43. For all the samples, the absolute errors are below 0.15 g L^{-1} , demonstrating an excellent agreement between methods. Regarding the evolution of both acids, it was as expected: L-malic decreased and L-lactic acid increased till the stabilization at the end of the process. The same biosensors were used for all the analysis, retaining more than the 91 and 93 % of the initial sensitivity of the L-lactate and the L-malate biosensor, respectively.

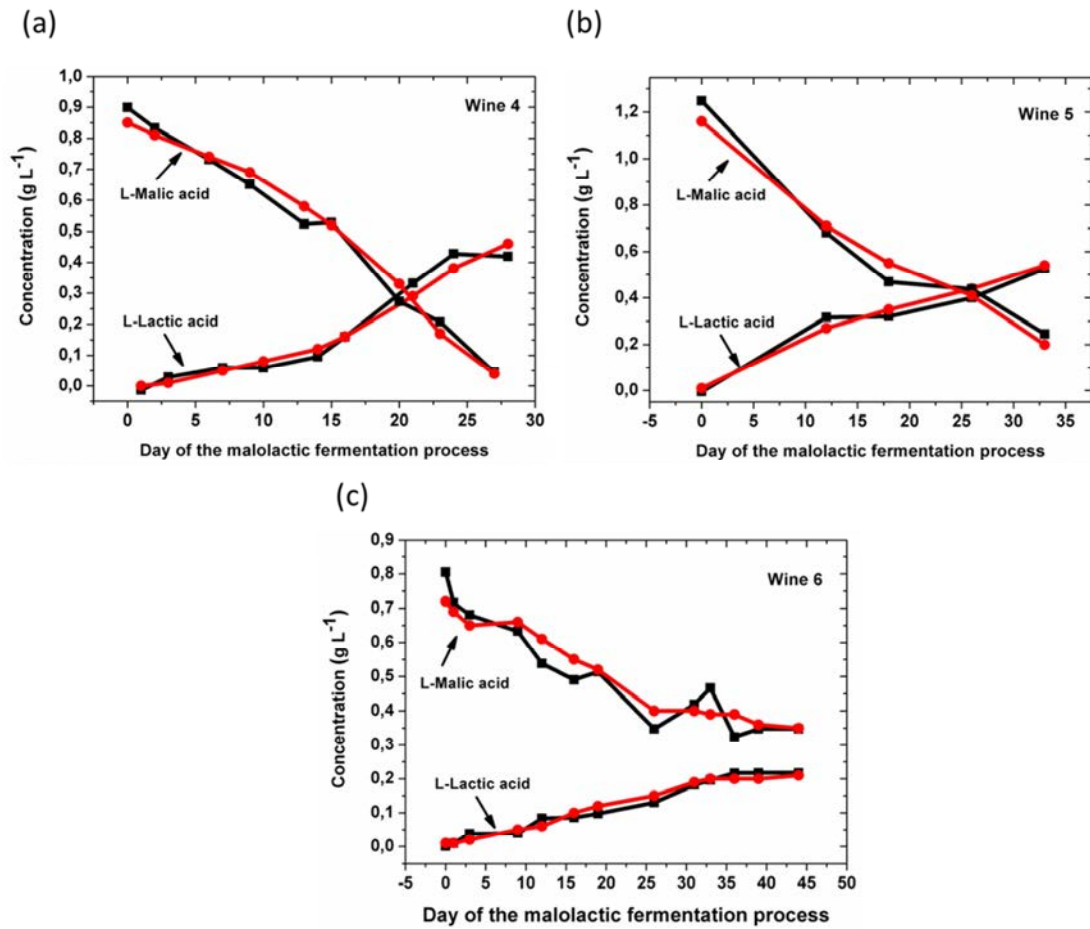


Figure 4.43. Analysis of wine samples collected during the malolactic fermentation process for three red wines. Black lines show the values of the L-lactic and the L-malic acid concentration determined by the proposed device. Red lines correspond to the results obtained with the colorimetric standard method for the same samples.

4.5 Multiparametric system based on an electronic tongue for the analysis of Cava wines

Cava is a quality sparkling wine produced in Spain. As a product with a designation of origin, Cava wine has to meet certain quality requirements throughout its production process; therefore, the analysis of several parameters is of great interest. In this work, an electronic tongue for the analysis of Cava wine is described. The system is constituted by an array of microsensors formed by one conductivity sensor, one redox potential (ORP) sensor, and two amperometric gold microelectrodes, together with six ISFETs sensitive to pH, Na⁺, K⁺, Ca²⁺, Cl⁻, and CO₃²⁻. For the data treatment, two different multivariate methods are used: linear discriminant analysis (LDA) and partial least squares (PLS). A set of 78 Cava wine samples has been analyzed with this electronic tongue.

4.5.1 Characterization of the sensors

ISFET for pH control and those with selective membrane to Na⁺, K⁺, Ca²⁺, Cl⁻, and CO₃²⁻ were calibrated with the multi-ISFET meter. The analytical performance obtained with three sensors of each type is shown in Table 4.16. All sensors had a typical Nernstian response, a linear range of two (Cl⁻ and CO₃²⁻), three (Na⁺ and K⁺) or more decades (Ca²⁺) with a significant coefficient of regression and a low LOD (by the cross-point method recommended by IUPAC for potentiometry [43]). The analytical parameters obtained with the multi-ISFET meter were very similar to those reported previously using conventional devices [44, 45], demonstrating the good performance of the multi-ISFET meter. Besides, the device allowed six simultaneous measurements of ISFETs without electrical interference between them.

Table 4.16. Response characteristics obtained from the calibration curves for each type of ISFET using the multi-ISFET meter.

Parameter	Sensitivity / mV dec ⁻¹	Linear Range / M	R ²	LOD / M
pH	54.2 ± 0.5	pH 1.56–11.42	0.9998 (n = 10)	-
Na ⁺	54.0 ± 0.4	2.1 × 10 ⁻⁵ –2.2 × 10 ⁻²	0.9994 (n = 6)	5.9 × 10 ⁻⁶
K ⁺	57.0 ± 0.8	2.0 × 10 ⁻⁵ –2.1 × 10 ⁻²	0.9996 (n = 7)	1.8 × 10 ⁻⁶
Ca ²⁺	28.6 ± 0.6	5.9 × 10 ⁻⁷ –1.9 × 10 ⁻²	0.9998 (n = 9)	1.9 × 10 ⁻⁷
Cl ⁻	-59 ± 1	2.0 × 10 ⁻⁴ –2.1 × 10 ⁻²	0.9998 (n = 4)	2.8 × 10 ⁻⁵
CO ₃ ²⁻	-58 ± 2	2.1 × 10 ⁻⁴ –2.2 × 10 ⁻²	0.9993 (n = 4)	3.0 × 10 ⁻⁵

For the conductivity sensor, the values of potential obtained using the multiparametric system for the five KCl solutions are shown in Figure 4.44. A linear

correlation between the values of potential and the resistivity (σ , inverse of conductivity) observed with a slope of $1.99 \text{ mV } \Omega^{-1} \text{ cm}^{-1}$ in the range from 0.80 mS cm^{-1} to 13.07 mS cm^{-1} and a coefficient of regression (r) of 0.999.

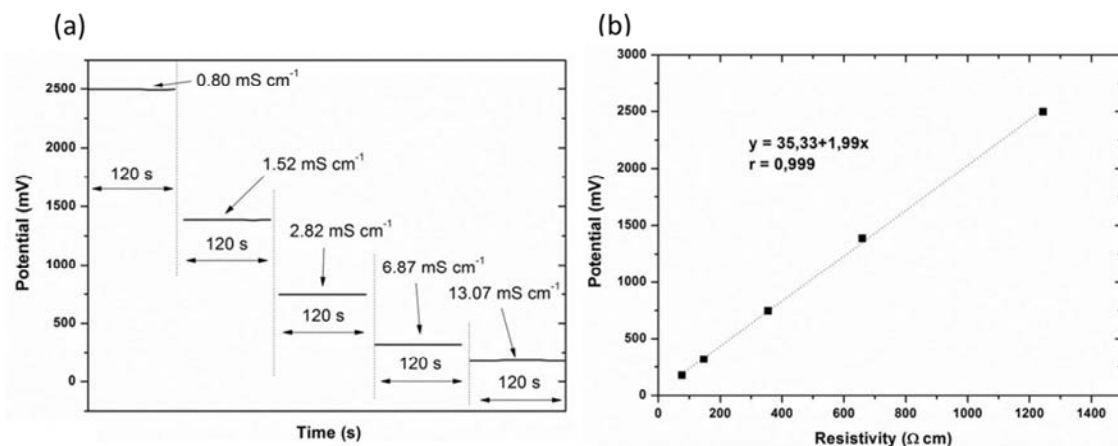


Figure 4.44. Results obtained for the conductivity measurements: (a) Recording of potential variation for different conductivity solutions. (b) Calibration curve obtained using values of resistivity measured with the commercial equipment vs. values of potential obtained with the system. Dotted line shows the linear fitting.

For the ORP sensor, two standard solutions of 220 mV and 468 mV were used. Using the multiparametric system, the redox potentials recorded were $189.5 \pm 0.7 \text{ mV}$ and $449.5 \pm 0.5 \text{ mV}$, respectively. These values were in good agreement with those obtained by the Autolab equipment, which were $194.2 \pm 0.1 \text{ mV}$ and $450.9 \pm 0.1 \text{ mV}$, respectively.

For the amperometric sensors successive additions of 0.1 M potassium ferricyanide solution were done in order to obtain a concentration range between 0.1 mM to 5 mM. Both amperometric terminals (AMP1 and AMP2) were tested by triplicated. Figure 4.45 shows the measurements and comparison with the commercial equipment. As expected, the cathodic current increases with the analyte concentration in a reproducible way for the two amperometric terminals and the commercial equipment. Calibration curves were obtained for the three cases in the range from 0 mM to 5 mM. The linear regression showed a slope of $-4.47 (\pm 0.01) \mu\text{A mM}^{-1}$ for AMP1 and $-4.44 (\pm 0.01) \mu\text{A mM}^{-1}$ for AMP2, which were in good accordance with the value of $-4.48 \mu\text{A mM}^{-1}$ obtained with the Autolab. The intercept of the regressions was also practically the same and the regression coefficient was 0.999 for all the cases.

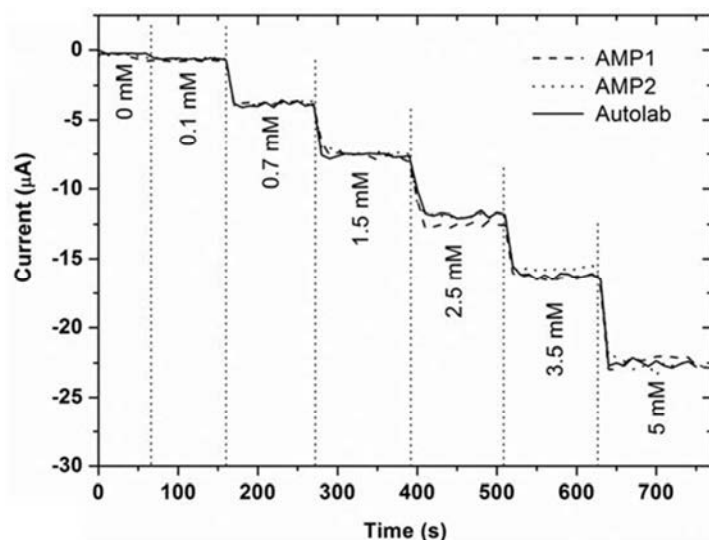


Figure 4.45. Results obtained for the amperometric measurements for successive additions of potassium ferricyanide in 0.1 M KNO_3 background solution: AMP1 (dashed line), AMP2 (dotted line) and Autolab (full line).

4.5.2 Analysis Cava Wine samples

4.5.2.1 Classification of the samples

With the data obtained from the different variables, LDA was performed. The confusion matrix of the obtained model and the percentages of sensitivity and specificity for the four of Cava Wine classes are shown in Table 4.17. The sensitivity corresponds to the samples of each group correctly classified by the LDA model; meanwhile the specificity is evaluated as the samples of different groups correctly rejected by the model. The “Reserva” samples are especially well adjusted, with only one sample wrong associated to “Gran Reserva”. Moreover, “Young” and “Gran Reserva” are well-classified between them, therefore the system was able to discriminate very different aging times (9–15 months or more than 30 months for “Young” and “Gran Reserva”, respectively). Nevertheless, “Reserva” overlapped easier with samples of their border (15–30 samples). The values of specificity were above 90% in all cases and the total sensitivity of prediction was 87%. It is also important to highlight the high percentage of sensitivity and specificity achieved for the Rosé class samples, which demonstrates the great discrimination capacity of the system formed by electrochemical micro-sensors.

Table 4.17. Confusion matrix for the Cava wine samples obtained with the LDA model using the cross-validation method.

Classes	Prediction				Sensitivity (%)	Specificity (%)
	Young	Reserva	Gran Reserva	Rosé		
Young	16	2	0	2	80	97
Reserva	0	24	1	0	96	91
Gran Reserva	0	3	13	0	81	98
Rosé	2	0	0	15	88	97

4.5.2.2 Quantification of Legal Parameters

PLS regression was carried out for quantifying several chemical parameters of the samples already analyzed with standard methods. These parameters were related to the legal limits, such as the total acidity (more than 5 g L⁻¹), pH (between 2.8 and 3.3) and VAD (between 10.8 % and 12.8 %) [46]. The prediction set was formed by four “Young” samples (Y 3336, 3709, 4956, 5219), six “Reserva” samples (R 2719, 2929, 3727, 5241, 5608, and 5962), four “Gran Reserva” samples (GR 2720, 3182, 4183, and 5220) and four Rosé samples (Ro 2978, 3103, 4814, and 5017). The results were summarized in Table 4.18. The interpolated values were in good agreement with the data obtained using standard methods for the three parameters. The relative errors were mainly below 9%. Especially good results were obtained for pH and VAD prediction, with relative errors below 5%. The results for VAD were significant since there was no specific sensor for this parameter. Values for total acidity were also quite accurate considering that it was a global parameter that included all titratable acids, mainly tartaric acid, but also lactic acid, malic acid, citric acid, etc., and again no specific sensor was used.

Table 4.18. Results of legal parameter quantification with the electronic tongue using PLS-1 regression. Standard method data were provided by IRTA-INCAVI.

Sample ¹	Total Acidity / g L ⁻¹			pH			VAD (%)		
	Standard Method	Electronic Tongue	Relative Error (%)	Standard Method	Electronic Tongue	Relative Error (%)	Standard Method	Electronic Tongue	Relative Error (%)
Y 3336	6.5	5.9	8.5	3.04	3.23	6.1	11.75	11.97	1.8
Y 3709	6.1	6.0	1.3	3.01	3.17	5.4	12.15	11.97	1.5
Y 4956	6.5	6.1	6.4	2.94	2.95	0.3	11.85	11.87	0.2
Y 5219	6.7	6.2	8.1	3.03	3.07	1.3	11.55	11.82	2.4
R 2719	5.5	5.8	5.0	3.31	3.35	1.2	13.00	12.06	7.2
R 2929	6.1	6.1	0.4	3.07	3.08	0.4	12.30	11.86	3.5
R 3727	6.1	6.2	0.9	2.96	3.04	2.8	11.75	11.90	1.3
R 5241	5.8	6.4	11.0	3.43	3.44	0.4	12.05	11.76	2.4
R 5608	6.2	6.1	2.4	2.94	3.15	7.3	12.15	11.92	1.9
R 5962	5.6	6.1	9.0	3.08	3.08	0.1	12.10	11.89	1.7
GR 2720	5.5	5.7	4.4	3.15	3.05	3.2	12.85	12.05	6.2
GR 3182	5.5	6.1	11.6	3.02	3.00	0.6	12.15	11.91	2.0
GR 4183	5.5	5.6	1.3	3.02	3.04	0.7	12.40	12.07	2.7
GR 5220	6.5	7.0	7.4	2.93	3.10	5.9	11.75	12.01	2.2
Ro 2978	5.5	5.9	7.8	3.35	3.19	4.9	12.20	12.15	0.4
Ro 3103	6.2	6.7	7.8	3.01	3.04	1.0	12.20	12.11	0.7
Ro 4814	5.8	6.0	3.2	3.00	3.10	3.4	12.30	11.96	2.8
Ro 5017	5.5	6.1	11.3	3.02	3.05	1.1	12.05	11.99	0.5
	Mean Relative Error		6.0	Mean Relative Error		2.6	Mean Relative Error		2.3

¹ Y: Young; R: Reserva; GR: Gran Reserva; Ro: Rosé.

4.5.2.3 Quantification of other parameters

Other parameters related with the tartaric stabilization, glycerol and methanol (and related to the final quality of the samples) were determined with PLS regressions. The comparative results obtained with the proposed system and standard methods are shown in Table 4.19, showing a good agreement between methods (relative errors below 15 %). Besides, the mean errors were below 6.0% for the four parameters analyzed. The best results were obtained for conductivity prediction. Again, glycerol and methanol were determined with no specific sensors, with good accuracy.

As conclusion, a compact electronic tongue has been developed and applied to measure Cava wines. The electronics used (multi-ISFET meter and multisensor meter) have been fabricated according to microsensor requirements and taking into account the minimum energy consumption. This power consumption is below 10 mA if we consider the measurement with the 10 microsensors simultaneously every 15 min. This means that the equipment could work continuously up to 150 h using a standard 9 V battery.

Comparing the results obtained with this system with them obtained with other electronic tongues for Cava wine analysis [47-49], this system is able to determine simultaneously up to seven important chemical parameters, apart from the qualitative analysis, thanks to the hybrid nature of the electrochemical sensors (potentiometric, amperometric, and conductimetric). Moreover, this e-tongue uses small and low-power equipment for measurement, instead of bench-top laboratory equipment, and microsensors, which are easy to miniaturize and integrate with the electronics.

In conclusion, the good results obtained both for classification and quantification analyses confirm the viability of the multiparametric system. Additionally, the use of portable meters together with electrochemical microsensors fabricated with semiconductor technology provide an advantageous combination for rapid and feasible in-field measurements, not only for the wine industry but for food quality control in general.

Table 4.19. Results of quality parameter quantification with the electronic tongue using PLS-1. Standard method data were provided by IRTA-INCAVI.

Sample ¹	Potassium / m L ⁻¹			Conductivity mS cm ⁻¹			Glycerol g L ⁻¹			Methanol mg L ⁻¹				
	Standard Method	Electronic Tongue	Relative Error (%)	Standard Method	Electronic Tongue	Relative Error (%)	Standard Method	Electronic Tongue	Relative Error (%)	Standard Method	Electronic Tongue	Relative Error (%)		
Y 3336	355	360	1.3	1.34	1.33	0.9	5	5.5	9.7	29	30	3.8		
Y 3709	433	423	2.4	1.42	1.32	6.9	4.9	5.4	10.0	29	28	2.3		
Y 4956	326	328	0.6	1.29	1.26	2.1	-	-	-	30	30	1.2		
Y 5219	332	332	0.0	1.38	1.32	4.3	5.3	5.2	1.7	29	30	5.0		
R 2719	550	487	11.4	1.79	1.66	7.5	6.1	6.2	2.2	31	34	10.6		
R 2929	360	395	9.7	1.29	1.28	0.9	5.1	5.7	12.2	30	32	5.7		
R 3727	300	332	10.7	1.21	1.21	0.3	5.6	5.4	2.8	30	30	0.0		
R 5241	372	315	15.4	1.19	1.13	5.3	5.1	5.6	9.5	30	30	1.3		
R 5608	379	418	10.3	1.31	1.31	0.1	5.8	5.8	0.7	29	31	6.1		
R 5962	320	334	4.4	1.2	1.19	0.5	5.5	5.7	2.9	28	30	7.5		
GR 2720	544	518	4.7	1.73	1.70	1.6	6.9	6.3	8.1	31	32	3.0		
GR 3182	321	327	1.9	1.14	1.16	2.0	5.1	5.4	6.1	30	30	1.5		
GR 4183	391	408	4.2	1.42	1.41	0.6	5.5	5.4	2.5	28	31	10.8		
GR 5220	300	301	0.2	1.33	1.29	2.9	5.1	5.3	4.4	29	28	2.3		
Ro 2978	430	452	5.1	1.29	1.41	9.1	5.4	5.9	8.5	38	33	13.4		
Ro 3103	367	346	5.6	1.44	1.31	9.4	5.4	5.7	4.9	38	36	5.5		
Ro 4814	459	398	13.4	1.39	1.33	4.0	5.5	5.8	5.8	36	32	12.0		
Ro 5017	318	306	3.6	1.22	1.20	1.7	5.4	5.7	6.2	27	30	9.7		
Mean Relative Error			5.8	Mean Relative Error			3.3	Mean Relative Error			5.8	Mean Relative Error		5.6

¹ Y: Young; R: Reserva; GR: Gran Reserva; Ro: Rosé.

4.6 References

1. Fazio, T. and C.R. Warner, *Food Additives and Contaminants*, 1990. **7**(4): p. 433-454.
2. Adams, J.B., *Food Chemistry*, 1997. **59**(3): p. 401-409.
3. International Organisation of Vine and Wine (OIV), *International Standard for the Labeling of Wines*. 2012,.
4. Paul, F., *Mitteilung Klosterneuburg Serie A*,, 1958. **8**: p. 21-27.
5. Ripper, M., *Journal fur praktische Chemie/Chemiker-Zeitung* 1892. **46**: p. 428-473.
6. International Organization of Vine and Wine (OIV), *Compendium of International Methods of Analysis of Wines and Musts (OIV-MA-AS323-04C)*. 2009,
7. Usseglio-Tomasset, L.a.B.P.D., *Vini d'Italia* 26, 1984. **5**: p. 7-14.
8. Kalimuthu, P., et al., *Analytical Chemistry*, 2010. **82**(17): p. 7374-7379.
9. Molinero-Abad, B., et al., *Analytica Chimica Acta*, 2014. **812**: p. 41-44.
10. Rawal, R. and C.S. Pundir, *Biochemical Engineering Journal*, 2013. **71**: p. 30-37.
11. Osborne, B.G. and J.F. Tyson, *International Journal of Food Science and Technology*, 1988. **23**(6): p. 541-554.
12. Ruiz-Capillas, C. and F. Jimenez-Colmenero, *Food Additives and Contaminants Part a-Chemistry Analysis Control Exposure & Risk Assessment*, 2008. **25**(10): p. 1167-1178.
13. Segundo, M.A., J. Lima, and A. Rangel, *Analytica Chimica Acta*, 2004. **513**(1): p. 3-9.
14. Falcone, F. and K.C. Maxwell, *Journal of Agricultural and Food Chemistry*, 1992. **40**(8): p. 1355-1357.
15. Oliveira, S.M., et al., *Journal of Agricultural and Food Chemistry*, 2009. **57**(9): p. 3415-3422.
16. Bartroli, J., et al., *Analytical Chemistry*, 1991. **63**(21): p. 2532-2535.
17. Atanassov, G., et al., *Analysis*, 2000. **28**(1): p. 77-82.
18. Huang, Y.L., J.M. Kim, and R.D. Schmid, *Analytica Chimica Acta*, 1992. **266**(2): p. 317-323.
19. Azevedo, C.M.N., et al., *Analytica Chimica Acta*, 1999. **387**(2): p. 175-180.
20. Alegret, S., et al., *Electroanalysis*, 1991. **3**(4-5): p. 349-354.
21. Jimenez, C., Bratov, A., Abramova, N., Baldi, A., *ISFET Based Sensors: Fundamentals and Applications*, A.S. Publishers, Editor. 2006. p. 151-196.
22. Ribereau-Gayon, P., et al., *Handbook of Enology*. 2 ed. Vol. 1, The Microbiology of Wine and Vinifications. 2006: John Wiley & Sons Ltd,.
23. International Organisation of Vine and Wine (OIV), *International code of enological practices*. 2017,.
24. International Organization of Vine and Wine (OIV), *Compendium of International Methods of Analysis. Volatile acidity (OIV-MA-AS313-02)*. 2015.
25. Becker, T., et al., *Journal of Biotechnology*, 1993. **31**(3): p. 267-275.
26. Lenghor, N., et al., *Talanta*, 2002. **58**(6): p. 1139-1144.
27. Araujo, C.S.T., et al., *Food Chemistry*, 2005. **92**(4): p. 765-770.
28. Eschenbruch, R., *American Journal of Enology and Viticulture*, 1974. **25**(3): p. 157-161.
29. Inczèdy, J., T. Lengyel, and A.A. Ure, *Compendium of analytical nomenclature IUPAC*. 1998: Oxford Blackwell Science.
30. Sassolas, A., L.J. Blum, and B.D. Leca-Bouvier, *Biotechnology Advances*, 2012. **30**(3): p. 489-511.
31. Berg, J.M., J.L. Tymoczko, and L. Stryer, *The Michaelis-Menten Model Accounts for the Kinetic Properties of Many Enzymes*, in *Biochemistry*. 2002, W H Freeman: New York.
32. Cho, J.H., M.C. Shin, and H.S. Kim, *Sensors and Actuators B-Chemical*, 1996. **30**(2): p. 137-141.
33. Silk, T., et al., *Synthetic Metals*, 1998. **93**(1): p. 59-64.
34. Lehr, I.L. and S.B. Saidman, *Corrosion Science*, 2007. **49**(5): p. 2210-2225.
35. Fruton, J.S., *Journal of Biological Chemistry*, 1934. **105**(1): p. 79-85.
36. Grundig, B., et al., *Journal of Electroanalytical Chemistry*, 1995. **395**(1-2): p. 143-157.

37. Schuhmann, W., et al., *Journal of Biotechnology*, 1993. **27**(2): p. 129-142.
38. Zeng, J., et al., *Journal of Electroanalytical Chemistry*, 2006. **595**(2): p. 152-160.
39. *Nicotinamide cofactor dependent oxidoreductions*, in *Enzymes synthetic organic chemistry*, C.H. Wong and G.M. Whitesides, Editors. 1994, Pergamon. p. 131-153.
40. Borsook, H. and G. Keighley, *Oxidation reduction potential of ascorbic acid (Vitamin C)*. Proceedings of the National Academy of Sciences of the United States of America, 1933. **19**: p. 875-878.
41. Li, Y.F. and R.Y. Qian, *Electrochimica Acta*, 2000. **45**(11): p. 1727-1731.
42. Matencio, T., J.M. Pernaut, and E. Vieil, *Journal of the Brazilian Chemical Society*, 2003. **14**(1): p. 90-96.
43. Buck, R.P. and E. Lindner, *Recommendations for nomenclature of ion-selective electrodes. IUPAC recommendations 1994*. Pure and Applied Chemistry, 1994. **66**(12): p. 2527-2536.
44. Artigas, J., et al., *Computers and Electronics in Agriculture*, 2001. **31**(3): p. 281-293.
45. Gutierrez, M., et al., *Analyst*, 2010. **135**(7): p. 1718-1725.
46. *Regulatory Board of Cava. Pliego de Condiciones Denominación de Origen Protegida "Cava"*. Available online:<http://www.docava.es/wp-content/uploads/2015/05/PLIEGO-DOP-CAVA.pdf> (accessed on 25 August 2016).
47. Ceto, X., et al., *Food Research International*, 2014. **55**: p. 455-461.
48. Ceto, X., et al., *Electroanalysis*, 2014. **26**(7): p. 1504-1512.
49. Ceto, X., et al., *Electroanalysis*, 2011. **23**(1): p. 72-78.

Chapter 5: Conclusions

1. Several sensors have been fabricated with microelectronic technology. These sensors are pH-ISFETs and ISFETs with ion selective membranes, microelectrodes with platinum and gold as electroactive metal for amperometric, conductimetric and ORP measurements. The amperometric sensors have been modified with enzymatic membranes to obtain biosensors.
2. These (bio)sensors have been characterized with electrochemical techniques to assess their response characteristics.
3. Microanalytical flow systems have been fabricated with low-cost and fast-prototyping polymers, such as PSA and PMMA, manufactured with micromilling and CO₂-laser ablation techniques. These flow systems have been applied to the automatization of the analytical detection of some parameters of interest in the wine industry.
4. A microanalytical flow system for monitoring **the free and total SO₂** concentration in wines samples has been developed and evaluated. This system incorporates a gas-diffusion membrane to separate the analyte from the sample avoiding interferences and uses as detector a pH-ISFET. Profiting the acid/basic characteristics of the analytes, indirect detection of pH is carried out. In order to detect total SO₂ the system incorporates a cell for the sample treatment.
 - Once optimized, this system has a sensitivity (slope) of $-49.6 \pm 0.7 \text{ mV dec}^{-1}$ ($r = 0.998$) in a range of 1 mg L^{-1} - 60 mg L^{-1} for free SO₂ and $-49.4 \pm 0.7 \text{ mV dec}^{-1}$ ($r = 0.998$) in a range of 30 mg L^{-1} - 300 mg L^{-1} for total SO₂. The limit of detection (LOD) is 0.5 mg L^{-1} .
 - This system has been evaluated with 70 wine samples and compared with two reference methods. Results have demonstrated that there is a good correlation between both methods. An underestimation of values obtained with the microanalytical flow system for free sulfur dioxide determination in white wines is present. These lower values could be associated to a lower rate of SO₂ diffusion through the membrane in the microanalytical flow system, mainly for the white wine. Even though, it is shown that this system could be feasible for a rapid and automatic analysis of wine in the cellar. It is worthwhile to notice that best comparative results are obtained with Paul method, which is an accredited laboratory method.
5. A microanalytical flow system based on the above principle for monitoring the **free SO₂ and acetic acid** concentration in wines has been fabricated and evaluated. This

system has to be applied in wine barrels and has to accomplish some size and volume requirements. For that reason, a more compact and smaller assembly has been fabricated joining the gas diffusion cell with the sensor cell.

- Once optimized, this system has a sensitivity (slope) of $-56.1 \pm 0.5 \text{ mV dec}^{-1}$ ($r = 0.997$) in a range of $5 \text{ mg L}^{-1} - 60 \text{ mg L}^{-1}$ for free SO_2 and $-32.4 \pm 1.8 \text{ mV dec}^{-1}$ ($r = 0.999$) in a range of $150 \text{ mg L}^{-1} - 1400 \text{ mg L}^{-1}$ for acetic acid. The LOD obtained is 4.2 mg L^{-1} for free SO_2 .
 - This system was applied to wine samples analysis. Results were compared with standard methods for free SO_2 and acetic acid. Values for red wines showed a quite good correlation between both methods either for acetic acid and SO_2 parameters. Even for samples that had been spiked with extra acetic acid the errors were very low. For rosé wines, negative error's values for SO_2 indicate an underestimation of the concentration for the proposed method, related to the low diffusion rate through the membrane for low SO_2 concentrations. The results for white wines were more dispersed. For acetic acid, samples with high content of sugar and cava type interfered in the analysis, providing higher values, For SO_2 analysis, the error was acceptable for the three samples except for the sample sparkling sample, where it is supposed that the carbonic acid is interfering.
6. A microanalytical flow system for monitoring the malolactic fermentation (MLF) process in red wine samples has been developed. This objective has been carried out in several steps:
- 6.1. An amperometric bienzymatic **L-lactate biosensor** based on the modification of the microelectrodes with the enzymes lactate oxidase (LOX) and horseradish peroxidase (HRP) has been fabricated and optimized. Different strategies of immobilization have been studied. The immobilization procedure by means of electropolymerization and entrapment of the enzymes in a polypyrrole matrix has been chosen for its superior response characteristics.
- This biosensor presented a sensitivity of $(-135 \pm 6) \times 10^2 \mu\text{A M}^{-1} \text{ cm}^{-2}$ ($r = 0.998$) in a range of $1 \times 10^{-6} \text{ M} - 1 \times 10^{-4} \text{ M}$ of L-lactate with a LOD of $5 \pm 0.2 \times 10^{-7} \text{ M}$.

- The biosensor response remained stable and kept over 90 % of the initial sensitivity for 42 days, showing an excellent the working stability.
- This biosensor has been applied to the monitoring of the L-lactic acid in samples recollected during the MLF process. The results show an excellent agreement between the biosensor and the standard method values.

6.2. An amperometric bienzymatic **L-malate biosensor** based on the modification of the microelectrodes with the malate dehydrogenase (MDH) and diaphorase (DP) as enzymes, nicotinamide adenine dinucleotide (NAD⁺) as co-factor and a redox mediator has been fabricated and optimized. In that case, the immobilization procedure chosen has been directly the one used for the L-lactate biosensor, electropolymerization and entrapment of the enzymes and bioreagents in a polypyrrole matrix. For this biosensor, the redox mediator and the architecture of the membrane has been optimized. The mediator that has provided better results has been the Hexaammineruthenium (III) chloride (HAR). The better architecture has consisted on de the deposition of two PPy layers, the first one entrapping HAR and the second one entrapping MDH and DP. The bienzymatic reaction was completed adding the NAD⁺ in solution.

- This biosensor presented a sensitivity of $1365 \pm 110 \text{ mA M}^{-1} \text{ cm}^{-2}$ ($r = 0.998$, $n = 5$) in a concentration range of $1 \times 10^{-7} \text{ M} - 1 \times 10^{-6} \text{ M}$ of L-malate with a LOD of $6.3 \times 10^{-8} \text{ M}$.
- The biosensor response remained stable and kept over 90 % of the initial sensitivity for 36 days, showing an excellent the working stability.
- This biosensor has been applied to the monitoring of the L-lactic acid in samples recollected during the MLF process. The results show an excellent agreement between the biosensor and the standard method values.

6.3. A microanalytical flow system containing the two biosensors described above for the simultaneous determination of L-lactate and L-malate has been designed, fabricated and optimized. In order to have a more compact system a special silicon chip has been designed and fabricated containing all the

microelectrodes. The enzymatic membranes have been electrosynthesized according to the procedure developed before. The system has been successfully validated in samples recollected during the MLF process.

7. A multiparametric analytical system based on all the microsensors described in the point 1 has been designed, developed and evaluated. The analysis of Cava wine samples has been assessed with the combination of the multisensor array and chemometric tools, which is an electronic tongue.
 - The use of Linear Discriminant Analysis allowed to classify the Cava wines according to the ageing time ("Young", "Reserva", "Gran Reserva" and Rosé) with a total sensitivity of prediction of 87%.
 - The use of Partial Least Squares regressions allowed to quantify the total acidity, pH, volumetric alcoholic degree, potassium, conductivity, glycerol and methanol parameters in the Cava wines with mean relative errors below 6%.

Conclusions in Spanish

1. Varios sensores se han fabricado con tecnología microelectrónica. Estos sensores son ISFETs de pH e ISFETs con membranas selectivas a iones, microelectrodos de platino y oro para medidas amperométricas, conductimétricas y de ORP. Los electrodos amperométricos se han modificado con membranas enzimáticas para obtener biosensores.
2. Estos (bio)sensores han sido caracterizados con técnicas electroquímicas para evaluar sus características de respuesta.
3. Los sistemas de flujo microanalítico se han fabricado con polímeros de bajo costo, como el PSA y el PMMA, y técnicas de prototipado rápido de ablación y láser de CO₂. Estos sistemas de flujo se han aplicado a la automatización de la detección analítica de algunos parámetros de interés en la industria vitivinícola.
4. Se ha desarrollado y evaluado un sistema de flujo microanalítico para monitorizar la concentración de SO₂ libre y total en muestras de vinos. Este sistema incorpora una membrana de difusión de gas para separar el analito de la muestra evitando interferencias y utiliza como detector un ISFET de pH. Aprovechando las características ácido/base de los analitos, se realiza la detección indirecta del pH. Con el fin de detectar el SO₂ total, el sistema incorpora una celda para el tratamiento de la muestra.
 - Una vez optimizado, este sistema tiene una sensibilidad (pendiente) de $-49,6 \pm 0,7 \text{ mV dec}^{-1}$ ($r = 0,998$) en un rango de 1 mg L^{-1} - 60 mg L^{-1} para SO₂ libre y $-49,4 \pm 0,7 \text{ mV Dec}^{-1}$ ($r = 0,998$) en un intervalo de 30 mg L^{-1} - 300 mg L^{-1} para el SO₂ total. El límite de detección (LOD) es de $0,5 \text{ mg L}^{-1}$.
 - Este sistema ha sido evaluado con 70 muestras de vino y comparado con dos métodos de referencia. Los resultados han demostrado que existe una buena correlación entre ambos métodos. Se observa una subestimación de los valores obtenidos con el sistema de flujo microanalítico para la determinación de dióxido de azufre libre en los vinos blancos. Estos valores más bajos podrían estar asociados a una menor difusión de SO₂ a través de la membrana en el sistema de flujo microanalítico. Sin embargo, se demuestra que este sistema podría ser factible para un análisis rápido y automático del vino en la bodega. Vale la pena notar que los mejores resultados comparativos se obtienen con el método de Paul, que es un método de laboratorio acreditado.

5. Se ha fabricado y evaluado un sistema de flujo microanalítico basado en el principio anterior para el control de la concentración de SO₂ libre y ácido acético en los vinos. Este sistema tiene que ser aplicado en barricas de vino y tiene que cumplir con algunos requisitos de tamaño y volumen. Por esta razón, se ha fabricado un dispositivo más compacto y más pequeño que unifica la celda de difusión de gas con la celda del sensor.
- Una vez optimizado, este sistema tiene una sensibilidad (pendiente) de $-56,1 \pm 0,5 \text{ mV dec}^{-1}$ ($r = 0,997$) en un rango de 5 mg L^{-1} - 60 mg L^{-1} para SO₂ libre y $-32,4 \pm 1,8 \text{ mV Dec}^{-1}$ ($r = 0,999$) en un intervalo de 150 mg L^{-1} - 1400 mg L^{-1} para ácido acético. El LOD obtenido es de $4,2 \text{ mg L}^{-1}$ para el SO₂ libre.
 - Este sistema se aplicó al análisis de muestras de vino. Los resultados se compararon con los métodos estándar para SO₂ libre y ácido acético. Los valores de los vinos tintos mostraron una buena correlación entre ambos métodos, tanto para el ácido acético como para SO₂. Incluso para las muestras a las que se le habían añadido ácido acético extra, los errores fueron muy bajos. Para los vinos rosados, los valores de error negativo para SO₂ indican una subestimación de la concentración para el método propuesto, relacionada con la baja difusión a través de la membrana para concentraciones bajas de SO₂. Los resultados para los vinos blancos fueron más dispersos. Para el ácido acético, las muestras con alto contenido de azúcar y tipo cava interfirieron en el análisis, proporcionando valores más altos. Para el análisis de SO₂, el error fue aceptable para las tres muestras excepto para la muestra de espumoso, donde se supone que el ácido carbónico interfiere.
6. Se ha desarrollado un sistema de flujo microanalítico para controlar el proceso de fermentación maloláctica (MLF) en muestras de vino tinto. Este objetivo se ha llevado a cabo en varias etapas:
- 6.1. Se ha fabricado y optimizado un biosensor amperométrico bienzimático de L-lactato basado en la modificación de los microelectrodos con las enzimas lactato oxidasa (LOX) y HRP peroxidasa. Se han estudiado diferentes estrategias de inmovilización. El procedimiento de inmovilización por electropolimerización y atrapamiento de las enzimas en una matriz de polipirrol ha sido elegido por sus características de respuesta superiores.

- Este biosensor presentó una sensibilidad de $(-135 \pm 6) \times 10^2 \mu\text{A M}^{-1} \text{cm}^{-2}$ ($r = 0,998$) en un rango de $1 \times 10^{-6} \text{ M} - 1 \times 10^{-4} \text{ M}$ de L-lactato con un LOD de $5 \pm 0,2 \times 10^{-7} \text{ M}$.
- La respuesta del biosensor permaneció estable y mantuvo más del 90% de la sensibilidad inicial durante 42 días, mostrando una estabilidad de trabajo excelente.
- Este biosensor se ha aplicado al control del ácido L-láctico en muestras recogidas durante el proceso de la MLF. Los resultados comparativos con el método estándar son excelentes.

6.2. Se ha fabricado y optimizado un biosensor amperométrico para L-malato basado en la modificación de los microelectrodos con las enzimas malato deshidrogenasa (MDH) y diaforasa (DP), la nicotinamida adenina dinucleótido (NAD^+) como co-factor y un mediador redox. En este caso, el procedimiento de inmovilización elegido ha sido directamente el utilizado para el biosensor de L-lactato, electropolimerización y atrapamiento de las enzimas y biorreactivos en una matriz de polipirrol. Para este biosensor se ha optimizado el mediador redox y la arquitectura de la membrana. El mediador que ha proporcionado mejores resultados ha sido el cloruro de Hexaamminorutenio (III) (HAR). La mejor arquitectura ha consistido en la deposición de dos capas de PPy, la primera atrapando HAR y la segunda atrapando MDH y DP. La reacción bienzimática se completó añadiendo el NAD^+ en solución.

- Este biosensor presentó una sensibilidad de $1365 \pm 110 \text{ mA M}^{-1} \text{cm}^{-2}$ ($r = 0,998$, $n = 5$) en un intervalo de concentración de $1 \times 10^{-7} \text{ M} - 1 \times 10^{-6} \text{ M}$ de L-malato con un LOD de $6,3 \times 10^{-8} \text{ M}$.
- La respuesta del biosensor permaneció estable y mantuvo más del 90% de la sensibilidad inicial durante 36 días, mostrando una estabilidad de trabajo excelente.
- Este biosensor se ha aplicado al monitoreo del ácido L-láctico en muestras recogidas durante el proceso de MLF. Los resultados muestran una excelente concordancia entre el biosensor y los valores del método estándar.

6.3. Se ha diseñado, fabricado y optimizado un sistema de flujo microanalítico que contiene los dos biosensores descritos anteriormente para la determinación simultánea de L-lactato y L-malato. Para tener un sistema más compacto se ha

diseñado y fabricado un chip especial de silicio que contiene todos los microelectrodos. Las membranas enzimáticas han sido electrosintetizadas de acuerdo con el procedimiento desarrollado anteriormente. El sistema ha sido validado con éxito en muestras recogidas durante el proceso MLF.

7. Se ha diseñado, desarrollado y evaluado un sistema analítico multiparamétrico basado en todos los microsensores descritos en el punto 1. El análisis de las muestras de vino de Cava ha sido evaluado con la combinación de la matriz multisensor y las herramientas quimiométricas, que es una lengua electrónica.
 - El uso del Análisis Discriminador Lineal permitió clasificar los vinos de Cava según el tiempo de crianza ("Young", "Reserva", "Gran Reserva" y Rosado) con una sensibilidad total de predicción del 87%.
 - El uso de regresiones de mínimos cuadrados parciales permitió cuantificar los parámetros de acidez total, pH, grado alcohólico volumétrico, potasio, conductividad, glicerol y metanol en los vinos de Cava con errores relativos medios por debajo del 6%.

Annex: published articles included in the thesis

Multisensor Portable Meter for Environmental Applications

P. Giménez-Gómez, R. Escudé-Pujol, C. Jiménez-Jorquera, and M. Gutiérrez-Capitán

Abstract—In recent years, the development of information and communication technologies has notably improved the water management processes, but the technologies for water quality control still leave much scope for improvement. Specially, *in situ* and inline water monitoring has an increasing interest in order to take decisions at real time. The main drawbacks of the current portable meters are their high cost and their high power consumption. In this paper, it is proposed a portable compact meter for measuring simultaneously oxidation–reduction potential, conductivity, temperature, and amperometric parameters like chlorine. This system includes microsensors fabricated with microelectronic technologies, and a commercial temperature sensor, all them allowing a very low power consumption. Validation of the system has been carried out using standard solutions and comparing the results with commercial sensors. The response characteristics of sensors, in terms of sensitivity and repeatability, showed good agreement with those obtained with standard equipment using the same microelectrodes.

Index Terms—Portable equipment, microsensors, water monitoring, multiparametric analysis.

I. INTRODUCTION

IN RECENT years the water sector has become a widespread user of Information and Communication Technologies (ICT) for planning and operation. These technologies are needed not only to comply with stricter regulations and safety measures, rising quality standards and challenging social and environmental demands but also to face serious problems of aging infrastructure, which includes leakage and quality issues related to the water supply network. On the other hand, the supply of drinking water that is healthy, clean and palatable is a fundamental requirement of the European drinking water directive. World Health Organization (WHO) guidelines for drinking water [1] are used as a basis for the standards in the Drinking Water Directive (DWD) [2]. Currently there are many multi-parametric probes in the market for in-line measurement of the most common

chemical-physical parameters: pressure, temperature, pH, turbidity, chlorine, colour, Total Organic Carbon (TOC), oxidation reduction potential (ORP) and conductivity [3], [4].

Some of these probes have been tested under several projects [5] and the results concluded that they do not accomplish all the requirements for a widespread remote water monitoring: they are expensive, they are large size probes, they require high maintenance, and they have a high power consumption (around 3 W). These drawbacks prevent their widespread use. In general terms, these inconveniences are related to the technology of sensors used: the sensors have big sizes and are expensive. Therefore the miniaturization of the sensor is envisaged as an alternative [6], [7] and specially microelectrodes fabricated with semiconductor technology which are robust, reproducible, have low output impedance, low fabrication and maintenance costs and they are easy to integrate with the electronic circuitry [8]–[12].

Concerning the measurement equipment, a miniaturized potentiostat fabricated in a silicon chip using CMOS technology was described [13]. Although the dimensions of this chip can be a few millimeters, it has been customized for a specific use, rather than intended for general uses. An alternative to obtain versatile small instruments for multiparametric applications at minimum cost is the use of commercial integrated circuits (IC) such as power supplies, analog to digital converters and microcontrollers [14], [15]. Therefore, the main components of the bench-top analytical tools can be replaced by standard ICs. The reduced size of these systems implies reduced fabrication and maintenance costs, as well as lower power consumption. The price and the weight is considerably less than commercial equipment. Besides, these ICs are manufactured in many different configurations to meet with the experimental requirements. In fact, there are several commercially available mini-potentiostats which have been used in environmental [16] and biomedical [17] applications.

In this work, the design and development of a portable meter for simultaneous measurement of conductivity, oxidation-reduction potential (ORP), temperature and amperometric parameters like chlorine is described. The sensors used have been fabricated using standard microfabrication techniques. This provides as major advantages low energetic consumption and high portability. A similar system was already developed in our group for pH, ORP, conductivity and temperature applied to samples of environmental interest [18]. In this new equipment, the electrical components of the circuits have been updated to reduce the size of the meter. Besides, a miniaturized potentiostat with two channels has been

Manuscript received June 26, 2015; revised July 15, 2015; accepted July 21, 2015. Date of publication July 22, 2015; date of current version September 14, 2015. This work was supported by the Spanish Research and Development National Program from the Ministerio de Economía y Competitividad (MINECO) through the Project TEC2011-29045-C04-01. The work of P. Giménez-Gómez was supported by the Spanish MINECO through the Formación de Personal Investigador (FPI) Program. The associate editor coordinating the review of this paper and approving it for publication was Dr. Chirasree Roychaudhuri.

The authors are with the Instituto de Microelectrónica de Barcelona, Consejo Superior de Investigaciones Científicas, Bellaterra 08193, Spain (e-mail: pablo.gimenez@csic.es; roger.escude@imb-cnmi.csic.es; cecilia.jimenez@csic.es; manuel.gutierrez@csic.es).

Color versions of one or more of the figures in this paper are available online at <http://ieeexplore.ieee.org>.

Digital Object Identifier 10.1109/JSEN.2015.2460011

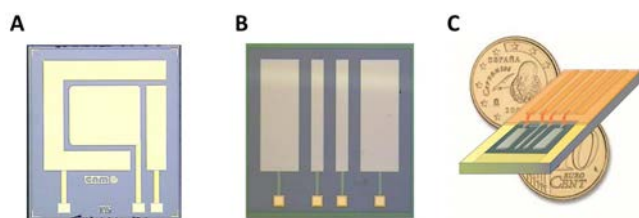


Fig. 1. Schematic view of the chips used: (A) Three-electrode cell. (B) Four-electrode cell. (C) Scheme of a packaged microsensors.

incorporated for measuring two amperometric parameters –i.e. dissolved oxygen, chlorine–, expanding the multiparametric applications of the system. Instead of a modular architecture, the developed device has a compact configuration with a different circuit and an isolated ground for each parameter to avoid electrical interferences. The validation of the whole system has been carried out with standard aqueous solutions for each parameter and results have been compared with those obtained from commercial equipment.

II. EXPERIMENTAL

A. Reagents and Solutions

All reagents used were provided by Sigma-Aldrich or Panreac and they were of high purity, analytical grade or equivalent. All solutions were prepared using de-ionized water.

Five solutions containing different concentrations of potassium chloride (KCl), were prepared in order to obtain conductivities in the range between 0.80 and 13.07 mS/cm. A standard solution of 1416 μ S/cm at 25 °C (Crison Instruments) was used for the repeatability study during conductivity tests. ORP standard solutions with nominal potentials of 220 mV and 468 mV at 25 °C were used as received. For amperometric measurements, a 0.1 M potassium ferricyanide ($K_3[Fe(CN)_6]$), solution, a 0.1 M KNO_3 (a 40 ppm free chlorine stock solution prepared from sodium hypochlorite (NaOCl 10-15 %) and a 0.1 M potassium phosphate buffer (KH_2PO_4) at pH 5.5 were prepared. Ethanol 96% and 6 M sulfuric acid (H_2SO_4 96%) were used for the electrodes cleaning.

B. Devices Used

Platinum thin-film electrodes were fabricated according to standard photolithographic technology. The steps involved in the fabrication are explained elsewhere [19]. Two different chips were used: (i) a four-electrode cell in a 3 mm \times 3 mm silicon chip for conductivity and ORP measurements, and (ii) a three-electrode cell in a 3 mm \times 3.5 mm silicon chip which contains a working electrode (1.62 mm²), a counter electrode (2.08 mm²) and a reference electrode (0.64 mm²) for amperometric measurements. Fig. 1 shows a picture of the chips used. The chips were wire-bonded on a printed-circuit board (PCB) and packaged using Ebecryl photocurable polymer following a standardized photolithographic process developed at the IMB-CNM [20].

An Ag/AgCl (3.0 M KCl) double junction reference electrode (Orion 92-02-00, Thermo Fisher Scientific Inc.,

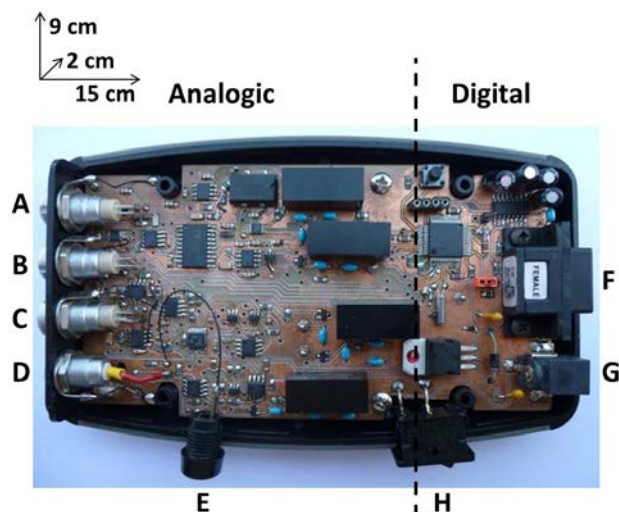


Fig. 2. View of the multiparametric system: (A) Conductivity connector. (B) Temperature connector. (C) Bipotentiostat module connector. (D) ORP connector. (E) Reference for ORP measures connector. (F) Mini-USB connector. (G) Power supply (12 V) connector. (H) On/Off switch.

Beverly, USA) was used for ORP and amperometric measurements. A Pt counter electrode (Radiometer Analytical, Lyon, France) was also used to complete the electrochemical cell. All experiments were performed at room temperature.

The conductivity of the solutions was verified using a commercial conductivity meter, Crison Micro CM 2202, before and after each measurement, being the value quite stable.

The results from the ORP and the amperometric tests were compared with the data obtained with a μ -Autolab potentiostat/galvanostat (Ecochemie, Utrecht, The Netherlands), using GPES 4.7 software package (General Purpose Electrochemical System).

C. Measurement Equipment and Electronics

The proposed system was designed and fabricated at the IMB-CNM premises. The electronic board was designed with Allegro PCB Designer and Layout Plus software (Cadence Design Systems, Bracknell, UK). The fabrication of the board was molded using a PhotoMap s43 milling machine (LPKF Laser & Electronics AG, Garbsen, Germany).

A picture of the final hardware is showed in Fig. 2. The size of the system is 10 \times 9 \times 2 cm. Capital letters indicate the five connectors for the electrodes, the mini Universal Serial Blues connector (USB, B-type) for the external communication with the PC and the power supply connector.

Analog electronics allowed generating and receiving the signals from the four microsensors. Temperature was recorded using a resistance temperature detector (RTD) Pt-100 of four wires (Pico Technology, St Neots, UK). Conductivity measurements were carried out using an alternating current (AC) source, at a fixed frequency of 5 kHz and a peak-to-peak voltage of 8 V, connected to the two external electrodes, and recording the signal (in mV) between the two internal electrodes. The ORP electrode was directly connected to the acquisition module and the potential (in mV) was measured

against the reference electrode. For amperometric measurements, a three-electrode microsensor was used. An electrical voltage was fixed between the reference and the working electrodes and the current that flowed between the working and the counter electrodes (in nA) was recorded. This current depended on the concentration of the analyte in solution. Then, the current values were converted to voltage values using a current-voltage (I-V) converter. The device had two amperometric terminals (AMP1 and AMP2) that could be used simultaneously. The equipment had a bi-potentiostat configuration based on two different I-V converters with the same reference and counter electrodes. These two electrodes could be either commercial ones, or those integrated in the same chip of the working electrode. In this sense, a hardware interface was developed which allowed choosing the configuration of the electrochemical cell.

The digital interface permitted to establish the communication between the user and the analog electronic part. The main IC was the ADUC848BSZ62-5 microcontroller (μC) (Analog Devices, Norwood, USA). This μC was composed by a central processing unit (CPU), some memories, digital and analog ports and some communications units. One of the memories (E2PROM) contained the programmed code, which was sequentially executed by the μC . This code was programmed in C++ language using the development kit μVision 4.02 (Keil Elektronik, Grasbrunn, Germany).

D. Software for Data Collection

The visualization of the results and the configuration of the measurement parameters were carried out employing a virtual instrument (VI). The VI was programmed with LabVIEW 2013 (National Instruments, Austin, USA). This is a modular, versatile, quick and intuitive software program which provides a clear working environment to the user. The communication with the analytical device can be performed through the different connections of the PC: serial, GPIB, parallel, USB, etc. [21]. The use of VI under the graphical LabVIEW environment is advantageous for electrochemical measurements due to the flexible programming and the easy-to-use, reliable and expandable instruments obtained [22], [23].

A general image of this software interface is showed in Fig. 3. This interface permits to enter the time between measurements (Fig. 3, B), and the voltages fixed for the amperometric electrodes (D); the visualization of the values obtained for the five parameters: ORP (in mV), conductivity (mV or mS/cm), temperature (in $^{\circ}\text{C}$) and the amperometric parameters (AMP1 and AMP2, in nA) (Fig. 3, A). The interface shows two dynamic graphs with the evolution of the different parameters over time: F for ORP, Conductivity or Temperature, and G for the two amperometric channels (AMP1 or AMP2). Besides, the panel incorporates commands to store the obtained values in spreadsheet file format, easily exported to other applications like Notepad, EXCEL or ORIGIN (C). Finally, the instrument includes an "Exit program" button in order to finish the measurements (E).

A scheme of the whole system formed by the bipotentiostat module, a laptop PC with the Labview software and the

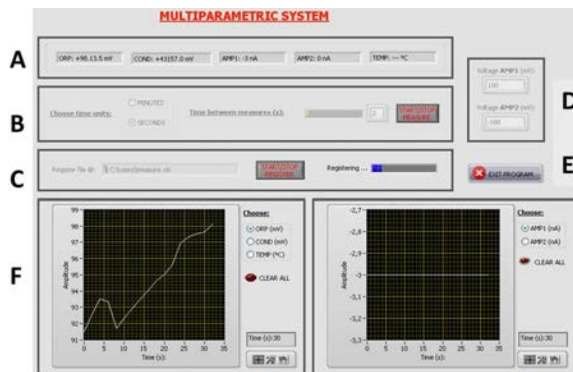


Fig. 3. Labview interface screen: (A) Signal measured for the four parameters. (B) Command to indicate the time between measurements. (C) Command to choose the registration file. (D) Command to fix voltages for the amperometric electrodes. (E) Button to stop the measurements. (F) Dynamic graph for ORP, conductivity or temperature. (G) Dynamic graph for amperometric measurements.

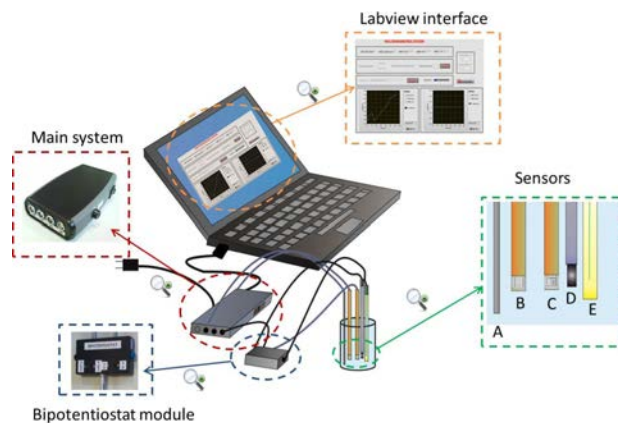


Fig. 4. Scheme of the whole multisensor equipment. In the detailed sensor scheme, (A) temperature sensor, (B) conductivity or ORP sensor, (C) amperometric sensor; (D) counter electrode and (E) reference electrode.

measurement cell with the different microsensors is showed in Fig. 4.

E. Methodology of Evaluation

An activation procedure was performed to the microsensors [24] before the measurements. Firstly, they were carefully cleaned with 96% ethanol, H_2SO_4 6M, deionized water and finally dried with nitrogen. Then, an electrochemical activation was performed in 0.1 M KNO_3 solution where the electrode was cycled from +0.8 V to -2.2 V at 100 mV/s for 15 times.

In order to test the developed equipment, measurements of conductivity, ORP and amperometric responses were performed and compared with the results provided by commercial equipments. Moreover, the possible cross-talk interference between ORP and conductivity measurements, due to the application of an AC source through the solution, was evaluated.

For conductivity tests, five KCl solutions of 0.80 mS/cm, 1.52 mS/cm, 2.82 mS/cm, 6.87 mS/cm and 13.07 mS/cm were

prepared in order to evaluate the system in a wide range. A Pt four-electrode microsensor was immersed in each solution and the signal was recorded every 10 s during 2 min using the developed electronic system. A study of repeatability was carried out using a standard solution with nominal conductivity of $1416 \mu\text{S}/\text{cm}$, which was measured six times consecutively. This solution was chosen because its conductivity value is close to that of the drinking water.

For ORP tests, a Pt four-electrode microsensor and a commercial reference electrode were immersed in the standard solutions of 220 mV and 468 mV. The potential given by the system was recorded every 1 s during 3 min. This measurement was repeated three times for each ORP solution. As before, the ORP testing was completed with a study of repeatability. In this case, the 220 mV standard solution was measured six times consecutively with the same sensor. This solution was chosen because its ORP value is close to that of the drinking water.

For amperometric tests, a Pt three-electrode microsensor as working electrode, a commercial counter electrode and a commercial reference electrode were used. In order to evaluate the system performance, the ferricyanide/ferrocyanide ($\text{Fe}(\text{CN})_6^{3-}/\text{Fe}(\text{CN})_6^{4-}$) redox process was considered. A potential of +75 mV that allowed the reduction of ferricyanide to ferrocyanide was applied. Then, calibration curves were performed in triplicate by addition of increasing concentrations of potassium ferricyanide in a 0.1 M KNO_3 background electrolyte solution in a range from 0 mM to 5 mM. Continuous stirring was used during all the measurements to ensure the homogeneity of the solution. For each ferricyanide addition, the current was recorded every 1 s during 2 min. This study was performed for the two amperometric terminals of the electronic device.

After testing the system for ferricyanide, its feasibility for free chlorine detection was checked. This analyte is an important parameter to control the quality of drinking water. In order to detect the reduction of the free chlorine in a 0.1 M phosphate buffer pH 5.5, a potential of +350 mV was fixed and chronoamperometric measurements were carried out by triplicated using one of the amperometric terminals of the multisensor portable meter. The range studied was between 0 and 1.32 ppm of free chlorine, in accordance with the concentrations found in drinking water. The potential was shifted to +350 mV after 30 s of magnetic stirring and the cathodic current was then recorded for 30 s. The overall time for one analysis in batch was 60 s. Since solutions of free chlorine are unstable, the stock solution for calibration was analyzed in parallel with the standard DPD colorimetric method, using a commercial kit (Pocket Colorimeter II for Chlorine, HACH Company, Loveland, USA) [24].

For the evaluation of cross-talk interference, simultaneous measurements of ORP and conductivity were performed using the multiparametric system. Firstly, ORP standard solutions of 220 mV and 468 mV were measured by triplicated with the two microsensors every 1 s during 5 min. Then, the value of conductivity for the five KCl solutions (with a conductivity range from 1 to 13 mS/cm) was evaluated together with the ORP every 10 s during 100 s.

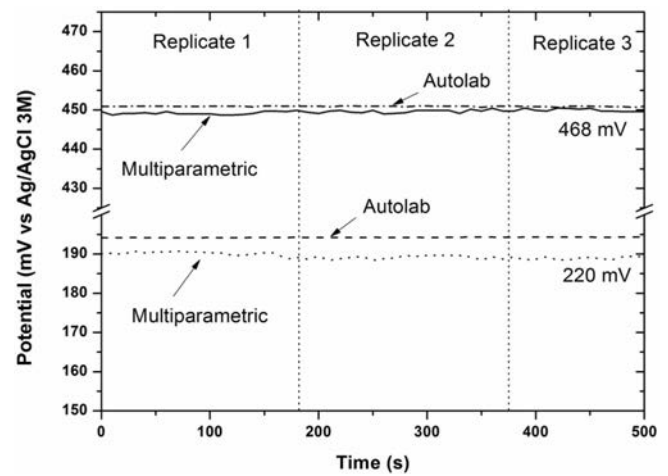


Fig. 5. ORP recording for the standard solutions: 220 mV (dotted line) and 468 mV (full line) with the multiparametric system; and 220 mV (dashed line) and 468 mV (dot-dashed line) with the Autolab equipment. The three replicates are separated by vertical dotted lines.

All measurements were performed at room temperature, 25°C .

III. RESULTS AND DISCUSSION

The equipment was tested firstly individually for each parameter and afterwards a cross-talk test was performed

A. ORP Tests

Two standard solutions of 220 mV and 468 mV were used for ORP measurements. Fig. 5 shows the signal obtained for the three replicates during 3 min and the comparison with the commercial μ -Autolab equipment. For the multiparametric system, the mean potentials recorded were 189.5 mV and 449.6 mV, respectively. These values were in good agreement with those obtained by the μ -Autolab equipment, which were 194.2 mV and 450.9 mV, respectively. The repeatability study for the 220 mV solution showed a standard deviation of 0.7 mV and a coefficient of variation of 0.4 % ($n = 6$), demonstrating a good performance of the system for the ORP measurement. Regarding temperature effect, this sensor has a temperature coefficient of $-1.6 \text{ mV}/^\circ\text{C}$, as reported elsewhere [18].

B. Conductivity Tests

The signal obtained using the conductivity output for the five KCl solutions is shown in Fig. 6A. As can be seen, the signal is stable for all conductivities. Besides, a clear correlation between values of potential and the resistivity (σ , inverse of conductivity) obtained with the commercial conductivity meter was observed (Fig. 6B). A linear relationship was obtained, with a slope of $1.99 \text{ mV}/(\Omega \cdot \text{cm})$ in the range from 0.80 mS/cm to 13.07 mS/cm conductivities and a coefficient of regression (r) of 0.999. The repeatability study for a $1416 \mu\text{S}/\text{cm}$ solution showed a standard deviation of $10 \mu\text{S}/\text{cm}$ and a coefficient of variation of 0.7 % ($n = 6$), demonstrating again a good performance of the system for the conductivity measurement. Conductivity is also affected by temperature being the temperature coefficient of $2.17\%/^\circ\text{C}$ [18].

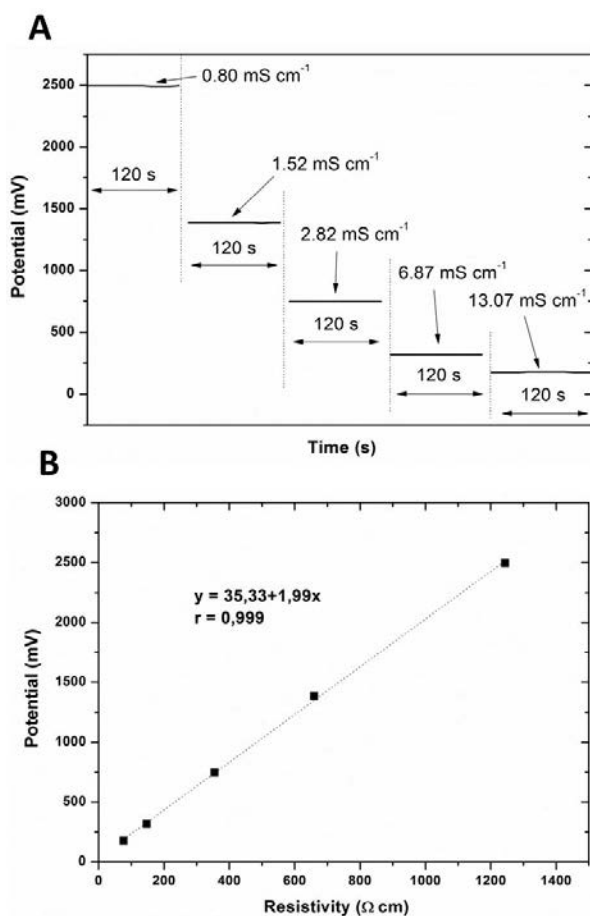


Fig. 6. Results obtained for the conductivity measurements: (A) Recording of potential variation for different conductivity solutions. (B) Calibration curve obtained using values of resistivity measured with the commercial equipment vs. values of potential obtained with the system. Dotted line shows the linear fitting.

C. Amperometric Tests

Firstly, ferricyanide was used for testing the electronic system and to compare the analytical signals with those from the commercial equipment. After that, the detection of free chlorine was evaluated in order to check the feasibility of the proposed system for a real application.

According to previous studies, a potential of +75 mV was chosen to measure ferricyanide reduction. Successive additions of 0.1 M potassium ferricyanide solution were carried out in order to obtain a concentration range between 0.1 mM to 5 mM. Both amperometric terminals (AMP1 and AMP2) were tested by triplicated. Fig. 7A shows the current obtained and the comparison with the commercial equipment. As expected, the cathodic current increased with the analyte concentration in a reproducible way for the two amperometric terminals and for the commercial equipment. The linear regression of the calibration curve showed a slope of $-4.47 (\pm 0.01) \mu\text{A}/\text{mM}$ for AMP1 and $-4.44 (\pm 0.01) \mu\text{A}/\text{mM}$ for AMP2, which were in good accordance with the value of $-4.48 \mu\text{A}/\text{mM}$ obtained with the μ -Autolab. The intercept of the regressions was also practically the same and the regression coefficient was 0.999 for all the cases.

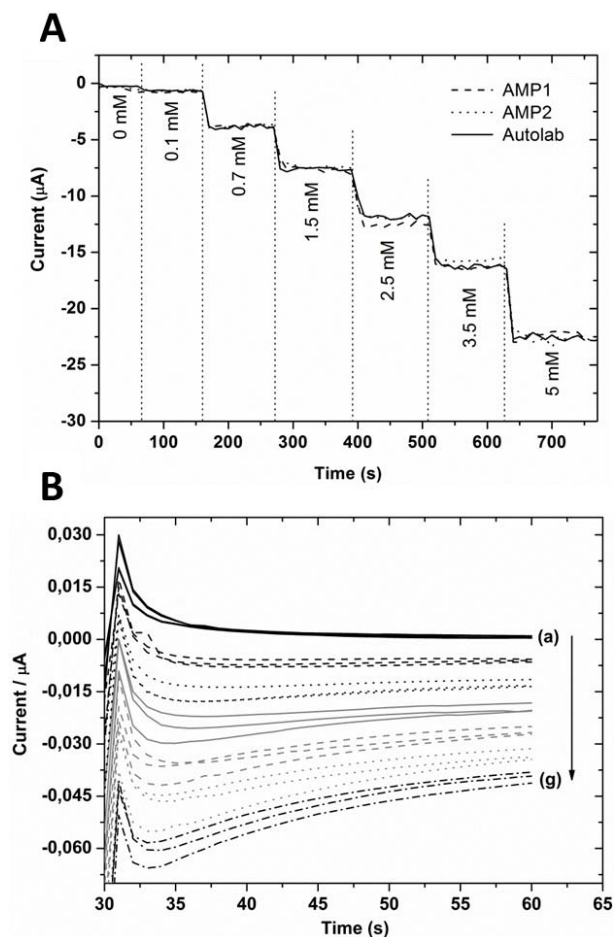


Fig. 7. (A) Recording for amperometric signal for successive additions of potassium ferricyanide in 0.1 M KNO_3 background solution: AMP1 (dashed line), AMP2 (dotted line) and Autolab (full line); (B) Chronoamperometric response recorded by triplicated in presence of 0 ppm (a), 0.22 ppm (b), 0.44 ppm (c), 0.66 ppm (d), 0.88 ppm (e), 1.1 ppm (f) and 1.32 ppm (g) of free chlorine.

Once demonstrated the good performance of the amperometric electronics, it was applied to the detection of free chlorine. For that a potential of +350 mV was fixed against the reference electrode and chronoamperometric analysis was performed in a concentration range between 0 ppm and 1.32 ppm. The signal recording for the different concentrations is shown in Figure 7B. As can be seen, the cathodic current increased with the free chlorine concentration. Each concentration was analyzed by triplicated. The calibration curve obtained in the studied range had a slope of $-31 \text{ nA}/\text{ppm}$ and a regression coefficient of 0.999.

D. Cross-Talk Interference Tests

It is well known that the AC signal that passes through the solution for conductivity measurements could affect the potentiometric (ORP) signal. In this equipment each sensor circuit was isolated and therefore this effect is removed. However, a test to demonstrate that the electronics were well isolated was carried out. Firstly, ORP and conductivity were measured simultaneously using two ORP standard solutions $200 \pm 3 \text{ mV}$ and $444 \pm 5 \text{ mV}$, respectively. Values for conductivity corresponded to $10.5 \text{ mS}/\text{cm}$ and $4.8 \text{ mS}/\text{cm}$,

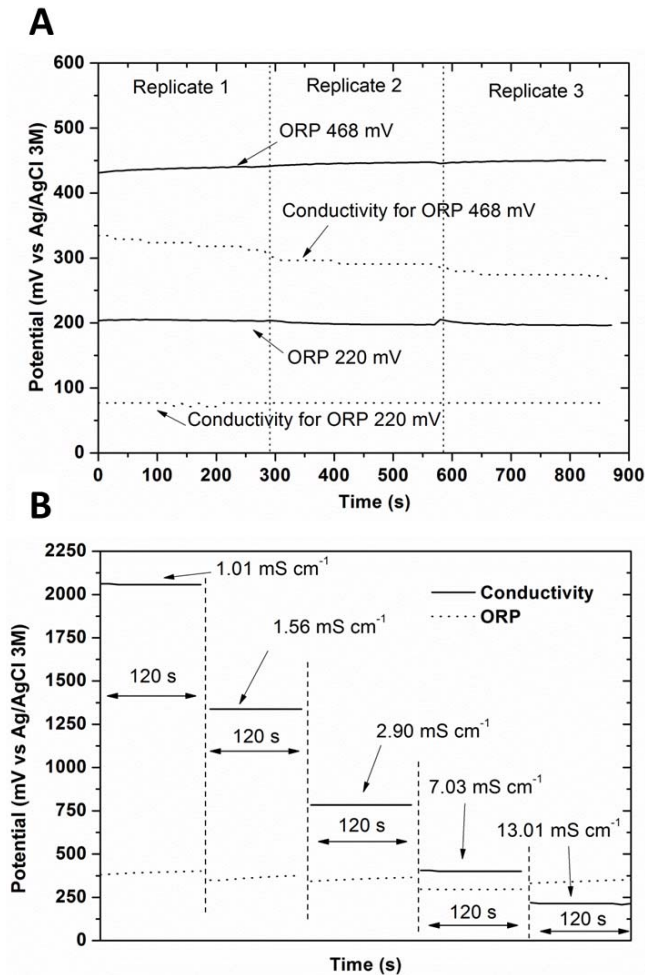


Fig. 8. Study of cross-talk between conductivity and ORP measurements. (A) Recording of ORP (full lines) and conductivity (dotted lines) in ORP commercial solutions. (B) Recording of conductivity (full line) and ORP (dotted line) in KCl solutions.

respectively. As shown in Fig. 8A for the 468 mV solution, the slight decrease of signal for conductivity measurements indicates an increase of conductivity probably due to the carbonation of the solution. It is worthwhile to note that this solution is not buffered meanwhile the 220 mV solution is buffered and the conductivity is higher and more stable.

In a second experiment, variation of conductivity in a range from 1 to 13 mS/cm was performed and ORP was also recorded (Fig. 8B).

The potential registered by the conductivity microsensors showed a variation as expected, with a slope of $1.98 \text{ mV}/(\Omega \cdot \text{cm})$ and a coefficient of regression of 0.999, in good agreement with the previous conductivity results. On the other hand, the values of potential recorded by the ORP microsensor remained fairly constant, despite the increasing KCl concentration, since no species with redox properties were added.

IV. CONCLUSIONS

A compact multiparametric meter for measuring ORP, conductivity, temperature and two amperometric signals has been developed and tested in this work. The electronics have

been fabricated according to microsensors requirements and taking into account the minimum energy consumption. This depended on the working mode of the device. During the measurement of the five microsensors simultaneously, there is a peak consumption of 140 mA. However, this value is reduced to 5 mA (sleep mode) when the microsensors are not working. Therefore, if the measurement is defined every 15 min, for example, the equivalent power consumption will be lower than 6 mA and the device could work continuously up to 200 h using a standard battery supply of 9 V.

Besides, the communication between the PC and the equipment could be performed using a wireless protocol, such as a Wi-Fi interface using low power RF transceiver IC (i.e. MRF24WB0MA from Microchip, USA) or a low power consumption ZigBee interface (i.e. XBee-PRO 802.15.4 OEM RF from DIGI International, USA). A Bluetooth interface based on wireless technology (i.e. from Laird Technologies, USA) could be another alternative, but the power consumption increases compared to the other options.

The comparative results with commercial equipment's for each parameter have demonstrated the good performance of the developed equipment. Simultaneous measurements of all parameters, including conductivity, can be carried out without any electrical interference thanks to the circuit design. This is achieved thanks to each parameter's circuitry is powered individually and has its own isolated signal ground. Therefore, a fully deployable multisensor equipment has been developed to perform in-field analysis for environmental monitoring.

REFERENCES

- [1] *Guidelines for Drinking-Water Quality*, 3rd ed. Geneva, Switzerland: World Health Organization Press, 2008.
- [2] *EU Directive 98/33/EC on the Quality of Water Intended for Human Consumption*, European Council, Brussels, Belgium, Nov. 1998.
- [3] Thermo Fisher Scientific Inc., Waltham, MA, USA. (Apr. 2015). *Orion Star A329 pH, ISE, Conductivity, Dissolved Oxygen, RDO and Temperature Portable Waterproof Multiparameter Meter*. [Online]. Available: <http://www.thermoscientific.com/content/tfs/en/product/orion-star-a329-ph-ise-conductivity-dissolved-oxygen-portable-multiparameter-meter.html#sthash.uNOSHKon.dpuf>
- [4] Thermo Fisher Scientific Inc., Waltham, MA, USA. (2014). *Thermo Scientific Orion Meter Brochure*. [Online]. Available: <http://www.thermoscientific.com/content/dam/tfs/ATG/EPD/EPD%20Documents/Catalogs%20&%20Brochures/Water%20Analysis%20Instruments%20and%20Supplies/Meters/B-ORIONMETERS-E-1014-RevA-web.pdf>
- [5] A. Monsorez. (Oct. 2011). *Deliverable 2.1.1, State of the Art Report of Chemical Sensors for Early Warning Systems, Version 2. SecurEau project, No 217976*. [Online]. Available: http://www.secureau.eu/fileadmin/Secureau/Deliverables_PU/V02_WP2_D2_1_1_SiteWeb.pdf
- [6] F. Attivissimo, C. G. C. Carducci, A. M. L. Lanzolla, A. M. L. Massaro, and M. R. Vadrucchi, "A portable optical sensor for sea quality monitoring," *IEEE Sensors J.*, vol. 15, no. 1, pp. 146–153, Jan. 2015.
- [7] C. Chen, F. Tsow, K. D. Campbell, R. Iglesias, E. Forzani, and N. Tao, "A wireless hybrid chemical sensor for detection of environmental volatile organic compounds," *IEEE Sensors J.*, vol. 13, no. 5, pp. 1748–1755, May 2013.
- [8] P. Ciosek *et al.*, "Potentiometric studies and various applications of solid state electrodes based on silicon and epoxy glass structures—An overview," *Electroanalysis*, vol. 21, nos. 17–18, pp. 1895–1905, Sep. 2009.
- [9] C. Jimenez *et al.*, "Development of a multiparametric system based on solid-state microsensors for monitoring a nuclear waste repository," *Sens. Actuators B, Chem.*, vol. 91, nos. 1–3, pp. 103–108, Jun. 2003.
- [10] L. Moreno i Codinachs *et al.*, "Integrated multisensor for FIA-based electronic tongue applications," *IEEE Sensors J.*, vol. 8, no. 5, pp. 608–615, May 2008.

- [11] J. Rothe, O. Frey, A. Stettler, Y. Chen, and A. Hierlemann, "Fully integrated CMOS microsystem for electrochemical measurements on 32×32 working electrodes at 90 frames per second," *Anal. Chem.*, vol. 86, no. 13, pp. 6425–6432, Jul. 2014.
- [12] D. M. Wilson, S. Hoyt, J. Janata, K. Booksh, and L. Obando, "Chemical sensors for portable, handheld field instruments," *IEEE Sensors J.*, vol. 1, no. 4, pp. 256–274, Dec. 2001.
- [13] B. Bozorgzadeh, D. P. Covey, C. D. Howard, P. A. Garris, and P. Mohseni, "A neurochemical pattern generator SoC with switched-electrode management for single-chip electrical stimulation and $9.3 \mu\text{W}$, $78 \text{ pA}_{\text{rms}}$, 400 V/s FSCV sensing," *IEEE J. Solid-State Circuits*, vol. 49, no. 4, pp. 881–895, Apr. 2014.
- [14] A. F. D. Cruz, N. Norena, A. Kaushik, and S. Bhansali, "A low-cost miniaturized potentiostat for point-of-care diagnosis," *Biosensors Bioelectron.*, vol. 62, pp. 249–254, Dec. 2014.
- [15] G. Rocchitta *et al.*, "Simultaneous telemetric monitoring of brain glucose and lactate and motion in freely moving rats," *Anal. Chem.*, vol. 85, no. 21, pp. 10282–10288, Nov. 2013.
- [16] F. Rueda-Holgado, E. Bernalte, M. R. Palomo-Marín, L. Calvo-Blázquez, F. Cereceda-Balic, and E. Pinilla-Gil, "Miniaturized voltammetric stripping on screen printed gold electrodes for field determination of copper in atmospheric deposition," *Talanta*, vol. 101, pp. 435–439, Nov. 2012.
- [17] A. J. Veloso *et al.*, "Miniaturized electrochemical system for cholinesterase inhibitor detection," *Anal. Chim. Acta*, vol. 774, pp. 73–78, Apr. 2013.
- [18] J. Orozco, A. Baldi, R. Baena, A. Cadarso, A. Bratov, and C. Jimenez, "Portable system based on microsensors for environmental monitoring applications," *Meas. Sci. Technol.*, vol. 18, no. 3, pp. 935–940, Mar. 2007.
- [19] J. Orozco, G. Suárez, C. Fernández-Sánchez, C. McNeil, and C. Jiménez-Jorquera, "Characterization of ultramicroelectrode arrays combining electrochemical techniques and optical microscopy imaging," *Electrochim. Acta*, vol. 53, no. 2, pp. 729–736, Dec. 2007.
- [20] A. Bratov, J. Muñoz, C. Dominguez, and J. Bartroli, "Photocurable polymers applied as encapsulating materials for ISFET production," *Sens. Actuators B, Chem.*, vol. 25, nos. 1–3, pp. 823–825, Apr. 1995.
- [21] A. Durán, M. Cortina, L. Velasco, J. A. Rodríguez, S. Alegret, and M. del Valle, "Virtual instrument for an automated potentiometric e-tongue employing the SIA technique," *Sensors*, vol. 6, no. 1, pp. 19–29, Jan. 2006.
- [22] A. Economou, S. D. Bolis, C. E. Efstathiou, and G. J. Voliakakis, "A 'virtual' electroanalytical instrument for square wave voltammetry," *Anal. Chim. Acta*, vol. 467, nos. 1–2, pp. 179–188, Sep. 2002.
- [23] Z. Stević, Z. Andjelković, and D. Antić, "A new PC and LabVIEW package based system for electrochemical investigations," *Sensors*, vol. 8, no. 3, pp. 1819–1831, Mar. 2008.
- [24] R. Olivé-Monllau *et al.*, "Flow injection analysis system based on amperometric thin-film transducers for free chlorine detection in swimming pool waters," *Talanta*, vol. 77, no. 5, pp. 1739–1744, Mar. 2009.



P. Giménez-Gómez was born in Madrid, Spain. He received the degree in chemical engineering (5-year degree) from the University of Murcia, Spain, in 2008, and the M.S. degree in electrochemistry (conducting polymers) from the Polytechnic University of Cartagena, Spain, in 2011. He is currently pursuing the Ph.D. degree in electrochemistry with the Instituto de Microelectrónica de Barcelona (IMB–CNM), CSIC.

He was an Environmental, Quality, and Health Controller in an industrial waste treatment company from Abengoa, Cartagena, Spain, from 2008 to 2009. He has worked for two years as a Researcher with the Center of Electrochemistry and Intelligent Materials, University of Cartagena. His job was focused on the study and development of conducting polymers and their applications. After it, he worked during almost one year as a Researcher in the development of electrically conductive ceramics materials with the Institute for Manufacturing Technologies of Ceramic Components and Composites, Stuttgart, Germany. He is currently pursuing the Ph.D. degree with IMB–CNM, CSIC, with the financial support through a research studentship of the FPI Program of the MINECO, Spain. His research interest includes the surface modification of amperometric biosensor for the control of chemical analytes in food industry or cell cultures and the design and development of lab-on-chip devices based on fast prototyping.



R. Escudé-Pujol was born in Barcelona, Spain. He received the B.S. and M.S. degrees in electronic and automation engineering from the Polytechnic University of Catalunya, Spain, in 2004.

He has been involved in the engineering service for electronic systems and applications with the Instituto de Microelectrónica de Barcelona, CSIC, since 2004. He has co-authored four articles and holds one patent. His main research interest is the development of prototype electronic sensors based on silicon technology for electrochemical applications.



C. Jiménez-Jorquera was born in Barcelona, Spain. She received the Ph.D. degree in chemistry from the Universitat Autònoma de Barcelona (UAB), Spain, in 1994.

She made a post-doctoral stage with the Institute of Microtechnology, University of Neuchâtel, Switzerland, from 1993 to 1994. She worked with UAB as an Assistant Professor from 1994 to 1996. She was with the School of Environmental Engineering as a Full Professor (Mollet, Spain) from 1997 to 1999. She joined the Chemical Transducer

Group, IMB–CNM, in 2000, where she was the Leader from 2003 to 2013. She was a member of the Science and Physics Technology Area Committee of CSIC from 2008 to 2012.

She is a Specialist in the development of biochemical sensors, mainly electrochemical semiconductor-based sensors based on ion selective field effect transistors, metal thin film microelectrodes, microelectrode arrays, and interdigitated electrodes. Her research is focused on the application of biosensors to areas, such as environmental control, industrial processes monitoring, mainly in food industry, clinical, and biomedical analysis, and cell culture's monitoring. She is also a Specialist in the development of integrated analytical microsystems. She has authored over 70 articles in SCI journals.



M. Gutiérrez-Capitán was born in Sabadell, Spain. He received the Ph.D. degree in analytical chemistry from the Universitat Autònoma de Barcelona, Spain, in 2008, for a thesis devoted to the application of potentiometric electronic tongues in agricultural, environmental, and clinical monitoring.

He has been with the Chemical Transducers Group, Instituto de Microelectrónica de Barcelona, CSIC, Spain, since 2008, where he received the Juan de la Cierva Scholarship in 2010. He has authored 20 articles in international scientific journals and four book chapters. His research interests include sensor arrays and electronic tongues, biochemical sensors made from microelectronic technology, miniaturized fluidic systems for analytical purposes, and new sensor platforms based on nanostructured materials (carbon nanotubes, graphene, and metal nanoparticles).



Contents lists available at ScienceDirect

Analytica Chimica Acta

journal homepage: www.elsevier.com/locate/aca

Monitoring of malolactic fermentation in wine using an electrochemical bienzymatic biosensor for L-lactate with long term stability



Pablo Giménez-Gómez^a, Manuel Gutiérrez-Capitán^a, Fina Capdevila^b, Anna Puig-Pujol^b, César Fernández-Sánchez^a, Cecilia Jiménez-Jorquera^{a,*}

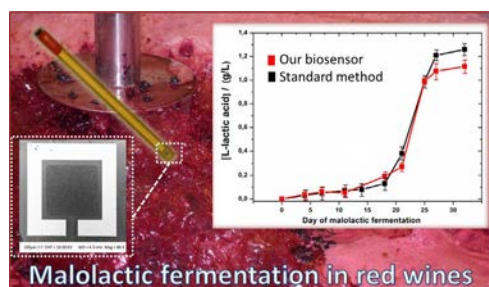
^a Instituto de Microelectrónica de Barcelona (IMB-CNM), CSIC, Campus UAB, 08193 Bellaterra, Spain

^b Institut Català de la Vinya i el Vi (IRTA-INCAVI), Plaça Àgora 2, 08720 Vilafranca del Penedès, Spain

HIGHLIGHTS

- Biosensor for L-lactate based on an electrosynthesized PPy film.
- Extended lifetime of over 40 days.
- Application to L-lactate acid monitoring during the malolactic fermentation process.

GRAPHICAL ABSTRACT



ARTICLE INFO

Article history:

Received 2 September 2015

Received in revised form

26 October 2015

Accepted 23 November 2015

Available online 30 November 2015

Keywords:

Amperometric biosensor

Bienzymatic membrane

Electrosynthesized polypyrrole

L-lactic acid analysis

Wines

Malolactic fermentation

ABSTRACT

L-lactic acid is monitored during malolactic fermentation process of wine and its evolution is strongly related with the quality of the final product. The analysis of L-lactic acid is carried out off-line in a laboratory. Therefore, there is a clear demand for analytical tools that enabled real-time monitoring of this process in field and biosensors have positioned as a feasible alternative in this regard. The development of an amperometric biosensor for L-lactate determination showing long-term stability is reported in this work. The biosensor architecture includes a thin-film gold electrochemical transducer selectively modified with an enzymatic membrane, based on a three-dimensional matrix of polypyrrole (PPy) entrapping lactate oxidase (LOX) and horseradish peroxidase (HRP) enzymes. The experimental conditions of the biosensor fabrication regarding the pyrrole polymerization and the enzymes entrapment are optimized. The biosensor response to L-lactate is linear in a concentration range of 1×10^{-6} – 1×10^{-4} M, with a detection limit of 5.2×10^{-7} M and a sensitivity of $-(13500 \pm 600) \mu\text{A M}^{-1} \text{cm}^{-2}$. The biosensor shows an excellent working stability, retaining more than 90% of its original sensitivity after 40 days. This is the determining factor that allowed for the application of this biosensor to monitor the malolactic fermentation of three red wines, showing a good agreement with the standard colorimetric method.

© 2015 Elsevier B.V. All rights reserved.

* Corresponding author. Instituto de Microelectrónica de Barcelona (IMB-CNM), CSIC, Campus de la UAB, 08193 Bellaterra, Barcelona, Spain.

E-mail address: cecilia.jimenez@csic.es (C. Jiménez-Jorquera).

1. Introduction

Measuring and controlling L-lactic acid concentrations is

required in fields as diverse as sport medicine [1], medical control [2] or food industry [3]. L-lactic acid is used as an indicator to monitor fermentation processes and its concentration is also strongly related to the flavor or the texture of the original product [4]. Also, L-lactic acid is applied as acidifier, preservative and pH regulator in confectionary industry [5], in fruit and vegetables industry or in the winemaking industry [6], among others. In the winemaking industry, the L-lactic acid concentration is related to the quality of the final product [7]. It is produced mainly in the malolactic fermentation, in which the transformation of the malic acid into L-lactic acid and CO₂ takes place. Wine L-lactic acid concentrations can increase up to 3 g L⁻¹ (0.028 M). In some elaboration processes, L-lactic acid is added as acidifier during the alcoholic fermentation in order to improve its clarification and guarantee the flavor during the aging of the wine. The presence of L-lactic acid improves the sensorial qualities of wine, its freshness and contributes to the chemical and microbiological stability. In addition, it increases the total acidity and the buffer capacity of the wine. Therefore, the control of the L-lactic acid concentration can be used as a quality indicator of the final wine.

There are conventional analytical procedures for the determination of L-lactic acid in wines based on chromatography [8] and colorimetric methods [9]. In general, these methods require costly equipment and are time consuming, given that the analysis is carried out in an external laboratory. Therefore, in order to follow the fermentation process in real time, in field monitoring of L-lactic acid concentration would be desirable. In this context, biosensor devices emerge as a feasible alternative [10], and those based on electrochemical methods have shown to be very convenient. Electrochemical biosensor devices show several advantages, such as low detection limits, a wide linear response range or high selectivity and reproducibility [11]. Among them, amperometric sensors based on redox reactions catalyzed by oxidoreductase enzymes have been of widespread use [12]. These enzymes show additional advantages like their natural origin and no toxicity, high specificity and stability under moderate working conditions of pH and temperature. One of the most common strategies for the L-lactate determination makes use of L-lactate dehydrogenase (LDH) in presence of NAD⁺/NADH as coenzyme [13]. However, the derived biosensor devices show several drawbacks related to the necessity of incorporating the NAD⁺ cofactor, which in turn requires the implementation of a potential step once the sensor response is recorded in order to regenerate it. This step is carried out at relatively high potentials (above 300 mV), and this can cause interferences of other electroactive species present in the samples. Another alternative is the use of LOX as recognition element. This enzyme catalyzes the L-lactate oxidation to produce pyruvate and hydrogen peroxide in the presence of dissolved oxygen. The hydrogen peroxide can then be reduced and the resulting cathodic current is stoichiometrically related to the L-lactate concentration in the sample. Here, the main drawback is that a high over-potential for the direct detection of H₂O₂ is needed and this again can cause interferences of other oxidizable species present in the samples. In order to circumvent this difficulty, a LOX based biosensor comprising an electrochemical dissolved oxygen sensor was reported [14]. Other more widespread strategies are based on the incorporation of a second enzyme, namely horseradish peroxidase (HRP) that catalyzes the reduction of H₂O₂ to H₂O in the presence of a suitable redox mediator that is concomitantly oxidized [15–17]. Detection of these oxidized species takes place at low enough potentials to avoid any possible interference from the sample. Moreover, the resulting biosensor shows enhanced sensitivity thanks to the application of the LOX/HRP cascade enzyme reaction [18].

One of the main drawbacks of biosensor devices is the limited lifetime mainly related to the biomolecules stability and the

procedure applied for their incorporation onto the transducer surface. Therefore, the chosen immobilization procedure has to be studied in detail and optimized in order to maximize the working stability over time. The enzyme entrapment in three-dimensional matrices [19,20] proved to be a good alternative due to the simple fabrication and the not required modification of the enzyme structure, which improves the lifetime of the biosensor. Besides, the enzyme entrapment in a membrane of a conducting polymer by electropolymerization is a common strategy in amperometric biosensors [21–23]. A one-step controlled process is carried out under potentiostatic (set potential) or galvanostatic (set current) conditions in a solution containing the monomer and the enzymes. Both approaches induce the oxidation of the monomer and the formation of an electrogenerated polymer layer, which physically entrap the enzymes, thus maintaining their original activity [24]. Conducting polymers, in particular PPy, have a stable electrical conductivity and can be electrogenerated under biocompatible conditions, in agreement with the enzyme requirements. The improved lifetime of biosensors fabricated using conducting polymers has been demonstrated [25]. Regarding to L-lactate biosensors, few works have been reported based on a two enzyme co-immobilization process onto the transducer surface using polymers. They make use of the polymer as a surface for the further enzyme physical adsorption [26] or covalent immobilization [27], but no paper has been reported describing the simultaneous one-step immobilization of LOX and HRP enzymes in an electro-synthesized PPy matrix.

In this work, the development and characterization of a new biosensor for L-lactate determination based on the co-immobilization of LOX and HRP in an electro-synthesized PPy film is described for first time. A thin-film gold microelectrode selected as the electrochemical transducer allows working with very small volumes and thus reducing reagent consumption during the polymer electro-synthesis. The fabrication of the enzymatic membrane has been optimized with respect to the electro-synthesis conditions and LOX:HRP ratio within the PPy membrane. L-lactate detection has been carried out by chronoamperometry in solutions containing potassium ferrocyanide as redox mediator. The analytical characteristics of the biosensor in terms of selectivity, sensitivity, linear range, limit of detection and working stability have been assessed and compared with other similar electrochemical biosensors. This sensor stands out for its extended lifetime of over 40 days and the successful application to the L-lactic acid monitoring during the malolactic fermentation process of three different red wines, obtaining concentration values in excellent agreement with those obtained using the standard colorimetric method.

2. Materials and methods

2.1. Reagents and solutions

All reagents used were of high purity, analytical grade or equivalent and were purchased from Sigma–Aldrich, unless stated otherwise. All solutions were prepared using de-ionized water. For the cleaning of the electrodes, ethanol 96% and 6 M sulfuric acid (H₂SO₄) were used. 5-μL 0.8 U μL⁻¹ Lactate oxidase (LOX, from *Pediococcus* sp., lyophilized powder, ≥20 U mg⁻¹ solid) aliquots were prepared and stored in a freezer at -20 °C. Horseradish peroxidase (HRP, type VI-A, essentially salt-free, lyophilized powder, 250–330 U mg⁻¹ solid) was stored in a refrigerator at 4 °C and used as received. Pyrrole (reagent grade, 98%) was distilled every week and stored in a freezer at -20 °C. A 0.05 M phosphate buffer solution (PB) prepared with potassium phosphate monobasic (KH₂PO₄) was used for all the optimization and electrochemical characterization experiments.

A set of PB solutions containing 2 mM of potassium ferrocyanide ($K_4[Fe(CN)_6]$), 2 mM of ι -lactate (L-(+)-Lactic acid, $\geq 98\%$), 0.2 U LOX and a different HRP concentrations (0.2 U, 2.0 U, 4.0 U, 6.0 U, 8.0 U and 10.0 U), were prepared for the optimization of the LOX:HRP ratio. For the fabrication and optimization of the PPy film, several PB solutions containing different reagents and concentrations were used in order to find the best electro-synthesis conditions. The reagents were 0.1 M lithium perchlorate ($LiClO_4$), 0.1 M potassium chloride (KCl), 0.1 M potassium nitrate (KNO_3), pyrrole in a range of 0.2 M–0.8 M, LOX from 2 U to 6 U and HRP from 40 U to 120 U. For the chronoamperometric ι -lactate detection, a PB solution containing 0.1 M KCl, 2 mM of $K_4[Fe(CN)_6]$ and a ι -lactate concentration from 1×10^{-7} M to 1×10^{-3} M was used. During the interference study, a PB solution with 0.1 M KCl, 2 mM $K_4[Fe(CN)_6]$ and 1×10^{-5} M of the analyzed interfering compounds was prepared. The interferents considered were glycerol, glucose, ethanol, fructose, tartaric acid (all them purchased from Panreac, Spain), acetic acid, ι -Malate (L(-)-Malic acid, $\geq 99\%$), gluconic acid and ascorbic acid (Fluka, Spain).

2.2. Devices and equipment

The thin-film gold electrodes used as transducers were fabricated on silicon substrates at the Instituto de Microelectrónica de Barcelona (IMB-CNM) according to standard microelectronic technology [28]. The chip size was 3×3.5 mm² and included a cell with two electrodes, namely the working electrode with an area of 1.62 mm² and the counter electrode with an area of 2.27 mm² (Fig. S1a, in the Supporting Information (SI)). The chips were wire-bonded on a printed-circuit board (PCB) and packaged using Ebecryl photocurable polymer following a standardized photolithographic process developed at the IMB-CNM [29].

In order to ensure a low consumption of reagents during the polymer film fabrication, a 20 μ L poly(methyl methacrylate) (PMMA) cell was designed and fabricated using a CO₂-laser system (Epilog Mini 24, Epilog Laser, United States). The cell was formed by two 3 mm \times 30 mm \times 20 mm PMMA layers. The bottom one was milled to host the transducer. The top layer was also machined to define the well of the electrochemical cell. Both parts were fixed with screws and an O-ring was used to avoid the fluid leakage. A 2-mm diameter stainless steel wire and a 0.5 mm diameter silver wire were used as counter and pseudo-reference electrode, respectively. A schematic picture of the assembled structure and an image of the actual configuration are showed in Fig. S1B and S1C, respectively, in the SI.

The electrochemical measurements were performed with an Autolab electrochemical workstation (PGSTAT-100 potentiostat – galvanostat, Ecochemie, Utrecht, The Netherlands) controlled using a PC with GPES (General Purpose Electrochemical System) software. During the biosensor characterization, the three-electrode cell was completed with a Ag/AgCl (3.0 M KCl) double junction (Orion 92-02-00, Thermo Fisher Scientific Inc., Beverly, USA) as reference electrode, and the integrated on chip auxiliary electrode as counter. Polystyrene 96-well ELISA plates (Corning Incorporated, United States) and a Thermo Electron Multiskan EX plate reader (Thermo Fisher Scientific) were used for the optimization of the LOX:HRP concentration ratio off chip by recording the absorbance at 405 nm. For the morphological characterization of the polypyrrole films, an atomic force microscope (AFM, Nanoscope IV from Veeco, USA) operated in tapping mode, a scanning electron microscope (SEM, Auriga from Carl Zeiss, Spain) operated at 5–10 kV and a focused ion beam equipment (FIB, Crossbeam 1560 XB from Carl Zeiss) were used.

2.3. LOX:HRP ratio assessment

The optimization of the LOX:HRP ratio was carried out off-chip in solution, using a low-binding ELISA microtiter plate. 100- μ L PB solutions containing 0.1 M KCl, 2 mM of potassium ferrocyanide, 2 mM of ι -lactate and different amounts of the two enzymes were prepared in independent wells. The LOX activity was set to 0.2 U and six concentrations of HRP (0 U, 2 U, 4 U, 6 U, 8 U and 10 U) were tested. Therefore, the LOX:HRP ratios studied were 1:0, 1:10, 1:20, 1:30, 1:40. Triplicates of each solution were analyzed. Solutions were stirred for 45 s and then left for 10 min under quiescent solutions for the enzymatic reactions to take place. Then, absorbance values for each well were recorded at a wavelength of 405 nm. This value was chosen taking into account the potassium ferricyanide absorbance spectrum [30].

2.4. Enzymatic membrane fabrication

Before the electro-synthesis of the PPy layer, the gold electrodes were activated according to previous works by our group [28]. Firstly, they were carefully cleaned using 96% ethanol, H₂SO₄ 6 M and deionized water. Then, an electrochemical activation was performed in 0.1 M KNO₃ solution by applying 20 cyclic voltammetric scans in a potential range from +0.8 V to –2.2 V at 100 mV s⁻¹. The effectiveness of this activation process was verified in a 0.1 M KNO₃ solution containing 1 mM potassium ferrocyanide [31].

The PPy film electrodeposition process was optimized by studying the influence of several chemical parameters of the pre-polymerization solution such as nature of the required counterion (or dopant agent) to carry out the polymer electro-synthesis, the pyrrole concentration and the amount of enzymes on the resulting biosensor response. The nature of the counter-ion has a high relevance in the morphology of the electro-generated PPy layer [32]. During the oxidation of the monomer, the generated radical cations react with other radical cations present in the sample for obtaining polymeric chains and their positive charge are compensated by the counter-ion. Then, three electrolytes ($LiClO_4$, KNO_3 and KCl) were tested in PB containing 0.5 M pyrrole, 4 U of LOX and 80 U of HRP. The counter-ion concentration was fixed to 0.1 M [25]. Then the effect of the monomer concentration and the concentration of both enzymes were sequentially studied in PB solutions. Four pyrrole concentrations from 0.2 M to 0.8 M, and three LOX:HRP concentrations (2:40, 4:80 and 6:120, in U) were selected. The LOX:HRP ratio was set following the results of the absorbance measurements carried out as described above. All measurements were done in triplicate.

Electro-synthesis of all the PPy films was carried out under potentiostatic conditions at a set potential of +0.85 V (vs. Ag pseudo-ref. electrode). In order to ensure the reproducibility of the PPy film thickness, the charge accumulated during the electro-generation was fixed to 500 mC cm⁻² [33]. This charge guarantees an efficient enzyme entrapment inside the polymer matrix. Finally, the biosensors were rinsed with PB in order to remove the enzymes physically adsorbed on the PPy film and stored in PB at 4 °C when not in use.

2.5. Electrochemical measurements

The process associated with the presented ι -lactate biosensor is based on the oxidation of the ι -lactate to pyruvate and hydrogen peroxide (H₂O₂) in presence of LOX (Fig. S2, in the SI). The hydrogen peroxide is then reduced in presence of HRP and the HRP is re-generated thanks to the potassium ferrocyanide mediator, which is

oxidized to ferricyanide. This is again reduced back to ferrocyanide by applying an adequate potential and the recorded faradaic current is stoichiometrically related to the L-lactate concentration in the sample.

The biosensor response was evaluated by chronoamperometry setting an overpotential of +0.075 V (vs. Ag/AgCl, 3 M), at which ferricyanide generated during the bienzymatic process is effectively reduced. The biosensor was calibrated in 10 mL PB solutions containing 2 mM ferrocyanide and L-lactate in a concentration range between 1×10^{-7} M and 1×10^{-3} M. Each L-lactate concentration was measured in triplicate.

The biosensor performance was assessed in terms of sensitivity, linear range and limit of detection to L-lactate. For the optimized biosensor, studies of repeatability, reproducibility and working stability were carried out using three biosensors fabricated under the same experimental conditions.

Selectivity studies were carried out in PB solutions containing 0.1 M KCl, 2 mM ferrocyanide and 1×10^{-5} M concentrations of glucose, glycerol, gluconic acid, L-malate, tartaric acid, fructose, acetic acid, ethanol or ascorbic acid interferences.

The working stability of the developed biosensor was tested by carrying out periodic calibrations in the L-lactate concentration range from 1×10^{-6} M to 1×10^{-4} M. The calibrations were carried out every 2 or 4 days during 52 days. The biosensor was stored in PB at 4 °C between calibrations.

2.6. Analysis of real samples coming from wine malolactic fermentation processes

In order to evaluate the applicability of the developed biosensor to the malolactic fermentation monitoring, the analysis of real wine samples provided by the Catalan Institute of Vineyard and Wine (IRTA-INCAVI) was carried out. Three red wines based on Marcelanne, Petit Verdot and Syrah grape varieties, were tested. These wines were from the 2013 vintage and their vineyards were harvested in the region of Tarragona (Spain). When the alcoholic fermentation was completed, selected bacteria of strain of *Oenococcus oeni* were inoculated to induce the malolactic fermentation. For each wine, samples collected along this fermentation process, with a concentration of L-lactic acid in a range of $0\text{--}2 \times 10^{-2}$ M ($0\text{--}1.7$ g L⁻¹), were analyzed. They were eleven samples for the “Wine 1” (Marcelanne) in an interval of 45 days, 5 samples for the “Wine 2” (Petit Verdot) in an interval of 16 days and 8 samples for the “Wine 3” (Syrah) in an interval of 30 days were analyzed with the proposed biosensor. For measuring, a 1:100 sample dilution was done in order to adjust the L-lactic acid concentration to the linear range of the amperometric biosensor. Results were compared with the standard enzymatic method used by the IRTA-INCAVI. This method is based on the enzymatically catalyzed reaction between the L-lactate and NAD⁺ to produce NADH, whose concentration is stoichiometrically related to the L-lactic acid concentration in the samples. The change of NADH concentration is measured spectrophotometrically at 340 nm [34].

3. Results and discussion

3.1. Study of the LOX:HRP ratio in the cascade reaction

In order to assess the optimal enzyme ratio whose coupled activity provided with the best analytical signal, solutions containing different LOX:HRP proportions were analyzed, as described in the experimental section. As it is shown in Fig. S3 in the SI, the absorbance value increased with the HRP activity and levels off at concentration values above 4 U. This HRP activity is related to the

LOX:HRP ratio of 1:20, which was chosen for the biosensor fabrication.

3.2. Optimization of the polymer electrogeneration conditions

The methodology used for the PPy electrogeneration is critical for the biosensor fabrication. In order to obtain a fast, easy and totally controlled method, potentiostatic conditions were proposed. A preliminary study by cyclic voltammetry was done in order to set the potential. First and second cyclic voltammograms during PPy electrogeneration are showed and compared to the background solution cyclic voltammogram in Fig. S4A (in the SI). The fast increase of current at potentials above +0.60 V (vs Ag pseudo-ref. electrode) in the pyrrole containing solution was related to the monomer oxidation-polymerization. A quasi-reversible signal at a half wave potential of +0.23 V was also recorded, which can be ascribed to the polymer film oxidation and reduction processes. From these results, the selected potential was set at +0.85 V (vs. Ag pseudo-ref. electrode) and applied for 1 min. In order to ensure the reproducibility of the PPy film thickness, the charge accumulated during the PPy formation was fixed to 500 mC cm⁻². An example of the chronoamperometric response obtained under these conditions is shown in Fig. S4B (in the SI).

The influence of three different counter ions (Cl⁻, NO₃⁻ or ClO₄⁻) on the PPy electropolymerization was assessed in terms of the sensitivity values achieved with the corresponding biosensors. Calibration curves were recorded in PB solutions containing 0.1 M KCl and L-lactate in a concentration range from 1×10^{-7} M to 1×10^{-3} M. The highest sensitivity was obtained when the PPy was generated in the presence of Cl⁻ ions ($-95 \times 10^2 \mu\text{A M}^{-1} \text{cm}^{-2}$), while values of $-81 \times 10^2 \mu\text{A M}^{-1} \text{cm}^{-2}$ and $-69 \times 10^2 \mu\text{A M}^{-1} \text{cm}^{-2}$ were obtained with NO₃⁻ and ClO₄⁻ ions respectively. The lower sensitivity obtained with these ions may be related to their oxidative power that could affect the enzyme activity. Indeed, preliminary studies carried out with HRP entrapped in PPy films showed the significant decrease of the enzyme activity when ClO₄⁻ ions were used (data not shown).

The effect of the monomer concentration on the biosensor response was studied in PB solutions containing 4 U LOX, 80 U HRP and 0.1 M KCl. Fig. S5A (in the SI) depicts the biosensor sensitivity related to the monomer concentration. It is shown that the highest sensitivity was achieved for a 0.4 M pyrrole concentration. At higher concentrations of monomer, the sensitivity and the linear range of the biosensor decreased. This could be related to the generation of a thicker polymer layer that negatively affected the diffusion of the redox mediator from the bulk of the solution to reach the electrode solution interface [35]. Also, at concentrations of pyrrole below 0.4 M no response of the biosensor was recorded. This could be related to the formation of a very thin polymer layer, which contained a low amount of enzymes entrapped in its structure.

Finally, the effect of the LOX and HRP concentrations was evaluated in PB containing 0.4 M pyrrole and 0.1 M KCl. Three LOX:HRP concentrations (2:40, 4:80 and 6:120, in U) were tested, keeping the LOX:HRP ratio to 1:20. As can be seen in Fig. S5B (in the SI), the highest sensitivity and widest linear range were achieved for the 4:80 U LOX:HRP concentration. Low enzyme concentrations resulted in a low amount of entrapped enzymes and a poor sensitivity. On the other hand, for high enzyme concentrations, the rate of the polypyrrole film formation decreased drastically (more than 30 min were required to reach the set charge of 500 mC cm⁻²). This could be due to different effects: blocking of the transducer surface by enzyme adsorption which results in the recording of non-faradaic currents and thus of no biosensor response and, lower polymerization rate due to the high

concentration of enzymes in solution.

As a summary, and based on the above described experiments, the optimum conditions for the electrosynthesis of the enzyme containing PPy film on the surface of the thin-film gold transducers were the following: potentiostatic conditions at +0.85 V (vs. Ag pseudo-ref. electrode) for 60 s and 500 mC cm⁻² charge, in a PB solution containing 0.4 M pyrrole, 0.1 M KCl, 4 U of LOX and 80 U of HRP.

3.3. Morphological characterization of the PPy/LOX:HRP film

The thickness of the PPy film plays a significant role in the biosensor response. The thickness and the structure of the polymer matrix are related to the charge accumulated during the electro-generation process and the nature and concentration of the substances involved in it (monomer, enzymes and counter-ion) [36]. A SEM image in Fig. 1A shows the typical surface morphology of these films [37]. The roughness, opening, porosity and globular morphology of the polypyrrole film allow for the adequate enzyme loading and improve the electronic conductivity of the film. Fig. 1B depicts a SEM image of the silicon chip, with the PPy film selectively deposited on the working electrode. An AFM detailed image of the PPy surface shown in Fig. S6A in SI, gives more information about the surface morphology and roughness. A RMS roughness of 0.24 μm was obtained. The thickness of the polypyrrole film, measured by FIB, was between 1.30 and 1.40 μm (Fig. S6B, in SI).

3.4. Evaluation of the biosensor performance

Once the fabrication of the biosensor was optimized, chronoamperometric measurements were carried out at +0.075 V (vs Ag/AgCl) in PB containing 0.1 M KCl, 2 mM potassium ferrocyanide and increasing concentrations of L-lactate, in a range from 1 × 10⁻⁷ M to 1 × 10⁻³ M. The biosensor responses are shown in Fig. 2A. As expected a more negative current density for increasing L-lactate concentrations, was obtained. The current recorded in all cases increased and started to level off at 100 s time after initiated the measurement. This current was recorded for 200 s and the mean current value of the last 60 s (140–200 s) was used as the analytical signal. From this, it can be said that the sensor response was 100 s and the overall assay time is set to 200 s. The calibration curve is shown in Fig. 2B. A linear response was observed in a concentration range from 1 × 10⁻⁶ M to 1 × 10⁻⁴ M of L-lactate with a sensitivity of -135 ± 6 × 10² μA M⁻¹ cm⁻² (r = 0.998). A limit of detection (LOD) of 5 ± 0.2 × 10⁻⁷ M, calculated using the 3σ IUPAC criterion was obtained. For L-lactate concentration above

1 × 10⁻⁴ M, the enzymatic biosensor is saturated, according to the normal behavior of a Michaelis–Menten enzyme kinetics in biosensors. Regarding the reproducibility of the fabrication process, three different biosensors were calibrated on the same day, obtaining a relative standard deviation (R.S.D.) of the sensitivity lower than 4%.

The biosensor response to possible interferences was assessed. For that, glycerol, glucose, gluconic acid, fructose, acetic acid, citric acid, ethanol, L-malate, tartaric acid and ascorbic acid were considered. The corresponding chronoamperometric responses are shown in Fig. 3. Only a significant signal was obtained in the presence of ascorbic acid, due to its electrochemical oxidation at the measurement potential of +0.075 V [38]. However, red wines do not contain ascorbic acid [39] and it is not produced during the malolactic fermentation. These results demonstrate the high selectivity of the developed biosensor for the L-lactate determination.

The biosensor working stability with time was studied during 52 days. When not in use, the biosensor was stored in the PB solution at 4 °C. As can be seen in Fig. 4, a decrease of the sensitivity around 5% took place during the first five days, probably related to the loss of the enzyme attached by physical absorption on the PPy film or the more weakly entrapped in the PPy film (enzyme molecules closer to the outer surface of the polymer). After this time, the biosensor response remained stable and kept over 90% of the initial sensitivity value for 42 days. From the day 45, there was a sudden decrease of the response, which could be attributed to the denaturation of the immobilized enzymes. However, this decrease represented only around 20% of the initial sensitivity after 52 days of study.

3.5. Application of the biosensor in real samples from malolactic fermentation of wines

The proposed L-lactate biosensor was applied to the monitoring of the malolactic fermentation in three different red wines. Samples collected different days during the fermentation process were provided by the IRTA-INCAVI. The 1:100 diluted wine samples were analyzed in triplicate with the biosensor. In parallel, the same samples were analyzed by the IRTA-INCAVI with the colorimetric standard method. The results from both methods were compared by plotting the L-lactic acid concentration (in g L⁻¹) versus the day of the malolactic fermentation process. As shown in Fig. 5, there is an excellent agreement between the two values, with absolute errors below 0.09 g L⁻¹ in all the cases. The evolution of the lactic acid during the fermentation processes was as expected. There was

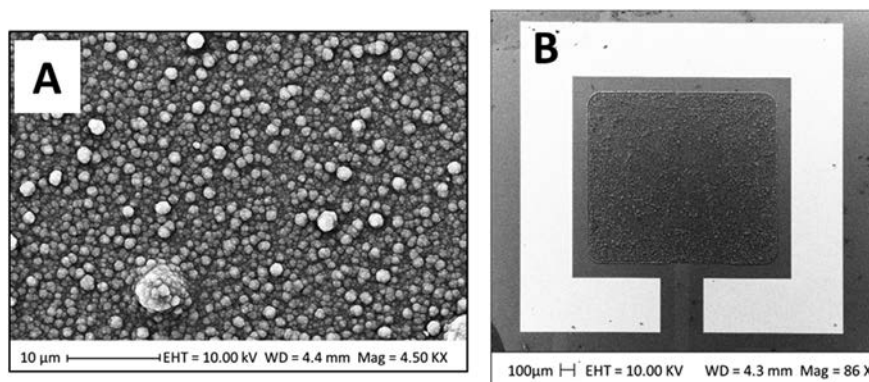


Fig. 1. SEM images of, (A) the PPy/LOX:HRP film; (B) the silicon chip showing the polymer film selectively deposited on the working electrode surface.

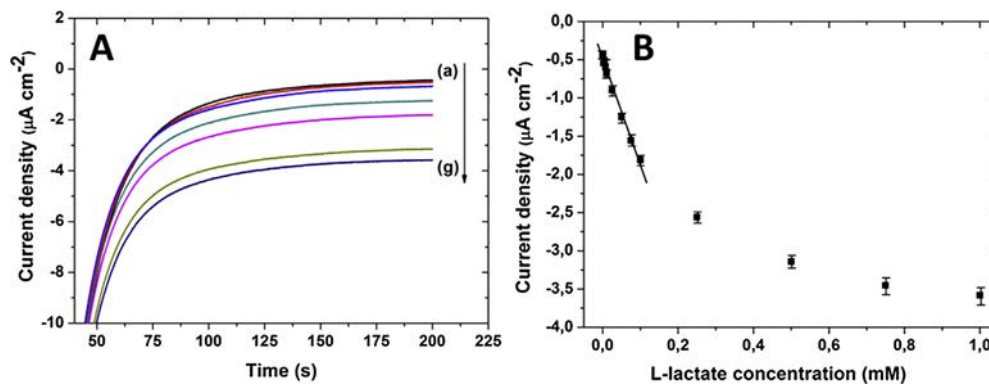


Fig. 2. A) Chronoamperometric response of the PPY/LOX:HRP biosensor for L-lactate concentrations from 5×10^{-7} M (a) to 1×10^{-3} M (g). B) Biosensor calibration curve. Each point represents the mean current value of three replicates recorded consecutively with the same biosensor, with the error bars being the corresponding standard deviation.

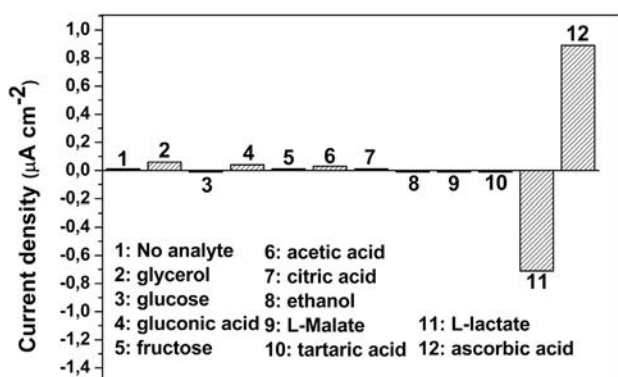


Fig. 3. Current density response of the biosensor in solutions containing interferences. All them are in a concentration of 1×10^{-5} M and are compared to the signal recorded in the background electrolyte (no analyte).

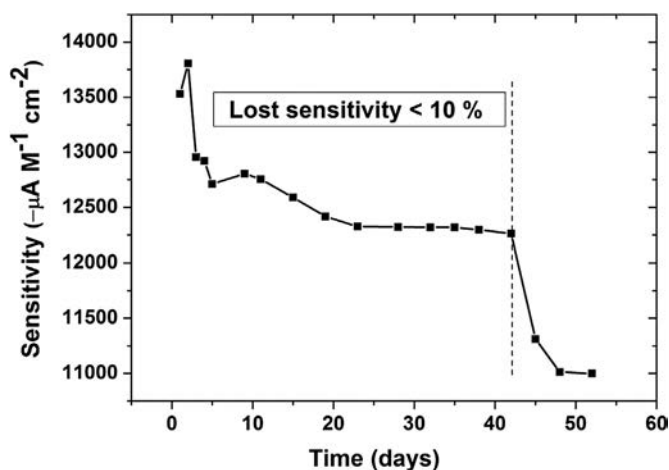


Fig. 4. Variation of the biosensor sensitivity along 50 days.

an initial slow formation, followed by an exponential increase and a final stabilization of the L-lactic acid concentration, which indicates the end of the malolactic fermentation. This behavior was particularly clear for “Wine 3”. However, for “Wine 1” and “Wine 2”, the concentration of L-lactic acid was still increasing, which means that the process of transformation of malic acid to L-lactic acid was still in progress.

During its application, the biosensor was calibrated four times within a range of 1×10^{-6} M to 5×10^{-4} M of L-lactate. These calibrations were carried out at the beginning, between the first and the second set of wines (30 analyses), between the second and the third set of wines (15 analyses) and at the end of the experiment (24 analyses). The results showed a stable sensor response, which retained over 90% of the initial value after completing all the analyses (see Table 1).

3.6. Comparison with other L-lactate electrochemical biosensors

The developed biosensor was compared with other electrochemical biosensors for L-lactate determination reported in the literature. The main characteristics of these devices are summarized in Table 2. Regarding the immobilization method, the proposed biosensor is the only one constructed by simultaneously entrapping both LOX and HRP in a PPy film, which simplifies the fabrication of the device. Also, biosensor production time is very short and reagent consumption is low.

The approach presented in this work clearly outperforms other devices in terms of operational stability and in terms of biosensor performance. It is worth mentioning that even though some of them show the required sensitivity and linear range for the measurement of L-lactic acid during the malolactic fermentation, all of them lack the long-term stability required to monitor this process, which usually takes place for up to 40 days in most wines. The proposed PPY/LOX:HRP biosensor, with a lifetime of 42 days is the only one that could be applied to this monitoring process.

It should also be highlighted that even though some of those biosensor devices have been applied to the L-lactic acid determination in real samples, such as beers, wines or milk, the long-term stability of the proposed biosensor enable the real-time of the malolactic fermentation using the same biosensor during all the process.

4. Conclusions

A bienzymatic amperometric biosensor based on the co-immobilization of LOX and HRP entrapped in an electropolymerized PPy film was developed and characterized for the L-lactic acid analysis in wine samples collected during the malolactic fermentation. The biosensor fabrication was optimized in terms of electrogeneration conditions. The analytical performance was thoroughly assessed and demonstrated that the developed

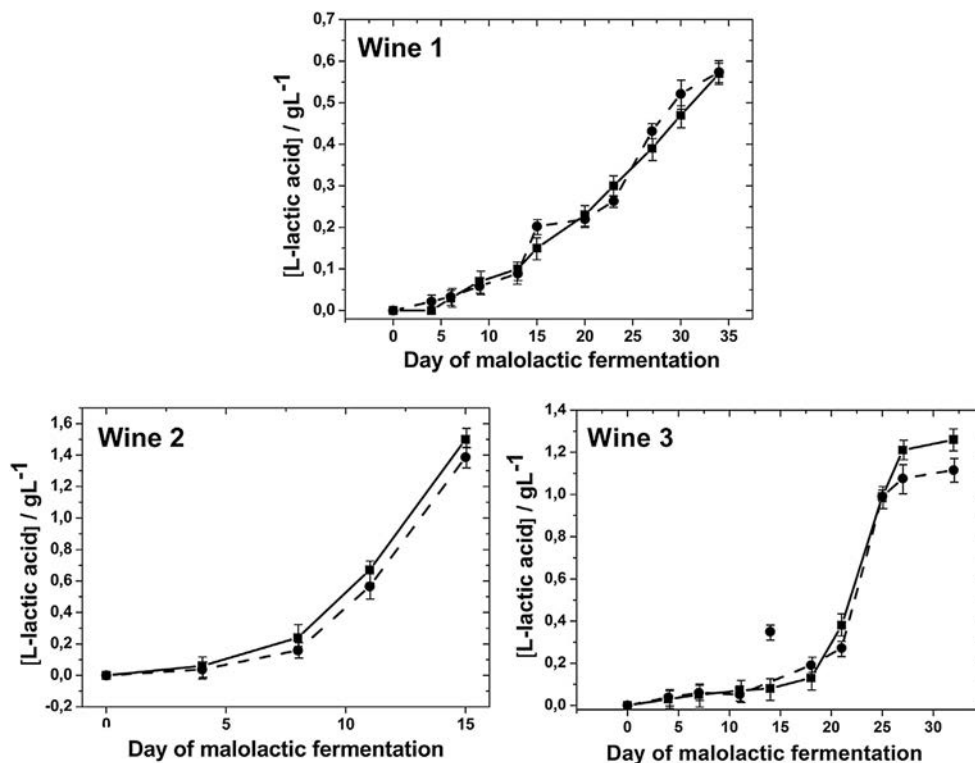


Fig. 5. Analysis of wine samples collected during the malolactic fermentation process for three red wines. Dashed lines and filled circles show the values of L-lactic acid obtained with the colorimetric standard method and solid lines and squares, those measured with the proposed PPY/LOX:HRP biosensor. In the case of the biosensor, the standard deviation values of three replicates are represented as error bars in the plot. In the case of the colorimetric method, the error bars represent the uncertainty at 95%.

Table 1

Data of calibration curves for L-lactate carried out during the analysis of the malolactic fermentation process of the three wines.

Calibration	Sensitivity ($\mu\text{A M}^{-1} \text{cm}^{-2}$)	R^2
1st	-13465	0.995
2nd	-12782	0.993
3rd	-12998	0.994
4th	-14064	0.993

biosensor presented a high sensitivity, a low LOD and a wide linear range, together with an excellent selectivity. Besides, the lifetime of the developed biosensor of more than 40 days is of key importance

for monitoring L-lactate in a real scenario.

In order to demonstrate the potential application in real samples, the monitoring of the L-lactic acid concentration during the malolactic fermentation in red wines was carried out and results were in excellent agreement with those obtained by the standard colorimetric method.

Taking into account the simplicity of the biosensor fabrication, its compatibility with the microelectronic technology, the long working stability and the characteristics of the response, the developed PPY/LOX:HRP biosensor for L-lactate acid determination represents a competitive and feasible approach for the online monitoring of malolactic fermentation in wineries.

Table 2

L-lactate electrochemical biosensors described in the literature.

Enzymes	Electrode	Mediator	Immobilization	Sensitivity	Linear range (M)	LOD (M)	Stability	Samples	Reference
LOX/ HRP	Carbon	Ferrocene	MWCNT/PS membrane	$116880 \mu\text{A M}^{-1} \text{cm}^{-2}$	1.1×10^{-6} -5.6×10^{-5}	5.6×10^{-7}	40% after 2 weeks	Wine Beer	[17]
LOX/ HRP	Carbon		Screen printed	$0.84 \mu\text{A M}^{-1} \text{L}$ (flow system)	1×10^{-5} - 2×10^{-4}	1×10^{-6}	90% after 50 injections	Yoghurt Milk	[16]
LOX/ HRP	Gold disk	TTF	MPA-SAM	$2711 \mu\text{A M}^{-1}$	4.2×10^{-7} -2×10^{-5}	4.2×10^{-7}	91% after 5 days	Synthetic wines	[15]
LDH	Glassy carbon		MWCNT-CHIT	$8300 \mu\text{A M}^{-1} \text{cm}^{-2}$	5×10^{-6} - 1.2×10^{-4}	7.6×10^{-7}	65% after 7 days		[40]
LOD/ LDH	ITO		PANI physical absorption	$0.038 \mu\text{A M}^{-1}$	1×10^{-4} - 1×10^{-3}	5×10^{-5}	3 weeks		[41]
LOD	Gold	PVI-Os	CNT-CHIT	$0.0197 \mu\text{A M}^{-1} \text{cm}^{-2}$	Up to 8×10^{-4}	5×10^{-6}			[42]
LOX/ HRP	Gold	Ferrocyanide	PPy entrapment	$14100 \mu\text{A M}^{-1} \text{cm}^{-2}$	1×10^{-6} - 1×10^{-4}	5×10^{-7}	90% after 42 days	Red wines	This work

* ITO: Indium tin oxide; TTF: Tetrathiafulvalene; PVI-Os: Polyvinylimidazole-Os; MWCNT: Multiwalled carbon nanotubes; PS: Polystyrene; MPA: 3-mercaptopropionic acid; SAM: Self-assembled monolayer; CNT: Carbon nanotubes; CHIT: Chitosan.

Acknowledgments

We acknowledge funding from the Spanish R & D National Program (MINECO, Project TEC2011-29045-C04-01 and 04). P. G.-G. is grateful to MINECO, Spain, for the financial support through a research studentship of the FPI Program. We also acknowledge the group of Dr. Iluminada Gallardo (Chemistry Department, Universitat Autònoma de Barcelona, Spain) for the support during the polymer distillation. The technical assistance of J.M. Ríos-Gallardo is highly appreciated.

Appendix A. Supplementary data

Supplementary data related to this article can be found at <http://dx.doi.org/10.1016/j.aca.2015.11.032>.

References

- [1] B. Sjodin, I. Jacobs, J. Svedenhag, Changes in onset of blood lactate accumulation (OBLA) and muscle enzymes after training at OBLA, *Eur. J. Appl. Physiol. Occup. Physiol.* 49 (1982) 45–57.
- [2] F. Valenza, G. Aletti, T. Fossali, G. Chevillard, F. Sacconi, M. Irace, L. Gattinoni, Lactate as a marker of energy failure in critically ill patients: hypothesis, *Crit. Care* 9 (2005) 588–593.
- [3] M.E. Stiles, Biopreservation by lactic acid bacteria, *Ant. Van Leeuwenhoek Int. J. Gen. Mol. Microbiol.* 70 (1996) 331–345.
- [4] E. Caplice, G.F. Fitzgerald, Food fermentations: role of microorganisms in food production and preservation, *Int. J. Food Microbiol.* 50 (1999) 131–149.
- [5] A.G. Larsen, F.K. Vogensen, J. Josephsen, Antimicrobial activity of lactic-acid bacteria isolated from sour doughs. Purification and characterization of bavaricin-a, a bacteriocin produced by *Lactobacillus-bavaricus* M1401, *J. Appl. Bacteriol.* 75 (1993) 113–122.
- [6] A. Lonvaud-Funel, Biogenic amines in wines: role of lactic acid bacteria, *Fems Microbiol. Lett.* 199 (2001) 9–13.
- [7] A. Lonvaud-Funel, Lactic acid bacteria in the quality improvement and depreciation of wine, *Ant. Van Leeuwenhoek Int. J. Gen. Mol. Microbiol.* 76 (1999) 317–331.
- [8] E.F. Lopez, E.F. Gomez, Simultaneous determination of the major organic acids, sugars, glycerol, and ethanol by HPLC in grape musts and white wines, *J. Chromatogr. Sci.* 34 (1996) 254–257.
- [9] S.B. Barker, W.H. Summerson, The colorimetric determination of lactic acid in biological material, *J. Biol. Chem.* 138 (1941) 535–554.
- [10] L. Rassaei, W. Olthuis, S. Tsujimura, E.J.R. Sudholter, A. van den Berg, Lactate biosensors: current status and outlook, *Anal. Bioanal. Chem.* 406 (2014) 123–137.
- [11] D.W. Kimmel, G. LeBlanc, M.E. Meschievitz, D.E. Cliffl, Electrochemical sensors and biosensors, *Anal. Chem.* 84 (2012) 685–707.
- [12] S.W. May, Applications of oxidoreductases, *Curr. Opin. Biotechnol.* 10 (1999) 370–375.
- [13] A. Silber, C. Brauchle, N. Hampp, Dehydrogenase-based thick-film biosensors for lactate and malate, *Sens. Actuators B Chem.* 18 (1994) 235–239.
- [14] E.B. Makovos, C.C. Liu, Measurements of lactate concentration using lactate oxidase and an electrochemical oxygen sensor, *Biotechnol. Bioeng.* 27 (1985) 167–170.
- [15] M. Gamella, S. Campuzano, F. Conzuelo, J.A. Curiel, R. Muñoz, A.J. Reviejo, J.M. Pingarron, Integrated multienzyme electrochemical biosensors for monitoring malolactic fermentation in wines, *Talanta* 81 (2010) 925–933.
- [16] F. Ghamouss, S. Ledru, N. Ruille, F. Lantier, M. Boujtitia, Bulk-modified modified screen-printing carbon electrodes with both lactate oxidase (LOD) and horseradish peroxidase (HRP) for the determination of L-lactate in flow injection analysis mode, *Anal. Chim. Acta* 570 (2006) 158–164.
- [17] S. Perez, E. Fabregas, Amperometric bienzymatic biosensor for L-lactate analysis in wine and beer samples, *Analyst* 137 (2012) 3854–3861.
- [18] A. Chaubey, B.D. Malhotra, Mediated biosensors, *Biosens. Bioelectron.* 17 (2002) 441–456.
- [19] A.M. Herrero, T. Requena, A.J. Reviejo, J.M. Pingarron, Determination of L-lactic acid in yoghurt by a bienzyme amperometric graphite-Teflon composite biosensor, *Eur. Food Res. Technol.* 219 (2004) 556–559.
- [20] E.I. Iwuoha, A. Rock, M.R. Smyth, Amperometric L-lactate biosensors: 1. Lactic acid sensing electrode containing lactate oxidase in a composite poly-L-lysine matrix, *Electroanalysis* 11 (1999) 367–373.
- [21] M. Aizawa, S. Yabuki, Electrochemical characteristics of an enzyme-immobilised conducting polymer membrane, in: *51st Annual Meeting Chemical Society*, 1985, p. 6.
- [22] Y.M. Uang, T.C. Chou, Fabrication of glucose oxidase/polypyrrole biosensor by galvanostatic method in various pH aqueous solutions, *Biosens. Bioelectron.* 19 (2003) 141–147.
- [23] H.Y. Wang, S.L. Mu, Bioelectrochemical characteristics of cholesterol oxidase immobilized in a polyaniline film, *Sens. Actuators B Chem.* 56 (1999) 22–30.
- [24] M.A. Rahman, P. Kumar, D.S. Park, Y.B. Shim, Electrochemical sensors based on organic conjugated polymers, *Sensors* 8 (2008) 118–141.
- [25] S.S. Razola, B.L. Ruiz, N.M. Diez, H.B. Mark, J.M. Kauffmann, Hydrogen peroxide sensitive amperometric biosensor based on horseradish peroxidase entrapped in a polypyrrole electrode, *Biosens. Bioelectron.* 17 (2002) 921–928.
- [26] A. Chaubey, K.K. Pande, V.S. Singh, B.D. Malhotra, Co-immobilization of lactate oxidase and lactate dehydrogenase on conducting polyaniline films, *Anal. Chim. Acta* 407 (2000) 97–103.
- [27] V. Casimiri, C. Burstein, Co-immobilized L-lactate oxidase and L-lactate dehydrogenase on a film mounted on oxygen electrode for highly sensitive L-lactate determination, *Biosens. Bioelectron.* 11 (1996) 783–789.
- [28] J. Orozco, G. Suarez, C. Fernandez-Sanchez, C. McNeil, C. Jimenez-Jorquera, Characterization of ultramicroelectrode arrays combining electrochemical techniques and optical microscopy imaging, *Electrochim. Acta* 53 (2007) 729–736.
- [29] A. Bratov, J. Munoz, C. Dominguez, J. Bartroli, Photocurable polymers applied as encapsulating materials for ISFET production, *Sens. Actuators B Chem.* 25 (1995) 823–825.
- [30] M.H. Chakrabarti, E.P.L. Roberts, Analysis of mixtures of ferrocyanide and ferricyanide using UV-visible spectroscopy for characterisation of a novel redox flow battery, *J. Chem. Soc. Pak.* 30 (2008) 817–823.
- [31] J. Wang, Study of the Electrode Reactions, New York, 2000.
- [32] X. Wang, P. Sjöberg-Eerola, J.-E. Eriksson, J. Bobacka, M. Bergelin, The effect of counter ions and substrate material on the growth and morphology of poly(3,4-ethylenedioxythiophene) films: towards the application of enzyme electrode construction in biofuel cells, *Synth. Met.* 160 (2010) 1373–1381.
- [33] L. Zhu, R. Yang, J. Zhai, C. Tian, Bienzymatic glucose biosensor based on co-immobilization of peroxidase and glucose oxidase on a carbon nanotubes electrode, *Biosens. Bioelectron.* 23 (2007) 528–535.
- [34] H. Möllering, *Methods of Enzymatic Analysis*, Verlag Chemie, France, 1985, pp. 39–47.
- [35] J.H. Cho, M.C. Shin, H.S. Kim, Electrochemical adsorption of glucose oxidase onto polypyrrole film for the construction of a glucose biosensor, *Sens. Actuators B Chem.* 30 (1996) 137–141.
- [36] T. Silk, Q. Hong, J. Tamm, R.G. Compton, AFM studies of polypyrrole film surface morphology – I. The influence of film thickness and dopant nature, *Synth. Met.* 93 (1998) 59–64.
- [37] I.L. Lehr, S.B. Saidman, Corrosion protection of iron by polypyrrole coatings electrosynthesised from a surfactant solution, *Corros. Sci.* 49 (2007) 2210–2225.
- [38] J.S. Fruton, Oxidation-reduction potentials of ascorbic acid, *J. Biol. Chem.* 105 (1934) 79–85.
- [39] P. Ribéreau-Gayon, D. Dubordieu, B. Donèche, A. Lonvaud, in: *The Microbiology of Wine and Vinifications*, John Wiley & Sons, L, USA, 2006, p. 236.
- [40] C.A. Marquette, A. Degiuli, L.J. Blum, Electrochemiluminescent biosensors array for the concomitant detection of choline, glucose, glutamate, lactate, lysine and urate, *Biosens. Bioelectron.* 19 (2003) 433–439.
- [41] Y.-C. Tsai, S.-Y. Chen, H.-W. Liaw, Immobilization of lactate dehydrogenase within multiwalled carbon nanotube-chitosan anhanocompo site for application to lactate biosensors, *Sens. Actuators B Chem.* 125 (2007) 474–481.
- [42] X.Q. Cui, C.M. Li, J.F. Zang, S.C. Yu, Highly sensitive lactate biosensor by engineering chitosan/PVI-Os/CNT/LOD network nanocomposite, *Biosens. Bioelectron.* 22 (2007) 3288–3292.

Article

Portable Electronic Tongue Based on Microsensors for the Analysis of Cava Wines

Pablo Giménez-Gómez ¹, Roger Escudé-Pujol ¹, Fina Capdevila ², Anna Puig-Pujol ², Cecilia Jiménez-Jorquera ¹ and Manuel Gutiérrez-Capitán ^{1,*}

¹ Instituto de Microelectrónica de Barcelona (IMB-CNM), CSIC Campus UAB, 08193 Cerdanyola del Vallès, Spain; pablo.gimenez@csic.es (P.G.-G.); roger.escude@csic.es (R.E.-P.); cecilia.jimenez@csic.es (C.J.-J.)

² Institut Català de la Vinya i el Vi (IRTA-INCAVI), Plaça Àgora 2, 08720 Vilafranca del Penedès, Spain; finacapdevila@gmail.com (F.C.); apuigpujol@gencat.cat (A.P.-P.)

* Correspondence: Manuel.Gutierrez@csic.es; Tel.: +34-93-594-7700; Fax: +34-93-580-0267

Academic Editors: Takeshi Onodera and Kiyoshi Toko

Received: 30 August 2016; Accepted: 24 October 2016; Published: 27 October 2016

Abstract: Cava is a quality sparkling wine produced in Spain. As a product with a designation of origin, Cava wine has to meet certain quality requirements throughout its production process; therefore, the analysis of several parameters is of great interest. In this work, a portable electronic tongue for the analysis of Cava wine is described. The system is comprised of compact and low-power-consumption electronic equipment and an array of microsensors formed by six ion-selective field effect transistors sensitive to pH, Na⁺, K⁺, Ca²⁺, Cl⁻, and CO₃²⁻, one conductivity sensor, one redox potential sensor, and two amperometric gold microelectrodes. This system, combined with chemometric tools, has been applied to the analysis of 78 Cava wine samples. Results demonstrate that the electronic tongue is able to classify the samples according to the aging time, with a percentage of correct prediction between 80% and 96%, by using linear discriminant analysis, as well as to quantify the total acidity, pH, volumetric alcoholic degree, potassium, conductivity, glycerol, and methanol parameters, with mean relative errors between 2.3% and 6.0%, by using partial least squares regressions.

Keywords: portable equipment; electrochemical microsensors; electronic tongue; multiparametric analysis; Cava wine samples

1. Introduction

Multiparametric analysis is a key issue for quality assurance in many different areas of interest, such as the industrial processes [1], the food industry [2], clinical diagnostics [3], or environmental monitoring [4]. In order to obtain real-time information about the composition of a sample, automatic and portable systems for decentralized analysis are highly valuable. A promising alternative is the application of electronic tongues, which generate multivariate analytical data, enlarging the number of parameters that can be determined simultaneously [5]. An electronic tongue entails the use of an array of sensors with partially-selective responses, plus a multivariate chemometric tool, and permits qualitative and/or quantitative applications in liquid media [6,7]. Among the different chemical sensors, microelectrodes fabricated with semiconductor technology present some advantages that make them particularly suitable for integration into arrays for on-site measurements, such as the miniaturization, robustness, high reproducibility, low output impedance, mass fabrication, and ease of integration with the electronic circuitry [8,9].

The applicability of electronic tongues has been especially relevant in food quality control and safety, where the increasing demand on a sustainable and high-quality production has promoted the development of more automated and precise analytical systems for monitoring [10,11]. Wine is one of

the most used beverages to test the viability of these systems [12]. Cava is a quality sparkling wine protected under a designation of origin (D.O.) in Spain, which is produced mostly in the Penedès region. Unlike most wines, sparkling wines are characterized by the presence of CO₂ in solution, which is produced by a second alcoholic fermentation, and a biological aging in contact with lees under anaerobic conditions for at least nine months in the bottle [13]. It is significant to mention the complexity of the Cava wine as a sample, given the drastic changes in the chemical composition (CO₂, sugars, ethanol, pH, amino acids), physical properties (turbidity, density, color), and varietal aromas produced by these fermentation and aging processes [14]. Only one research group from the Universitat Autònoma de Barcelona has approached the analysis of Cava with electronic tongue systems. This group was able to classify Cava wine samples according to the content of sugar added [15] and to the aging time in bottle [16], as well as to determine the sugar and the total dry extract by using a voltammetric electronic tongue based on modified graphite-epoxy electrodes. In another work, the use of enzyme-modified sensors in the array allowed the quantification of different phenolic indices in Rosé Cava wines [17]. However, these systems were limited to the determination of just a few parameters, so it is necessary to develop more versatile and innovative tools for the analysis of Cava wine.

Most electronic tongue systems reported until now for food quality are laboratory versions [10,11], partly due to the use of large-sized sensors and data collection equipment. On one hand, the miniaturization of the electronic tongue has been approached by using individual wire electrodes [18] or developing integrated arrays of sensors. Usually, these arrays have a planar configuration and include layers of conductive inks or pastes sequentially deposited onto insulating and chemically-inert substrates. Depending on the thickness of these layers, integrated arrays of sensors have been fabricated by using screen-printed methods (thick-film technology) and applied as portable devices for monitoring drinking waters [19] and beer discrimination [20]. Additionally, thin-film technologies have been also used to fabricate integrated multisensor systems combined with flow injection analysis [9] and portable taste sensors [21], both by using standard photolithographic techniques.

On the other hand, an alternative to obtaining versatile portable instruments for multiparametric applications at a minimum cost is the use of commercial integrated circuits (IC), such as power supplies, analog-to-digital converters, and microcontrollers [22]. The reduced size of these systems implies reduced fabrication and maintenance costs, as well as lower power consumption. In a previous paper [23], we developed and tested a compact multisensor meter, whose electronics were fabricated according to microsensor requirements and took into account the minimum energy consumption and its portability. In this work, we have fabricated a multi-ion-selective field effect transistor (ISFET) meter able to simultaneously measure up to six ISFETs, with the same requirements of portability and low power consumption. The two compact meters have been used together to perform the multiparametric analysis with an array of microsensors fabricated with microelectronic technology. This combination supposes an advance to achieve a portable electronic tongue system. The array of microsensors was formed by one conductivity sensor, one redox potential (ORP) sensor, and two amperometric gold microelectrodes, which were measured with the multisensor meter, together with six ISFETs sensitive to pH, Na⁺, K⁺, Ca²⁺, Cl⁻, and CO₃²⁻, measured with the multi-ISFET meter. For the data treatment, two different multivariate methods were used: linear discriminant analysis (LDA) and partial least squares (PLS). A set of 78 Cava wine samples was analyzed with the electronic tongue. The system demonstrated its reliability for Cava wines according to the aging time, as well as the quantification of some chemical parameters with high accuracy.

2. Materials and Methods

2.1. Reagents and Solutions

All reagents used were of high purity, analytical grade or equivalent. All solutions were prepared with de-ionized water. For ISFET calibration, stock solutions with ionic salts with concentrations of

10^{-4} , 10^{-2} , and 1.0 M were prepared. In the case of those sensitive to cations (Na^+ , K^+ , and Ca^{2+}), the corresponding chloride salts were considered. For the Cl^- and CO_3^{2-} ions, solutions of NaCl and NaHCO_3 , respectively, were prepared. For the pH ISFET calibration, a universal buffer solution containing 0.04 M boric acid, 0.04 M acetic acid, 0.04 M phosphoric acid, and 0.1 M KNO_3 as a background was prepared. A solution containing 0.1 M KNO_3 was used to activate the amperometric gold electrodes. In order to calibrate the conductivity sensor, two different standard solutions from Crison (Barcelona, Spain), with nominal values of 1413 $\mu\text{S}/\text{cm}$ and 147 $\mu\text{S}/\text{cm}$, were utilized. Two standard redox solutions from Panreac (Barcelona, Spain), with values of 468 mV and 220 mV (at 25 °C vs. Ag/AgCl), were used to test the ORP sensor. For the ISFET measurements, a reference solution containing an average concentration of the main species present in wine was prepared. The composition of this solution has been reported elsewhere [24].

2.2. Cava Wine Samples

A total set of 78 Cava wine samples from different producers were analyzed. All samples were produced and bottled in the Catalonia region and they are all commercially available. Samples were selected according to their type, taking into account their vintage time as categorized by the Regulatory Board of Cava [25]: 20 “Young” samples (9–15 months), 25 “Reserva” samples (15–30 months), and 16 “Gran Reserva” samples (more than 30 months). Moreover, a set of 17 “Rosé” Cava samples were included in this study. These samples were mainly from the Penedès region (Spain). White Cava wines were obtained mainly from Macabeu, Xarel·lo, and Parellada grape varieties, although Chardonnay and/or Subirat parent may also be used, that is, the five different white grape varieties authorized by Regulatory Board of Cava [25]. For Rosé cava wines, Trepát, Monastrell, Grenache Noir, and/or Pinot Noir might be used.

Volumetric alcoholic degree (VAD), total acidity, pH, potassium ion, conductivity, glycerol, and methanol were analyzed with reference/standard methods [26,27] in all 78 Cava samples at the Catalan Institute of Vine and Wine (IRTA-INCAVI) in order to compare and evaluate the results of the developed electronic tongue.

2.3. Sensors and Devices Used

A set of ISFET sensors were fabricated using standard microelectronic technology [28]. One ISFET was used for measuring pH and the rest were modified with polymeric membranes sensitive to Na^+ , K^+ , Ca^{2+} , Cl^- , and CO_3^{2-} ions. Polymeric membranes were based on photocurable polymers with commercial ionophores from Fluka (Buchs, Switzerland). The ionophores used in each case were: 4-tert-butylcalix [4] arenetetraacetic acid tetraethyl ester (Ionophore X) for Na^+ , valinomycin (Ionophore I) for K^+ , N,N,N',N'-tetracyclohexyl-3-oxapentanediamide (Ionophore II, ETH 129) for Ca^{2+} , tridodecylmethylammonium chloride for Cl^- , and 4-butyl- α,α,α -trifluoroacetophenone (Ionophore IV) for CO_3^{2-} . All of these ionophores are selective to the principal ion, but are not specific and they present a certain degree of cross-response to other ions in solution. Membrane composition and preparation has been presented elsewhere [29–32]. An Orion 90-02-00 double junction Ag/AgCl reference electrode (Thermo Electron, Waltham, MA, USA) with 0.1 M CH_3COOLi solution in its outer chamber was employed for all of the potentiometric measurements.

Sensors based on a platinum four-electrode configuration were employed as the conductivity sensors and ORP sensors. Their fabrication and characterization are reported elsewhere [33]. Finally, two conventional thin-film gold electrodes, also fabricated according to standard photolithographic techniques, were employed to perform chronoamperometric measurements. The amperometric cell contained the working electrode, a platinum electrode as a counter electrode (Radiometer, Lyon, France), and an $\text{Ag}/\text{AgCl}/10\%$ (w/v) KNO_3 reference electrode (Metrohm 0726 100, Herisau, Switzerland).

All of these microsensors present a long-term stability above seven months with discrete calibrations in aqueous solutions [29–33]. However, their lifetimes are, in fact, limited by their use,

so that in a continuous monitoring application, for example in Cava wine production, their response characteristics (sensitivity, selectivity) would degrade within 2–3 months. This effect is noticed especially in ISFET sensors due to the leaching of the ionophores out of the polymeric membrane [29].

2.4. Measurement Equipment

The measurements with the conductivity sensor, the ORP sensor, and the two amperometric gold electrodes were performed with a multisen-someter constructed through the MATLAB software. A detailed explanation of the electronic designs, software for data collection, and global performance of this equipment is presented in [23].

For the measurements with the six ISFETs, the analog electronic was fabricated. The circuit board was designed with the Agilent PCB Designer PCB Design Tools (Cadence Design Systems, Berkeley, CA, USA). The board was fabricated using a 2-layer FR4 single in-plane layout (LPC1114) machine (LPC1114 PCB Cards, Germany). The size of the system is 150 mm × 80 mm. The PCB was assembled by the PCB manufacturer. The power supply area, digital part, and digital ISFET analog part, the connection between the digital and analog parts were digital and analog ICs. The analog part of the circuit was designed to obtain the real-time continuous measurement of the six ISFETs, such that the real-time measurement of the six ISFETs, ISFET channel current was measured by the ISFET gate current. The current was measured by applying the 90 mV and reversing the ISFET gate potential (and the ISFET gate potential (analyte) concentration is related with the analyte concentration in solution.

The digital interface permitted the establishment of communication between the user and the analog electronic part. The main IC was the ADUC88BSZ6256 microcontroller (Analog Devices, Norwood, MA, USA). This chip is composed of peripheral processor (CPU), digital and analog parts, analog outputs and standard communication protocols of the CMOS (EMPIRES) (EMPIRES) embedded processor (EMPIRES) which was also executed by the μ S. The code was programmed in the IC through a programming kit 4.0V (Keil 4.02, Keil, Electronics, Germany). The finalization of the result of the configuration of the measurement parameters were accomplished by using the graphical user interface (GUI) of the LabVIEW (National Instruments, Austin, TX, USA). This is a universal, and intuitive, quick and intuitive software program which provides a rich working environment to the user.

A scheme of the whole system for the portable laptop PC with the software, software and the measurement with the different sensors shown in Figure 1.

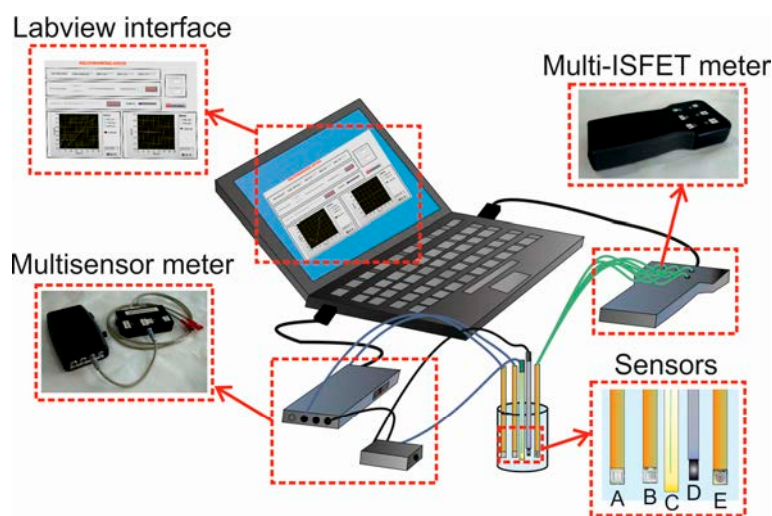


Figure 1. Scheme of the whole measurement system. In detail: (A) conductivity or ORP sensor; (B) amperometric sensor; (C) reference electrode; (D) counter electrode; and (E) ISFET.

2.5. Characterization of Sensors and Electronics

For the evaluation of the new multi-ISFET meter, the response characteristics of ISFETs sensitive to the different ions considered were studied. The response characteristics were evaluated

2.5. Characterization of Sensors and Electronics

For the evaluation of the new multi-ISFET meter, the response characteristics of ISFETs sensitive to the different ions considered were studied. The response characteristics were evaluated by calibration in response to the principal ion. These calibration curves were obtained by means of the method of the analyte addition: the variation of potential originated by the addition of accumulated microvolumes of stock ion solutions (10^{-4} , 10^{-2} , and 1.0 M) in 25 mL of de-ionized water was measured and registered by the new equipment. In the case of the pH ISFET, microvolumes of 1 M NaOH solution were added to a 50 mL of universal buffer solution to change pH from 2 to 12. Then, the potential (in mV) was plotted versus the logarithm of the activity of the principal ion ($\log a_x$ or pH), where the sensitivity, limit of detection, or linear range of each potentiometric sensor were extracted. All of these experiments were performed at room temperature by using three different ISFETs of each type, prepared under the same experimental conditions.

Moreover, two platinum four-electrode sensors and two thin-film gold electrodes were firstly chemically cleaned, followed by an electrochemical activation carried out in 0.1 M KNO₃ where the electrode was cycled from +0.8 V to −2.2 V at least 20 times. These sensors were also characterized before the analysis using the multisensor meter. The response characteristics are reported in [23], including the conductivity calibration and the ORP test obtained with the four-electrode sensors.

2.6. Electronic Tongue Measurement Procedure

The analysis was directly carried out in the Cava sample, previously degassed by magnetic stirring. No measurement replications were done in order to get a rapid analysis and prevent changes of the Cava wine, as well as to minimize the formation of CO₂ bubbles onto the sensor surface.

Once calibrated, the six ISFETs (one for each ion considered) were immersed in the Cava wine and the potentials (in mV vs. Ag/AgCl) were recorded every 10 s for 30 s using the multi-ISFET meter. The output values corresponding to the relative measurements of each ISFET with respect to the reference solution, which was checked periodically, were used as analytical signals for the models. This is a common strategy to correct the possible drift of the ISFET sensors.

Once the good behavior of the two platinum four-electrode sensors and two thin-film gold electrodes was confirmed, they were immersed in the Cava wine sample and the signals were recorded every 1 s for 30 s using the multisensor meter. In the case of the amperometric measurements, one gold electrode was set to an overpotential of +1.01 V (vs. Ag/AgCl), at which the polyphenols are probably oxidized. The other gold electrode was set to +1.31 V (vs. Ag/AgCl), related with the oxidation of gold from the electrode [2].

The measurements with these two devices were performed sequentially, first with the multi-ISFET meter and then with the multisensor meter. Therefore, a complete analysis of one Cava wine sample took around 2 min under batch conditions.

2.7. Data Treatment and Analysis

Once all of the samples were passed through the sensors, a data matrix was constructed with the different variables to be used as the input of the chemometric tools. In this study, the input data were composed by 10 variables, as shown in Table 1.

Table 1. Variables considered for constructing the models.

Equipment	Sensors	Variables
Multi-ISFET meter	Six ISFETs	pH, Na ⁺ , K ⁺ , Ca ²⁺ , Cl [−] , and CO ₃ ^{2−}
Multisensor meter	Two four-electrode sensors Two gold electrodes	Conductivity and ORP Current at +1.01 V and +1.31 V

These data were treated using different multivariate methods. The linear discriminant analysis (LDA) was utilized to achieve a good classification model for the Cava wine samples. Discriminant analysis is a supervised method, since it is used to build linear combinations of the original variables for a number of pre-specified classes (model). These combinations are later used for allocating new and unknown samples to the most probable class. Another important application of discriminant analysis is to help in interpreting differences between groups of samples.

The partial least squares (PLS) regression was employed to perform the quantification of different parameters of the samples. PLS is a method for multivariate calibration that finds the combinations of the original variables (components or factors) that will best predict the values of the parameters analyzed, by maximizing the covariance between the matrices. In this work, the PLS-1 variant (one PLS model per each parameter) was used in order to obtain more accurate predictions.

For the two methods, the original values were previously autoscaled—all of the variables were centered and set to a standard deviation equal to 1, to avoid variables from having a different influence on the model. Additionally, all of the obtained models were centered. On one hand, the Mahalanobis method, for measuring the distance of an observation to the centers of the groups, together with the leave-one-out cross validation method were used for the LDA model. On the other hand, the classical non-linear iterative (NIPALS) algorithm, together with the test-set validation technique, was used for the PLS regressions. In this case, a fixed calibration set composed of 60 Cava wine samples was chosen. Meanwhile, the prediction set consisted of 18 samples. To control all of these parameters and to perform the analyses, the Unscrambler v.9.1 informatics package (CAMO ASA, Oslo, Norway) was used.

3. Results and Discussion

3.1. Characterization of Sensors and Electronics

ISFET sensors selective to pH, Na⁺, K⁺, Ca²⁺, Cl⁻, and CO₃²⁻ were calibrated with the new device. Three sensors of each type were connected and measured simultaneously with the multi-ISFET meter. The response characteristics obtained are shown in Table 2. The limit of detection is calculated by the cross-point method recommended by IUPAC for potentiometry [34]. As can be observed, all of the sensors presented a Nerstian response for at least a two-decade linear range with a high significant regression coefficient (R²). In fact, these analytical parameters obtained with the new device are very similar to those reported previously for ISFETs with the same membrane composition [24,29–31], also in terms of the limit of detection. These results demonstrate the good performance of the developed equipment. Simultaneous measurements of six ISFETs can be carried out without any electrical interference thanks to the circuit design, which is a key issue for an electronic tongue system. Therefore, this multi-ISFET meter was used to perform the analysis of the Cava wine samples.

Table 2. Response characteristics obtained from the calibration curves for each type of ISFET using the multi-ISFET meter.

Parameter	Sensitivity (mV/dec) ¹	Linear Range (M)	R ²	Limit of Detection (M)
pH	54.2 (0.5)	pH 1.56–11.42	0.9998 (n = 10)	-
Na ⁺	54.0 (0.4)	2.1 × 10 ⁻⁵ –2.2 × 10 ⁻²	0.9994 (n = 6)	5.9 × 10 ⁻⁶
K ⁺	57.0 (0.8)	2.0 × 10 ⁻⁵ –2.1 × 10 ⁻²	0.9996 (n = 7)	1.8 × 10 ⁻⁶
Ca ²⁺	28.6 (0.6)	5.9 × 10 ⁻⁷ –1.9 × 10 ⁻²	0.9998 (n = 9)	1.9 × 10 ⁻⁷
Cl ⁻	-59 (1)	2.0 × 10 ⁻⁴ –2.1 × 10 ⁻²	0.9998 (n = 4)	2.8 × 10 ⁻⁵
CO ₃ ²⁻	-58 (2)	2.1 × 10 ⁻⁴ –2.2 × 10 ⁻²	0.9993 (n = 4)	3.0 × 10 ⁻⁵

¹ Standard deviation of three different ISFET is indicated in brackets.

3.2. Classification of the Cava Wine Samples

With the data obtained from the different variables, LDA was performed. The confusion matrix of the obtained model is presented in Table 3, together with the percentages of sensitivity and specificity

for the four groups. The sensitivity corresponds to the samples of each group correctly classified by the LDA model, while the specificity is calculated as the samples of different groups correctly rejected by the model. As shown in Table 3, especially good results are obtained in the prediction of the Reserva class samples, with just one sample confused with the Gran Reserva class. Looking more in detail at the specificity of classification, it is observed that no Young sample is confused with Gran Reserva, and, conversely, no Gran Reserva sample is confused with Young. This is because the system is able to discriminate very different aging times that are 9–15 months (Young) and more than 30 months (Gran Reserva). On the other hand, the Reserva class has an aging time in between (15–30 months) and, therefore, it is more likely to overlap with the borderline samples. However, the values of specificity are above 90% in all cases and the total sensitivity of prediction is 87%. It is also important to highlight the high percentage of sensitivity and specificity achieved for the Rosé class samples, which demonstrates the great discrimination capacity of the system formed by just electrochemical microsensors.

Table 3. Confusion matrix for the Cava wine samples obtained with the LDA model using the cross-validation method.

Classes	Prediction				Sensitivity (%)	Specificity (%)
	Young	Reserva	Gran Reserva	Rosé		
Young	16	2	0	2	80	97
Reserva	0	24	1	0	96	91
Gran Reserva	0	3	13	0	81	98
Rosé	2	0	0	15	88	97

3.3. Quantification of Legal Parameters

Next, a PLS regression was realized in order to assess if the system was able to quantify some chemical parameters of the samples already analyzed with standard methods. These parameters are of interest to meet the legal limits, such as the total acidity, pH, and VAD. These legal limits are fixed between 10.8% and 12.8% for VAD, between 2.8 and 3.3 for pH, and at least 5 g/L for total acidity [35]. For the regression, the prediction set was formed by 18 Cava wine samples, whose data was not included in the calibration process: four Young (Y 3336, 3709, 4956, 5219), six Reserva (R 2719, 2929, 3727, 5241, 5608, and 5962), four Gran Reserva (GR 2720, 3182, 4183, and 5220), and four Rosé (Ro 2978, 3103, 4814, and 5017). The results are shown in Table 4. As can be seen, the interpolated values are in good agreement with the data obtained using standard methods for the three parameters. In general, the relative errors are below 9%. Especially good results are obtained for pH and VAD prediction, with relative errors below 5%. The results for VAD are significant since there is no specific sensor for this parameter. Values for total acidity are also quite accurate considering that it is a global parameter that includes all titratable acids, mainly tartaric acid, but also lactic acid, malic acid, citric acid, etc., and again no specific sensor is used.

3.4. Quantification of Other Parameters

PLS regressions were also used to determine other parameters of interest, such as potassium and conductivity, which are related with the tartaric stabilization, and glycerol and methanol, both related with the final sensory quality of the Cava wine. The data for the prediction set obtained with our system and with standard methods are shown in Table 5. The values obtained with both methods are also in good agreement, with relative errors below 15%. As can be seen, the mean errors are below 6.0% for the four parameters. The best results are obtained for conductivity prediction. Again, glycerol and methanol are determined with no specific sensors, with good accuracy.

Table 4. Results of legal parameter quantification with the electronic tongue using PLS-1 regression. Standard method data were provided by INCAVI.

Sample ¹	Total Acidity (g/L)			pH			VAD (%)		
	Standard Method	Electronic Tongue	Relative Error (%)	Standard Method	Electronic Tongue	Relative Error (%)	Standard Method	Electronic Tongue	Relative Error (%)
Y 3336	6.5	5.9	8.5	3.04	3.23	6.1	11.75	11.97	1.8
Y 3709	6.1	6.0	1.3	3.01	3.17	5.4	12.15	11.97	1.5
Y 4956	6.5	6.1	6.4	2.94	2.95	0.3	11.85	11.87	0.2
Y 5219	6.7	6.2	8.1	3.03	3.07	1.3	11.55	11.82	2.4
R 2719	5.5	5.8	5.0	3.31	3.35	1.2	13.00	12.06	7.2
R 2929	6.1	6.1	0.4	3.07	3.08	0.4	12.30	11.86	3.5
R 3727	6.1	6.2	0.9	2.96	3.04	2.8	11.75	11.90	1.3
R 5241	5.8	6.4	11.0	3.43	3.44	0.4	12.05	11.76	2.4
R 5608	6.2	6.1	2.4	2.94	3.15	7.3	12.15	11.92	1.9
R 5962	5.6	6.1	9.0	3.08	3.08	0.1	12.10	11.89	1.7
GR 2720	5.5	5.7	4.4	3.15	3.05	3.2	12.85	12.05	6.2
GR 3182	5.5	6.1	11.6	3.02	3.00	0.6	12.15	11.91	2.0
GR 4183	5.5	5.6	1.3	3.02	3.04	0.7	12.40	12.07	2.7
GR 5220	6.5	7.0	7.4	2.93	3.10	5.9	11.75	12.01	2.2
Ro 2978	5.5	5.9	7.8	3.35	3.19	4.9	12.20	12.15	0.4
Ro 3103	6.2	6.7	7.8	3.01	3.04	1.0	12.20	12.11	0.7
Ro 4814	5.8	6.0	3.2	3.00	3.10	3.4	12.30	11.96	2.8
Ro 5017	5.5	6.1	11.3	3.02	3.05	1.1	12.05	11.99	0.5
	Mean Relative Error		6.0	Mean Relative Error		2.6	Mean Relative Error		2.3

¹ Y: Young; R: Reserva; GR: Gran Reserva; Ro: Rosé.

Table 5. Results of quality parameter quantification with the electronic tongue using PLS-1. Standard method data were provided by INCAVI.

Sample ¹	Potassium (mg/L)			Conductivity (mS/cm)			Glycerol (g/L)			Methanol (mg/L)		
	Standard Method	Electronic Tongue	Relative Error (%)	Standard Method	Electronic Tongue	Relative Error (%)	Standard Method	Electronic Tongue	Relative Error (%)	Standard Method	Electronic Tongue	Relative Error (%)
Y 3336	355	360	1.3	1.34	1.33	0.9	5	5.5	9.7	29	30	3.8
Y 3709	433	423	2.4	1.42	1.32	6.9	4.9	5.4	10.0	29	28	2.3
Y 4956	326	328	0.6	1.29	1.26	2.1	-	-	-	30	30	1.2
Y 5219	332	332	0.0	1.38	1.32	4.3	5.3	5.2	1.7	29	30	5.0
R 2719	550	487	11.4	1.79	1.66	7.5	6.1	6.2	2.2	31	34	10.6
R 2929	360	395	9.7	1.29	1.28	0.9	5.1	5.7	12.2	30	32	5.7
R 3727	300	332	10.7	1.21	1.21	0.3	5.6	5.4	2.8	30	30	0.0
R 5241	372	315	15.4	1.19	1.13	5.3	5.1	5.6	9.5	30	30	1.3
R 5608	379	418	10.3	1.31	1.31	0.1	5.8	5.8	0.7	29	31	6.1
R 5962	320	334	4.4	1.2	1.19	0.5	5.5	5.7	2.9	28	30	7.5
GR 2720	544	518	4.7	1.73	1.70	1.6	6.9	6.3	8.1	31	32	3.0
GR 3182	321	327	1.9	1.14	1.16	2.0	5.1	5.4	6.1	30	30	1.5
GR 4183	391	408	4.2	1.42	1.41	0.6	5.5	5.4	2.5	28	31	10.8
GR 5220	300	301	0.2	1.33	1.29	2.9	5.1	5.3	4.4	29	28	2.3
Ro 2978	430	452	5.1	1.29	1.41	9.1	5.4	5.9	8.5	38	33	13.4
Ro 3103	367	346	5.6	1.44	1.31	9.4	5.4	5.7	4.9	38	36	5.5
Ro 4814	459	398	13.4	1.39	1.33	4.0	5.5	5.8	5.8	36	32	12.0
Ro 5017	318	306	3.6	1.22	1.20	1.7	5.4	5.7	6.2	27	30	9.7
	Mean Relative Error		5.8	Mean Relative Error		3.3	Mean Relative Error		5.8	Mean Relative Error		5.6

¹ Y: Young; R: Reserva; GR: Gran Reserva; Ro: Rosé.

4. Conclusions

A compact electronic tongue has been developed and applied to measure Cava wines. The electronics used (multi-ISFET meter and multisensor meter) have been fabricated according to microsensor requirements and taking into account the minimum energy consumption. This power consumption is below 10 mA if we consider the measurement with the 10 microsensors simultaneously every 15 min. This means that the equipment could work continuously up to 150 h using a standard 9 V battery.

This electronic tongue has been applied to the analysis of 78 Cava wine samples. The qualitative results confirm that the device is capable of classifying the samples according to the aging time and to distinguish the Rosé samples from the white Cava wine samples with a high sensitivity and specificity. In addition, the application of the PLS technique to the collected data permits the quantification of some chemical parameters of interest in the final product. Some of these parameters have legal limits to accomplish, such as the total acidity, pH, and VAD. In general, the relative errors are below 10%. The best results are obtained for pH, VAD, and conductivity predictions with mean relative errors below 4%. The good accuracy obtained for the determination of VAD, glycerol, and methanol is especially relevant since there are no specific sensors for these parameters.

Compared with other electronic tongues for Cava wine analysis [15–17], this system is able to determine simultaneously up to seven important chemical parameters, apart from the qualitative analysis, thanks to the hybrid nature of the electrochemical sensors (potentiometric, amperometric, and conductimetric). Moreover, this e-tongue uses small and low-power equipment for measurement, instead of bench-top laboratory equipment, and microsensors, which are easy to miniaturize and integrate with the electronics.

In conclusion, the good results obtained both for classification and quantification analyses confirm the viability of the multiparametric system. Additionally, the use of portable meters together with electrochemical microsensors fabricated with semiconductor technology provide an advantageous combination for rapid and feasible in-field measurements, not only for the wine industry but for food quality control in general.

Acknowledgments: We acknowledge funding from the Spanish R & D National Program (MINECO, Projects TEC2011-29045-C04-01 and TEC2014-54449-C3-1-R). P.G.-G. is grateful to MINECO, Spain, for the financial support through a research studentship of the FPI Program. The technical assistance of Juan Manuel Ríos-Gallardo is highly appreciated.

Author Contributions: P.G.-G., C.J.-J. and M.G.-C. designed the experiments and analyzed the data; F.C. and A.P.-P. selected the Cava wine samples and performed the analysis by standard methods; R.E.-P. developed the electronic devices and the Labview interface of control; P.G.-G. performed the experiments. All authors have written, read and revised the manuscript.

Conflicts of Interest: The authors declare no conflict of interest.

References

1. Amodio, M.; Brattoli, M.; Dambrosio, P.; de Gennaro, L.; de Gennaro, G.; Loiotile, A.D.; Trizio, L. Odour Impact Assessment by a Multiparametric System (Electronic Noses/CH4-NMHC Analyser). In *Nose 2012: 3rd International Conference on Environmental Odour Monitoring and Control*; DelRosso, R., Pierucci, S., Klemes, J.J., Eds.; Aidic Servizi Srl: Milano, Italy, 2012; Volume 30, pp. 199–204.
2. Gutierrez, M.; Llobera, A.; Ipatov, A.; Vila-Planas, J.; Minguez, S.; Demming, S.; Buttgenbach, S.; Capdevila, F.; Domingo, C.; Jimenez-Jorquera, C. Application of an E-Tongue to the Analysis of Monovarietal and Blends of White Wines. *Sensors* **2011**, *11*, 4840–4857. [[CrossRef](#)] [[PubMed](#)]
3. Totu, E.E.; Manuc, D. Multisensor for Clinical Analysis with Impact on Public Health Evaluation. *Rev. Chim.* **2008**, *59*, 947–951.
4. Praveena, S.M.; Aris, A.Z. A baseline study of tropical coastal water quality in Port Dickson, Strait of Malacca, Malaysia. *Mar. Pollut. Bull.* **2013**, *67*, 196–199. [[CrossRef](#)] [[PubMed](#)]
5. Guth, U.; Vonau, W.; Zosel, J. Recent developments in electrochemical sensor application and technology—A review. *Meas. Sci. Technol.* **2009**, *20*, 042002. [[CrossRef](#)]

6. Holmberg, M.; Eriksson, M.; Krantz-Rülcker, C.; Artursson, T.; Winquist, F.; Lloyd-Spetz, A.; Lundström, I. 2nd Workshop of the Second Network on Artificial Olfactory Sensing (NOSE II). *Sens. Actuators B Chem.* **2004**, *101*, 213–223. [[CrossRef](#)]
7. Vlasov, Y.; Legin, A.; Rudnitskaya, A.; Di Natale, C.; D'Amico, A. Nonspecific sensor arrays (“electronic tongue”) for chemical analysis of liquids (IUPAC Technical Report). *Pure Appl. Chem.* **2005**, *77*, 1965–1983. [[CrossRef](#)]
8. Rothe, J.; Frey, O.; Stettler, A.; Chen, Y.H.; Hierlemann, A. Fully Integrated CMOS Microsystem for Electrochemical Measurements on 32×32 Working Electrodes at 90 Frames Per Second. *Anal. Chem.* **2014**, *86*, 6425–6432. [[CrossRef](#)] [[PubMed](#)]
9. Codinachs, L.M.I.; Baldi, A.; Merlos, A.; Abramova, N.; Ipatov, A.; Jimenez-Jorquera, C.; Bratov, A. Integrated multisensor for FIA-based electronic tongue applications. *IEEE Sens. J.* **2008**, *8*, 608–615. [[CrossRef](#)]
10. Baldwin, E.A.; Bai, J.H.; Plotto, A.; Dea, S. Electronic Noses and Tongues: Applications for the Food and Pharmaceutical Industries. *Sensors* **2011**, *11*, 4744–4766. [[CrossRef](#)] [[PubMed](#)]
11. Rodríguez-Méndez, M.L. *Electronic Noses and Tongues in Food Science*; Elsevier Inc.: Oxford, UK, 2016; pp. 151–273.
12. Zeravik, J.; Hlavacek, A.; Lacina, K.; Skladal, P. State of the Art in the Field of Electronic and Bioelectronic Tongues-Towards the Analysis of Wines. *Electroanalysis* **2009**, *21*, 2509–2520. [[CrossRef](#)]
13. Buxaderas, S.; López-Tamames, E. Chapter 1-Sparkling Wines: Features and Trends from Tradition. In *Advances in Food and Nutrition Research*; Jeyakumar, H., Ed.; Academic Press: Waltham, MA, USA, 2012; Volume 66, pp. 1–45.
14. Pozo-Bayón, M.Á.; Martínez-Rodríguez, A.; Pueyo, E.; Moreno-Arribas, M.V. Chemical and biochemical features involved in sparkling wine production: From a traditional to an improved winemaking technology. *Trends Food Sci. Technol.* **2009**, *20*, 289–299. [[CrossRef](#)]
15. Ceto, X.; Gutierrez, J.M.; Moreno-Baron, L.; Alegret, S.; del Valle, M. Voltammetric Electronic Tongue in the Analysis of Cava Wines. *Electroanalysis* **2011**, *23*, 72–78. [[CrossRef](#)]
16. Ceto, X.; Capdevila, J.; Puig-Pujol, A.; del Valle, M. Cava Wine Authentication Employing a Voltammetric Electronic Tongue. *Electroanalysis* **2014**, *26*, 1504–1512. [[CrossRef](#)]
17. Ceto, X.; Capdevila, J.; Minguez, S.; del Valle, M. Voltammetric BioElectronic Tongue for the analysis of phenolic compounds in rose cava wines. *Food Res. Int.* **2014**, *55*, 455–461. [[CrossRef](#)]
18. Ouyang, Q.; Zhao, J.W.; Chen, Q.S. Classification of rice wine according to different marked ages using a portable multi-electrode electronic tongue coupled with multivariate analysis. *Food Res. Int.* **2013**, *51*, 633–640. [[CrossRef](#)]
19. Garcia-Breijo, E.; Atkinson, J.; Gil-Sanchez, L.; Masot, R.; Ibanez, J.; Garrigues, J.; Glanc, M.; Laguarda-Miro, N.; Olguin, C. A comparison study of pattern recognition algorithms implemented on a microcontroller for use in an electronic tongue for monitoring drinking waters. *Sens. Actuator A Phys.* **2011**, *172*, 570–582. [[CrossRef](#)]
20. Blanco, C.A.; de la Fuente, R.; Caballero, I.; Rodriguez-Mendez, M.L. Beer discrimination using a portable electronic tongue based on screen-printed electrodes. *J. Food Eng.* **2015**, *157*, 57–62. [[CrossRef](#)]
21. Tahara, Y.; Nakashi, K.; Ji, K.; Ikeda, A.; Toko, K. Development of a Portable Taste Sensor with a Lipid/Polymer Membrane. *Sensors* **2013**, *13*, 1076–1084. [[CrossRef](#)] [[PubMed](#)]
22. Cruz, A.F.D.; Norena, N.; Kaushik, A.; Bhansali, S. A low-cost miniaturized potentiostat for point-of-care diagnosis. *Biosens. Bioelectron.* **2014**, *62*, 249–254. [[CrossRef](#)] [[PubMed](#)]
23. Gimenez-Gomez, P.; Escude-Pujol, R.; Jimenez-Jorquera, C.; Gutierrez-Capitan, M. Multisensor Portable Meter for Environmental Applications. *IEEE Sens. J.* **2015**, *15*, 6517–6523. [[CrossRef](#)]
24. Gutierrez, M.; Llobera, A.; Vila-Planas, J.; Capdevila, F.; Demming, S.; Buttgenbach, S.; Minguez, S.; Jimenez-Jorquera, C. Hybrid electronic tongue based on optical and electrochemical microsensors for quality control of wine. *Analyst* **2010**, *135*, 1718–1725. [[CrossRef](#)] [[PubMed](#)]
25. Ministerio de Agricultura, Pesca y Alimentación. Ministerio de Agricultura, Pesca y Alimentación. ORDEN de 14 de Noviembre de 1991 por la que se Aprueba el Reglamento de la Denominación “Cava” y de su Consejo Regulador. In *BOE-A-1991-28079*; Secretaría General Técnica: Madrid, Spain, 1991; p. 37587.
26. Community Methods for the Analysis of Wines. Available online: <http://eur-lex.europa.eu/legal-content/EN/TXT/?qid=1477386665745&uri=CELEX:31990R2676> (accessed on 25 August 2016).

27. Compendium of International Methods of Wine and Must Analysis. Available online: <http://www.oiv.int/public/medias/2624/compendium-2016-en-vol1.pdf> (accessed on 25 August 2016).
28. Jiménez, C.; Bratov, A.; Abramova, N.; Baldi, A. ISFET based sensors: fundamentals and applications. In *Encyclopedia of Sensors*; Grimes, C.A., Dickey, E.C., Pishko, M.V., Eds.; American Scientific Publishers: New York, NY, USA, 2005; Volume X.
29. Artigas, J.; Beltran, A.; Jimenez, C.; Baldi, A.; Mas, R.; Dominguez, C.; Alonso, J. Application of ion sensitive field effect transistor based sensors to soil analysis. *Comput. Electron. Agric.* **2001**, *31*, 281–293. [[CrossRef](#)]
30. Bratov, A.; Abramova, N.; Dominguez, C. Investigation of chloride sensitive ISFETs with different membrane compositions suitable for medical applications. *Anal. Chim. Acta* **2004**, *514*, 99–106. [[CrossRef](#)]
31. Makarychev-Mikhailov, S.; Goryacheva, O.; Mortensen, J.; Legin, A.; Levitchev, S.; Vlasov, Y. Carbonate sensors based on 4-hexyltrifluoroacetophenone modified by acceptor substituents in phenyl ring. *Electroanalysis* **2003**, *15*, 1291–1296. [[CrossRef](#)]
32. Beltran, A.; Artigas, J.; Jimenez, C.; Mas, R.; Bartroli, J.; Alonso, J. Development of durable nitrate-selective membranes for all-solid state ISE and ISFET sensors based on photocurable compositions. *Electroanalysis* **2002**, *14*, 213–220. [[CrossRef](#)]
33. Orozco, J.; Baldi, A.; Baena, R.; Cadarso, A.; Bratov, A.; Jimenez, C. Portable system based on microsensors for environmental monitoring applications. *Meas. Sci. Technol.* **2007**, *18*, 935–940. [[CrossRef](#)]
34. Buck, R.P.; Lindner, E. Recommendations for nomenclature of ion-selective electrodes (IUPAC recommendations 1994). *Pure Appl. Chem.* **1994**, *66*, 2527–2536. [[CrossRef](#)]
35. Regulatory Board of Cava. Pliego de Condiciones Denominación de Origen Protegida “Cava”. Available online: <http://www.docava.es/wp-content/uploads/2015/05/PLIEGO-DOP-CAVA.pdf> (accessed on 25 August 2016).



© 2016 by the authors; licensee MDPI, Basel, Switzerland. This article is an open access article distributed under the terms and conditions of the Creative Commons Attribution (CC-BY) license (<http://creativecommons.org/licenses/by/4.0/>).



Analysis of free and total sulfur dioxide in wine by using a gas-diffusion analytical system with pH detection



Pablo Giménez-Gómez^a, Manuel Gutiérrez-Capitán^a, Anna Puig-Pujol^b, Fina Capdevila^b, Sergio Muñoz^c, Andreu Tobeña^c, Antoni Miró^d, Cecilia Jiménez-Jorquera^{a,*}

^a Instituto de Microelectrónica de Barcelona (IMB-CNM), CSIC, Campus UAB, 08193 Bellaterra, Spain

^b Institut Català de la Vinya i el Vi (IRTA-INCAVI), Plaça Àgora 2, 08720 Vilafranca del Penedès, Spain

^c BioSystems S.A., c/ Costa Brava 30, 08030 Barcelona, Spain

^d Linking Innovations, S.L., c/ Costa Brava 22, 1^a, 08030 Barcelona, Spain

ARTICLE INFO

Article history:

Received 15 April 2016

Received in revised form 2 February 2017

Accepted 6 February 2017

Available online 8 February 2017

Keywords:

Free and total sulfur dioxide

Flow-system

Gas-diffusion

pH-ISFET

Wine monitoring

ABSTRACT

The use of sulfur dioxide as preservative in winemaking industry has a direct impact on wine quality. The standard methods to analyze this parameter require several processes and are time consuming. In this paper a simple and rapid analytical method for free and total sulfur dioxide detection is proposed. This method is based on the separation of the analyte from the sample with a permeable gas diffusion membrane and its indirect detection with a pH sensor. The system has been validated and optimized for free sulfur dioxide detection in the range of 1–60 mg L⁻¹ and for total sulfur dioxide in the range of 30–300 mg L⁻¹ with a limit of detection of 0.5 mg L⁻¹. Validation of the system has been carried out using a total of 70 samples of white and red wines and two standard methods, the Ripper and the Paul method. The obtained values have demonstrated a good agreement for both methods.

© 2017 Elsevier Ltd. All rights reserved.

1. Introduction

Sulfur dioxide is added to wine during winemaking to prevent the microbial spoilage, oxidation and color changes due to undesirable enzymatic and non-enzymatic reactions (Fazio & Warner, 1990). It is present in wine in two forms, as free sulfur – this is basically under the form of HSO₃⁻, which is the antioxidant portion, and a small amount of dissolved SO₂ – and sulfur bound with acetaldehyde, some polyphenols, ketones, sugars or acids. The sum of both corresponds to the total sulfur dioxide (Eschenbruch, 1974).

Monitoring of total and free SO₂ content in wine is critical during wine storage and processing to ensure protection from chemical and microbiological agents and to adhere to prevailing legislation. The presence of even low concentrations of SO₂ can induce severe diseases in people with allergic illness or food intolerance symptoms (Adams, 1997). Furthermore, high concentrations of sulfur dioxide affect the final quality of the wine, mainly the smell and the taste and can inhibit the malolactic fermentation. The maximum level of total and free sulfur dioxide is fixed in the European Community by the International Organisation of Vine

and Wine (OIV) and it depends on the type of wine (up to 150 mg L⁻¹ for red wines and up to 400 mg L⁻¹ for sweet white wines). If the total sulfur dioxide content exceeds 10 mg L⁻¹, it must be expressed on the label of the wine bottle (International Organization of Vine and Wine, 2015). The analysis of SO₂ is also important during winemaking in order to control the sulfur dioxide decrease and the right amount of sulfur dioxide to add.

There are three standard methods for the determination of sulfur dioxide in wine proposed by the OIV. The Paul method, also known as the aeration-oxidation method, is the official method. In that method, the free sulfur dioxide is volatilized and carried through a separate container by a stream of air or nitrogen where it is fixed and oxidized with a dilute and neutral H₂O₂ solution. Then, the sulfuric acid formed is determined by titration with a standard NaOH solution. Free sulfur dioxide is purged from the wine by entrainment at low temperature (10 °C), while total sulfur dioxide is purged from the wine by entrainment at high temperature (approximately 100 °C) (Paul, 1958). However, this method is tedious since it requires flushing of the sample, use large sample volumes and the precision depends on the experience of the technician. The Ripper method is based on an iodimetric titration (Ripper, 1892). This is the most widely used in cellars due to its simplicity and short analysis time. Nevertheless, it suffers from many interferences and the end point observation in red wines is

* Corresponding author.

E-mail address: cecilia.jimenez@csic.es (C. Jiménez-Jorquera).

difficult due to the use of colorimetric indicators. The third recommended method is based on theoretical models (International Organization of Vine and Wine, 2009a) and allows calculating the molecular sulfur dioxide content as percentage of free SO₂ according to pH, temperature and alcoholic strength (Usseglio-Tomasset, 1984).

Alternative methods based on direct detection of sulfur dioxide in wine are electrochemical biosensors. They have a high selectivity due to the use of enzymatic recognition (Kalimuthu, Tkac, Kappler, Davis, & Bernhardt, 2010; Molinero-Abad, Alonso-Lomillo, Dominguez-Renedo, & Arcos-Martinez, 2014; Rawal & Pundir, 2013). However, these biosensors suffer from low stability due to the inactivation of the bio-elements.

Other alternatives to standard methods that permit the automation of the analysis are those based on flow analysis mainly using flow injection analysis (FIA) (Osborne & Tyson, 1988; Ruiz-Capillas & Jimenez-Colmenero, 2008) and Sequential Injection analysis (SIA) (Segundo, Lima, & Rangel, 2004). The most interesting aspect of these methods is that they allow the separation of the analyte from the sample using a diffusion cell and a hydrophobic membrane. The methodology is based on the acid/base characteristics of sulfur dioxide. The sample is acidified to pH lower than 1 to convert all sulfur dioxide to the SO₂ form. This gas is diffused through the gas permeable membrane and collected by an acceptor stream. The most usual detection technique is colorimetric having a reagent on the acceptor channel such as pararosaniline (Falcone & Maxwell, 1992; Oliveira, Lopes, Toth, & Rangel, 2009), *p*-aminoazobenzene (Bartoli, Escalada, Jorquera, & Alonso, 1991), malachite green (Atanassov, Lima, Mesquita, Rangel, & Toth, 2000) or luminol (Huang, Kim, & Schmid, 1992). Some of these techniques were commercialized in the past (i.e. FIAstar analytical system from FOSS), however, they have been substituted by other detection techniques due to the toxicity of the colorimetric reagents and the use of expensive complex measuring devices.

Amperometric detection using non-modified glassy carbon electrodes (Azevedo, Araki, Toma, & Angnes, 1999) or modified electrodes (Thanh, Decnopweever, & Kok, 1994) implemented in FIA systems have also been described in the literature. The main problem of this detection method was the loss of sensitivity of electrodes. An alternative detection method using a pH-ISFET (Ion-Sensitive Field-Effect Transistor) combined with a FIA system was proposed in (Alegret et al., 1991a). These authors evaluated the system with water solutions but no wine samples were analyzed. However the paper pointed out the interest of using ISFETs as pH sensors. ISFETs are sensors fabricated with microelectronic technology. Their functioning is based on a MOS (Metal-Oxide Semiconductor) transistor with a Si₃N₄ dielectric membrane instead of a metal. This membrane behaves in a similar way as a glass electrode, therefore ISFETs have potentiometric response and follow Nerstian law. Nevertheless, due to their semiconductor device characteristics, they have several advantages, such as small size, they have the dimensions of a chip, in this case 3 × 3 mm², they are solid state by nature as they are fabricated on silicon, they are mass fabricated, and show a short response time and long term stability (Jimenez, Abramova, & Baldi, 2005).

Today's winemakers are moving away from manual titrations, color indicators, time consuming aeration-oxidation (AO) tests and dilution calculations to more accurate, more automatic and faster methods. It is crucial that instruments deliver information quickly, inexpensively and with high accuracy. For example, commercial methods like WineScan™ from FOSS use a gas separation method to extract the SO₂ from the sample and a FTIR (Fourier Transform Infrared Spectroscopy) interferometer that scans the full infrared spectrum. This system is rapid, automatic and can measure other parameters than SO₂. However, this equipment requires laboratory infrastructure.

The aim of the present work is the development and validation of a simple, selective, automatic and rapid method for the determination of free and total sulfur dioxide in wine samples. The detection method is based on pH detection of a stream containing the SO₂ of the sample collected through a gas permeable membrane. For that a continuous flow system with a gas-diffusion cell and a pH-ISFET has been fabricated. This system has no matrix interferences and allows a rapid detection with low-reagent consumption. The flow system has been optimized and validated with seventy wine samples and two different methods, the iodimetric method and the Paul method.

2. Material and methods

2.1. Chemicals and reagents

All reagents used were of high purity, analytical grade or equivalent and were purchased from Sigma-Aldrich (Spain), unless stated otherwise. All solutions were prepared using de-ionized (DI) water. A solution containing 0.1 M sodium hydroxide (NaOH), 5% (v/v) glycerol and 0.1 M sodium sulfite (Na₂SO₃) was used as stock for preparing the calibration solutions and renewed every 10 days (Bartoli, Escalada, Jorquera, & Alonso, 1991). Calibration solutions containing different concentrations of Na₂SO₃ with 12% (v/v) ethanol absolute (Panreac, Spain) were prepared every day from this stock. A solution containing 2 × 10⁻⁵ M Na₂SO₃ and 0.02 M sodium chloride (NaCl) was used as carrier solution. A 4 M NaOH solution was used for the wine sample digestion. A set of hydrochloric acid (HCl) solutions in the range from 0.1 M to 4 M was used for sample pH adjustment (Acid solution 1) and another set in a range from 10⁻⁷ M to 10⁻³ M for carrier solution pH adjustment (Acid solution 2).

2.2. Devices and flow system

A scheme of the flow system is illustrated in Fig. 1. Two peristaltic pumps (403U/VM3, Watson Marlow, UK) were used to pump carrier and sample solutions. Teflon pump tubes had an internal diameter of 1.0 mm (Teknokroma, Barcelona, Spain) and Polyether ether ketone (PEEK) tubes connecting different devices had 0.75 mm of inner diameter (Teknokroma). In order to separate the analyte from the sample a gas-diffusion module was used. A more detailed scheme of the gas-diffusion cell is shown in Fig. S1, in the Supporting Information (SI). This is fabricated by micromilling (Roland MDX-40, Roland Digital Group Iberia, Spain) with polymethyl methacrylate (PMMA) and contains a polyvinylidene fluoride (PVDF, VHP09050 Durapore®, Hydrophobic Plain White, 0.22 μm pore size, from Merck Millipore, Darmstadt, Germany) gas-permeable membrane. This type of hydrophobic membrane has already demonstrated a good performance for the proposed application (Kuban, Janos, & Kuban, 1998). The measurement cell hosting a pH-ISFET and a Ag/AgCl (3.0 M KCl) double junction reference electrode (Orion 92-02-00, Thermo Fisher Scientific Inc., Beverly, USA) was also fabricated with PMMA and aluminum (Fig. S2, in SI). The pH-ISFETs used in this work were fabricated under clean room conditions according to standard photolithography techniques at the Instituto de Microelectrónica de Barcelona (IMB-CNM, CSIC) (Jimenez-Jorquera, Orozco, & Baldi, 2010). The electrochemical cell was connected to a data-acquisition card (NI USB 6259, National Instruments, Austin, TX), and the instrumentation was completed with a PC. The communication between the PC and the data-acquisition card was performed through a USB board and employing software programmed with LabView 2013 graphic language (National Instruments).

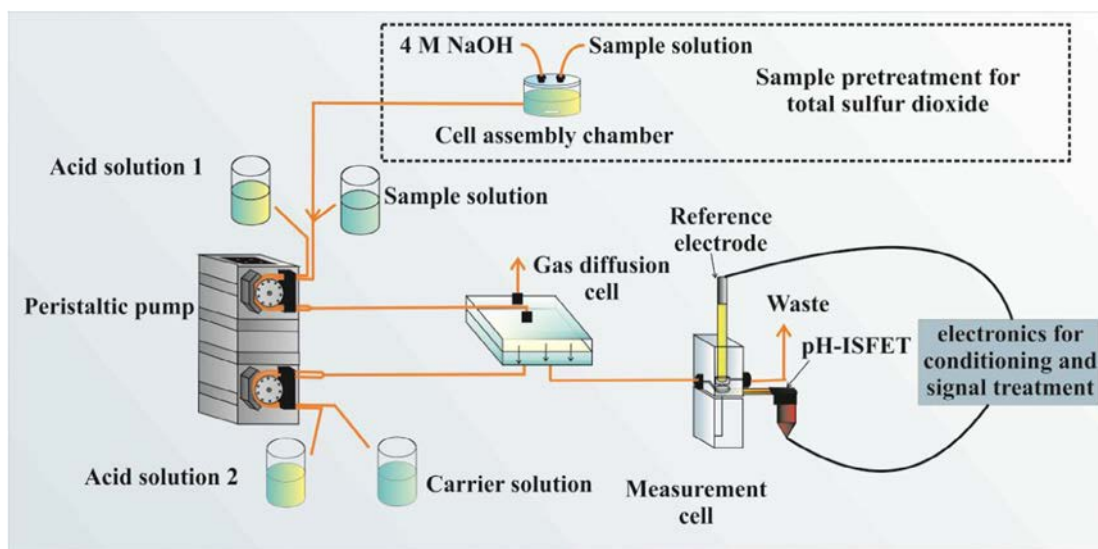


Fig. 1. Scheme of the flow system used for the determination of free and total sulfur dioxide.

2.3. Flow system design and methodology for free and total sulfur dioxide determination

As shown in Fig. 1, for free SO_2 measurement, the sample or calibration solution was pumped and mixed 1:1 in volume with a HCl solution (Acid solution 1) to convert all the hydrogen sulfite present to SO_2 . In parallel, the pH of the carrier solution was also adjusted by mixing 1:1 in volume with the Acid solution 2. When the sample stream arrived to the gas-diffusion cell, the SO_2 diffused through the membrane and it was collected by the acceptor solution. The diffusion ratio depends on the gas concentration but also on the gradient of concentration and the time of contact between both sides of the membrane, as well as on the pH of the carrier solution. This step was performed under continuous flow conditions for 5 min in order to ensure the effective mixing of solutions and the efficient diffusion process. After this time, the pH change generated in the carrier solution due to the SO_2 was measured with the ISFET (in mV) under stop-flow conditions during 2 min for each sample and the analytical signal collected was the mean potential value of the last 30 s. The obtained signal was correlated to the concentration of free sulfur dioxide in the sample. The calibration of the system was performed in triplicate using five solutions in the range $1\text{--}60\text{ mg L}^{-1}$ of SO_2 in DI water with 12% (v/v) ethanol. In order to obtain the calibration curve, this signal (in mV) was plotted versus the logarithm of the SO_2 concentration (in mg L^{-1}). The consumption of sample for each measurement was 2.5 mL.

For the determination of total SO_2 , the sample was treated with an alkaline solution in order to release all the bound sulfur dioxide of the wine sample (Sarudi & Kelemen, 1998). This pretreatment was carried out in a cell assembly made of PMMA with a 3 mL chamber placed in the sample channel before the diffusion cell (Fig. 1). For the sample treatment, 1.5 mL of sample was mixed with 1.5 mL of 4 M NaOH and let to react. After the treatment of the sample was completed, the sample (pH around 11) was mixed with a high concentration of HCl (Acid solution 1) to reduce in situ the pH value below 1. The flow system for the carrier channel was the same as described above for the determination of free SO_2 . Five solutions of sulfur dioxide in the range $30\text{--}300\text{ mg L}^{-1}$ were used to obtain the calibration curve. In this case, 1.5 mL of sample was used for each measurement.

2.4. Optimization of the flow system and analytical assessment

Several hydrodynamic parameters of the flow system were optimized in order to improve the analytical characteristics of sulfur dioxide detection. For that, chemical parameters were initially fixed. The carrier solution was fixed considering that SO_2 is a weak acid species and forms bisulfite (HSO_3^-) and sulfite (SO_3^{2-}) as conjugate bases. In order to obtain a stable, reproducible and linear pH change with the concentration of SO_2 , the carrier solution used was $2 \times 10^{-5}\text{ M Na}_2\text{SO}_3$ which allows a rapid chemical equilibrium. Previous tests demonstrated that if no conjugated species are used (i.e. water with a salt), the baseline signal is not stable due to pH variations. Besides, the pH change due to the presence of SO_2 is not reproducible and linear. The low concentration of sulfite chosen is related to its low buffering capacity, which allows a higher jump of pH against the presence of SO_2 and therefore better sensitivity. This carrier solution was adjusted initially at pH 4 (with an Acid solution 2 channel of $2 \times 10^{-4}\text{ M HCl}$) because at this pH the predominant species is bisulfite. This carrier solution contained also 0.02 M NaCl in order to adjust the ionic strength so that the response of the pH-ISFET sensor is not affected (Alegret et al., 1991b). The Acid solution 1 was HCl 4 M to reduce the pH of the sample below 1 and achieve complete conversion to gaseous SO_2 . A set of calibration solutions in the range from 30 to 300 mg L^{-1} of total sulfur dioxide were used to perform the calibration in triplicate.

Regarding the hydrodynamic parameters, the length of the tubes for mixing the sample with the HCl 4 M was a critical parameter to achieve the pH adjustment. The optimization of tubes' length was carried out for the determination of total sulfur dioxide since a more drastic change in pH is required (from pH 11 to 1). Two lengths of tubes (10 and 20 cm) were checked using a flow rate of 1.00 mL min^{-1} . The alkaline pretreatment of the sample was performed by mixing (1:1 in volume) the sample with NaOH 4 M during 3 min under stop flow conditions. The influence of four different flow rates (0.25, 0.50, 0.75 and 1.00 mL min^{-1}) was also checked. In relation to the performance of the gas-diffusion cell, a test was undertaken to see if the diffusion of SO_2 could be improved stopping the flow – after the 5 min under continuous flow – for 2 min before the analysis. Moreover, the flow mode – parallel current and countercurrent flow – in both sides of the membrane was also checked.

Regarding the alkaline pretreatment of the sample for the determination of total sulfur dioxide, the time of digestion in stop flow (1, 2 or 3 min) and the stirring conditions were optimized by using a set of 16 wine samples and comparing the results obtained with the equipment specified in Section 2.5 based on the iodimetric method.

In order to avoid the hysteresis and the clogging of the diffusion membrane, a method for cleaning the system was proposed and tested. The aim was to recover the baseline of the carrier solution after each measurement with wine samples. For that, a HCl solution with a concentration in the range from 0.1 M to 1 M was flowed at 1 mL min^{-1} through the wine sample channel between 1 and 5 min.

After the hydrodynamic parameters were fixed, the chemical parameters were optimized. The HCl concentration of the Acid solution 1 channel was tested in order to assure the total conversion of hydrogen sulfite to sulfur dioxide in the sample. The experiments consisted on mixing (1:1 in volume) a set of 3 wine samples with a set of HCl solutions (Acid solution 1). These solutions were from 0.1 M to 1 M and from 1 M to 4 M HCl for the free and total sulfur dioxide, respectively. The final pH of the mixed solution was checked using a pH-meter for ensuring a pH value below 1. In the same way, the HCl concentration in the Acid solution 2 channel was varied (from 10^{-7} M to 10^{-3} M) to study five different pH values of the carrier solution, specifically pH 3.50, 4.00, 4.75, 6.00 and 6.50.

Finally, the matrix effect was tested in the presence of some substances contained in wine that could affect the response of the system. For that, calibration curves in a range from 1 to 60 mg L^{-1} of free SO_2 were carried out adding an average concentration of several compounds in the calibration solutions (Hans-Ferdinand & Jackson, 1998). First 12% ethanol, then the most common ions ($7.75 \text{ mg L}^{-1} \text{ NO}_3^-$, $500 \text{ mg L}^{-1} \text{ H}_2\text{PO}_4^-$, $700 \text{ mg L}^{-1} \text{ SO}_4^{2-}$, $210 \text{ mg L}^{-1} \text{ K}^+$, $107.2 \text{ mg L}^{-1} \text{ Mg}^{2+}$, $90.6 \text{ mg L}^{-1} \text{ Ca}^{2+}$ and $100 \text{ mg L}^{-1} \text{ Cl}^-$) and finally adding 5 g L^{-1} of acid malic and 2.5 g L^{-1} of tartaric acid.

2.5. Analysis of wine samples

For the validation of the system four sets of wine samples were analyzed. First a calibration was carried out to check that the system was working correctly and to interpolate the signal obtained from each sample in the calibration curve for both free and the total SO_2 to obtain the sulfur dioxide value. In order to check the repeatability of the system and the drift of the ISFET, a control solution of 15 mg L^{-1} and 80 mg L^{-1} (for free and total SO_2 detection respectively) was measured every five samples. The signal obtained was used as the baseline for correcting the calibration curve.

Firstly, a set of 27 samples were used to validate the flow system against an analytical equipment based on iodimetric determination, *SO₂-Matic 23* (Crison Instruments, Barcelona, Spain). This equipment is based on the Ripper method (International Organization of Vine and Wine, 2009b) and works in a range from 0 to 640 mg L^{-1} of SO_2 and has a resolution of 1 mg L^{-1} . Among them, 14 wine samples were used for the analysis of free sulfur dioxide: 4 white wines (CW1, CW2, CW3, CW4) and 10 red wines (CR1 to CR10). 13 wine samples were used for the determination of total sulfur dioxide: 7 white wines (CW5 to CW10) and 6 red wines (CR2, CR3, CR4, CR10, CR11, CR12).

A second set of 43 wine samples was provided by the Institut Català de la Vinya i el Vi (IRTA-INCAVI) which is an accredited laboratory (ISO 17025). These wines were analyzed by the Paul method (International Organization of Vine and Wine, 2009c). This laboratory has a procedure to regularly validate the method, which consists on a weekly analysis of duplicates of real samples. In order

to determine the accuracy of the method, duplicates of a standard solution are performed monthly and the measurement of uncertainty at 95% is periodically calculated from the results of inter-comparison analysis with other accredited laboratories. The standard solution used is prepared in the laboratory by making additions of sodium meta-bisulfite in a wine matrix without SO_2 . Its concentration is changed every month in order to cover all the accredited range. This validation protocol makes an important difference compared to analyses that could be carried out in non-accredited laboratories and provides a higher reliability of the SO_2 values. Samples analyzed with this method and the flow system were: 10 white wines (W1–W10) and 15 red wines (R1–R15) for free sulfur dioxide and 8 white wines (W11–W18) and 10 red wines (R16–R25) for the determination of total sulfur dioxide.

3. Results and discussion

3.1. Optimization of the flow system variables

The length of the tubes for mixing the sample with the acid solution 1 was firstly optimized using the total sulfur dioxide system and a calibration range of $30\text{--}300 \text{ mg L}^{-1}$. For a 10 cm coil the slope of the regression curve was $-34.7 \pm 0.4 \text{ mV dec}^{-1}$ and for a 20 cm coil $-38.7 \pm 0.5 \text{ mV dec}^{-1}$. The reason for the lower sensitivity when using a shorter coil is due to the final pH of the sample solution: pH was close to 0 at the end of the 20 cm coil, meanwhile this pH was close to 1 when the 10 cm coil was used. The conversion of sulfite species to sulfur dioxide was more efficient at pH near 0. Therefore, the 20 cm coil was chosen for the next measurements.

Regarding the optimization of the flow rate, the sensitivity of the calibration curves (in absolute value) increased until a rate of 0.75 mL min^{-1} (Fig. 2A). However, a rate of 0.50 mL min^{-1} was chosen considering that the difference of sensitivity between both rates ($-38.0 \pm 0.6 \text{ mV dec}^{-1}$ and $-39.0 \pm 0.7 \text{ mV dec}^{-1}$ for 0.50 mL min^{-1} and 0.75 mL min^{-1} , respectively) does not justify the higher consumption of reagents at 0.75 mL min^{-1} .

The use of parallel current and countercurrent flow in both sides of the diffusion cell was evaluated. The results showed a 40% higher sensitivity for the countercurrent flow (slopes of $-40.0 \pm 0.3 \text{ mV dec}^{-1}$ and $-25.5 \pm 0.7 \text{ mV dec}^{-1}$ for counter and parallel current, respectively). Also, a test increasing the time of contact by stopping the flow for 2 min after the 5 min of continuous flow in both sides of the membrane was carried out. However, no significant improvement was obtained (slope of $-39.3 \pm 0.6 \text{ mV dec}^{-1}$ for 5 min in continuous flow plus 2 min in stop flow vs. $-40.0 \pm 0.3 \text{ mV dec}^{-1}$ for just 5 min in continuous flow) and therefore the process was performed without stopping the flow.

For total SO_2 detection, SO_2 bound to aldehydes and ketones must be released under basic conditions. The alkaline pretreatment of the sample was optimized in the chamber defined in Section 2.3 using red and white wine samples in a range of sulfur dioxide from 30 to 105 mg L^{-1} . The best results in terms of accuracy were obtained using an initial stirring step of 3 s and then allowing reacting without stirring for 3 min before driving the sample to the flow system. The relative errors between the values obtained with the iodimetric method and the proposed system were below 10% after this pretreatment optimization.

The proposed method for cleaning the system using HCl was checked for the determination of total sulfur dioxide in five white and red wine's samples, in a range from 15 to 63 mg L^{-1} . Results for the best cleaning conditions (0.3 M HCl, 3 min) can be seen in Fig. 2B. Under these optimized conditions, the recovery of the base-

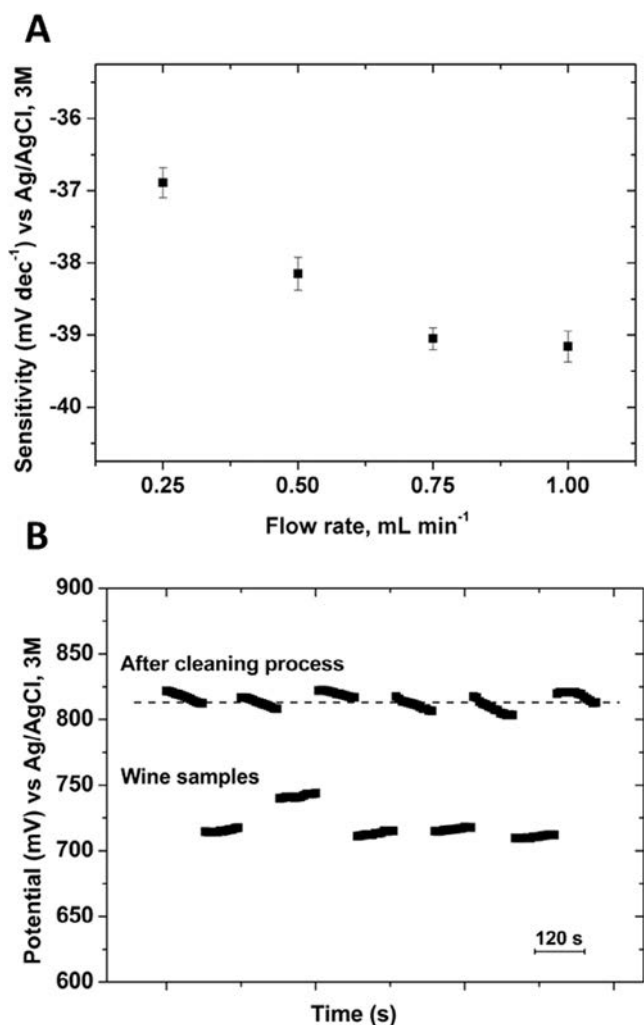


Fig. 2. (A) Sensitivity obtained with the total sulfur dioxide system in the range from 30 to 300 mg L⁻¹ versus the pump flow rate used. Standard deviations of three calibrations carried out consecutively with the same pH-ISFET are drawn as error bars. (B) Signal recorded with the pH-ISFET in the total sulfur dioxide system for five different wine samples and recovery of the baseline after the cleaning process with 0.3 M HCl.

line after each sample was almost complete. For these five measurements, the ISFET signal (in mV) obtained for the baseline after each cleaning process had a relative standard deviation (RSD) of 5.1%.

Regarding to the HCl concentration used in the Acid solution 1 channel, 0.6 M and 4 M were chosen for the determination of free and total sulfur dioxide, respectively. These concentrations were chosen to assure a pH below 1 in the sample solution when it reaches the gas-diffusion membrane thus having all sulfite compounds in the form of SO₂. These were checked with wine samples tested by triplicate. For Acid solution 2 channel, five HCl solutions in a range from 10⁻⁷ M to 10⁻³ M were tested to adjust the pH of the carrier solution in a range from 3.5 to 6.5. The solutions (Acid solution 2 and carrier solution) were prepared separately and mixed under dynamic conditions to assure the stability of the bisulfite, which is unstable at low pH. The results of this study showed that the best sensitivity (-49.1 ± 0.5 mV dec⁻¹) and linear range was obtained when a 2 × 10⁻⁶ M HCl was used in this channel, being the final pH value of the carrier solution 6 (Fig. S3). Considering the chemical equilibriums involved, the predominant specie is SO₂ for pH below 1 but between pH 3 and 6, bisulfite is

the predominant specie. Therefore, at pH 6 all the SO₂ gas diffused from the sample is converted to bisulfite upon contact with the carrier solution. In conclusion, this pH 6 is optimal because it is basic enough to favor a good diffusion of the SO₂ through the membrane, but in turn acid enough to achieve a rapid pH change.

As a summary, the optimum conditions for sulfur dioxide determination were the following: A carrier solution containing 2 × 10⁻⁵ M Na₂SO₃ and 0.02 M NaCl. The pH of this carrier solution was adjusted to pH 6 with a 2 × 10⁻⁶ M HCl solution present in the Acid solution 2 channel. Sample solutions were mixed with the Acid solution 1 (HCl 0.6 M and HCl 4 M for the determination of free and total sulfur dioxide, respectively) to get a value of pH lower than 1. For total SO₂ analysis, a pretreatment process was carried out consisting on adding the same volume of sample and NaOH 4 M in the pre-treatment chamber. Then, the mixture was stirred for 3 s and kept in stop flow during 3 min to achieve complete release of bound SO₂.

3.2. Evaluation of the system response

Using the optimized experimental conditions described above, triplicate calibrations for the free sulfur dioxide system in a concentration range from 1 to 60 mg L⁻¹ and for the total sulfur dioxide in a concentration range from 30 to 300 mg L⁻¹ were carried out. In Fig. 3A and C are depicted the pH-ISFET signals and in Fig. 3B and D, the calibration plots for free and total sulfur dioxide respectively. A linear decrease of the potential (in mV) recorded by the pH-ISFET with the increasing concentration of sulfur dioxide was observed in both cases. The sensitivity (slope) was -49.6 ± 0.7 mV dec⁻¹ (r = 0.998) and -49.4 ± 0.7 mV dec⁻¹ (r = 0.998) for the free and total sulfur dioxide determination, respectively. The limit of detection (LOD) was 0.5 mg L⁻¹ (calculated according to the IUPAC criterion for potentiometric sensors (Inczèdy, Lengyel, & Ure, 1998)).

To study the matrix effect, a calibration in a range from 1 to 60 mg L⁻¹ SO₂ was performed in a solution containing 12% ethanol resulting in a regression curve $E(\text{mV}) = -46.3 \log[\text{SO}_2] + 297.4$ (r = 0.996). Then, common ions were added in this solution giving a curve $E(\text{mV}) = -44.1 \log[\text{SO}_2] + 292.6$ (r = 0.998). Finally, malic and tartaric acid were added, resulting in a similar calibration curve, $E(\text{mV}) = -45.5 \log[\text{SO}_2] + 294.2$ (r = 0.996). These results demonstrate that the presence of ethanol in the calibration solution is decreasing the sensitivity, maybe due to a reduction of the diffusion coefficient of SO₂ through the membrane. Therefore, this compound was used for next experiments in the calibration solution.

During the optimization of the proposed flow system, a unique gas-diffusion membrane was used for a total number of 204 tests, without any decrease of the SO₂ diffusion rate.

3.3. Analysis of wine samples

Once optimized, the system was evaluated with wine samples. A previous calibration was carried out for each set of wine and control solutions of 15 mg L⁻¹ and 80 mg L⁻¹ for free and total SO₂ to check the stability of the system were measured every five samples. These control solutions showed coefficients of variation of 7 and 1% respectively that demonstrates the repeatability of the system.

Two gas-diffusion membranes were used along all these tests (total of 236). The membrane was changed when a decrease higher than 10% in the interpolated concentration of SO₂ was obtained in the control solutions. Unlike the aqueous solutions used during the optimization of the system, the complexity of the wine matrix affected the gas-diffusion membrane, blocking it after 148 consecutive tests.

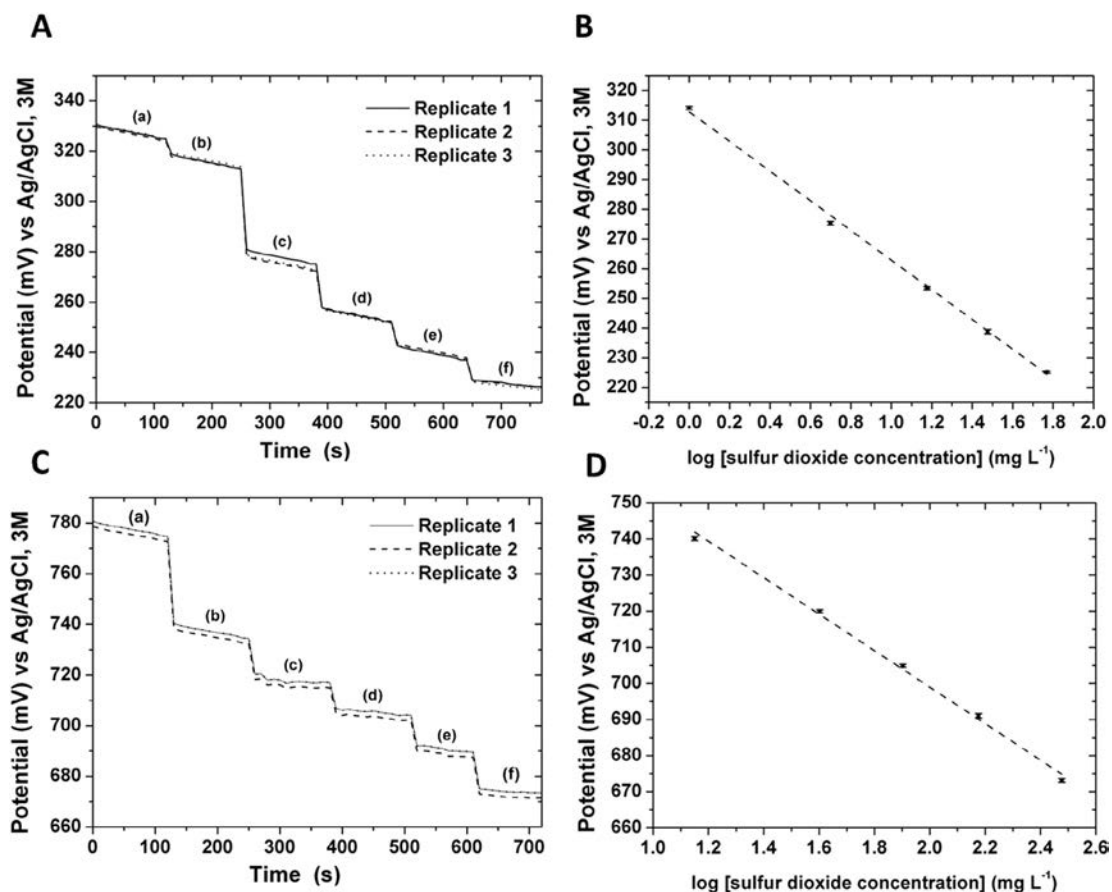


Fig. 3. (A) pH-ISFET signals recorded by triplicate for the free sulfur dioxide system in presence of (a) 0 mg L⁻¹, (b) 1 mg L⁻¹, (c) 5 mg L⁻¹, (d) 15 mg L⁻¹, (e) 30 mg L⁻¹ and (f) 60 mg L⁻¹ of sulfur dioxide. (B) Calibration curve obtained for the free sulfur dioxide system. (C) pH-ISFET signals recorded by triplicate for the total sulfur dioxide system in presence of (a) 0 mg L⁻¹, (b) 30 mg L⁻¹, (c) 40 mg L⁻¹, (d) 80 mg L⁻¹, (e) 150 mg L⁻¹ and (f) 300 mg L⁻¹ of sulfur dioxide. (D) Calibration curve obtained for the total sulfur dioxide system. Standard deviation of triplicated calibrations is drawn as error bars.

Firstly, two sets of 14 and 13 wines for free and the total sulfur dioxide determination, respectively, were analyzed with the flow system and the results were compared with the values obtained with commercial equipment using the iodimetric method. Results of this analysis are shown in Tables S1 and S2 (in the SI) for free and total sulfur dioxide, respectively. For the free sulfur dioxide determination, the relative errors are above -25%, being lower for red wines. The negative values of these errors indicate an underestimation of values for the flow method. These lower values could be associated to a lower rate of SO₂ diffusion through the membrane in the flow system. The lowest values for white wines could be associated with the high volatility of free sulfur in white wines, having in consideration that the wine is opened to the air while the system is performing the analysis (for 5 min). On the other hand, the interferences (mainly ascorbic acid and polyphenols) present for the iodimetric method could cause an extra consumption of iodine during the titration. For total sulfur dioxide, the relative errors are below 16% for both types of wine samples. Among these samples, 10 and 13 average values for free and total sulfur dioxide, respectively, were within the confidence interval of the iodimetric method.

The differences between both methods separating white and red wines were analyzed by the least squares method plotting the data of the flow system vs. the iodimetric method. The results are shown in Fig. 4 and Table 1. For free sulfur dioxide the slope and the correlation coefficient are close to 1 indicating a good agreement between both methods. However, a negative value of the intercept, higher for white wines, indicates an underestimation

of the values obtained with the flow system as was discussed previously. The results of the least square analysis for total sulfur dioxide were the worst due to the variance introduced by the treatment of the sample for releasing the bounded sulfur dioxide. Slopes are close to 1 but regression coefficients are not fitting ideal behavior, especially for white wines samples. The intercept value is higher than for free sulfur dioxide determination, although the uncertainty intervals include zero. This high value is more accentuated for white wines maybe due to the narrow range of concentrations analyzed.

A second set of 43 samples was analyzed by the accredited IRTA-INCAVI laboratory using the Paul method and the flow system (Tables S3 and S4 (in SI)). As shown, for values of free sulfur dioxide lower than 16 mg L⁻¹, the relative errors were high. We can distinguish those values near to 20 mg L⁻¹ for the Paul method (w2, w5, w6, w7, w9) that are showing errors around -40% and those values below 3 mg L⁻¹ with errors above 100% (w10, R4, R13, R14). This last case seems to be related with the limit of quantification of our method. For values above 20 mg L⁻¹ the error is below 10%. However, most of the mean values obtained (corresponding to 16 wine samples) were within the confidence interval of the Paul method.

For total sulfur dioxide, the relative errors were in general below 15% that is quite acceptable. In addition, the mean values of 16 wine samples obtained were within the confidence interval of the Paul method.

The results comparing both methods with the least squares regression are shown in Table 1 and Fig. 5. For free sulfur dioxide

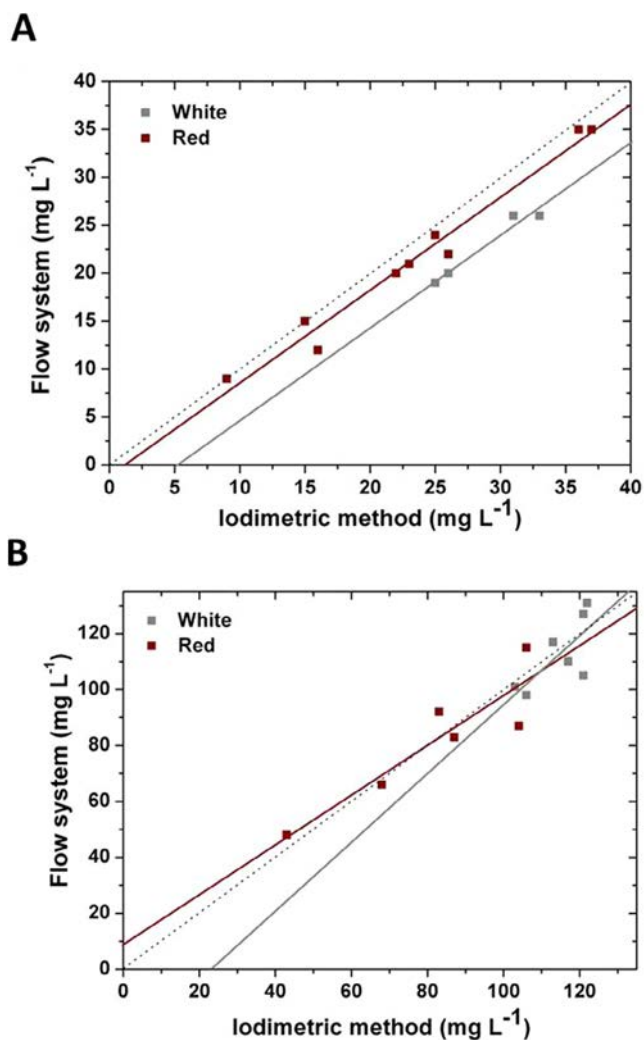


Fig. 4. Results obtained from the least squares analysis using the iodimetric method and the flow system. (A) Free sulfur dioxide determination and (B) total sulfur dioxide determination. The dotted line corresponds to ideal correlation between methods.

the slope in both cases, red and white wines, is close to 1, but again the values of a negative intercept for white wine indicates that the flow system underestimates the SO_2 content due to a low diffusion rate of the SO_2 through the membrane. However, this value is lower than for the Ripper method, which is in accordance with the different sign of errors seen in Table S3. For red wines, the positive value of the intercept indicates the opposite effect, an overestimation of the flow method in accordance with positive values of errors shown in Table S3. On the other hand, for total sulfur dioxide determination, the values of slope and regression coefficient are

Table 1
Least squares parameters obtained comparing the flow system and the iodimetric method (Ripper method) and the Paul method. The uncertainty intervals are calculated at the 95% confidence level.

	Free sulfur dioxide			Total sulfur dioxide		
	Slope	Intercept	r	Slope	Intercept	r
<i>Ripper method</i>						
White wine	1.0 ± 0.1	-4.7 ± 4.2	0.966	1.2 ± 0.5	-25.7 ± 58.8	0.657
Red wine	1.0 ± 0.1	-1.1 ± 1.4	0.985	0.9 ± 0.2	9.8 ± 17.1	0.885
<i>Paul Method</i>						
White wine	0.9 ± 0.2	-2.2 ± 4.9	0.782	1.0 ± 0.1	-3.1 ± 6.1	0.986
Red wine	1.0 ± 0.1	3.4 ± 2.0	0.956	0.9 ± 0.1	4.1 ± 5.2	0.972

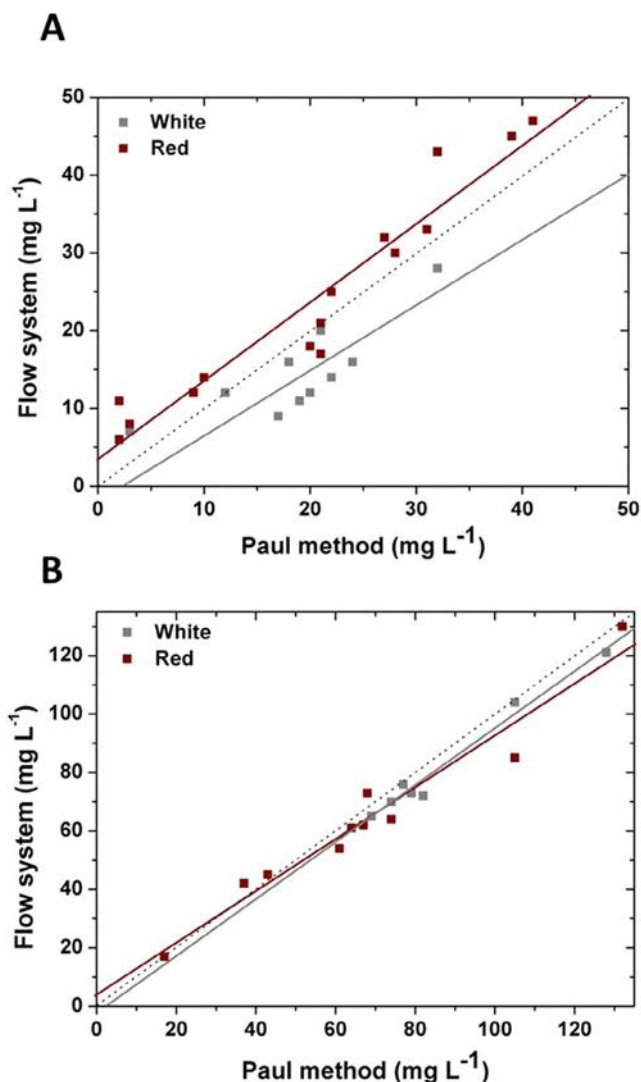


Fig. 5. Results obtained from the least squares analysis using the Paul method and the flow system. (A) Free sulfur dioxide determination and (B) total sulfur dioxide determination. The dotted line corresponds to ideal correlation between methods.

close to 1 indicating a good correlation between both methods. Again the values of intercept indicate certain systematic deviation with the same tendency as for free SO_2 .

4. Conclusions

A flow system for the determination of free and total sulfur dioxide in wine has been fabricated, characterized and evaluated with wine samples. This analytical system uses a gas-diffusion cell

to separate SO₂ from the sample matrix thus avoiding usual interferences for this analyte. The treatment of the sample for detection of total sulfur dioxide is implemented in the same flow system, thus improving the time of the analysis. An indirect detection method is proposed, using a pH-ISFET. This sensor provides advantages like short response time, long-term stability and easy calibration. An optimization of the chemical and the hydrodynamic parameters of the system have concluded in a highly efficient flow system with a sampling rate of 10 min and 15 min per sample for free and total sulfur dioxide respectively which improves the 30 min of the existing methods. The results have demonstrated the feasibility of the proposed system, obtaining a detection range from 1 to 60 mg L⁻¹ and from 30 to 300 mg L⁻¹ for the determination of free and total sulfur dioxide, respectively, with a LOD of 0.5 mg L⁻¹. The evaluation of the system with 70 wine samples and the comparison with two reference methods, the Ripper iodometric method and the Paul titrimetric method, has demonstrated that there is a good correlation between both methods. However, an underestimation of values obtained with the flow system for free sulfur dioxide and white wines is present almost in all sets. This difference between white and red wines is indicating a kind of interference or matrix effect. Most experiments will be carried out to evaluate this effect.

Even though, it is shown that this system could be feasible for a rapid and automatic analysis of wine in the cellar. It is worthwhile to notice that best comparative results are obtained with Paul method, which is an accredited laboratory method.

Acknowledgments

P.G.-G. is grateful to MEINCOM, Spain, for the financial support through a research studentship of the FPI Program. The support of the Electrochemistry-Science and Technology PhD program from the Universitat Autònoma de Barcelona (UAB), Spain, is also acknowledged. This work has made use of the Spanish ICTS Network MICRONANOFABS partially supported by MEINCOM.

Appendix A. Supplementary data

Supplementary data associated with this article can be found, in the online version, at <http://dx.doi.org/10.1016/j.foodchem.2017.02.026>.

References

- Adams, J. B. (1997). Food additive-additive interactions involving sulphur dioxide and ascorbic and nitrous acids: A review. *Food Chemistry*, *59*(3), 401–409.
- Alegret, S., Bartroli, J., Jimenez, C., Delvalle, M., Dominguez, C., Cabruja, E., & Merlos, A. (1991a). Flow-Through pH-ISFET as detector in automated determinations. *Electroanalysis*, *3*(4–5), 349–354.
- Alegret, S., Bartroli, J., Jimenez, C., Delvalle, M., Dominguez, C., Cabruja, E., & Merlos, A. (1991b). PH-ISFET with NMOS technology. *Electroanalysis*, *3*(4–5), 355–360.
- Atanassov, G., Lima, R. C., Mesquita, R. B. R., Rangel, A., & Toth, I. V. (2000). Spectrophotometric determination of carbon dioxide and sulphur dioxide in wines by flow injection. *Analisis*, *28*(1), 77–82.
- Azevedo, C. M. N., Araki, K., Toma, H. E., & Angnes, L. (1999). Determination of sulfur dioxide in wines by gas-diffusion flow injection analysis utilizing modified electrodes with electrostatically assembled films of tetra-ruthenated porphyrin. *Analytica Chimica Acta*, *387*(2), 175–180.
- Bartroli, J., Escalada, M., Jorquera, C. J., & Alonso, J. (1991). Determination of total and free sulfur-dioxide in wine by flow-injection analysis and gas-diffusion using para-aminazo benzene as the colorimetric-reagent. *Analytical Chemistry*, *63*(21), 2532–2535.
- Eschenbruch, R. (1974). Sulfite and sulfide formation during winemaking – Review. *American Journal of Enology and Viticulture*, *25*(3), 157–161.
- Falcone, F., & Maxwell, K. C. (1992). Simultaneous continuous-flow analysis of free and total sulfur-dioxide in wine. *Journal of Agricultural and Food Chemistry*, *40*(8), 1355–1357.
- Fazio, T., & Warner, C. R. (1990). A review of sulfites in foods – Analytical methodology and reported findings. *Food Additives and Contaminants*, *7*(4), 433–454.
- Hans-Ferdinand, L., & Jackson, J. F. (1998). *Wine analysis*. Springer.
- Huang, Y. L., Kim, J. M., & Schmid, R. D. (1992). Determination of sulfite in wine through flow-injection analysis based on the suppression of luminol chemiluminescence. *Analytica Chimica Acta*, *266*(2), 317–323.
- Inczedy, J., Lengyel, T., & Ure, A. A. (1998). *Compendium of analytical nomenclature IUPAC*. Oxford Blackwell Science.
- International Organization of Vine and Wine, (2009a). Compendium of International Methods of Analysis of Wines and Musts. (OIV-MA-AS323-04C).
- International Organisation of Vine and Wine (2009b). Compendium of international methods of analysis of wines and musts. Sulphur dioxide (OIV-MA-AS323-04A).
- International Organisation of Vine and Wine (2009c). Compendium of international methods of analysis of wines and musts. Sulphur dioxide (OIV-MA-AS323-04B).
- International Organisation of Vine and Wine (2015). International standard for the labelling of wines.
- Jimenez, C. B., Abramova, N., & Baldi, A. (2005). ISFET based sensors: fundamentals and applications. In C. A. Grimes, E. C. Dickey, & M. V. Pishko (Eds.), *Encyclopedia of Sensors*. New York: American Scientific Publishers.
- Jimenez-Jorquera, C., Orozco, J., & Baldi, A. (2010). ISFET based microsensors for environmental monitoring. *Sensors*, *10*(1), 61–83.
- Kalimuthu, P., Tkac, J., Kappler, U., Davis, J. J., & Bernhardt, P. V. (2010). Highly sensitive and stable electrochemical sulfite biosensor incorporating a bacterial sulfite dehydrogenase. *Analytical Chemistry*, *82*(17), 7374–7379.
- Kuban, P., Janos, P., & Kuban, V. (1998). Gas diffusion-flow injection determination of free and total sulfur dioxide in wines by conductometry. *Collection of Czechoslovak Chemical Communications*, *63*(6), 770–782.
- Moliner-Abad, B., Alonso-Lomillo, M. A., Dominguez-Renedo, O., & Arcos-Martinez, M. J. (2014). Sulfite oxidase biosensors based on tetrathiafulvalene modified screen-printed carbon electrodes for sulfite determination in wine. *Analytica Chimica Acta*, *812*, 41–44.
- Oliveira, S. M., Lopes, T. I. M. S., Toth, I. V., & Rangel, A. O. S. S. (2009). Development of a gas diffusion multicommuted flow injection system for the determination of sulfur dioxide in wines, comparing malachite green and pararosaniline chemistries. *Journal of Agricultural and Food Chemistry*, *57*(9), 3415–3422.
- Osborne, B. G., & Tyson, J. F. (1988). Flow-injection analysis – A new technique for food and beverage analysis. *International Journal of Food Science and Technology*, *23*(6), 541–554.
- Paul, F. (1958). *Die alkalimetrische Bestimmung der freien, gebundenen un gesamten schwefligen Säure mittels des Apparates von Lieb und Zacherl*. Mitteilung Klosterneuburg Serie A, 8, 21–27.
- Rawal, R., & Pundir, C. S. (2013). Development of electrochemical sulfite biosensor based on SOX/PBNPs/PPY modified Au electrode. *Biochemical Engineering Journal*, *71*, 30–37.
- Ripper, M. (1892). *Schweflige Säure in Weinen und deren Bestimmung*. *Journal für praktische Chemie/Chemiker-Zeitung*, *46*, 428–473.
- Ruiz-Capillas, C., & Jimenez-Colmenero, F. (2008). Determination of preservatives in meat products by flow injection analysis (FIA). *Food Additives and Contaminants Part A-Chemistry Analysis Control Exposure & Risk Assessment*, *25*(10), 1167–1178.
- Sarudi, I., & Kelemen, J. (1998). Determination of sulphur and total sulphur dioxide in wines by an ICP-AES method. *Talanta*, *45*(6), 1281–1284.
- Segundo, M. A., Lima, J., & Rangel, A. (2004). Automatic flow systems based on sequential injection analysis for routine determinations in wines. *Analytica Chimica Acta*, *513*(1), 3–9.
- Thanh, N. T. K., Decnopweever, L. G., & Kok, W. T. (1994). Determination of sulfite in wine by flow-injection analysis with indirect electrochemical detection. *Fresenius Journal of Analytical Chemistry*, *349*(6), 469–472.
- Usseglio-Tomasset, L. A. B. P. D. (1984). *La prima costante di dissociazione dell'acido solforoso*. *Vini d'Italia*, *26*(5), 7–14.



Contents lists available at ScienceDirect

Analytica Chimica Acta

journal homepage: www.elsevier.com/locate/aca

Robust L-malate bienzymatic biosensor to enable the on-site monitoring of malolactic fermentation of red wines



Pablo Giménez-Gómez^a, Manuel Gutiérrez-Capitán^{a,*}, Fina Capdevila^b, Anna Puig-Pujol^b, Cesar Fernández-Sánchez^a, Cecilia Jiménez-Jorquera^a

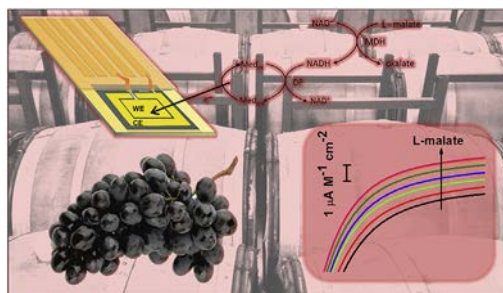
^a Instituto de Microelectrónica de Barcelona (IMB-CNM), CSIC, Campus UAB, 08193, Bellaterra, Spain

^b Institut Català de la Vinya i el Vi (IRTA-INCAVI), Plaça Agora 2, 08720, Vilafranca del Penedès, Spain

HIGHLIGHTS

- Bienzymatic electrochemical biosensor for L-malate.
- Malate dehydrogenase and diaphorase enzymes entrapped into an electrosynthesized polypyrrole film.
- Optimized redox mediator also incorporated into the polymeric film.
- Long-term stability for over 37 days.
- Application to L-malic acid determination during the malolactic fermentation of red wines.

GRAPHICAL ABSTRACT



ARTICLE INFO

Article history:

Received 21 June 2016

Received in revised form

2 November 2016

Accepted 29 November 2016

Available online 4 December 2016

Keywords:

Amperometric bienzymatic biosensor
Electrosynthesized polypyrrole membrane
Immobilization of redox mediator
L-malic acid analysis
Malolactic fermentation

ABSTRACT

Monitoring the malolactic fermentation process is strictly required to guarantee the sensorial quality and freshness of red wines. This could be achieved by in-field and real-time continuous measurements of L-malate concentration in the fermentation tanks. The potential of a miniaturized amperometric bienzymatic biosensor as an analytical tool to be applied in such scenario is described in this paper. The biosensor comprises a thin-film gold electrode as transducer, malate dehydrogenase (MDH) and diaphorase (DP) enzymes together with nicotinamide adenine dinucleotide (NAD⁺) cofactor as the selective receptor and an adequate redox mediator to record the corresponding amperometric signal. Three different biosensor architectures are studied, whose main differences lie in the immobilization of the different chemical components onto the electrode surface. In all cases a fast-electrosynthesized polypyrrole (PPy) membrane is generated for this purpose. The experimental conditions are optimized and the best architecture shows a sensitivity of $1365 \pm 110 \text{ mA M}^{-1} \text{ cm}^{-2}$ and a detection limit of $6.3 \times 10^{-8} \text{ M}$ in a concentration range of $1 \times 10^{-7} \text{ M} - 1 \times 10^{-6} \text{ M}$. The biosensor presents an excellent working stability as it retains above 90% of its sensitivity after 37 days, thus enabling the monitoring of the malolactic fermentation of three red wines. The obtained results show excellent agreement with the standard colorimetric method.

© 2016 Elsevier B.V. All rights reserved.

1. Introduction

L-malic acid is one of the principal organic acids in grapes [1]. It is mainly synthesized via glycolysis and its concentration depends

* Corresponding author. Instituto de Microelectrónica de Barcelona (IMB-CNM), CSIC, Campus de la UAB, 08193, Bellaterra, Barcelona, Spain.

E-mail address: manuel.gutierrez@csic.es (M. Gutiérrez-Capitán).

on the climatic conditions and temperature during harvesting and crushing of the grapes [2]. However, the presence of L-malic acid affects the final quality of the wine by deteriorating its biochemical and microbial stability, and hence its sensorial quality and freshness. This is why an adjustment of the acidity is performed in red wines by malolactic fermentation (MLF), wherein the L-malic acid, in a concentration of $1\text{--}3\text{ g L}^{-1}$ ($7.5 \times 10^{-3} \text{--} 2.2 \times 10^{-2}\text{ M}$), is converted to L-lactic acid and CO_2 by lactic acid bacteria action [3]. During alcoholic fermentation, yeast strain converts grape sugars, glucose and fructose, into ethanol. Once these sugars are consumed, the yeast concentration decreases and the lactic acid bacteria (LAB) perform the malolactic fermentation using the malolactic enzymes [4]. Natural or induced malolactic fermentation is carried out in the production of all red wines.

The conventional analytical methods for the determination of L-malic acid in wine are chromatography [5–7] and electrophoresis [8,9]. These methods require the use of bulky expensive equipment and are time consuming. Alternative enzymatic approaches based on the detection of nicotinamide adenine dinucleotide (NADH) by absorbance have been also reported [10]. In them, L-malic acid is oxidized to oxaloacetate in presence of NAD^+ and catalyzed by L-malate dehydrogenase (L-MDH) enzyme. Then, the produced NADH is detected by absorbance at 340 nm and stoichiometrically related to the L-malic acid in the sample. However, this procedure has to be carried out in an external laboratory and is reagent consuming. The application of biosensors for in-field determination of malic acid appears to be an excellent option for the strict and continuous control of this fermentation process. These are based on different enzymatic approaches [11–15], but the most applied one makes use of a cascade bienzymatic reaction involving the catalytic reactions of L-MDH enzyme in the presence of NAD^+ as co-factor, and consecutively of Diaphorase (DP) enzyme coupled to an appropriate redox mediator. The readout of this reaction can be carried out by spectrophotometry [16] or amperometry [17,18].

In this work, the potential of an amperometric biosensor for in-field detection of L-malate is presented. Amperometric biosensors are characterized by its small size, low manufacturing costs, potential portability for in-situ analysis, low volume reagent consumption, wide linear response range and high selectivity and reproducibility [19]. Different redox mediators can be selected to record the biosensor amperometric signal. The careful selection of a mediator is fundamental for the successful performance of the developed device [20]. In the case of those NAD^+ -dependent enzyme reactions, the mediator participates in the electrocatalytic regeneration of the NAD^+ cofactor. In this context, the most commonly used mediators are organics dyes [21] and inorganic redox ions [22]. Although the mediator is commonly added in solution during the biosensor performance, a lot of work has also been done on the incorporation of the mediator on the transducer surface together with the rest of biochemicals (enzymes and co-factors) in order to construct reagentless biosensors that are easier to use and show enhanced sensitivities [23]. Selective immobilization processes are based on physically entrapment in electro-polymerized layers, among others [24]. One very convenient polymer is polypyrrole (PPy) that can be easily processed in aqueous solutions at neutral pH, shows good biocompatibility, conductivity and stability.

In this work, a PPy layer has been generated on the surface of a thin-film gold electrode with the aim of entrapping the selected chemical components and thus constructing an electrochemical bienzymatic biosensor for the L-malate determination. Different redox mediators have been initially tested for selecting the most suitable one in terms of signal reversibility, low oxidation potential and compatibility with the PPy membrane. A comparative study has been then conducted with three different biosensor

architectures based on the partial or full immobilization of the required chemical reagents in the PPy membrane. The biosensor performances have been assessed in terms of working stability and analytical characteristics. The selected biosensor architecture has been eventually applied to the L-malic acid monitoring during the MLF of three red wines.

2. Materials and methods

2.1. Reagents and solutions

All reagents were of high purity, analytical grade or equivalent and were purchased from Sigma-Aldrich, unless stated otherwise. All solutions were prepared using de-ionized water. For the cleaning of the electrodes, ethanol 96% and 6 M sulfuric acid (H_2SO_4) were used. Diaphorase (DP, from *Clostridium kluyveri*, lyophilized powder, $3\text{--}20\text{ U mg}^{-1}$ solid) and β -Nicotinamide adenine dinucleotide hydrate (NAD^+ , $\geq 96.5\%$ enzymatic, from yeast) were stored in a freezer at $-20\text{ }^\circ\text{C}$ and used as received. $15\text{-}\mu\text{L}$ $2.4\text{ U }\mu\text{L}^{-1}$ Malate dehydrogenase (MDH, from porcine heart, freeze-dried material, $\geq 119\text{ U mg}^{-1}$ solid, Sorachim, S.A.) aliquots were prepared and stored in a freezer at $-20\text{ }^\circ\text{C}$. Pyrrole (reagent grade, 98%) was distilled and stored in a freezer at $-20\text{ }^\circ\text{C}$. A 0.05 M phosphate buffer solution (PB) prepared with potassium phosphate monobasic (KH_2PO_4) and adjusted at pH 7 with NaOH 0.1 M was used for all the optimization and electrochemical characterization experiments.

A set of PB solutions containing 2 mM of different compounds (2,6-Dichlorophenolindophenol sodium salt hydrate $\geq 90\%$, Gallo-cyanine 90%, Toluidine Blue O 80%, Nile Blue A $\geq 75\%$, 1,1'-Dimethylferrocene 95%, Methyl Red sodium salt, Tetrathiafulvalene 97%, Hexaammineruthenium (III) chloride ($\text{Ru}(\text{NH}_3)_6\text{Cl}_3$, 98%) (HAR) and Potassium ferricyanide ($\text{K}_3[\text{Fe}(\text{CN})_6]$, $\geq 99\%$)) were prepared for the optimization study of the redox mediator.

A set of PB solutions containing 2 mM potassium ferricyanide, 2 mM L-malate (L(-)-Malic acid, Reagent Plus $> 99.9\%$), 5 mM NAD^+ , 0.5 U DP and a different MDH activity (0 U, 1 U, 2 U, 3 U, 4 U and 5 U), were prepared for the optimization of the DP:MDH ratio. A set of PB solutions containing 2 mM potassium ferricyanide, 2 mM L-malate, 0.5 U DP, 3 U MDH and different NAD^+ concentrations (0 mM, 0.05 mM, 0.1 mM, 0.2 mM, 0.5 mM, 1 mM and 2 mM) were prepared for the optimization of the enzymes:co-factor ratio. For the chronoamperometric L-malate detection, a PB solution containing 0.1 M KCl, 5 mM NAD^+ and a L-malate concentration from $1 \times 10^{-7}\text{ M}$ to $1 \times 10^{-5}\text{ M}$ was used.

For the interference study, a PB solution with 0.1 M KCl, 5 mM NAD^+ and $5 \times 10^{-7}\text{ M}$ of the analyzed interfering compounds was prepared. The studied interferents were glycerol, glucose, gluconic acid, fructose, acetic acid, citric acid, ethanol, L-Lactate (L(+)-lactic acid, $\geq 99\%$), tartaric acid and ascorbic acid (all them purchased from Panreac, Spain).

2.2. Devices and equipment

The thin-film gold electrodes used as transducers were fabricated on silicon substrates at the Instituto de Microelectrónica de Barcelona (IMB-CNM) according to standard microelectronic technology [25]. The chip size was $3 \times 3.5\text{ mm}^2$ and included a cell with two electrodes, namely the working electrode (WE) with an area of 1.62 mm^2 and the counter electrode (CE) with an area of 2.27 mm^2 (Fig. S1 in Supporting Information (SI)). The chips were wire-bonded on a printed-circuit board (PCB) and packaged using Ebecryl photocurable polymer following a standardized photolithographic process developed at the IMB-CNM [26].

A 20- μL poly (methyl methacrylate) (PMMA) cell was fabricated

for the electrosynthesis of the polymeric membrane. Detailed information of this electrochemical cell is described in a previous work [27].

Cyclic voltammetry (CV) and chronoamperometry were performed at room temperature with an Autolab electrochemical workstation (PGSTAT-100 potentiostat – galvanostat, Ecochemie, Utrecht, The Netherlands) connected to a PC with GPES (General Purpose Electrochemical System) software. During the biosensor characterization, the three-electrode cell was completed with a Ag/AgCl (3.0 M KCl) double junction (Orion 92-02-00, Thermo Fisher Scientific Inc., Beverly, USA) reference electrode, and the integrated on-chip auxiliary electrode.

The morphological characterization of the polymeric films was carried out by scanning electron microscopy (SEM, Auriga from Carl Zeiss, Spain) and focused ion beam (FIB, Crossbeam 1560 XB from Carl Zeiss).

2.3. Optimization of the DP:MDH and (DP:MDH):NAD⁺ ratios

The enzymes and co-factor relative concentrations in solution were optimized in 96-well low-binding polystyrene ELISA plates (Corning Incorporated, United States) by absorbance measurements with a Thermo Electron Multiskan EX plate reader (Thermo Fisher Scientific). Firstly, DP:MDH ratio was studied using 100- μ L PB solutions containing 0.1 M KCl, 2 mM potassium ferricyanide, 2 mM L-malate and different amounts of the two enzymes. A fixed DP activity of 0.5 U was set and six activities of MDH (0 U, 1 U, 2 U, 3 U, 4 U and 5 U) were tested, these resulting in DP:MDH ratios of 1:0, 1:2, 1:4, 1:6, 1:8 and 1:10, respectively. Secondly, (DP:MDH):NAD⁺ ratio was optimized using 100- μ L PB solutions containing 0.1 M KCl, 2 mM potassium ferricyanide, 2 mM L-malate, 0.5 U DP, 3 U MDH and different amounts of NAD⁺ (0 mM, 0.05 mM, 0.1 mM, 0.2 mM, 0.5 mM, 1 mM and 2 mM) whose corresponding (DP:MDH):NAD⁺ ratios were 1:0, 1:2, 1:4, 1:6, 1:8 and 1:10, respectively. Each solution was analyzed in triplicate after being stirred for 45 s and then leaving it undisturbed for 10 min for the enzymatic reaction to take place. Then, the absorbance value of the unreacted potassium ferricyanide at 405 nm wavelength was recorded [28].

2.4. Voltammetric study with different redox mediators

Following previous studies on the electrocatalytic oxidation of NADH [29,30], eight organic compounds and two inorganic salts were tested as redox mediators. Cyclic voltammetric experiments were performed using the thin-film gold electrodes applied in this work, in 10 mL PB solutions (pH 7) containing 0.1 M KCl and 2 mM of each redox mediator. In the case of 1,1'-dimethylferrocene and tetrathiafulvalene, a 10% ethanol was added to the aqueous solutions in order to improve their solubility. The redox processes ascribed to each mediator were compared in terms of reversibility, current and redox potential values as well as solubility. Ideally, a mediator showing a fully reversible redox process taking place at low potentials, in order to avoid interferences from other species that may be present in the wine samples, and showing a high current density is pursued. Also, these species should have good water solubility to allow for the strict control of the polypyrrole membrane electrosynthesis.

The redox mediators that best met all these characteristics were incorporated into a PPy membrane generated on the transducer surface, as described below.

2.5. Electrosynthesis of the polymeric membranes

Before the electrogeneration of the PPy layer, the thin-film gold electrodes were cleaned and activated [25]. The conditions for the

electrosynthesis on the surface of the gold transducers were optimized elsewhere [27]. Using the PMMA cell mentioned above and a Ag wire as pseudo-reference electrode, a +0.85 V potential was applied in a PB solution containing 0.4 M pyrrole (monomer) and 0.1 M KCl (counter-ion). The PPy membrane was electrosynthesized in two consecutive potentiostatic steps. In the first step, the redox mediator was entrapped in a PPy membrane for ensuring the good electron transfer with the transducer surface and avoiding competition with the other species (enzymes and cofactor) during the membrane growth. The concentration of the redox mediator was fixed to 10 mM for ensuring its excess against the other chemical reagents involved in the bienzymatic process. The accumulation charge during this electrosynthesis was fixed to 250 mC cm⁻². In the second step, the enzymes (MDH and DP) and the cofactor (NAD⁺) were entrapped in a new PPy membrane, fixing the accumulation charge to 500 mC cm⁻². This accumulation charge enabled the efficient entrapment of enzymes as has been previously demonstrated by our group [27]. Current profiles recorded during the potentiostatic generation of the PPy/redox mediator and the PPy/enzyme films are depicted in Fig. S2 (in the SI).

Using these electrosynthesis conditions, three different biosensor architectures that differ in the immobilization of the different components, were assessed: Biosensor 1, the mediator was not immobilized and the sensor performance was tested in solutions containing the selected mediator; Biosensor 2, the NAD⁺ cofactor was not immobilized and the sensor performance was tested in solutions containing this cofactor and Biosensor 3, both the redox mediator and the cofactor were immobilized on the electrode surface.

2.6. Chronoamperometric measurements

Chronoamperometric measurements were carried out by applying a set overpotential that depended on the selected redox mediator. This potential allows re-oxidizing the reduced mediator generated during the bienzymatic process and the faradaic current recorded is stoichiometrically related to the L-malate concentration in the sample (see more details in Fig S3 in SI). The biosensors were calibrated in 10 mL PB solutions (pH 7) containing L-malate in a concentration range between 1 \times 10⁻⁷ M and 1 \times 10⁻⁵ M. All the measurements were done by triplicate.

Firstly, a study on the working stability of the different biosensor architectures was performed. The study consisted of periodic calibrations for over 40 days. The biosensors were stored in PB at 4 °C when not in use.

Once the more stable architecture was selected, the biosensor performance was assessed in terms of repeatability, reproducibility, sensitivity, linear range and limit of detection to L-malate using three biosensors fabricated under the same experimental conditions.

In order to evaluate the selectivity of the optimized biosensor, chronoamperometric measurements were performed in PB solutions containing 5 \times 10⁻⁷ M concentrations of glycerol, glucose, gluconic acid, fructose, acetic acid, citric acid, ethanol, L-lactate, tartaric acid, or ascorbic acid as interferences.

2.7. Analysis of real samples coming from wine malolactic fermentation processes

A study with wine samples was conducted in order to evaluate the applicability of the developed bienzymatic biosensor. Three red wines (2013 vintage, from Tarragona, Spain) based on Marcellane, Petit Verdot and Syrah grape varieties, were provided by the Catalan Institute of Vineyard and Wine (IRTA-INCAVI). In these

wines, the malolactic fermentation was induced by inoculation of a strain of *Oenococcus oeni* lactic acid bacteria. The analyzed samples were collected periodically during the malolactic fermentation process. They had a concentration of L-malic acid from 0 to 2×10^{-2} M ($0\text{--}2.5$ g L $^{-1}$). Ten samples from the Marcelanne wine ("Wine 1") along 32 days, 5 samples from the Petit Verdot wine ("Wine 2") along 15 days and 11 samples from the Syrah wine ("Wine 3") along 34 days were analyzed with the developed biosensor. These samples were diluted 1:20000 ("Wine 1"), 1:25000 ("Wine 2") and 1:10000 ("Wine 3") in PB solution to adjust the L-malic acid concentration to the linear range of the amperometric biosensor. The high sensitivity of the biosensor allowed these high dilutions of the wine samples, thus avoiding the potential matrix effects that could interfere in the determination. The results obtained were compared with the standard enzymatic method used by the IRTA-INCAVI. This is an enzymatic catalyzed reaction between the L-malate and the NAD $^{+}$ to produce NADH, whose concentration increase is measured by absorbance at 340 nm and stoichiometrically related to the L-malate concentration in the samples [10].

3. Results and discussion

3.1. Selection of the DP:MDH and (DP:MDH):NAD $^{+}$ ratios

The enzymes and cofactor relative concentrations were optimized and results are shown in Fig. 1. The absorbance value decreased with the increase of MDH activity up to 3 U, remaining constant for higher values. Thus, the optimum DP:MDH ratio was 1:6. Then, the DP and MDH activities were fixed to 0.5 U and 3 U, respectively, and the NAD $^{+}$ concentration was increased from 0 to 2 mM. The recorded absorbance values levelled off for NAD $^{+}$ concentrations above 0.5 mM. Thus, the (DP:MDH):NAD $^{+}$ ratio was set to 2:1. These ratios were selected for the further biosensor fabrication.

3.2. Selection of the redox mediator

All the selected redox mediators of this study have previously been applied in amperometric biosensing [29,30]. The corresponding cyclic voltammograms recorded with the thin-film gold electrodes are shown in Figs. S4 and S5 in SI. Unlike in those

reported studies that make use of these mediators, the expected quasi-reversible signals could not be recorded with all of them. This might be related to the use of a gold electrochemical transducer instead of the carbon-based transducers applied in those works. Table 1 includes the electrochemical parameters extracted from these voltammograms. Using the oxidation potential (E_{ox}) as the initial parameter to select these species, the lowest values were obtained for Gallocyanine, Toluidine Blue O and HAR (-250 mV, -275 mV and -180 mV, respectively). Among these three redox mediators, Gallocyanine and Toluidine Blue O showed a similar peak potential separation (ΔE_p), while this is about two times larger for HAR. Then, the ratio of oxidation to reduction peak currents was compared. Values around 1 indicate the absence of coupled chemical reactions. This is the case for Gallocyanine and HAR, while is around 2.1 for Toluidine Blue O. These three redox mediators showed oxidation peak current densities higher than $250 \mu\text{A cm}^{-2}$. Besides, all three are fully water soluble, therefore the electro-synthesis conditions of the PPy would not be modified by presence of any organic solvent.

Then, the electrogeneration of the PPy/mediator membrane on the surface of the gold transducers was carried out in solutions containing 10 mM of each of these three redox mediators. Toluidine Blue O formed a blue precipitate during the polymerization process. This is likely to be related to the polymerization of this redox mediator by the one-electron oxidation of the NH $_2$ containing moiety and the formation of a radical cation at the potential applied during the PPy electro-synthesis membrane [31]. By contrast, both Gallocyanine and HAR could be entrapped in the PPy membrane and the time to achieve an accumulation charge of 250 mC cm^{-2} was 70 and 30 s, respectively. The resulting membranes were rinsed with PB, tested by cyclic voltammetry and then stored immersed in PB solution at 4 °C until the following test. After 24 h, the PPy/Gallocyanine-modified transducer nearly lost all its voltammetric response and the PB solution turned blue-colored, meaning that the mediator leached from the polypyrrole membrane. This may be due to charge repulsion between the positively charged pyrrole and the Gallocyanine molecules during the PPy membrane electro-synthesis that would make these species not to be efficiently entrapped and thus to be easily leached. The same experiment was repeated with PPy/HAR-modified transducer, this keeping its voltammetric response after the 24-h period. Therefore, this redox mediator was selected for the fabrication of the biosensor architecture.

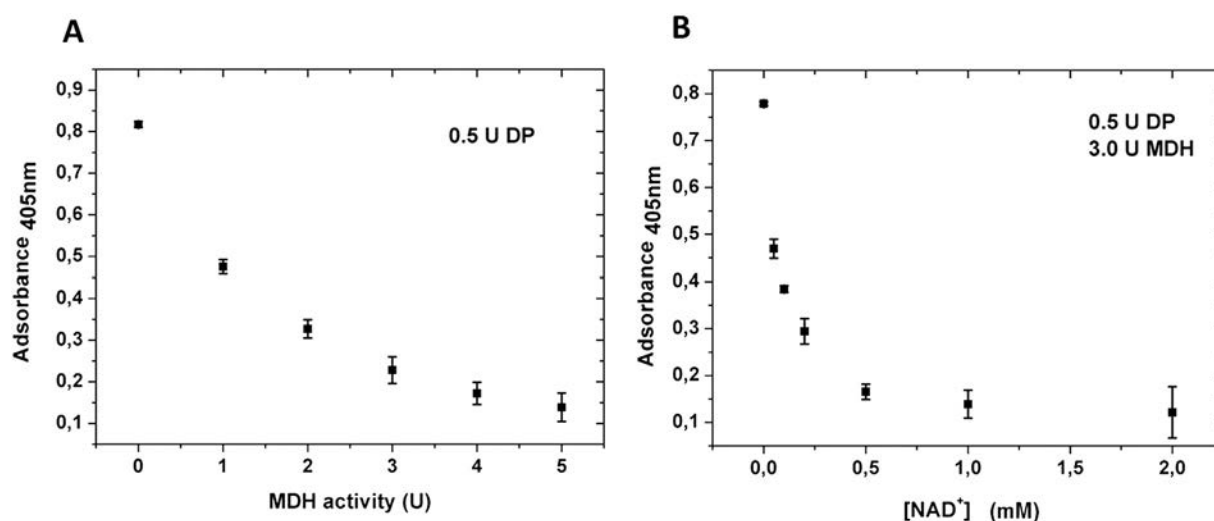


Fig. 1. Absorbance recording of ferricyanide for different biocomponents ratios a) DP:MDH and b) (DP:MDH):NAD $^{+}$. Measurements were carried out in PB solution containing 2 mM potassium ferricyanide, 2 mM L-malate and different concentration of DP, MDH and NAD $^{+}$. Each point corresponds to the mean value of three replicates and the error bars represents the standard deviation.

Table 1

Chemical structures of the studied redox mediators and their main redox values obtained in solution: oxidation potential (E_{ox}), peak potential separation (ΔE_p) and the ratio between the oxidation and the reduction peak currents (I_{ox}/I_{red}).

Redox mediator	Chemical structure	E_{ox}/mV	$\Delta E_p/mV$	$ I_{ox}/I_{red} $
2,6-Dichlorophenolindophenol sodium salt hydrate		10	55	0.4
Gallocyanine		-250	59	0.9
Toluidine Blue O		-274	66	2.1
Nile Blue A ^a		-	-	-
1,1'-Dimethylferrocene		68	57	1.7
Methyl Red		126	205	0.9
Ferrocene		190	85	1.3
Tetrathiafulvalene		110	94	1.8
Hexaammineruthenium (III) chloride	[Ru(NH ₃) ₆]Cl ₃	-180	80	0.9
Potassium ferricyanide(III)	K ₃ [Fe(CN) ₆]	220	120	0.8

^a There is no signal of the oxidation peak current.

3.3. Selection of the biosensor architecture

The working stability of the three different biosensor architectures, described in Section 2.5, was analyzed for over 40 days. The lifetime estimated from the percentage of the initial sensitivity kept over time, is shown in Fig. 2. In the three cases, an initial decrease of the sensitivity is observed during the first eight days, probably related to partial leaching of the chemical species not tightly immobilized within the PPy membrane. This decrease was more pronounced for biosensor 3 (all reagents in the PPy membrane), which lost 30% sensitivity after 5 days and 45% after 8 days, and biosensor 1 (redox mediator in solution), which lost 10% sensitivity after 3 days, 20% after 7 days and 40% after 18 days. However, biosensor 2 architecture (NAD⁺ in solution) just lost 10% after 37 days. The decrease in sensitivity of biosensor 1 and 3 is likely to be due to the fast decomposition of the entrapped NAD⁺ [32].

Biosensor 2 appeared to be the most suitable for the monitoring of L-malic acid during the red wine fermentation process, taking into account that it maintained around 90% of the initial sensitivity after 37 days. Then it suddenly decreased to 30% of the initial value after 42 days, probably due to the denaturation of the immobilized enzymes. This architecture was then selected and fully characterized, as described in the following sections.

3.4. Morphological characterization of the PPy films

The thickness and morphology of the electrogenerated PPy membranes are influenced by some experimental parameters, such as applied potential and accumulated charge during the electro-synthesis, counter-ion required for the PPy polymerization, as well as the chemical and biochemical species entrapped in the resulting membrane and present in the polymerization solution [33]. The

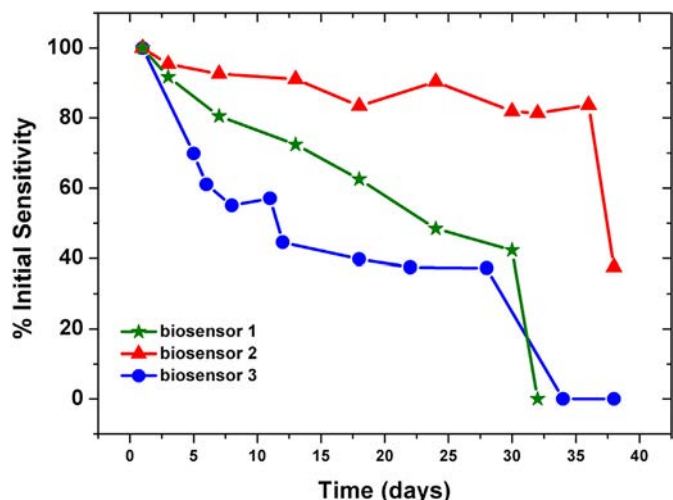


Fig. 2. Comparative study of the working stability along 38 days for the three proposed biosensor architectures: biosensor 1 (green colored stars), biosensor 2 (red colored triangles), and biosensor 3 (blue colored circles). (For interpretation of the references to colour in this figure legend, the reader is referred to the web version of this article.)

PPy membrane thicknesses, measured by FIB, (Fig. S6 in SI) was $1.3 \mu\text{m}$ and $2.5 \mu\text{m}$ for the PPy/HAR and the PPy/(DP:MDH) membranes, respectively. This difference is in accordance with the electrical charge associated to the electro-synthesis of both membranes, being twice for the PPy/(DP:MDH) membrane than that of the PPy/HAR one. An additional SEM image (Fig. S6 in SI) showed the homogeneity and roughness of the PPy membranes.

3.5. Evaluation of the biosensor performance

The optimized biosensor was calibrated by chronoamperometry in PB solutions containing 0.1 M KCl , 5 mM NAD^+ and a L-malate concentration ranging from $1 \times 10^{-7} \text{ M}$ to $1 \times 10^{-5} \text{ M}$. A -0.15 V potential (vs. Ag/AgCl) was chosen considering the voltammetric response of the selected redox mediator (Fig. S5 de la SI), at which the HAR reduced species generated by the enzymatic reaction are oxidized back to the HAR. Results are shown in Fig. 3A. The sensor response followed an exponential trend, and the current started to level off at 70 s time after initiating the measurement. The signal was recorded during 120 s and the mean current density value of

the last 20 s was used as analytical signal. As expected, the recorded current density increased with the L-malate concentration. Then, it can be said that the biosensor response was 70 s and the overall assay time was set to 120 s . The calibration curve is shown in Fig. 3B. A linear range was observed in a concentration range from $1 \times 10^{-7} \text{ M}$ – $1 \times 10^{-6} \text{ M}$ (1.3×10^{-5} – $1.3 \times 10^{-4} \text{ g L}^{-1}$) of L-malate with a sensitivity of $1365 \pm 110 \text{ mA M}^{-1} \text{ cm}^{-2}$ ($r = 0.998$, $n = 5$). A limit of detection of $6.3 \times 10^{-8} \text{ M}$, calculated using the 3σ IUPAC criterion, was obtained. For L-malate concentration above $1 \times 10^{-6} \text{ M}$, the biosensor response was saturated, this following the usual behavior of a Michaelis-Menten kinetic process. Regarding the biosensor reproducibility, three different devices were calibrated on the same day, obtaining a relative standard deviation (RSD) of the sensitivity lower than 10% .

The biosensor selectivity to L-malate was assessed considering the possible interferences found in wine. Results are shown in Fig. 4. Among all of them, just ascorbic acid produced a non-negligible biosensor response that is related to the irreversible electrochemical oxidation that starts at the applied potential of -0.15 V and whose maximum anodic peak current appears at -0.066 V [34]. Although ascorbic acid exists in small quantities in grapes (around 10 mg L^{-1} or $7.5 \times 10^{-5} \text{ M}$), it rapidly disappears during the fermentation and initial aeration processes [3]. Then, it is anticipated that the red wine samples coming from the

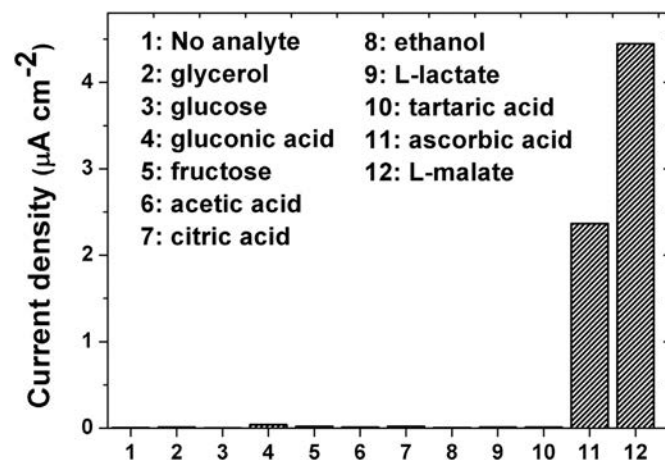


Fig. 4. Current density response of the biosensor in solutions containing different interferents at a concentration of $5 \times 10^{-7} \text{ M}$.

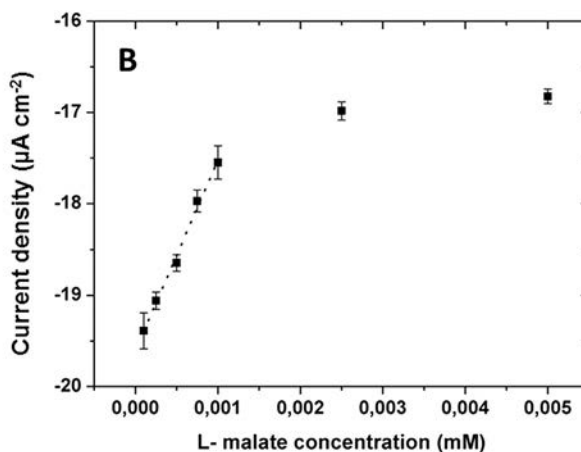
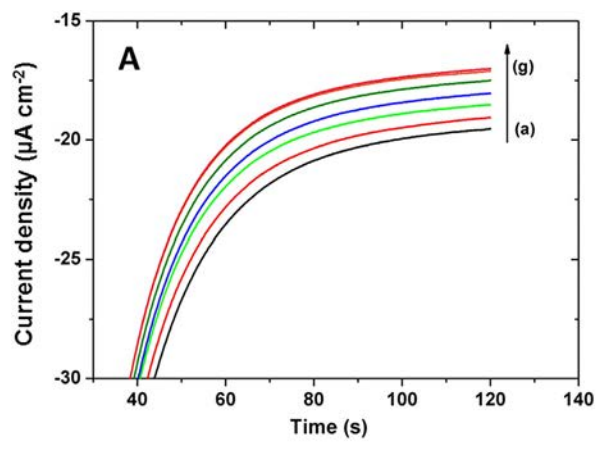


Fig. 3. A) Chronoamperometric response of the developed biosensor for L-malate concentrations in a range of $1 \times 10^{-7} \text{ M}$ (a) to $5 \times 10^{-6} \text{ M}$ (g). B) Calibration curve for L-malate representing the mean current value of three replicates recorded consecutively with the same biosensor. The error bars correspond to the standard deviation.

malolactic fermentation process would not contain ascorbic acid. Therefore, it can be stated that the L-malate determination is not affected by the presence of interferences.

3.6. Application of the biosensor in real wines samples from malolactic fermentation

The biosensor performance for the L-malate determination in wine samples collected during the malolactic fermentation was assessed. Fig. 5 shows the results of the analysis of samples collected from the fermentation process of three red wines and the values obtained with the standard colorimetric method. An excellent agreement was achieved with absolute errors below 0.2 g L^{-1} ($1.5 \times 10^{-3} \text{ M}$) in all the samples. As can be seen, almost all values obtained with the biosensor are within the uncertainty range at 95% of the standard method. The evolution of the malic acid during the fermentation processes was as expected. When the concentration of L-malic is below 0.3 g L^{-1} ($2.2 \times 10^{-3} \text{ M}$) for 3 consecutive determinations, the transformation to L-lactic acid ended. In this case, the three wines analyzed have completed this process. During the winemaking, the detection of this end point is very important in order to microbiologically stabilize the wine by adding sulphite on time. If not, the lactic acid bacteria begin to degrade the sugars, producing an increase of acetic acid concentration in wine. This affects negatively the taste and odor of the final product. It is worth mentioning that all measurements performed in this study were

carried out with the same biosensor, which retained the 90% of its initial sensitivity after analyzing more than 80 measurements, including all the wine samples as well as the calibrations carried out before and after the analysis of each wine.

3.7. Comparative study with other L-malate amperometric biosensors

Table 2 shows the analytical characteristics of the developed L-malate biosensor and other amperometric biosensors based on the use of MDH, previously reported. Regarding the application of coupled enzyme reactions, there is one biosensor using just MDH and most of them also incorporate DP for improving the sensitivity. The biosensor described in this work clearly outperforms the other approaches in terms of sensitivity and detection limit. This may be partially related with the immobilization of the chemical species in a conductive polypyrrole membrane synthesized under biocompatible conditions that may preserve the enzyme activity almost intact. Besides, using an electropolymerization approach such as the one described in this work enables the strict controlled deposition of the required chemical species making it compatible with the application of miniaturized transducers. By contrast, the estimated biosensor linear range is slightly shorter than that shown by other devices. This may be related to the limited amount of mediator entrapped in the polymer film compared with that when the mediator is kept in solution. Nevertheless, immobilizing the

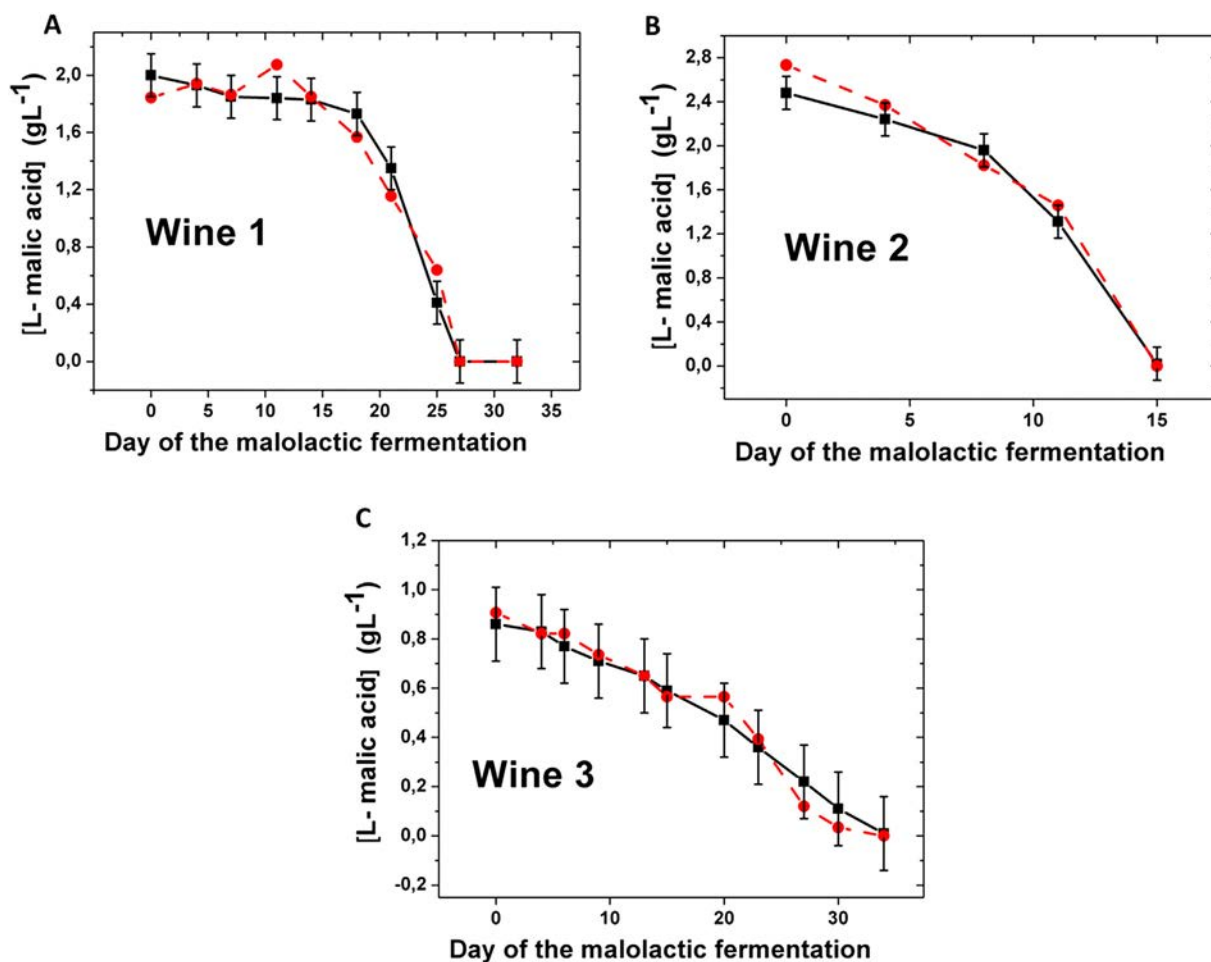


Fig. 5. Comparative analysis of wine samples collected during the malolactic fermentation process for three red wines. Dashed lines and circles show the values of L-malic acid measured with the developed biosensor and solid lines and squares, those obtained with the colorimetric standard method. The error bars represent the uncertainty at 95% in the case of the colorimetric method.

Table 2
L-malate amperometric biosensors based on MDH described in the literature.

Enzymes	Electrode	Mediator	Immobilization	Sensitivity ($\mu\text{A M}^{-1}$)	Linear range (M)	LOD (M)	Stability	Samples	Reference
MDH/DP	Carbon-paste	Ferricyanide in solution	Entrapment in the carbon paste	–	1.5×10^{-5} -1.5×10^{-3}	1.5×10^{-5}	90% after 1 month of storage	-	[35]
MDH/DP	Carbon	Ferricyanide in solution	Dialysis membrane	–	1×10^{-5} -1.3×10^{-3}	1×10^{-5}	100% after 5 month of storage or 5 assays	Wines	[36]
MDH	SWCNT		Physical absorption	4.55×10^{-1}	2×10^{-4} -8×10^{-4}	3.3×10^{-7}	75% after 5 measures	-	[37]
MDH/DP	Gold planar electrode	Ferricyanide in solution	Chitosan layers	5.50×10^{-4}	1.5×10^{-6} -5.2×10^{-4}	5.4×10^{-6}	63% after 7 days or 30 assays or 90% after 1 year of storage	Wines	[18]
MDH/DP	Gold disk	TTF	MPA-SAM and dialysis membrane	1.58×10^3	5.2×10^{-7} -2×10^{-5}	5.2×10^{-7}	90% after 7 days	Synthetic MLF	[17]
MDH/DP	Thin-film gold electrode	Hexaammineruthenium (III) chloride	PPy entrapment	2.18×10^4	1×10^{-7} -1×10^{-6}	6.3×10^{-8}	90% after 32 days or 80 assays	Red wines from MLF	This work

TTF: tetrathiafulvalene; MPA: 3-mercaptopropionic acid; SAM: self-assembled monolayer; SWCNT: single-wall carbon nanotubes.

mediator together with the enzymes is highly desirable in order to minimize the number of reagents added to the measuring solution.

A biosensor applied to the monitoring of the malolactic fermentation must show a long-term working stability under continuous use because the fermentation process takes around 30 days. Some of the biosensors in Table 2 show excellent storage stability values of months or even years. However, the working biosensor stability is significantly worse, this being restricted to few days and thus limiting the biosensor performance for the proposed application. The biosensor developed in this work maintains 90% of its initial sensitivity after 37 days in solution and continuous use, being the only amperometric biosensor based on MDH reported so far that could be applied to the real-time monitoring of malolactic fermentation processes. Finally, some biosensors have been applied to the determination of L-malate in wines samples and one of them has been tested in synthetic wines samples simulating the malolactic fermentation process. However, the biosensor presented in this work is the only one that has been assessed using real samples collected during the malolactic fermentation of red wines.

4. Conclusions

An electrochemical bioenzymatic biosensor for the determination of L-malate based on the co-entrapment of MDH and DP enzymes together with the redox mediator in an electrosynthesized PPy film has been developed. The study performed with 10 different redox mediators demonstrated that the Hexaammineruthenium (III) chloride was effectively entrapped in the PPy film. Although the incorporation of the NAD⁺ as enzymatic cofactor into the PPy membrane was also assessed, the working stability was limited by the chemical decomposition of NAD⁺. The results demonstrated that the developed biosensor presented a very high sensitivity with a low limit of detection. Besides, the biosensor retained more than 90% of its original sensitivity over 37 days of performance, allowing its successful application to the L-malic acid monitoring during the malolactic fermentation of three red wines.

Acknowledgements

We acknowledge funding from the Spanish R & D National Program (MINECO, Projects TEC2011-29045-C04-01/04 and TEC2014-54449-C3-1-R) and from the Generalitat de Catalunya (2014SGR1645). P. G.-G. is grateful to MINECO, Spain, for the financial support through a research studentship of the FPI Program. We also acknowledge the group of Dr. Iluminada Gallardo (Chemistry Department, Universitat Autònoma de Barcelona,

Spain) for the support during the polymer distillation.

Appendix A. Supplementary data

Supplementary data related to this article can be found at <http://dx.doi.org/10.1016/j.aca.2016.11.061>.

References

- [1] C.M. Ford, *The biochemistry of organic acids in the grape*, in: H. Gerós, M. Chaves, S. Delrot (Eds.), *The Biochemistry of the Grape Berry*, Bentham Books, 2012, pp. 67–88.
- [2] R.B. Boulton, et al., *Principles and Practices of Winemaking*, Springer Science + Business Media, New York, 1999.
- [3] P. Ribereau-Gayon, et al., *Handbook of enology*, in: 2 ed. *The Microbiology of Wine and Vinifications*, vol. 1, John Wiley & Sons Ltd., 2006.
- [4] M. Bony, et al., *Metabolic analysis of S-cerevisiae strains engineered for malolactic fermentation*, *Febs Lett.* 410 (2–3) (1997) 452–456.
- [5] M. Calull, R.M. Marce, F. Borrull, *Determination of carboxylic-acids, sugars, glycerol and ethanol in wine and grape must by ion-exchange high-performance liquid-chromatography with refractive-index detection*, *J. Chromatogr.* 590 (2) (1992) 215–222.
- [6] H. Kelebek, et al., *HPLC determination of organic acids, sugars, phenolic compositions and antioxidant capacity of orange juice and orange wine made from a Turkish cv. Kozan*, *Microchem. J.* 91 (2) (2009) 187–192.
- [7] R. Vonach, B. Lendl, R. Kellner, *High-performance liquid chromatography with real-time Fourier-transform infrared detection for the determination of carbohydrates, alcohols and organic acids in wines*, *J. Chromatogr. A* 824 (2) (1998) 159–167.
- [8] V.I. Esteves, et al., *Using capillary electrophoresis for the determination of organic acids in Port wine*, *Anal. Chim. Acta* 513 (1) (2004) 163–167.
- [9] I. Mato, S. Suarez-Luque, J.F. Huidobro, *Simple determination of main organic acids in grape juice and wine by using capillary zone electrophoresis with direct UV detection*, *Food Chem.* 102 (1) (2007) 104–112.
- [10] OIV-MA-AS313-11, *L-malic Acid: Enzymatic Method* (OIV Compendium Ed. 1990, Revised by 377/2009), International Organisation of Vine and Wine (OIV), 2009.
- [11] B. Bucur, et al., *Strategies to develop malic acid biosensors based on malate quinone oxidoreductase (MQO)*, *Biosens. Bioelectron.* 21 (12) (2006) 2290–2297.
- [12] M. Esti, et al., *Electrochemical biosensors for monitoring malolactic fermentation in red wine using two strains of Oenococcus oeni*, *Anal. Chim. Acta* 513 (1) (2004) 357–364.
- [13] A.M. Gurban, et al., *Malate biosensors for the monitoring of malolactic fermentation: different approaches*, *Anal. Lett.* 39 (8) (2006) 1543–1558.
- [14] F. Mazzei, F. Botre, G. Favero, *Peroxidase based biosensors for the selective determination of D, L-lactic acid and L-malic acid in wines*, *Microchem. J.* 87 (1) (2007) 81–86.
- [15] F. Gallarta, F. Javier Sainz, C. Saenz, *Fluorescent sensing layer for the determination of L-malic acid in wine*, *Anal. Bioanal. Chem.* 387 (6) (2007) 2297–2305.
- [16] J.F.S. de Santana, M.F. Belian, A.F. Lavorante, *A spectrophotometric procedure for malic acid determination in wines employing a multicommutation approach*, *Anal. Sci.* 30 (6) (2014) 657–661.
- [17] M. Gamella, et al., *Integrated multienzyme electrochemical biosensors for monitoring malolactic fermentation in wines*, *Talanta* 81 (3) (2010) 925–933.
- [18] R. Monosik, et al., *Comparison of biosensors based on gold and nanocomposite electrodes for monitoring of malic acid in wine*, *Cent. Eur. J. Chem.* 10 (1)

- (2012) 157–164.
- [19] D. Grieshaber, et al., Electrochemical biosensors - sensor principles and architectures, *Sensors* 8 (3) (2008) 1400–1458.
- [20] A. Chaubey, B.D. Malhotra, Mediated biosensors, *Biosens. Bioelectron.* 17 (6–7) (2002) 441–456.
- [21] D.D. Schlereth, E. Katz, H.L. Schmidt, Surface-modified gold electrodes for electrocatalytic oxidation of NADH based on the immobilization of phenoxazine and phenothiazine-derivatives on self-assembled monolayers, *Electroanalysis* 7 (1) (1995) 46–54.
- [22] M. Somasundrum, J. Hall, J.V. Bannister, Amperometric NADH determination via both direct and mediated electron-transfer by NADH oxidase from *thermus-aquaticus* YT-1, *Anal. Chim. Acta* 295 (1–2) (1994) 47–57.
- [23] E. Barendrecht, Chemically and physically modified electrodes- Some new developments, *J. Appl. Electrochem.* 20 (2) (1990) 175–185.
- [24] F.R.R. Teles, L.R. Fonseca, Applications of polymers for biomolecule immobilization in electrochemical biosensors, *Mater. Sci. Eng. C-Biomim. Supramol. Syst.* 28 (8) (2008) 1530–1543.
- [25] J. Orozco, et al., Characterization of ultramicroelectrode arrays combining electrochemical techniques and optical microscopy imaging, *Electrochim. Acta* 53 (2) (2007) 729–736.
- [26] C. Jimenez-Jorquera, J. Orozco, A. Baldi, ISFET based microsensors for environmental monitoring, *Sensors* 10 (1) (2010) 61–83.
- [27] P. Gimenez-Gomez, et al., Monitoring of malolactic fermentation in wine using an electrochemical bienzymatic biosensor for L-lactate with long term stability, *Anal. Chim. Acta* 905 (2016) 126–133.
- [28] M.H. Chakrabarti, E.P.L. Roberts, Analysis of mixtures of ferrocyanide and ferricyanide using UV-Visible spectroscopy for characterisation of a novel redox flow battery, *J. Chem. Soc. Pak.* 30 (6) (2008) 817–823.
- [29] B. Gründig, et al., Mediator-modified electrodes for electrocatalytic oxidation of NADH, *J. Electroanal. Chem.* 395 (1995) 143–157.
- [30] W. Schuhmann, et al., Electrocatalytic oxidation of NADH at mediator-modified electrodes surfaces, *J. Biotechnol.* 27 (1993) 129–142.
- [31] J. Zeng, et al., Fabrication of poly(toluidine blue O)/carbon nanotube composite nanowires and its stable low-potential detection of NADH, *J. Electroanal. Chem.* 595 (2) (2006) 152–160.
- [32] Nicotinamide cofactor dependent oxidoreductions, in: C.H. Wong, G.M. Whitesides (Eds.), *Enzymes Synthetic Organic Chemistry*, Pergamon, 1994, pp. 131–153.
- [33] L.S. Curtin, G.C. Komplin, W.J. Pietro, Diffusive anion-exchange in polypyrrole films, *J. Phys. Chem.* 92 (1) (1988) 12–13.
- [34] H. Borsook, G. Keighley, Oxidation reduction potential of ascorbic acid (Vitamin C), *Proc. Natl. Acad. Sci. U. S. A.* 19 (1933) 875–878.
- [35] S. Miertus, et al., Amperometric biosensors based on solid binding matrices applied in food quality monitoring, *Biosens. Bioelectron.* 13 (7–8) (1998) 911–923.
- [36] J. Katrlík, et al., Biosensors for L-malate and L-lactate based on solid binding matrix, *Anal. Chim. Acta* 379 (1–2) (1999) 193–200.
- [37] A. Arvinte, L. Rotariu, C. Bala, Amperometric low-potential detection of malic acid using single-wall carbon nanotubes based electrodes, *Sensors* 8 (3) (2008) 1497–1507.